In-solution and physical state properties of polymer and lipid excipients and their effects on the supersaturation evolution of poorly water-soluble drugs

by

Jiahao Huang

A thesis

presented to the University of Waterloo

in fulfillment of the

thesis requirement for the degree of

Doctor of Philosophy

in

Pharmacy

Waterloo, Ontario, Canada, 2022

Examining Committee Membership

The following members served on the Examining Committee for this thesis. The decision of the Examining Committee is by majority vote.

External Examiner	Dr. Ping Lee Professor, Leslie Dan Faculty of Pharmacy, University of Toronto
Supervisor	Dr. Shawn Wettig Professor, School of Pharmacy; Assistant Vice President, Graduate Studies (Science)
Internal Members	Dr. Praveen Nekkar Rao Associate Professor, School of Pharmacy
	Dr. Roderick Slavcev Associate Professor, School of Pharmacy
Internal-External Member	Dr. Jean Duhamel Professor, Department of Chemistry; Director, Institute for Polymer Research

Author's Declaration

This thesis consists of materials that I authored and co-authored: see Statement of Contributions section. This is a true copy of the thesis, including any required final revisions, as accepted by my examiners.

I understand that my thesis may be made electronically available to the public.

Statement of Contributions

Jiahao Huang was the sole author of Chapters 1, 2, 3, 5 and 6 which were written under the supervision of Dr. Shawn Wettig and were not written for publication. Exception to sole authorship of material is as follow:

Research presented in Chapter 4:

Experimental studies of this chapter were planned by Jiahao Huang in consultation with Dr. Wettig. All experiments were carried out by Jiahao Huang at the University of Waterloo. The fluorescence spectroscopy and microscopy results of indomethacin-phospholipid section were published. Jiahao Huang was responsible for data analysis of the results and created the initial draft of the manuscript. Dr. Peter X Chen provided assistance in the analysis of fluorescence spectra results. Dr. Wettig edited the various drafts of the manuscript and contributed to the discussion of the experimental results and to the overall conclusions that resulted.

Citation:

Huang J, Chen PX, Wettig S. Fluorescence-based techniques to assess the miscibility and physical stability of a drug–lipid complex. Canadian Journal of Chemistry. 2019;97(6):496-503.

Abstract

Solubility has become an increasing issue for the pharmaceutical industry, as the advances in combinatorial chemistry and high throughput screening methods have resulted in an increase in the molecular weight and lipophilicity of new chemical entities. There is a constant need for the development of formulation strategies to address these challenges for the oral delivery of poorly soluble drugs. The supersaturated drug delivery system (SDDS) based on amorphous solid dispersion (ASD) is a novel strategy to increase solubility and dissolution of hydrophobic drug compounds in order to achieve an improved oral absorption. The kinetic solubility profile of an ASD formulation in aqueous environment depends on the buildup and maintenance of supersaturated drug solution, which are determined by parameters including drug amorphization state in ASD carrier, drug release from the carrier matrix, liquid-liquid phase separation (LLPS) and nucleation of supersaturated drug solution, and crystal growth rate of drug molecules. These factors are closely correlated to the solid-state and in-solution properties of ASD carrier materials. This thesis aims to investigate the effects of polymer and lipid materials on the LLPS, recrystallization profile, drug-carrier miscibility and dissolution behaviors of two model drugs, indomethacin (IDM) and apixaban (APX), in an effort to benefit both the investigation of fundamental mechanisms of drug supersaturation and the development of pharmaceutical excipients into ASD carriers.

Firstly, the LLPS behaviors of both drugs in the presence of polymer and lipid carriers were successfully characterized using the double wavelength UV extinction method. The LLPS behaviors of both drugs were depended on one or more of the following mechanisms: in-solution hydrogen bonding, drug aggregation facilitated by amphiphilic agents, micelle/vesicle incorporation, and ionization induced solubility enhancement. Polymer or lipid carrier can modify the LLPS behaviours of different drugs in completely different ways depending upon the nature of the drugs. The methodology is expected to serve the LLPS investigations of more types of drugs and excipients. Our work suggests that the effects of excipients on drug LLPS must be analyzed on a case by case basis, given the fact that an ASD carrier can behave markedly differently for different drug compounds.

Secondly, the supersaturation effects of polymer and lipid ASD carriers on IDM and APX under non-sink dissolution conditions were revealed using a solvent-shift method and compared with the identified LLPS properties. Results showed that the supersaturation behaviors of both drugs were influenced by ASD carriers by mechanisms that include in-solution hydrogen bonding, pH-induced

solubility change, solubilization, and reduced crystal growth rate. The recrystallization behaviors of both drugs did not necessarily align with the corresponding LLPS results, as LLPS properties were considered to influence the early stage of drug recrystallization. By comparing LLPS and supersaturation result for certain drug-excipient pairs, we also suggested that the different principles of characterization methods may induce variations in the characterization results. Therefore, multiple characterization methods should be combined to obtain accurate in-solution properties of drugs and excipients.

Thirdly, we successfully characterized the drug-excipient miscibility for IDM and APX under a solid state, aiming to analyze the amorphization and loading state of both drugs in different carriers. Meanwhile, the feasibility of using fluorescence techniques to evaluate drug-carrier miscibility was testified by various drug-excipient pairs. Spectral parameters including peak shape, peak intensity and peak wavelength were used to analyze drug-excipient miscibility and physical state of IDM and APX in ASD systems. Distribution of fluorescence intensity and birefringence properties of fluorescence microscopy were also used to analyze the drug-excipient miscibility. Our work suggests that the fluorescence spectroscopy and fluorescence microscopy must be combined to obtain the accurate drug amorphization state in ASD systems, as fluorescence spectroscopy alone may be ineffective in identifying the amorphous drug aggregates in ASD systems. The drug amorphization and loading states were used to analyze the drug release behavior that was closely associated with supersaturation buildup of an ASD formulation.

Lastly, ASDs for IDM and APX were prepared with polymers, lipids, and their combinations as carriers. The dissolution behaviors of prepared samples were tested under non-sink conditions where LLPS and recrystallization were expected to occur. The dissolution and supersaturation parameters were analyzed based on previously investigated properties including LLPS, solubilization, recrystallization, and drug amorphization state. For both IDM and APX, dissolution parameters were greatly influenced by carrier type in different manners. A given type of carrier could provide different effects when it was used to load different drugs. Preparation methods were found to bring inconsistent changes to different formulations. The disintegration, dissolution and dispersion of carrier materials were critical factors to determine the expression of carriers' ability to generate and maintain supersaturated drug solutions. The correlations between carriers' effect on crystalline solubility, LLPS, recrystallization, and dissolution parameters could only be established when drug carriers could rapidly and completely dissolve or disperse in dissolution media. The methodology and

implications provided by this study could be used to investigate the in-solution and physical-state properties of more types of poorly soluble drugs and potential ASD carriers, in order to benefit the development of ASD formulations.

Acknowledgements

Firstly, I would like to sincerely express my gratitude to my supervisor Dr. Shawn Wettig. I am grateful for his supportive and encouraging mentorship to lead me through the graduate program. His professionalism as an educator and passionate commitment to the Royal Canadian Air Force demonstrated a positive involvement in different aspects of the community, which had a significant impact on me. I feel lucky to work in the Wettig research group.

I would like to thank the members of my advisory committee, Dr. Jonathan Blay, Dr. Praveen Nekkar Rao, and Dr. Roderick Slavcev for their kind guidance over the years. Their constructive criticism helped me view my project from the perspectives of different expertise fields and led to important improvements. I am grateful to Dr. Ping Lee and Dr. Jean Duhamel for being part of my examining committee. I appreciate your time.

Dr. Monica Tudorancea is acknowledged for her support on the usage and maintenance of core lab facilities at the School of Pharmacy. I would like to thank Josie Orso Simon for providing support on using the Flex Lab instruments at the School of Pharmacy.

All members of the Wettig Lab are acknowledged for the supports and collaborations throughout my research journey. Thank you to Dr. Samantha Shortall and Dr. Shannon Callender for providing training on various lab instruments. I am grateful for Dr. Festo Damian and Dr. Peter X Chen for sharing knowledge on drug solubility and fluorescence experiments.

I am grateful for the financial support from University of Waterloo, School of Pharmacy, and Waterloo Institute for Nanotechnology.

Finally, I would like to acknowledge my fiancée, Shengwenjun Qi, for her unconditional support.

Dedication

I dedicate this thesis to my beloved family members.

Table of Contents

List of Figures

List of Tables

List of Abbreviations

API	Active pharmaceutical ingredient
APX	Apixaban
ATO	Compritol® 888 ATO,
ASD	Amorphous solid dispersion
BCS	Biopharmaceutical Classification System
CMC	Critical micelle concentration
DAPI	4′,6-diamidino-2-phenylindole
DMSO	Dimethyl sulfoxide
DPC	Drug-phospholipid complex
DSC	Differential scanning calorimetry
EC	Ethyl cellulose
FTIR	Fourier-transform infrared spectroscopy
G48	Gelucire® 48/16, PEG-32 stearate
GFP	Green fluorescent protein
GI	Gastrointestinal
GRAS	Generally recognized as safe
HPC	Hydroxypropyl cellulose
HPLC	High-performance liquid chromatography
HPMC	Hydroxypropyl methylcellulose
HPMCAS	Hydroxypropyl methylcellulose acetate succinate
HME	Hot melt extrusion
IDM	Indomethacin
LBF	Lipid based formulation

LLPS	Liquid-liquid phase separation
NCE	New chemical entities
PEG	Polyethylene glycol
PL	Phospholipid
PVP	Polyvinylpyrrolidone
PWSD	Poorly water-soluble drug
PXRD	Powder X-ray diffractometry
SA	Sodium alginate
SDDS	Supersaturated drug delivery system
SDS	Sodium dodecyl sulfate
SEM	Scanning electronic microscopy
SI	Sink index
SOL	Soluplus®, polyvinyl caprolactam-polyvinyl acetate-polyethylene glycol graft copolymer
TEM	Transmission electronic microscopy
UPLC	Ultra-performance liquid chromatography
UV	Ultraviolet

Chapter 1
Introduction

1.1 Solubility and dissolution enhancement of poorly water-soluble drugs for oral drug delivery

Oral delivery of drugs is by far the most common and the most preferred method for patients to take a prescribed medication [1,2]. In order to be successfully delivered by the oral route a drug must have some solubility in aqueous media [3–5]. If one considers that the majority of new molecules being developed (either through chemical synthesis or extraction from biological sources) as potential drugs have both low solubility and a low degree of permeability across biological membranes (a second important requirement that new drugs must possess) understanding the ways in which drug solubility can be modified is of critical importance [6,7]. An important starting point for such understanding is the Biopharmaceutical Classification System (BCS).

1.1.1 Biopharmaceutical Classification System

The BCS was proposed based on the mechanisms that the oral absorption of a drug in the gastrointestinal (GI) tract through passive diffusion is determined by the amount of drug in solution at the luminal-epithelial border and the diffusion rate of drug across the intestinal membrane [8,9]. The solubility and permeability of a drug are categorized as either high or low by the BCS system (Figure 1.1) and are constructively used to evaluate the potential of a drug compound to be influenced by formulation variables and physiological changes. A compound is considered to have high solubility if its largest dose strength can be fully dissolved in 250 mL GI medium from pH 1 to 7. BCS class I and III drugs with high solubility are not expected to be sensitive to formulation factors when developing immediate-release dosage forms. In contrast, the oral bioavailability of BCS class II and IV drugs with low solubility is more likely to be influenced by their physical states that determine the dissolution rate. In the pharmaceutical field, BCS provides guidance on the formulation strategies for new drug compounds and is used by regulatory agencies to determine whether bioequivalence studies or biowaivers are required for new strengths or modified formulations of approved drugs.

Solubility has become an increasingly important issue for the pharmaceutical industry. The advances in combinatorial chemistry and high throughput screening methods have resulted in an increase in the molecular weight and lipophilicity of new chemical entities (NCE), as these properties are expected to improve drug potency by increasing the drug-receptor interactions [10–12]. Over 40%

of the approved drugs and approximately 90% of the pharmaceutical compounds in the development pipeline are in the category of BCS class II and IV [13]. Despite the therapeutic potentials of certain NCEs, their development into oral drug products, which provide the best patient compliance, can be negatively influenced by the poor aqueous solubility associated with their large molecular sizes and lipophilic structures.

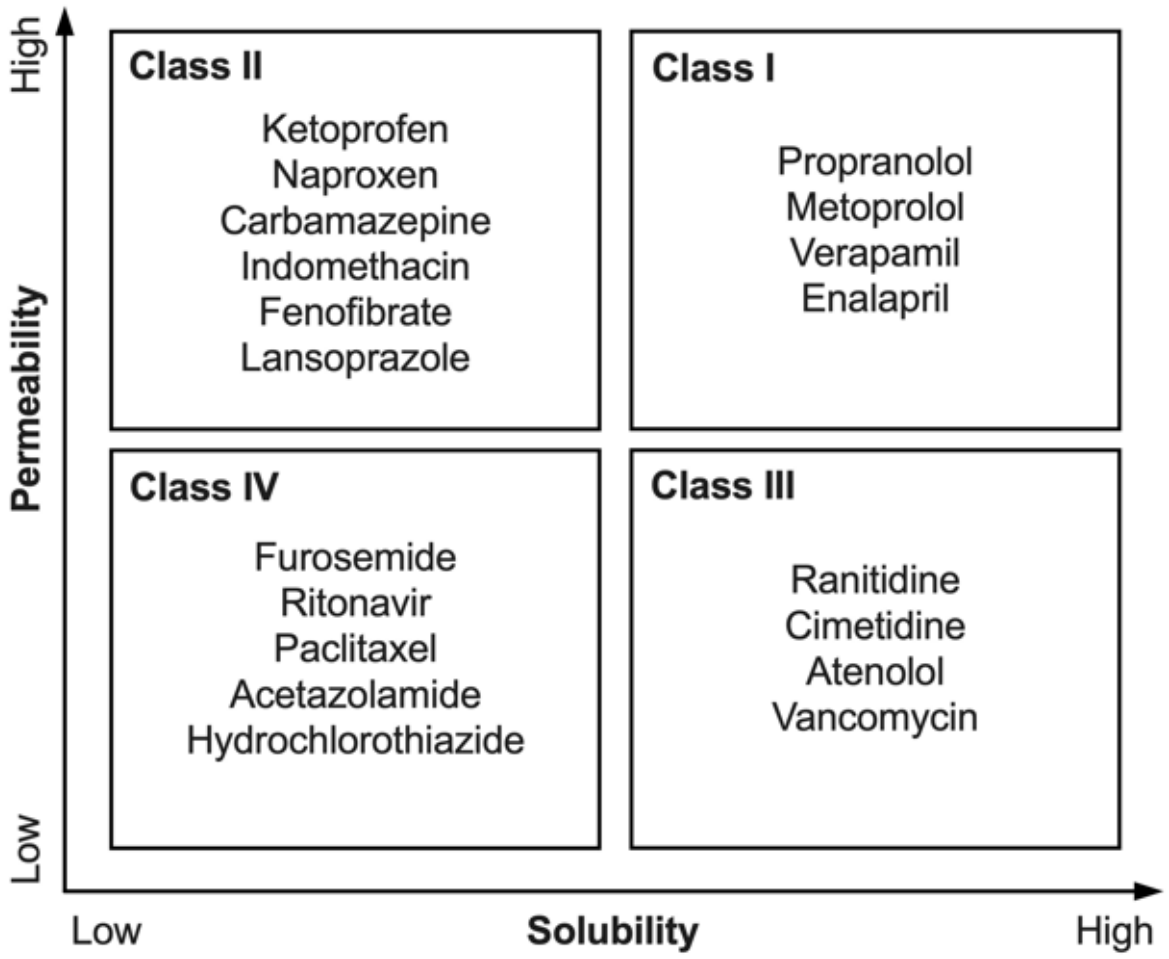

Figure 1.1. Illustration of Biopharmaceutical Classification System (BCS). Class I drug has a high solubility and high permeability; Class II drug has a low solubility and high permeability; Class III drug has a high solubility and low permeability; and Class IV drug has a low solubility and low permeability [14].

For a poorly water-soluble drug (PWSD) to be absorbed through the oral route and reach the blood circulation over its therapeutic threshold concentration, the required dissolution time may surpass its retention time in the GI tract. Therefore, an understanding of solubility and dissolution characteristics of a PWSD is essential for its formulation development.

1.1.2 Crystalline solubility and dissolution

A crystalline solid is characterized with a lattice structure with regular arrangement. Crystalline solubility describes an equilibrium between the solid and drug molecules that are in the solution phase, representing the concentration in the solution phase whereby the solvent is absent in the crystalline phase [15]. The equilibrium is described as [16]:

$$\ln\left(x_D^W \gamma_D^W\right) = \frac{\mu_D - \mu_0}{RT} \qquad \textbf{Equation 1.1}$$

where x_D^W is the mole fraction solubility of a crystalline drug (D) in water (W), γ_D^W is the activity coefficient of the drug at water saturation, μ_D and μ_0 are the chemical potentials of the crystalline drug and supercooled liquid form of the drug, R is the gas constant, and T is the temperature. In this context, the crystalline form of a drug is the most thermodynamically stable form, and its chemical potential is equivalent to that of the solute in a saturated solution. To reach this equilibrium, a solid crystalline drug undergoes a dissolution process when it is delivered to an aqueous medium. Dissolution can be divided into consecutive steps [11,17]. Firstly, the crystalline lattice of the solid drug is disrupted into isolated drug molecules, which is an endothermic process that requires the crystal packing energy/lattice energy to be overcome. Following this, with the input of cavitation energy, the breaking of hydrogen bonding of water enables the formation of cavity to host drug molecules. Lastly, favorable interactions form between the solvent and solute to finalize the dissolution process. This step is an exothermic process as the solvation energy is released to lower the Gibbs free energy of the system in order to reach equilibrium. For PWSDs, the crystal packing energy has a larger magnitude than cavitation and solvation energies, serving as the critical determinant of solubility and dissolution. The overall rate of these processes is referred to as dissolution rate, which can be described by the Whitney-Noyes equation:

$$\frac{dM}{dt} = \frac{DA}{h} \times (C_s - C) \approx \frac{DAC_s}{h} \qquad \textbf{Equation 1.2}$$

where M is the mass of solute, D is the intrinsic diffusion coefficient of solute, A is the surface area of solid particle, h is the thickness of the diffusion layer, C_S is the equilibrium solubility of the solute,

and C is the solute concentration in the dissolution medium. When a drug is delivered orally, h is determined by the intrinsic hydrodynamic conditions of the gastrointestinal tract, which generally cannot be changed from the formulation perspective [18]. The manipulation of other factors has led to the development of various solubility and dissolution enhancing technologies.

1.1.3 Solubility and dissolution enhancing technologies

Over the years, a variety of formulation strategies have been designed to improve solubility and dissolution to deliver hydrophobic compounds orally. Examples include pH adjustment, prodrug design, cocrystal formation, micro/nano pulverization, colloidal system design with surfactant micelles or lipid vesicles, cyclodextrin incorporation, drug incorporation into a mesoporous inorganic carrier, etc [19–25]. As introduced in the previous section, the Whitney-Noyes equation is the scientific foundation for considering most solubility-enhancing technologies that produce solid-state products. An increase in surface area (A) is enabled by the size reduction of active pharmaceutical ingredient (API) particles using either top-down technologies including ball milling, cryogenic grinding, nano-pulverization, or bottom-up generation of smaller crystals of API through technologies including supercritical fluid and freeze drying [26–30]. The surface tension of GI media can be decreased by the addition of surfactants to a formulation, so that the surface area that is accessible to the dissolution media is improved by facilitated wetting. The other major factor, equilibrium solubility (C_S), can be increased by chemical modifications including salt formation, co-crystals, and prodrugs. In the past two decades, there has been rising recognition that decreasing particle size or increasing dissolution rate and crystalline solubility are insufficient to achieve desired bioavailability for PWSDs. Interests in supersaturated drug delivery systems (SDDS) that are able to maintain a supersaturated concentration of drug have increased due to the ability to further improve the solubility of PWSD by incorporating amorphous drugs (as opposed to crystalline) which show higher solubility and faster dissolution than their crystalline counterparts [31,32]. An SDDS is a thermodynamically unstable system that is prone to changes in physical state [15]. An understanding of the scientific foundations and implications of SDDS is important for the development of relating formulations.

1.2 Theories of supersaturated drug delivery system (SDDS)

1.2.1 Solubility and dissolution advantages of an amorphous solid

A solid substance can exist in either a crystalline or an amorphous state. These two forms possess the same molecular composition but can show different physiochemical properties such as hardness, thermal conductivity, electrical resistivity, etc [33–35]. The pharmaceutical interests in amorphous solids focus on their increased solubilities compared with the respective crystalline drugs. The lack of crystalline structure or a long-range order of molecular packing of an amorphous drug provides higher Gibbs free energy in its delivery form [32]. It requires less energy input to break the solid into isolated molecules that can be solvated because the crystal lattice energy is absent.

The amorphous solubility of a solid substance is the equilibrium between amorphous solid and the liquid phase of its saturated solution, representing the concentration in solution phase whereby solvent is absent in amorphous solid phase. The concept is similar to crystalline solubility. However, from the thermodynamic perspective, such an equilibrium cannot exist because the amorphous form of a solid drug is not the most thermodynamic stable form, and there is a constant tendency for it to crystallize until the solution concentration reaches the crystalline solubility [14]. Nevertheless, if crystallization is slow, the nonequilibrium amorphous state can become metastable from the kinetic perspective. This enables the possibility that an amorphous drug can maintain its high Gibbs free energy prior to dissolution. At present, there is no characterization technique to directly measure the amorphous solubility of a drug. Amorphous solubility of a solid in water can be estimated by different approaches when the crystalline solubility is known [36–39]. The correlation between crystalline solubility and amorphous solubility is described in Equation 1.3:

$$C_a = C_s \times e^{-I(a)} \times e^{\frac{\Delta G}{RT}} \qquad \textbf{Equation 1.3}$$

where C_a is the amorphous solubility of the drug, C_S is the crystalline solubility of the drug, -I(a) is the activity coefficient of the amorphous drug at equilibrium, ΔG is the difference in the free energy of crystalline and amorphous form of the drug, R is the gas constant, and T is the temperature. ΔG is calculated based on the experimentally determined heat capacity of the crystal and supercooled liquid. -I(a) is determined by the mole fraction of water absorbed by amorphous drug as a function of relative humidity [15,40]. The flux across the GI membrane is dependent on the thermodynamic activity of a

solute, so that solutions enabled by the amorphous drug can exhibit improved flux compared to those enabled by the solubilized system at the same drug concentration [41,42].

1.2.2 Supersaturation

During dissolution of an amorphous solid, the chemical potential of a solute in solution is higher than that of a saturated solution. The solution is defined as a supersaturated solution, for which the supersaturation degree (S) is described as:

$$\ln S = \frac{\mu_S - \mu_D}{RT} = \ln \frac{x_S^W \gamma_S^W}{x_D^W \gamma_D^W} \qquad \textbf{Equation 1.4}$$

where μ_S is the chemical potential of the supersaturated solution, $\mu_D$is the chemical potential of the saturated solution, x_S^W is the mole fraction of a drug in the supersaturated solution, γ_S^W is the activity coefficient of the drug in the supersaturated solution, R is the gas constant, and T is the temperature. For the practical purpose of pharmaceutical development, it is assumed that γ_S^W equals to $\gamma_D^W$for simple aqueous media that do not contain substances with cavity structures like cyclodextrin [15]. In these circumstances, S is expressed by the ratio of $x_S^W$and x_D^W, and the supersaturation degree can be taken as the ratio of the molar concentrations:

$$S = \frac{C}{C_S} \qquad \textbf{Equation 1.5}$$

where C is the molar concentration of the drug in a supersaturated solution and C_S is the molar concentration of the saturated solution. The supersaturation degree is commonly used to quantify the dissolution performance of SDDS formulations and facilitate the design of experiment parameters for *in vitro* dissolution tests [43–45].

1.2.3 Crystallization and liquid-liquid phase separation

A superstrated solution is a thermodynamically unstable system that would precipitate to form a saturated solution as a way to lower the Gibbs free energy of the system. The attenuation of supersaturation is due to drug crystallization from solution, which involves a nucleation stage and a crystal growth stage [46,47]. Firstly, drug molecules in a supersaturated solution aggregate with each other when diffusing through the bulk solution under the thermodynamic driving force [48]. The size of the formed drug clusters is increased by the addition of drug monomers, leading to the formation of nuclei that act as centers of crystallization. A nucleus is understood as the minimum amount of new

phase that is capable of existing independently in the original phase. The rate of nucleation (J) is expressed by an Arrhenius reaction rate equation:

$$J = N_0 \cdot v \cdot \exp\left[-\frac{16f\gamma^3 v^2}{3k^3T^3(\ln S)^2}\right] \qquad \textbf{Equation 1.6}$$

where J is the rate of appearance of nuclei in a given volume, N_0 is the number of molecules of crystallizing phase in a volume unit, v is the frequency of molecular transport at the nucleus-liquid interface, f is nucleation factor, γ is the nucleus-solution interfacial tension, k is the Boltzmann constant, T is temperature, and S is supersaturation degree. The equation suggests that the nucleation rate increases with higher supersaturation degree, which has a profound impact on the design of SDDS, as a high supersaturation degree is desired for better bioavailability [49,50]. The nucleation rate can also be influenced by pharmaceutical excipients through the change in solution viscosity and therefore molecular transport [51,52]. Surface active agents bring dual effects to the nucleation rate. On the one hand, they can solubilize drug molecules and incorporate them into a micelle/vesicle phase, decreasing the free drug concentration in the bulk solution phase and therefore the supersaturation degree [53,54]. On the other hand, interfacial tension between nucleating clusters and the solution phase may be lowered by surfactants to facilitate recrystallization [55–57]. The overall influence of surfactants is determined by the competition of reverse effects on supersaturation degree and wetting.

Crystal growth happens immediately after nucleation, resulting from the diffusion of drug particles to the surface of nuclei and incorporation into crystal lattice structures [48]. The crystal growth rate is expressed by the increase in crystal radius (r) over time, which is calculated by the following equation:

$$\frac{dr}{dt} = \left[DvN_A/(r + \frac{D}{k})\right] \cdot (C - Cs) \qquad \textbf{Equation 1.7}$$

where D is the diffusion coefficient of crystalline compound in a given solution, v is the frequency of molecular transport at the nucleus-liquid interface, k is the surface integration factor, N_A is Avogadro's constant, C is the drug concentration in bulk solution phase, and C_S is the equilibrium crystalline solubility of the drug. Similar to nucleation, a higher supersaturation degree is associated with faster crystal growth. D and v can be altered by the viscosity change in the presence of excipients. The surface integration can be modified if there is adsorption between crystal surface and excipients.

Another route for a supersaturated solution to lower the Gibbs free energy is known as liquid-liquid phase separation (LLPS), which can occur in the absence of recrystallization [58]. Similar to the initiation of nucleation, drug molecules in the bulk phase of a supersaturated solution aggregate with each other upon diffusion. Before the formation of nuclei (i.e. the minimum amount of new phase that is capable of existing independently), the aggregate forms a liquid phase with an uneven distribution and fluctuation of solute concentration. The liquid phase then splits into two immiscible liquid phases, a water-rich phase and a drug-rich phase, in the absence of formation of solid crystalline phase. The LLPS mechanism can be understood by the diagram of mixing free energy versus composition of two partially miscible liquids as shown in Figure 1.2 (in this case amorphous drug is considered as supercooled liquid) [59].

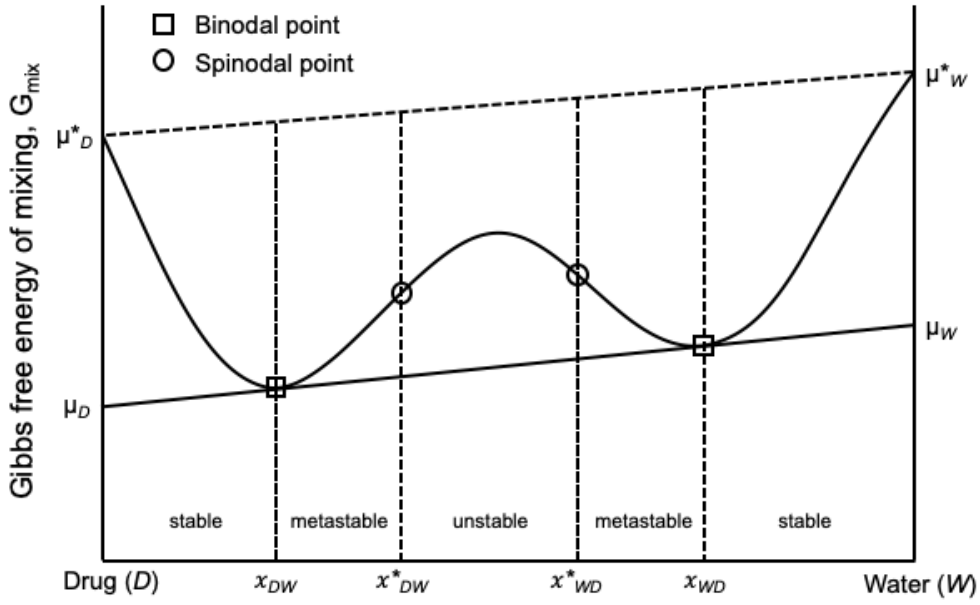

Figure 1.2. Gibbs free energy of mixing versus composition diagram for two immiscible liquids. Figure adapted from Reference [15], with permission from Elsevier.

Starting from the right side of the x-axis that represents pure water (W), the free energy of mixing becomes lower (i.e., ΔG is negative) when the amorphous drug (D) is added to the system until reaching the point x_{WD}. This means that the mixing of two phases is thermodynamically favored until the drug concentration reaches its miscibility limit in water, which is the amorphous solubility of

the drug. Similarly, starting from the left side of the x-axis that represents the pure drug, the mixing is also thermodynamically favored until reaching the composition of x_{DW} that corresponds to the miscibility of water in the drug. At the compositions of x_{WD} and x_{DW}, the net ΔG is lower than that for all other compositions, and these two compositions are referred to as binodal points for mixtures of water and amorphous drug. At the binodal points, the chemical potential of all solution components is equal in each phase ($\mu_D=\mu_W$). x_{WD} is the water-rich phase that contains a small amount of drug dissolved in water, where the drug concentration equals the amorphous solubility. x_{DW} is the drug-rich phase that contains a small amount of water mixed with amorphous drug. A miscibility gap is shown between the binodal points. Within this range, the spinodal points x^*_{WD} and x^*_{DW} represent the inflection points on the curve of free energy versus composition where $\partial^2G/\partial x^2 = 0$. Compositions between binodal and spinodal points (x_{WD} to x^*_{WD} and x_{DW} to x^*_{DW}) are metastable. Phase separation can occur while an energy barrier has to be overcome to form a new phase. Compositions between two spinodal points (x^*_{WD} and x^*_{DW}) are unstable, for which phase separation can occur spontaneously through spinodal decomposition to produce a water-rich phase and a drug-rich phase to lower the free Gibbs energy, and the process is referred to as LLPS. The drug-rich nanodroplets dissolve faster than crystalline drugs, attributed to the nanoscale and amorphous properties [42,60,61].

1.2.4 Experimental determination of liquid-liquid phase separation

The concept of LLPS has been used to understand the formation of amorphous nanoparticles in SDDS-enabled drug solutions and investigate the dissolution mechanisms of related formulations. There are different techniques that can be used to determine LLPS of supersaturated drug solutions. Light scattering is the most commonly used method to analyze the behaviors of supersaturated systems undergoing LLPS [62,63]. The solutions at this stage show distinct properties in terms of light transmittance and scattering. Ultraviolet (UV)/visible absorbance of a drug at its absorbing wavelength shows a change in linearity with regard to drug concentration when LLPS occurs. Correspondingly, light scattering can be detected at a non-absorbing wavelength for the drug during phase separation. This method is often associated with the solvent shift method, where a drug solution in a water-miscible organic solvent is titrated into water. When reaching a certain drug concentration, drug-rich nanodroplets form through spinodal decomposition due to the addition of drug solution to an unstable region. For ionizable drugs, pH solubilization can be used to create a drug solution with high concentration, followed by a constant change in pH to decrease the degree of ionization of the drug. The LLPS onset for the drug can be calculated by its solubility at the pH value where light

scattering is first detected. A limitation of this method is that the determined LLPS onset of a drug might be higher than the theoretical value due to the solubility increase of the drug in the presence of the organic solvent.

Fluorescence spectroscopy is another widely used technique to determine LLPS [58,64]. A fluorescence probe that is sensitive to environmental polarity changes, such as pyrene, can be used to characterize drug-rich phases which form when the amorphous solubility of a drug is exceeded. Fluorescence probes tend to interact with the drug-rich phase through hydrophobic interactions, and therefore their emission spectra change due to the probe preferentially being found in a less polar environment. By monitoring the emission spectrum as a function of drug concentration, the LLPS onset of the drug can be determined. For fluorescence spectroscopy to be effective it is important that drug molecules are not autofluorescent so that the emission spectra of fluorescence probes are not convoluted.

Ultracentrifugation can also be used to determine LLPS [65]. The separation of two phases by ultracentrifugation is based on the different density of two phases. Here it is important that the system undergoes minimal change in the physical state during centrifugation, and the centrifugation parameters can realize an effective separation, both of which can be compromised in a practical manner. An effective ultracentrifugation may require a long time (30-40 min) during which supersaturated solutions may evolve resulting in a change in physical state such as crystallization. Conversely, drug-containing nanodroplets with a size smaller than 50 nm could stay in the supernatant [66–69]. To solve this, a small amount of crystallization inhibitor can be added to maintain the physical state of testing samples [15]. Other characterization techniques include nuclear magnetic resonance spectroscopy, cryo-transmission, scanning electron microscopy, synchrotron radiation, etc [70–73].

1.3 Pharmaceutical application of amorphous solid dispersion

In order to take advantage of amorphous drug and SDDS in oral drug delivery, the amorphous solid dispersion (ASD) is the most common type of formulation used to carry amorphous drugs and achieve a supersaturated drug solution in GI fluids [74–76]. ASD has been established as a platform technology for the formulation of PWSD.

1.3.1 Preparation of solid dispersions

The term “solid dispersion” is defined as a dispersion of a solid drug in a solid matrix carrier which can be either a small molecule or a polymeric material. In 1961, the first solid dispersion formulation for pharmaceutical use was prepared by dispersing crystalline sulfathiazole into crystalline urea as a carrier to form a eutectic mixture as an oral dosage [77]. The formulation produced a microcrystalline suspension for sulfathiazole with a faster dissolution rate in water due to particle size reduction and facilitated wetting. Other carriers have mainly included sugars such as sorbitol and mannitol [78]. This type of SD was prepared using a melting method, whereby drug and carrier can crystallize simultaneously during the cooling process if they form a eutectic mixture. For a eutectic mixture, the melting point is lower than that for both drug and carrier. If the mixture of drug and carrier is not at the eutectic composition, the solid dispersion will be a mixture of micronized dispersion and a separated solid phase of drug or carrier. According to the literature, most of the first-generation solid dispersions studied were in fact not eutectic mixtures [79]. This type of mixture with crystalline drug and carrier was considered as the prototype of SD.

For the second generation of solid dispersions, amorphous polymeric materials were used as carrier for hydrophobic active pharmaceutical ingredients (API) [74]. Depending on drug-carrier miscibility and physical state of the API in formulation, these solid dispersions can be classified into amorphous solid solutions or amorphous solid suspensions. An amorphous solid solution contains drug and carrier that are fully miscible with each other and form a homogeneous dispersion. In contrast, an amorphous solid suspension contains two phases where the carrier is amorphous, and the API disperses in the carrier in a crystalline or partially amorphous state as a result of low miscibility between the API and polymeric carriers [80]. The crystallinity of the API is significantly reduced in both systems. Upon dissolution, the amorphous drug payload can dissolve in an aqueous environment fast and achieve a supersaturated state where the concentration of a drug is higher than its crystalline solubility, achieving the desired function of SDDS introduced previously. This type of solid dispersion is referred to as amorphous solid dispersions (ASD) and is the most investigated type to date.

Newer generations of solid dispersions have incorporated different types of additives to modify drug release rate and supersaturation behaviors. For example, insoluble polymeric materials are added to ASDs to adjust the drug release behaviors based on the different drug release mechanisms from soluble and insoluble carriers [81,82]. To deal with drug recrystallization during

dissolution and under storage copolymer surface active agents and emulsifiers are used either as carriers or additives based on drug-excipient interactions within the in-solution state and solid state [83–85]. A significant part of current solid dispersion research is focused on the development of novel ASD carriers, reducing drug recrystallization in the solid state and during dissolution and investigating related fundamental mechanisms.

1.3.2 Polymer based ASD

Polymeric materials are the most common type of ASD carriers. Examples of fully synthetic polymers are polyvinylpyrrolidone (PVP), poly (ethylene glycol) (PEG), polyvinyl caprolactam-polyvinyl acetate-polyethylene glycol graft copolymer (Soluplus®, SOL), derivatives of methacrylate copolymer (Eudragit® series), etc. Semi-synthetic polymers based on natural materials mainly include hydroxypropyl methylcellulose (HPMC), hydroxypropyl methylcellulose acetate succinate (HPMCAS), ethyl cellulose (EC), hydroxypropyl cellulose (HPC), chitosan, dextran, alginate, pectin, etc. Although other additives may be included in ASD formulations prepared using polymers, ASDs are mainly considered as two-component drug-polymer systems where drug-polymer interactions are the foundation for the design of ASD products. The understanding of drug-polymer interactions under the solid state and in the solution state is essential for the development of ASD formulations.

1.3.2.1 Drug-polymer interactions in the solid state

ASDs are mechanistically understood by viewing them as a two-component solution whereby drug and polymer serve as solute and solvent, respectively. Such two-component systems can form different structures depending on the composition and processing method [86]. When the drug loading amount is lower than the equilibrium solubility of the drug in a given polymer, the drug can be molecularly dispersed in the polymer matrix to form a thermodynamically stable system, as shown in Figure 1.3.

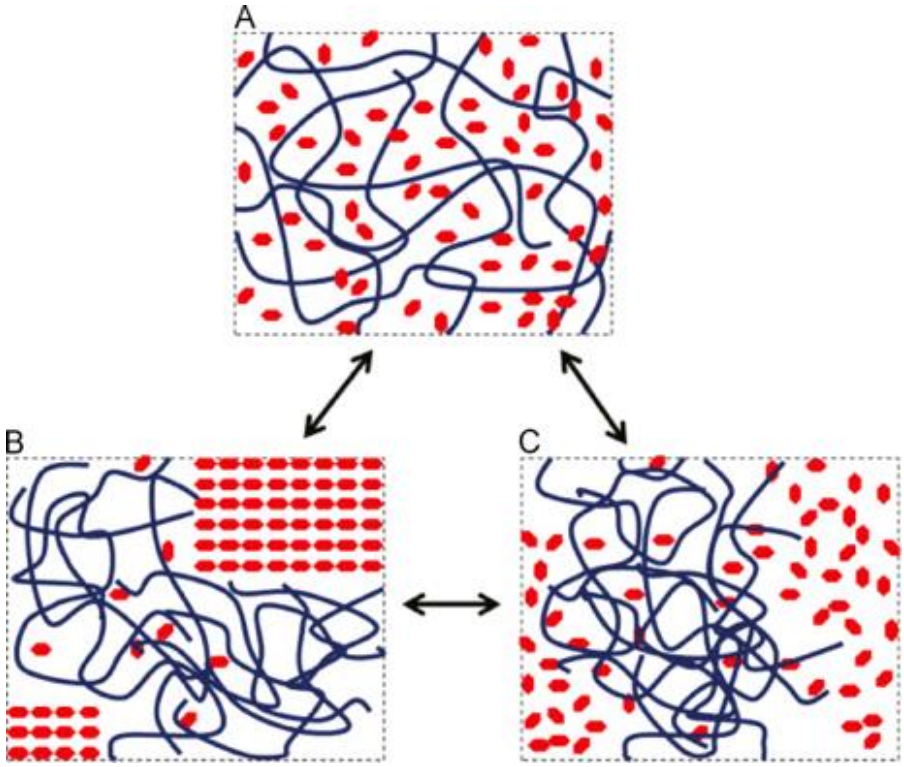

Figure 1.3. Different structures of a drug/polymer solid dispersion where hexagonal symbol represents drug molecule and curvy line represents polymer chain. (A) Drug is molecularly dispersed in polymer matrix; (B) Drug recrystallization occurs in solid dispersion; (C) Amorphous drug-rich domains mix with polymer matrix. Figure adapted from Reference [86], with permission from Elsevier.

For most drug-polymer pairs a thermodynamically stable state can only be achieved at low drug loading or high temperature due to low drug solubility in polymers [87]. When the drug loading exceeds its solubility in a polymer, temperature must be utilized to produce ASDs with molecularly dispersed drug. Upon cooling, the matrix system becomes a supersaturated system that is prone to phase separation. Drug-rich domains, where the drug may still exist in an amorphous state, can exist with molecularly miscible domains of drug and polymer. The amorphous drug-rich domains can further transform into the crystalline state, and the ASD becomes a semi-crystalline dispersion system. Phase separation and recrystallization are inevitable and irreversible during storage because of the thermodynamic driving force, compromising the solubility and dissolution enhancement of ASDs [88]. With this said, a thermokinetic stability can be achieved by prolonging the drug recrystallization process through the rational selection of polymeric carriers to restrict the molecular

mobility of an ASD, so that drug recrystallization can be effectively inhibited over the storage timescale of the product [15]. Stabilization is enabled by drug-polymer intermolecular interactions including hydrogen bonding, halogen bonding, Van der Waals forces, etc [89,90]. These interactions can be estimated using solubility parameters or experimentally determined by solid-state analytical techniques such as nuclear magnetic resonance, differential scanning calorimetry, Fourier transform infrared spectroscopy, etc [91–93]. The drug-polymer miscibility can be explained by the Flory Huggins theory and calculated using the following equation:

$$\frac{\Delta G_M}{RT} = n_{drug} \ln \Phi_{drug} + n_{polymer} \ln \Phi_{polymer} + n_{drug} \Phi_{polymer} X \qquad \textbf{Equation 1.8}$$

where ΔG_M is the free energy of mixing drug and polymer, n is the moles of drug or polymer, Φ is the volume fraction of drug or polymer, R is the ideal gas constant, and T is temperature. X represents the miscibility level of the drug-polymer system. X is experimentally determined by the melting point depression method, in which the melting point of a crystalline drug decreases due to interactions with polymer. X is then used to determine the stable, metastable, and unstable regions by generating spinodal and binodal points on the composition diagram. An example is shown in Figure 1.4 [94].

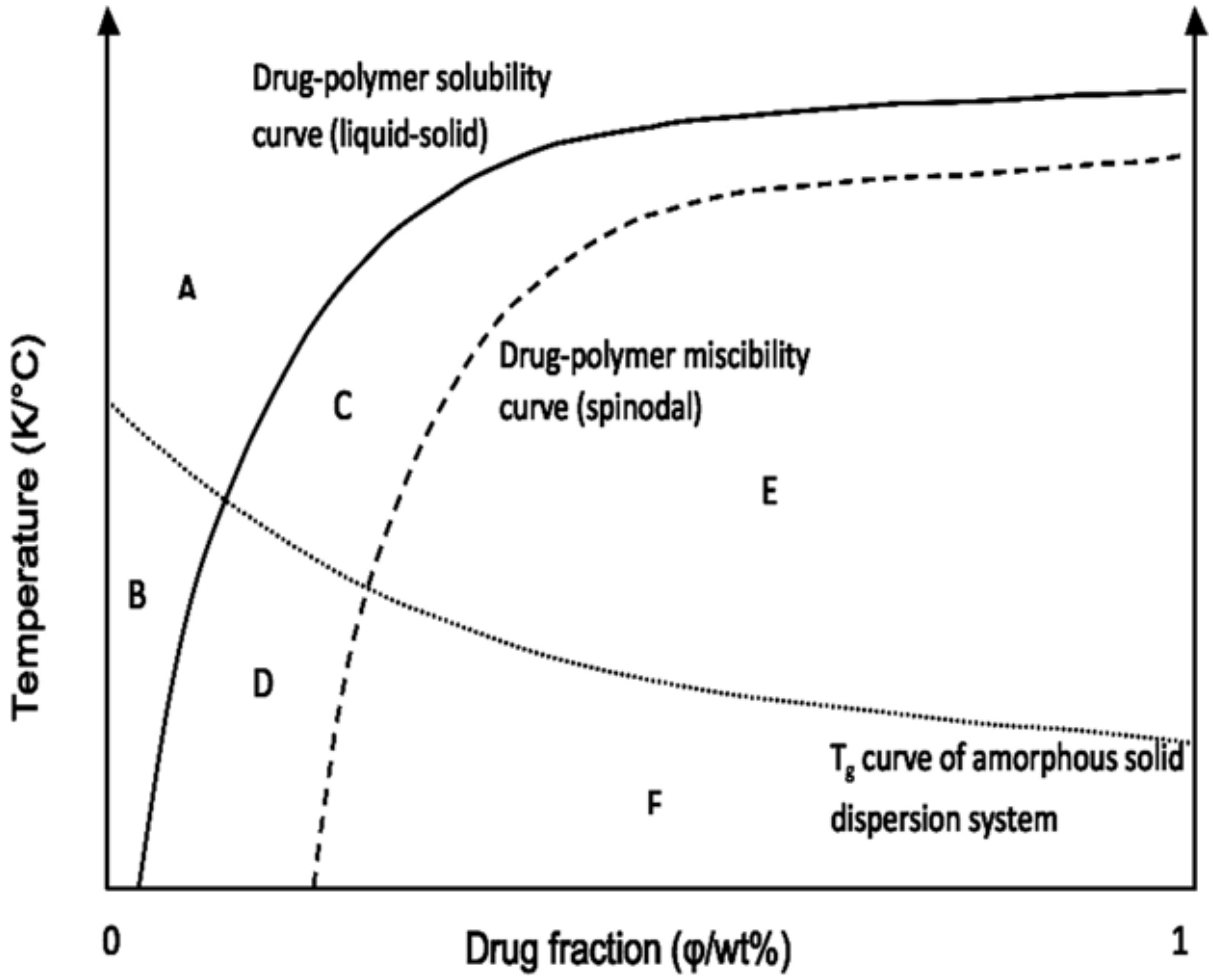

Figure 1.4. Phase diagram of a drug-polymer binary system based on Flory Huggins theory. Figure adapted from Reference [94], with permission from American Chemical Society.

Above the drug-polymer solubility curve, which is depicted by the X values described in Equation 1.8, region A and B represent a zone where drug-polymer compositions are stable. Below the drug-polymer solubility curve (i.e. temperature is lower than the equilibrium temperature) regions C and D represent the metastable zones where an energy barrier needs to be overcome for the initiation of an amorphous-amorphous phase separation. In the metastable region, the drug is supersaturated compared to its solubility in the polymer. An effective kinetic barrier can be achieved by the appropriate selection of polymer type for the ASD formulations that can slow the phase separation process, particularly for region D where the storage temperature is below the glass

transition temperature (T_g) for the drug-polymer system. Region E and F are unstable zones where recrystallization is thermodynamically favoured, and no energy is required for its development.

1.3.2.2 Drug release mechanism of ASD

There are different mechanisms for drug release from polymer based ASDs, depending on the physical state of drug and solubility properties of the drug carriers. If ASDs are formulated with insoluble carriers, the drug release follows a carrier-controlled mechanism, for which the rate limiting step is the diffusion of drug molecules through the polymeric matrix [74,95]. For swellable insoluble carriers, the diffusion layer surrounding the surface of the polymer carrier also acts as diffusion barrier for drug molecules. A portion of amorphized drug can be entrapped in these diffusion barriers with insufficient contact with the dissolution media. The general dissolution of these ASDs often shows sustained release profiles with a continuous increase in free drug concentration, which can be higher than the drug solubility due to the dissolution of amorphous drug. Without an instant release of the amorphous drug the supersaturation degree of the system upon dissolution is low and is associated with a weaker tendency for drug nucleation and recrystallization.

If drug carriers are soluble, the drug release mechanism can also be carrier-controlled due to the formation of a concentrated gel layer of drug carrier during dissolution, and the viscosity of this layer is high enough to act as a diffusion barrier for drug diffusion [96,97]. In this regard, the diffusion of the gel layer into the bulk solution phase is the rate-limiting step for the overall drug release rate. If drug carriers can dissolve instantly in water, the drug release profile follows a drug-controlled mechanism where drug molecules freely interact with dissolution media, and the overall drug release rate will depend on the physical properties of drug payloads (amorphization degree and amorphous solubility) [95,98]. Given a successful preparation of an ASD formulation where a large portion of drug is amorphous, the dissolution behavior can show a fast buildup to high degrees of supersaturation followed by a decrease in drug concentration (I.e. “desupersaturation”) due to nucleation and recrystallization. This type of dissolution behaviour is widely described as a “spring and parachute” profile (Figure 1.5), where the parameters of a spring stage (T_{max} and C_{max}) are determined by the dissolution of amorphous drug, and parachute characteristics are determined by the intrinsic recrystallization rate of drug, in-solution interactions between drug and polymer that influence nucleation and/or recrystallization, and the solubilization effect on drug carriers on the

crystalline solubility of drug [99–101]. This type of ASD has been widely developed for PWSDs to take the advantage of enhanced solubility in oral drug delivery.

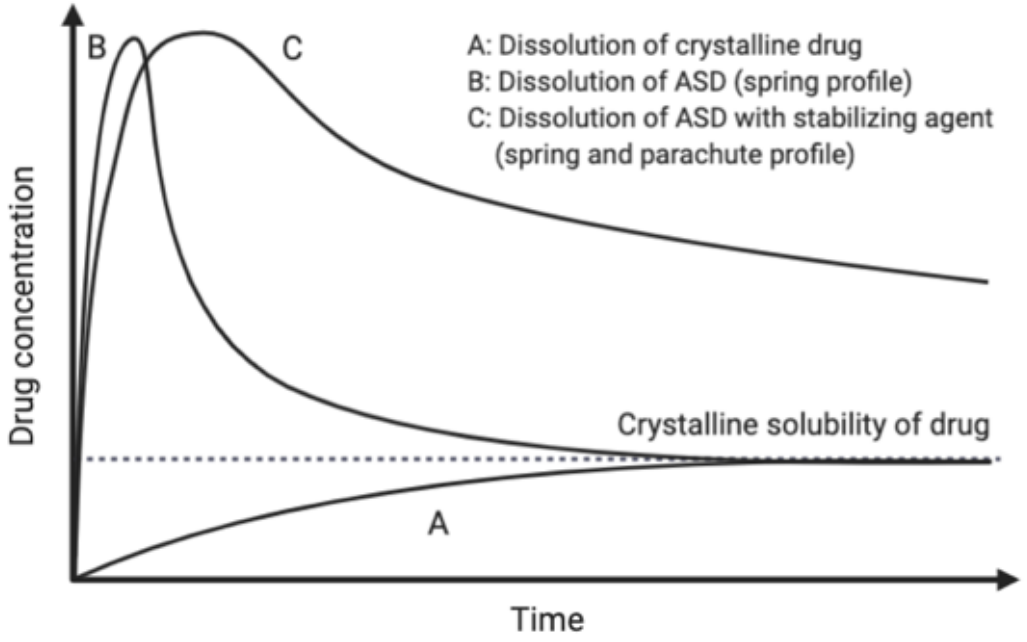

Figure 1.5. Spring and parachute concept to achieve high drug concentration for ASD during dissolution.

1.3.2.3 Drug-polymer interactions during dissolution

The mechanisms of how polymers maintain supersaturated drug solutions have been extensively investigated but have not reached a consensus so far. Hydrogen bonding and hydrophobic interactions have been commonly recognized as the main in-solution interactions between drug and polymer. For instance, the inhibiting effect of HPMC on drug nucleation had a positive correlation to the number of hydrogen bond receptors that a given drug possesses [102–104]. Nucleation was inhibited as nucleation energy is increased by the hydrogen bonding between drug and polymer [105–107]. The adsorption of polymer on the surface of drug clusters could prolong the process of both nucleation and crystal growth. This phenomenon is more effective when ASD carriers with lower hydrophilicity are used, as the adsorption between drug molecules and these materials are favoured by hydrophobic interactions. Other factors including steric hindrance, polymer rigidity and distribution

of functional groups also influence drug-polymer interactions and therefore overall drug release behaviors [108,109].

1.3.3 Lipid based ASD

Lipid based formulations (LBF) correspond to a wide range of formulations, either liquid or solid, that are composed of lipids, surfactants, cosolvents and drugs [110]. In the context of ASD, we focus on LBF formulations using lipid materials as solid carriers for amorphous PWSDs, comparable to the two-component drug-carrier system described above for polymeric ASD. Lipid-based ASDs have been less investigated in spite of the fact that lipid materials are widely used for other purposes in the pharmaceutical industry including as diluents, lubricants, emulsifiers and solubilizers [111–113]. Most lipid materials used as ASD carrier are modified long-chain fatty acids having amphiphilic structures, such as PEGylated stearate and glycerol stearate. They share the same mechanisms with polymeric ASDs in terms of drug loading, enabled by the solid-state hydrogen bonding and Van der Waals forces [114,115]. The phase transition temperature of a formulation is determined by the drug-lipid composition [116,117].

Phospholipid is another type of lipid carrier that can be used to formulate ASD, where these formulations may exist in a semi-solid status due to the low phase transition temperatures of phospholipids. Phospholipid based ASDs are also referred to as drug-phospholipid complexes (DPC), initially developed and patented as Phytosome® by an Italian pharmaceutical company for enhancing permeability of hydrophilic natural polyphenol compounds [118]. Phospholipids have structures that are similar to the lipid composition of the intestinal cell membrane, making them highly compatible with the human gastrointestinal environment and capable of incorporating into cell membrane to replace cellular phospholipids without damaging the cellular lipid bilayer [119,120]. Therefore drugs incorporated in DPCs can be effectively transported upon the absorption of phospholipids by the gut. The DPC drug delivery platform was also used to improve the dissolution profiles of PWSDs due to the surfactant-like properties of amphiphilic phospholipids. DPCs have been successfully applied to both synthetic and natural compounds, such as indomethacin, ibuprofen, probucol, celecoxib, amphotericin B, curcumin, silybin, rutin, baicalein, etc [121–129].

1.3.3.1 Drug-lipid interactions in the solid state

The major drug-lipid interactions in the solid state have been suggested to be hydrogen bonding and Van der Waals forces between drug molecules and both hydrophilic head structures and hydrophobic hydrocarbon tails of amphiphilic lipids [114,115]. According to Fourier-transform infrared spectroscopy (FTIR) results from different studies, the interactions between drug molecules and lipid polar heads are reflected by an intensity change of different functional groups of both drug and lipids [128,130]. For example, the infrared signal of the carboxylic monomer of indomethacin is reinforced by phospholipid after solvent evaporation preparation, and the hydrogen bonding of carboxylic dimer was weakened, both of which suggested the dispersion of IDM in phospholipid with reduced self-association of IDM molecules [131]. The stretching vibration signals of the -OH group of IDM's phenolic group, the -CH group on the fatty acid tails of the phospholipids, and the -C=O group on the polar head of the phospholipids can be masked by a broad peak observed for phospholipid based ASDs for different drugs [132]. NMR has also been used to confirm the interactions between drug and lipids. ^{1}H-NMR chemical shift could be observed at the polar head group of a phospholipid, where the bands of the quaternary ammonium group and the adjacent protons of the choline group showed a broadening and reduced intensity, suggesting the existence of solid-state interactions between the drugs and the polar heads of phospholipids [133,134]. The ^{31}P-NMR revealed an upfield change in the phosphorous chemical shift for the phospholipid after ASD preparation [133]. These studies demonstrate that a drug can exist in an amorphous state in lipid based ASDs, which can also be characterized using differential scanning calorimetry (DSC) and X-ray diffractometry (XRD) [124,126] both of which are common analytical methods used in pharmaceutical formulation. The elimination of peaks, emergence of new peaks or a change in peak shape or onset can be observed for lipid based ASDs compared with individual components. Due to the generally low melting point or phase transition temperature of lipid materials (i.e. <100 °C) and high melting points of drugs (i.e. > 150 °C), the physical state of a test sample could change during the temperature ramp of a DSC experiment. A portion of the drug molecules can be dissolved in the melting lipid to decrease the overall crystallinity of sample. To facilitate the analysis of the physical state of lipid based ASDs XRD is often used. The physical state of ASD samples remains unchanged during an XRD experiment and is described by the characteristics of crystalline peak signals. In our study, fluorescence spectroscopy and fluorescence microscopy have been successfully applied to the characterization of lipid based ASDs. The molecular miscibility of drug and lipid was reflected by the

change in emission spectra of drug molecules due to the varying polarity of their environment. The distribution of fluorescence intensity of a lipid based ASD is used as indicator for drug-lipid miscibility for fluorescence microscopy method.

1.3.3.2 Drug-lipid interactions during dissolution

While investigations into drug release mechanisms for lipid based ASDs are limited, the physical state and dispersion/dissolution behavior of lipids in water should be factors that influence the drug release mechanism, considering that lipid based ASDs are two-component drug-carrier systems with similar drug loading mechanisms to polymer ASDs. Amphiphilic lipids are considered as soluble carriers due to their ability to dissolve or disperse in water to form micelle/vesicle structures; however, the time required for amphiphilic lipids to completely disperse in water varies significantly with lipid type. According to different studies, drug release from phospholipid based ASDs can be slowed by the intermolecular complexation of phospholipid in water, even if the drugs exist in an amorphous state in the phospholipid carrier [129,135–137]. This mechanism is similar to the carrier-controlled mechanism where the drug release rate is controlled by the drug diffusion through diffusing barriers. In contrast, according to our results PEG-32 stearate could disperse in water instantly upon contacting water, resulting in a rapid drug release associated with high supersaturation that is prone to nucleation and recrystallization (see Chapter 5). Here the drug release mechanism is similar to the drug-controlled drug release mechanism for polymer based ASDs. Other factors including the drug-lipid ratio and preparation method are expected to influence drug release through these mechanisms.

The effect of lipid ASD carriers on drug supersaturation is rarely investigated; the dissolution of lipid based ASDs were tested in most studies under sink conditions where supersaturation does not occur [121,124,137]. Based on the similarities of amphiphilic lipids to surfactants, dispersed amphiphilic lipid carriers may impact drug supersaturation by similar mechanisms. Firstly, amphiphilic lipids above their critical micelle concentration can solubilize crystalline drug and therefore reduce the possibility for recrystallization by reducing the degree of supersaturation (i.e. reducing the concentration of drug in the bulk solution phase). Secondly, the hydrophobic tails of lipids can interact with drug molecules through hydrophobic interactions in water, thereby facilitating the aggregation of nuclei at the early stage of recrystallization [56]. Lastly, as introduced above, the adsorption of excipient on the surface of nuclei and small drug clusters can inhibit nucleation and

crystal growth by weakening the interactions between drug molecules. The overall effect of an amphiphilic lipid carrier results from the competing contribution of these mechanisms.

In addition to the small number of studies described above, studies of the effect of lipid carriers on the LLPS of a supersaturated drug solution do not seem to be found in the literature making it an entirely new area of research in drug delivery formulation science. It is of great interest to explore this effect as it is closely linked with nucleation and crystal growth of PWSD in an aqueous environment. This will be an important part of this study.

1.3.3.3 Polymer-lipid combination systems as ASD carriers

Individual polymers or lipids have been extensively used as ASD carriers, while their combination as binary ASD carriers are relatively less investigated. Most studies of ASDs based on a polymer-lipid combination directed more towards improving the poor dispersion of lipid material in aqueous environment rather than for increasing PWSD supersaturation. For example, Soluplus® was used to solidify a phospholipid based ASD for curcumin and improve its dispersibility and drug dissolution rate [138]. Similarly, PVP was used to improve the dispersibility and dissolution of a phospholipid based ASD for baicalein [129]. Here, the improvement was based on the leveled phase transition temperature of the amorphous baicalein formulation due to the introduction of the component (i.e. polymers) with a higher glass transition temperature. The intermolecular complexation of phospholipid can also be weakened by the addition of polymeric materials. Despite the application of polymer-lipid based ASD to improve drug dissolution, effects of these binary materials on the supersaturation behaviors of drug molecules are rarely investigated [139]. Their effects on the LLPS and drug supersaturation under non-sink dissolution conditions will be explored in this study.

1.3.4 Preparation of ASD

The preparation methods for ASD formulations can be generally divided into solvent methods and melting methods. Solvent-based methods rely on the evaporation of common solvents from the solutions of drug and carriers. Practical approaches mainly include the use of a rotary evaporator under reduced pressure, spraying drying and freeze drying. For rotary evaporation and spray drying, insufficient time is provided for drug recrystallization and crystal growth from the solution upon a fast evaporation of organic solvents at high temperature, so that drug can be produced

in an amorphous state loaded in carrier materials. For freeze drying, the solvent is removed from the frozen solution by sublimation at low temperature and reduced pressure. With drug-polymer interactions and restricted molecular mobility under low temperature, the aggregation and recrystallization of molecularly dispersed drug molecules in a frozen solution are inhibited during preparation. Drugs in the lyophilized ASDs can exist in an amorphous state or a nanocrystal state with significantly reduced crystallinity [140,141]. Other solvent-based methods, such as fluidized bed methods and or aerosol solvent extraction, are used relatively less often for ASD preparation [142,143].

For melting methods, drug and carrier are mixed at elevated temperature above their melting point or glass transition temperature, and the temperature is decreased to produce an ASD in which the drug exists in an amorphous state. The maintenance of an amorphous drug is based on the drug-polymer and drug-lipid interactions introduced previously. The most used melting technology is hot melt extrusion (HME). For a typical HME process, different compositions are fed into an extruder to undergo shearing, heating, plasticizing, and mixing at controlled conditions. The mixtures of drug and polymer are shaped by passing through a die opening and prepared as the ASD forms. HME has been successfully used to realize the large-scale preparation of ASD without the use of organic solvent [144].

1.4 Drugs and ASD carriers used in this study

Two model drugs, indomethacin (IDM) and apixaban (APX), were selected to evaluate the effects of different polymers and lipids on the LLPS and supersaturation behaviors of hydrophobic drug molecules. They were selected based on different considerations. IDM is a nonsteroidal anti-inflammatory drug prescribed to reduce pain, swelling and joint stiffness induced by arthritis, gout, or bursitis [145]. It is a weak acid drug with a pKa value of 4.5, showing a pH dependent solubility profile ranging from 1.15 μg/mL at pH 1.2 to 200 μg/mL at pH 6.8 [95]. Since the largest strength of IDM (50 mg for a single dose) cannot fully dissolve in 250 mL of gastrointestinal fluids, IDM is classified as a BCS class 2 drug with poor solubility. In the research fields of solubility and dissolution enhancement, IDM is a commonly used model to test the dissolution-related properties of novel drug carriers and investigate underlying mechanisms [95,139,146–148]. The intrinsic properties of IDM and derivative behaviors rendered by different dissolution enhancing technologies are clearly revealed. In this regard, novel properties and mechanisms of a formulation revealed by IDM could be

used to comprehensively compare with previous studies to obtain accurate evaluation. We proposed to use IDM as the first model to test the effects of different polymers, lipids, and their combinations on the in-solution and solid-state properties of drug molecules.

The second drug model, APX, was selected to investigate whether the revealed properties and underlying mechanisms for ASD carriers can translate to the formulation of a completely different drug compound. APX is a selective inhibitor for blood coagulation factor Xa used in preventing stroke and systemic embolism in nonvalvular atrial fibrillation [149]. It has a short history use since its first approval was in 2012. APX is a nonionized drug with a pKa of 13.12 and shows an aqueous solubility of approximately 40 μg/mL over the physiological pH range [150]. APX is classified as a BCS class 3 drug since its largest strength (5 mg) can be fully dissolved in 250 mL gastrointestinal fluid. From the BCS classification, one could expect a fast dissolution rate for this type of drug, and drug dissolution performance should not be limited by aqueous solubility or physical states such as particle size, crystal form, and solubilization state. Instead, APX is characterized with a slow dissolution rate in aqueous environments according to different studies [149,151–154]. For the commercial solid product of APX (Eliquis®), micronization technology is used to control the size with a cut-off of 89 μm for drug particles to facilitate dissolution, and a surface-active agent (sodium dodecyl sulfate, SDS) is added to improve the wetting of APX to meet the dissolution requirement [150]. Yong's group has developed co-crystals to improve the dissolution rate and equilibrium solubility for APX [152]. Solvate and polymorphic forms of APX were designed to provide APX with higher aqueous solubility in different pH conditions [153,155]. Several liquid formulations have also been developed by combining co-solvents and surfactants, providing a 10-fold increase in APX solubility [156]. In the field of ASD development, APX has been formulated into several polymeric carriers to improve dissolution performance [157,158]; however, limited information on fundamental aspects of APX ASDs was disclosed in these invention embodiments, such as comparison of drug carrier effects on APX dissolution rate, recrystallization behavior of APX under non-sink condition, APX physical state in different formulations, etc. At present, no information on the supersaturation and LLPS properties of APX is available, both of which are recognized as fundamental data to direct the development of ASD forms for poorly water-soluble drugs. Therefore, in this study, LLPS and supersaturation properties of APX were investigated in an aqueous environment. The chemical structures of IDM and APX are shown in Figure 1.6.

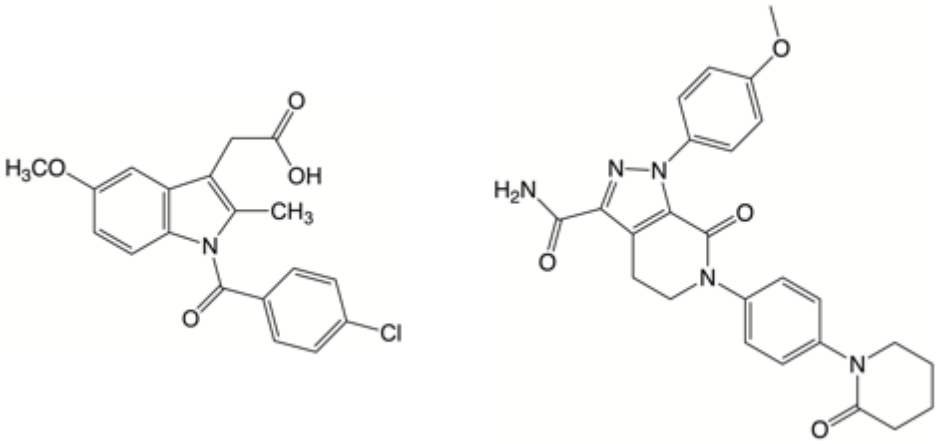

Figure 1.6. Chemical structures of indomethacin (left) and apixaban (right).

The selection of polymer and lipid ASD carriers for this study was based on different considerations. Firstly, selected drug carriers were expected to present different properties to cover general categories of polymer and lipid. For polymeric materials, solubility, dispersibility, and ionization ability are important factors to consider, as they have been recognized to influence drug dissolution and supersaturation. Solubility, amphiphilicity and swellability are considerations for lipid selection. Secondly, it was preferred that the drug carriers had unrevealed supersaturation properties. These newly revealed properties are expected to provide a better understanding of available pharmaceutical excipient candidates to serve the formulation development work. Lastly, considerations were given to excipients that were not conventionally used as ASD drug carriers, so that potential new applications can be suggested based on the findings of this study.

1.4.1 Polymer carriers used in this study

Poly (vinyl pyrrolidone) (PVP) was selected as soluble and non-ionizable hydrophilic polymer. PVP is a linear polymer of 1-vinyl-2-pyrrolidone monomers with varying molecular weight from 10,000 to 70,000. It is one of the most utilized polymers in the pharmaceutical industry for the use of oral drug delivery [97]. It can be used as binder, film former, suspending agent, emulsion stabilizer, etc. As a classic ASD carrier, PVP shows ideal hydrophilicity and fast dissolution in water which are favorable for the release and wetting of drug payloads [95]. In the solid state, PVP has been observed to complex with hydrophobic drugs thorough various interactions, including hydrogen bonding, Van der Waals forces, and electrostatic interactions [159]. The molecular mobility of

amorphized drug can be reduced by the interactions with the PVP polymer chain, so that nucleation and crystal growth are inhibited to maintain the drug in an amorphous state. The ability of PVP to maintain supersaturation of a drug varies when it was used for different drugs, depending on polymer grades, polymer-drug matching and preparation method [96,97]. PVP K90 was used in this study.

Soluplus® (SOL) was selected as amphiphilic copolymer for the study. SOL is a non-ionizable triblock graft copolymer of polyvinyl caprolactam–polyvinyl acetate–polyethylene glycol with a molecular weight range of 90,000 to 140,000 Da. SOL shows bifunctional characteristics as a matrix drug carrier and as a solubilizer for aqueous solutions and has been well utilized to formulate different hydrophobic drugs into ASDs [160]. Amorphized drugs can be maintained in the polymer chain of SOL, and a fast drug release can be achieved due to the fast dispersion of SOL in aqueous environment. SOL has also been observed to maintain supersaturation by decreasing the recrystallization of a dissolved drug in aqueous media, making it an ideal ASD carrier candidate for the formulation development of hydrophobic drugs [95,161].

Sodium alginate (SA) was selected as soluble and ionizable hydrophilic polymer. SA is the sodium salt of an anionic linear polysaccharide composed of β-(1→4)-linked d-mannuronic acid (M) and α-(1→4)-linked l-guluronic (G) residues. SA has been widely used in the food, pharmaceutical, bioengineering and textile industries, and is generally recognized as safe (GRAS) by different agencies due to its biocompatibility, biodegradability and non-toxic profile [162–166]. In the field of oral drug delivery, SA has mainly been used as a hydrogel, thickener, and as a base material for micro-/nanoparticles prior to its development as an ASD carrier in 2015 [167–169]. SA-based ASDs significantly improved the solubility and dissolution rates of several poorly water-soluble drugs under sink conditions, and effectively slowed down drug crystallization during storage [170,171]. When physically mixed with SA, several hydrophobic drugs showed an increased solubility and improved dissolution due to facilitated wetting induced by SA, making SA a favorable excipient for solid pharmaceutical developments [170]. The dissolution performance of SA-based ASDs significantly depended on the paring of drug and SA. When the solid-state drug-polymer interactions are weak, SA showed minimal effect on the dissolution rates of the drug payload. Several interesting results were noticed when viewing these studies in detail. There was no statistical difference in the dissolution efficacy between telmisartan-SA ASDs with drug-polymer ratios of 1:5, 1:7 and 1:9 under sink conditions, all of which showed significant improvement compared with unformulated telmisartan [170]. For the indomethacin-SA and lovastatin-SA systems, no statistically significant difference in

dissolution was found between drug-SA ratios from 1:1 to 1:5, all of which showed similar improvement for drug materials [171]. It was concluded that the hydrogen bonding interaction between drug and SA was an important factor for contributing to the dissolution enhancing ability of SA. We noticed that a sink condition with wetting agent (900 mL of 0.05 M pH 6.8 phosphate buffer with 0.1% SDS) was used in these studies for assessing the dissolution performances of SA-based ASDs, which could be ineffective in differentiating the dissolution behaviors of different ASD formulations with supersaturation abilities. Ionization of SA could also be an important mechanism for the enhanced dissolution of indomethacin or lovastatin, as these drugs are weak acids whose kinetic solubility profiles can benefit from the presence of alkalizers. This effect could be hidden when drug dissolution occurs in a buffered condition. The improved kinetic solubility profiles of these two drugs could result not only from the dissolution of an amorphous drug (having a high Gibbs free energy), but also from increased crystalline solubility. Therefore, in our study, the ionization of SA will be examined by comparing the dissolution behaviors of ionizable and non-ionizable drugs in the presence of SA under non-sink conditions without buffering agents. In this context, the supersaturation properties of SA would benefit the analysis of drug dissolution under non-sink conditions.

Of late, a few studies revealed the supersaturation properties of SA using different drugs including indomethacin, lovastatin, itraconazole and chlorthalidone [172,173]. In these cases, all drugs showed improved supersaturation to different degrees. Indomethacin and lovastatin had the best supersaturation improvement and recrystallization inhibition compared to drug alone. In contrast, the ability to maintain the supersaturation of itraconazole was weakened over time with a same amount of SA. The supersaturation of chlorthalidone was barely improved by SA and relied on the combination of SA and other excipients such as sodium dodecyl sulfate and other hydrophilic polymers. These results were in good agreement with previous studies, where the solubility, dissolution rate, and supersaturation of weak acid drugs were improved by SA more effectively than weak base drugs. Considering these findings and conclusions, SA was selected as a hydrophilic and ionizable polymer to test its effect on the supersaturation and LLPS of different types of drugs.

Ethyl cellulose (EC) was selected as insoluble polymeric carrier for the study. EC is a cellulose derivative where hydroxyl groups on the anhydroglucose units are partially replaced with ethyl ether groups, with a molecular weight ranging from 24,000 to 75,000. Based on the film forming ability and its insoluble nature, major pharmaceutical applications of EC include its use as a

coating agent, flavouring fixative, oral film base, and drug carrier for sustained release [174]. EC influences drug supersaturation through a different mechanism than that for soluble polymers as it is insoluble in water. Amorphized drug formulated with EC has a slow release by diffusing from the EC matrix and therefore can be maintained at a slightly higher concentration than the drug solubility. The effects of its combination with lipid carriers were of interest for this study. The structures of all polymers used in this study are shown in Figure 1.7.

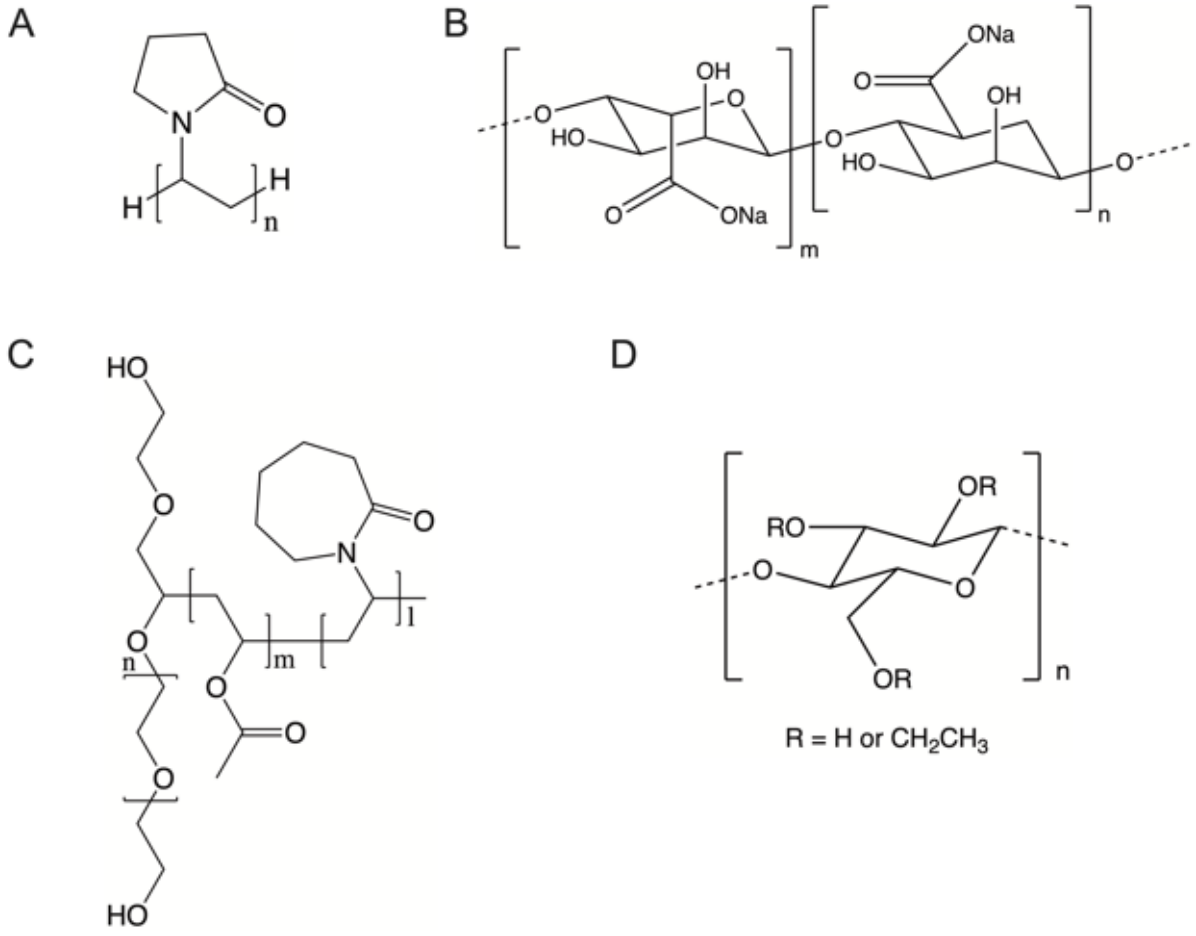

Figure 1.7. Chemical structures of (A) PVP, (B) SA, (C) SOL and (D) EC.

1.4.2 Lipid carriers used in this study

There are different methods for the categorization of lipid materials. For pharmaceutical lipid excipients, a classification system was developed to divide lipids (including surfactants) into different types based on their interactions with bulk water and at the water-air interface [175,176]. Type I

lipids are insoluble and non-swelling in water and include triglycerides, diglycerides, cholesterol and long-chain fatty acids. Type II lipids are insoluble and swellable lipids that can aggregate in water through the hydrophobic effect to form swollen lipid layer or vesicle structures. Examples include phospholipids and 2-monoacylglycerides. Type III lipids are soluble amphiphiles with lyotropic mesomorphic behaviors when at a high concentration. These lipids form unstable monolayers at water-air interfaces and can form micelles when the concentration is above their critical micelle concentration (CMC). Examples include bile salts, saponins, and sodium/potassium salts of long-chain fatty acids. In this study, one lipid of each type was selected.

Glycerol dibehenate, with a commercial name of Compritol® 888 ATO (ATO), was selected as type I insoluble and non-swellable lipid. ATO is a mixture of mono-, di-, and triesters of behenic acid, with a molecular weight of 1059.8 g/mol and an HLB value of 2. ATO can be used as sustained release matrix former and base material for solid lipid nanoparticle and nanostructured lipid carriers, taking advantage of its hydrophobic nature and ability to store drug in its spherical structure [113]. In terms of the application for solid dispersion, ATO has been mainly used as inert matrix to sustain the release of hydrophilic drugs. It has not been used for the purpose of maintaining supersaturation of hydrophobic drugs. Considering that certain insoluble polymeric materials can show a diffusion controlled supersaturated dissolution profile when combined with hydrophobic drugs, the ability of ATO to achieve a similar effect will be tested in this study. The investigation is expected to support the application of ATO as ASD drug carrier.

Phospholipid (PL) was selected as type II lipid with insoluble and swellable properties. The phospholipid used in this study (Sigma-Aldrich catalog no. P3644) contains 55% type IV-S L-α phosphatidylcholine, 25% phosphatidylethanolamine and other phospholipids, with an average molecular weight of 776 g/mol. Trace components in phospholipid including triglycerides and cholesterol are not routinely quantified. PL has been widely used in the pharmaceutical field as a wetting agent, emulsifier, solubilizer, and base material for liposome formation, all of which are based on the amphiphilic nature and vesicle forming ability of PL [177]. Like polymeric ASDs, an amorphized drug can be complexed with PL to form a lipid-based ASD, also referred to as drug-phospholipid complex (DPC) and realizes an improved drug dissolution rate. Such effects have been validated for DPC formulations of different synthetic drugs and naturally derived active ingredients. In spite of these applications, the ability of PL to maintain a supersaturated drug solution has been investigated to a negligible degree, creating an opportunity for the study of the fundamental properties

of PL important to its use as an ASD carrier able to achieve supersaturation of PWSDs. In this study, the effect of PL on the LLPS and supersaturation behaviors of IDM and APX were assessed.

PEG-32 stearate, with a commercial name of Gelucire® 48/16 (G48) was selected as a type 3 lipid being soluble with a defined CMC value. G48 is a non-ionizable PEGylated long chain fatty acid with a melting point of 48 °C and an HLB value of 16. G48 is supplied as pellets that rapidly dissolve in solution. With a CMC value of 153 ± 31 μg/mL, G48 can form micelle with an average size of 7 nm in water that can solubilize hydrophobic drugs or serve as an emulsifier for emulsions and self-emulsifying formulations [178,179]. Similar to SA, G48 has a relatively short history of use as an ASD carrier. Several of its fundamental properties including the formation of amorphous mixtures with certain drugs, dissolution improvement under sink condition, and the physical state of drugs in G48 based solid dispersions have been well investigated [180,181]; however, there is no data available that demonstrates its ability to influence supersaturated drug solutions. This makes G48 an ideal lipid candidate for this study. The chemical structures of PL, G48 and ATO were shown in Figure 1.8.

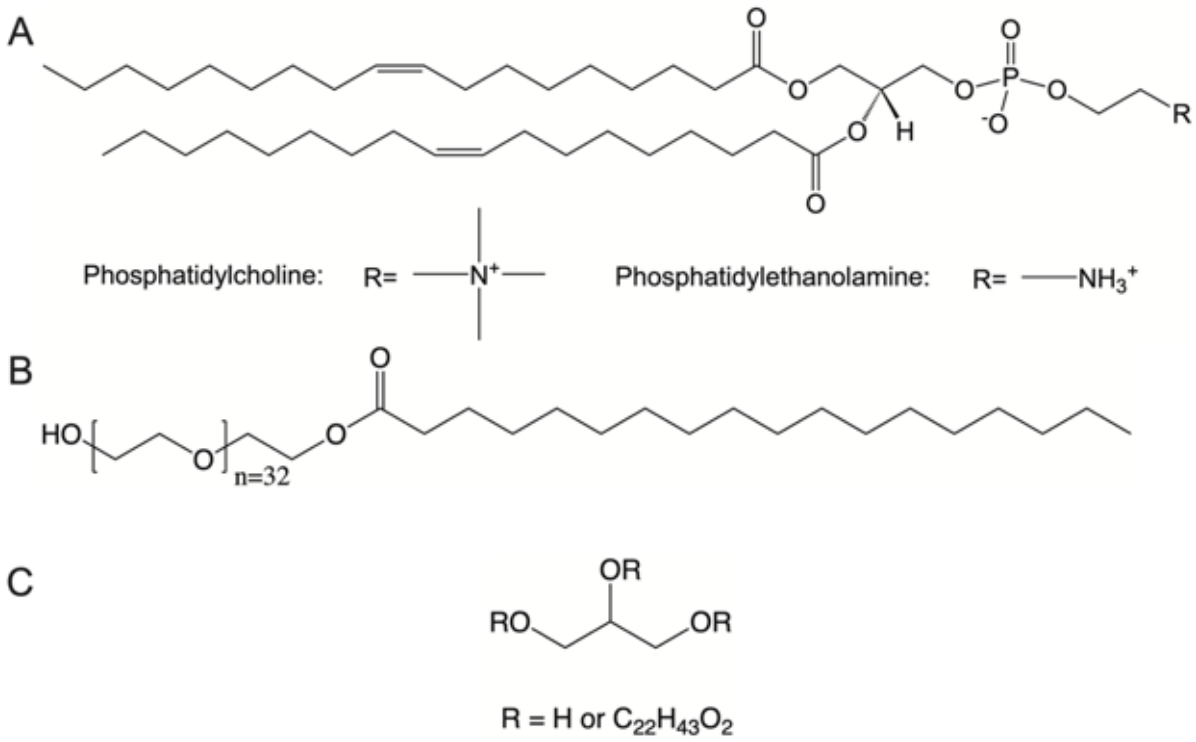

Figure 1.8. Chemical structures of (A) PL, (B) G48 and (C) ATO.

1.5 Project rationale, hypothesis and objectives

With an increasing number of drug compounds showing poor solubility and slow rates of dissolution there is a constant need for the development of formulation strategies able to address these challenges for the oral delivery of poorly soluble drugs. ASD formulations are widely used for this purpose by achieving a supersaturated solution where drug concentration can exceed the solubility of the drug, improving both solubility and dissolution rate of poorly soluble compounds. The kinetic solubility profile of an ASD formulation in aqueous environment depends on the buildup and maintenance of the supersaturated drug solution, which are determined by parameters including drug amorphization state in the ASD carrier, drug release from the carrier matrix, the LLPS and nucleation of supersaturated drug solution, and the crystal growth rate of drug molecules. These factors are closely correlated to the solid-state and in-solution properties of ASD carrier materials. A deep understanding of these properties will benefit both the development of pharmaceutical excipients into ASD carriers and the investigation of fundamental mechanisms of drug supersaturation.

1.5.1 Hypothesis

Both solid-state and in-solution behaviors of IDM and APX are influenced by polymer and lipid ASD carriers as well as their combinations. The evolution of LLPS of IDM and APX in water are affected by ASD carriers in different manners depending on the in-solution properties of carrier materials. As a transient state prior to the recrystallization process, the altered LLPS behaviors of IDM and APX may or may not determine the overall supersaturation evolution of these drugs over a long dissolution time. In a solid state, the application of fluorescence-based techniques for assessing drug amorphization state in carriers and drug-carrier miscibility could expand to all selected carrier materials, based on the previously developed methodology for IDM ASDs. Given that APX shows autofluorescence in solution, it should also occur in a solid state so that fluorescence techniques can be used to assess the miscibility between APX and excipients for solid samples. The dissolution and supersaturation behaviors of ASDs for IDM and APX prepared with polymer and lipid carriers are correlated with these properties.

1.5.2 Objectives

1) Determine the onset and duration of LLPS for IDM and APX in water containing pre-dissolved ASD carriers.

2) Investigate the recrystallization profiles of supersaturated solutions of IDM and APX under non-sink dissolution conditions with pre-dissolved ASD carriers.

3) Use fluorescence techniques to assess drug amorphization and drug-carrier miscibility for IDM and APX.

4) Evaluate dissolution and supersaturation behaviors of ASDs for IDM and APX prepared with polymer and lipid carriers under non-sink dissolution conditions.

5) Analyze the correlation between LLPS, recrystallization, drug-excipient miscibility and dissolution parameters of ASDs for IDM and APX, and analyze the determinant factors for the kinetic-solubility profiles of an ASD.

For this research, both well utilized and novel characterization methods were used to determine different parameters involved in the elucidation of dissolution mechanisms and formulation development of ASDs of IDM and APX. Comprehensively comparing these results will help understand the role of each parameter in determining different aspects of dissolution behaviors (i.e. supersaturation buildup rate, supersaturation maintenance, maximum achievable drug concentration, etc.). The applicability of these characterization methods will be demonstrated by the results of different drug-excipient pairs and the methods are expected to serve the assessment of novel ASD. The revealed mechanisms including LLPS, recrystallization, drug-excipient miscibility, and dissolution behaviors of IDM and APX are expected to benefit the formulation development of ASDs using polymer and/or lipid carriers.

Chapter 2
Effect of polymers and lipids on the liquid-liquid phase separation of IDM and APX

2.1 Abstract

Liquid-liquid phase separation (LLPS) is a transient physical state whereby a supersaturated solution splits into two liquid phases to lower the Gibbs free energy of the system without the occurrence of recrystallization. The concept of LLPS has been used to understand the formation of amorphous nanoparticles in drug solutions enabled by SDDS and direct the development of ASD formulations. The purpose of this chapter was to investigate the effect of different drug carriers on the LLPS properties of IDM and APX in aqueous media. The characterizations were conducted using a double wavelength UV extinction method upon the titration of a stock drug solution in organic solvent into aqueous substrate pre-dissolved with ASD carriers. For IDM, the LLPS onset was delayed, and the duration was prolonged to different degrees by different ASD carriers with different mechanisms. A synergistic effect on the stabilization of LLPS of IDM was observed when PVP and PL were co-dissolved. For APX, the LLPS onset could be delayed, maintained, and promoted by different ASD carriers. All polymer-lipid combinations showed an averaged effect on the stabilization of LLPS of APX with regard to individual carriers. The same carrier compound was able to elicit different effects on the LLPS of different drugs, suggesting that the carrier effect on drug LLPS did not follow a single mechanism. The LLPS data revealed in this chapter will be used to analyze the correlation between LLPS and supersaturation decay profiles of IDM and APX in the presence of different ASD carriers.

2.2 Introduction

LLPS is a transient physical state for a supersaturated solution to split into a water-rich phase and a drug-rich phase without forming a solid crystalline phase [15,42]. The drug concentration of the water-rich phase equals the amorphous solubility of the drug, and therefore provides the highest solute thermodynamic activity and flux across gastrointestinal membranes that are favorable for the oral absorption of poorly water-soluble drugs [42,95]. The drug-rich phase is composed of aggregates of amorphous drug. Due to the nanoscopic and amorphous nature, this phase provides a faster dissolution rate than the crystalline drug, and rapidly equilibrates in aqueous media to serve as a drug

reservoir to replenish the absorbed drug. A stabilized and prolonged LLPS is expected to benefit the maintenance of supersaturation achieved by ASD formulations and achieve optimal drug absorption.

Light scattering is the most common indicator to detect LLPS in a solution. Thomson's methodology to characterize the binodal and spinodal concentrations of protein-water systems using light scattering was adapted to evaluate the LLPS behavior of a pharmaceutical compound in aqueous media [182]. When the incident light enters a liquid sample, the transmitted light is attenuated due to scattering and absorption. At the absorbing wavelength of a completely dissolved substance, the extinction is a result of UV absorption of the solute. At a non-absorbing wavelength, without the absorbance by a solute, extinction cannot be detected until the light is scattered by the formation of a second phase which is not fully miscible with the original phase. The extinction values at both wavelengths are obtained for a series of drug solutions with different concentrations that are prepared by the constant addition of a stock drug solution in organic solvent into aqueous substrate. This approach is convenient and uses common equipment but has a significant limitation of overestimating the point of LLPS due to the increasing drug solubility in the presence of organic solvent. Fluorescence spectroscopy is an alternative approach to determine LLPS. The change in the emission of a fluorescence probe reflects the altered polarity of its environment due to the partitioning of the probe into a specific phase [183,184]. A supersaturated solution before LLPS is homogeneous, and the probe is dissolved in the aqueous phase with a high polarity. When two phases form through LLPS, the hydrophobic probe tends to localize within the drug-rich phase through hydrophobic interactions, providing an environment of decreasing polarity for fluorophores. When drug recrystallization occurs, fluorescence probes are not incorporated into the crystal lattice of drug compounds, partitioning from the drug-rich phase back into to the aqueous phase, which is reflected by a change in fluorescence due to the increase in polarity of the aqueous phase. Pyrene is an environment sensitive fluorescence probe that is commonly used for this purpose. The ratio of intensity of its first and third vibronic fluorescence peaks is used to assess the environment polarity, where a larger I_1/I_3 corresponds to a more polar environment [185]. The limitation of this method is that LLPS could be promoted by the presence of the fluorescence probe, as the aggregation of the amorphous drug is facilitated by the fluorophores through hydrophobic interactions. The autofluorescent properties of drug compounds may also interfere with the probe spectrum. Other characterization methods include ultracentrifugation and nuclear magnetic resonance spectroscopy to identify the solution properties of distinct phases upon LLPS [58,70].

Considering that the autofluorescence properties from IDM and APX may interfere with the emission spectra of a probe, and the amphiphilic ASD carriers used to formulate IDM and APX could alter the aggregation behavior of a probe, we selected the double wavelength UV extinction method to characterize supersaturated drug solutions prepared by the titration of the organic solution of the drug into. Effects of different polymer and lipid carriers on the LLPS of IDM and APX were revealed. The LLPS behaviors of APX with and without ASD carrier were demonstrated for the first time to the best of our knowledge. The information obtained in this study will be used as the basis to analyze the ability of these excipients to maintain supersaturated concentrations of IDM and APX.

2.3 Materials and methods

2.3.1 Materials

Indomethacin (IDM, purity > 97.5%) and ethyl cellulose were purchased from Fisher Scientific (Hampton, NH, USA). Apixaban (APX, purity > 99%) was purchased from HuiRui Chemical Technology Co., Ltd (Shanghai, China). Poly (vinyl pyrrolidone) (PVP) K90 and phospholipid were purchased from Sigma-Aldrich (Mississauga, ON. Canada). The phospholipid used in this study (Sigma-Aldrich catalog no. P3644) contains 55% phosphatidylcholine, 25% phosphatidylethanolamine and other phospholipids, with an average molecular weight of 776 g/mol. Polyvinyl caprolactam-polyvinyl acetate-polyethylene glycol graft co-polymer (Soluplus®, SOL) was a gift from BASF (Ludwigshafen, Germany). Sodium alginate (CAS number: 9005-38-3) was obtained from Acros Organics (USA). PEG-32 stearate (Gelucire® 48/16, G48) and glyceryl behenate (Compritol® 888 ATO) were a gift from Gattefosse (Saint-Priest, France). Ethanol and dimethyl sulfoxide (DMSO) of high-performance liquid chromatography (HPLC) grade were purchased from Fisher Scientific (Hampton, NH, USA). Water used in this study was obtained from a Millipore Milli-Q system.

2.3.2 Determination of equilibrium solubility of IDM and APX in water

The equilibrium solubility (C_S) of IDM was determined in pure water using a shake flask method. An excess amount (10 mg) of crystalline IDM and 10 mL of pure water were added to a sealed conical tube and equilibrated in an incubating microplate shaker (Fisher Scientific, Hampton, NH, USA) at 37 ± 0.1 ˚C and 500 rpm for 48 h. The obtained samples were filtered through 0.22 μm PES membranes. The concentration of IDM sample was determined by a UV spectrometer based on a

Beer-Lambert calibration curve at 318 nm. The same procedure was used for APX, where 278 nm was used instead of 318 nm.

2.3.3 Calculation of dissolution dose and excipient concentration for IDM and APX

For the LLPS study solutions of ASD carriers of different concentrations were used to measure their effects on the phase separation of supersaturated solutions of IDM and APX. The concentrations were calculated based on doses of IDM and APX that will be used for dissolution tests. For this study, the dissolution and supersaturation behaviors of IDM and APX were evaluated under non-sink dissolution conditions corresponding to the finite volume of GI fluid, where nucleation and recrystallization happen when a large drug dose is given [95]. The sink index (SI) was used to quantify the non-sink degree as described in the following equation:

$$SI = C_S \times V / dose \qquad \textbf{Equation 2.1}$$

where C_S is the equilibrium solubility of a crystalline drug, V is the volume of dissolution medium, and "dose" is the drug amount added to the dissolution medium. The SI value was set to 0.1 for all recrystallization and dissolution tests in this study with the exception of the two-stage dissolution tests, where the volume of the dissolution medium was changed between the two stages. Using the experimentally determined IDM equilibrium solubility (8.1 ± 0.14 μg/mL), an SI of 0.1 translates to a single dose of approximately 20.28 mg of IDM for a 250-mL volume of dissolution medium. The drug-excipient ratio used in this study was 1:4 for recrystallization tests, dissolution tests, and ASD preparations, requiring approximately 81 mg excipient (i.e. 20.28 mg × 4 = 81.12 mg) for a 250-mL dissolution medium, giving an approximate excipient concentration of 320 μg/mL. For APX (C_S = 36.1 ± 0.5 μg/mL), an SI of 0.1 translates to a single dose of approximately 90 mg for a 250-mL volume of dissolution medium. As for IDM a drug-excipient ratio of 1:4 was used for the dissolution tests, requiring approximately 360 mg excipient (i.e. 90 mg × 4 = 360 mg) for 250-mL of dissolution medium, giving an approximate excipient concentration of 1440 μg/mL. In this chapter, 320 μg/mL and 1440 μg/mL were used as the lowest and highest concentrations for the excipient solutions that were used to determine the LLPS behaviors of supersaturated solutions of IDM and APX. A mid-level of concentration was set to be 800 μg/mL, corresponding to the amount of excipient in 250-mL water when 50 mg drug is dissolved. For the preparation of ASD carrier solutions, a required amount of carrier material was added to water in a sealed container and stirred for 12 hours. The obtained aqueous media were filtered using a Buchner funnel with filter paper before LLPS experiment.

2.3.4 UV double wavelength method to determine liquid-liquid phase separation

2.3.4.1 Parameter optimization for LLPS experiment

The LLPS of IDM and APX supersaturated solutions were determined using a UV double-wavelength extinction method on a SpectraMax M5 plate reader (Molecular Devices, LLC., CA, USA). Measurements were conducted for a series of drug solutions prepared by titration of a concentrated stock solution (prepared in organic solvent) into water. Parameter optimization was conducted to select stirring rate, organic solvent used for the stock solution, stock solution concentration and UV wavelength for different drugs based on different considerations.

The stirring rate was selected based on two considerations. Firstly, a high stirring rate is required to achieve a fast distribution of the organic stock solution in aqueous media. Secondly, in a practical sense, it is preferred that the stir bar fully immerses in the media under the selected stirring rate (i.e. the upper edge of the stir bar should be below the liquid level of the vortex center), in order to avoid titration of the organic stock solution directly onto the surface of the stirring bar that could result in solvent evaporation due to exposure to air. Therefore, 800 rpm was selected for the LLPS experiment.

The concentration of drug stock solution in organic solvent was determined by two considerations. The titration process associated with UV determination is designed to be finished within 1 hour, considering that long stirring of a supersaturated solution can result in recrystallization before the amorphous solubility can be reached. Additionally, the total volume of organic solvent titrated should be less than 5% of the volume so as to minimize changes in the properties of the media. Our preliminary results suggested that a stock solution of 5 mg/mL for IDM needed to be prepared by dissolving 50 mg IDM in 10 mL of anhydrous ethanol at room temperature. For APX a stock solution of 15 mg/mL APX was prepared by dissolving 150 mg of APX in 10 mL of DMSO at room temperature.

The absorbing and non-absorbing wavelengths for IDM were selected as 318 nm (λ_{max} for IDM) and 450 nm, respectively. The absorbing and non-absorbing wavelengths for APX were selected as 330 nm and 450 nm, respectively. 330 nm was used for APX rather than the λ_{max} of 278 nm since our preliminary studies showed that UV absorbance of APX at 278 nm ranged from 3.55 to 3.96 when APX concentration increased from 0 µg/mL to 400 µg/mL, significantly exceeding the recommended testing range for UV absorbance of 2.0. The high absorbance value obtained for the

blank sample (media alone) was due to the absorbance of the polystyrene microplate at low UV ranges (260 nm to 280 nm). Therefore, a wavelength with lower absorbance efficiency for the plate background was selected. The absorbance of APX at 330 nm shows linearity with increasing APX concentration, following the Beer-Lambert law.

2.3.4.2 LLPS determination of IDM and APX supersaturated solutions

50 mL of pure water and excipient solutions of 320 µg/mL, 800 µg/mL, and 1440 µg/mL were used as titration substrates and maintained at 37 ± 0.2 ˚C. An IDM stock solution of 5 mg/mL was used to titrate the aqueous solution in 50 µL increments under a constant stirring rate of 800 rpm. After stirring for 30 s, 100 µL sample was withdrawn and replaced with the same amount of aqueous solution to maintain a constant volume. The UV extinction values for the withdrawn sample were measured at 318 nm and 450 nm. The LLPS concentration of IDM was calculated by the intersection of two trendlines observed in the UV extinction-concentration scatter plots at 450 nm. All experiments were repeated for 3 times. For APX as described above a stock solution of 15 mg/mL was used, and UV extinction values were measured at 330 nm and 450 nm with all other procedures kept the same.

2.3.5 Surface tension measurement of excipient solutions

The surface tension of the excipient solutions was tested using the Du Noüy ring method on a Lauda TE 3 tensiometer (Lauda, Germany) equipped with a platinum-iridium alloy Du Noüy ring with a circumference of 6.001 cm (radius = 0.955 cm). Excipient solutions with different concentrations were maintained at 37 ± 0.2 °C by a circulating water bath. The testing ring was cleaned and flamed to dry before each measurement. The surface tension of a solution was determined by the average result of 3 consecutive measurements with a difference of no greater than ± 0.1 mN/m. A Harkins-Jordan correction was applied to the surface tension values as recommended by the instrument manufacturer. All experiments were conducted in triplicate.

2.3.6 Viscosity measurement of excipient solutions

The viscosities of excipient solutions were tested at 37 °C using a capillary method on a m-VROC viscometer equipped with a circulating water bath. Before testing, excipient solutions were freshly prepared and maintained at 37 °C in a water bath. The 1-mL glass syringe used to load the samples was kept in an oven at 37 °C before testing. Testing samples were loaded in the glass syringe

and introduced into the instrument at a constant rate of 0.5 mL/min for 2.1 seconds (controlled by the syringe pump built into the instrument). The viscosity value of each sample was calculated as the average result of three consecutive measurements. All experiments were repeated in triplicate.

2.4 Results

2.4.1 LLPS of IDM in pure water

The UV extinctions of IDM in pure water at both the absorbing and non-absorbing wavelengths are shown in Figure 2.1. When IDM concentration was gradually increased the UV extinction at 318 nm showed a linear increase following the Beer-Lambert law, indicating that IDM molecules were in a fully dissolved state. When the IDM concentration reached a certain value, the UV signal at 318 nm started to lose its linearity and showed a further increase until crystal precipitation was observed. The concentration corresponding to this distinct change corresponds to the initiation of LLPS. At the non-absorbing wavelength of 450 nm, the UV extinction intensity remained close to the baseline during the titration, which was evidence that the liquid system remained a single-phase system and no phase induced light scattering was present. At a critical concentration point, the UV signal at 450 nm increased substantially with a continuous increase until precipitation was observed. This critical IDM concentration where the UV signals changed significantly was taken as the LLPS onset of the IDM supersaturated solutions. The concentration was calculated from the intersection of two trendlines before and after the critical concentration. The LLPS onset of IDM in pure water was determined to be 46 ± 2 µg/mL.

2.4.2 Effect of polymers on the LLPS of IDM

As shown in Figure 2.2, The LLPS behaviors of IDM could be influenced by polymer and/or lipid excipients in different manners. In the presence of PVP at concentrations of 320 µg/mL, 800 µg/mL, and 1440 µg/mL, the LLPS onset of IDM remained constant and equal to 47.6 ± 1.1 µg/mL, 47.7 ± 1.5 µg/mL, and 48.5 ± 1.6 µg/mL, respectively, which were comparable to the value of 46 ± 2 µg/mL obtained for pure water (Section 2.4.1). The LLPS onset values did not show any significant changes with PVP concentration.

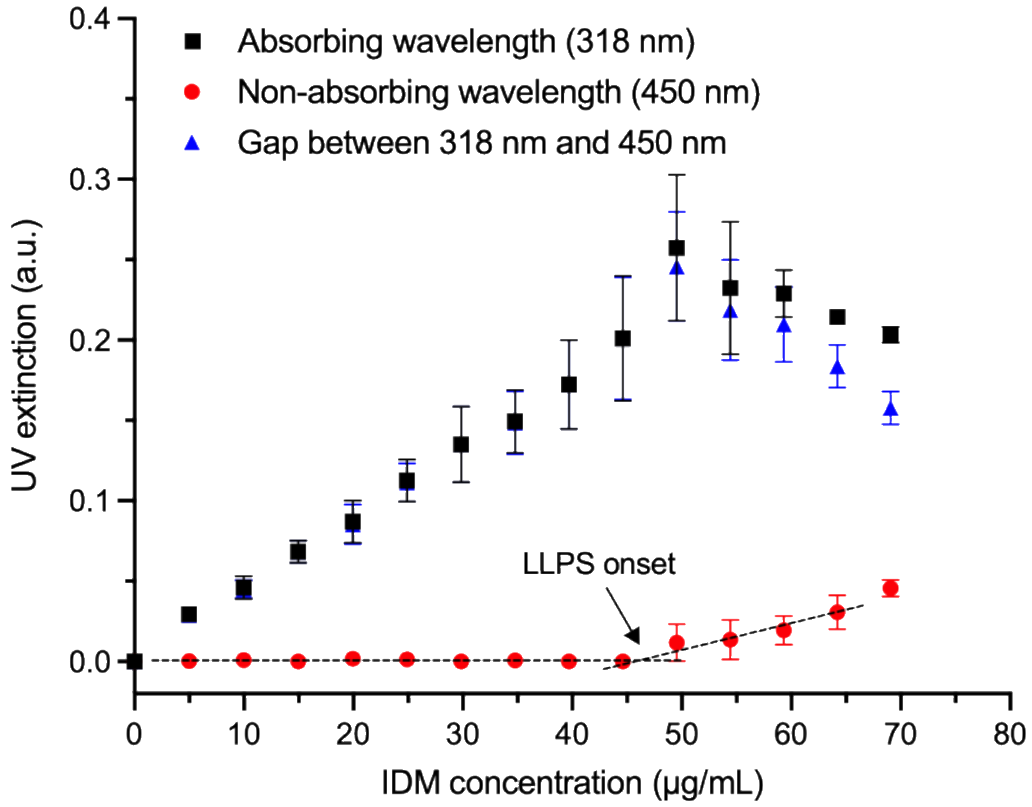

Figure 2.1. UV extinctions at different wavelengths for IDM solutions in water.

The amphiphilic polymer SOL showed a significantly delayed effect on the LLPS of IDM. In the presence of SOL with lowest concentration (320 μg/mL), no LLPS was observed for IDM within the tested drug concentration range of 200 μg/mL. It was noted that the UV extinction of IDM at 450 nm continuously increased with drug concentration since the starting point, which could be a result of drug incorporation into SOL micelles. The ionizable polymer SA effectively delayed the LLPS onset for IDM to different degrees, as a function of polymer concentration. With a low concentration (320 μg/mL), the IDM LLPS concentration was approximately 17.8 times the IDM crystalline solubility (8.1 ± 0.14 μg/mL, determined in section 2.3.2). With further increasing SA concentration, no LLPS of the IDM supersaturated solution could be observed within the tested range. Finally the LLPS behavior of IDM was essentially unchanged in the presence of EC, suggesting that the insoluble excipient did not interfere with the phase separation of the dissolved drug.

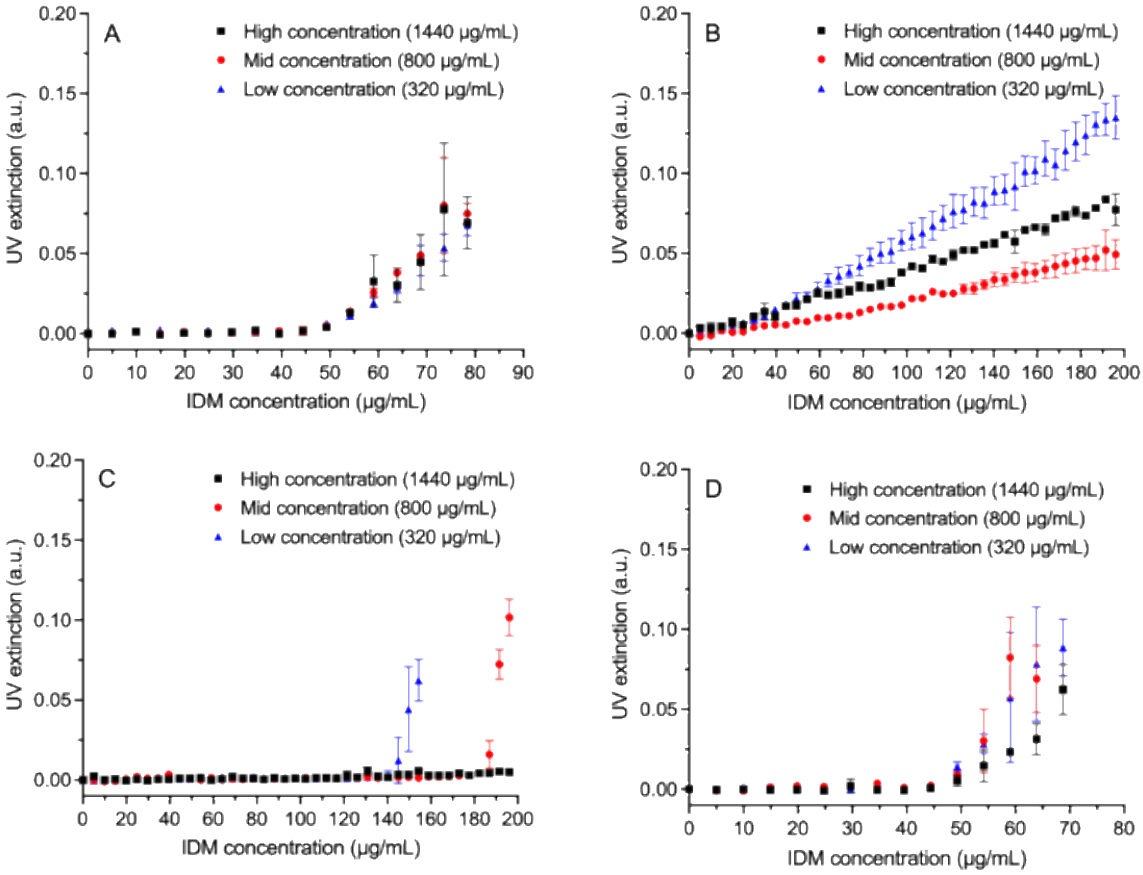

Figure 2.2. UV extinctions at 450 nm for IDM solutions with pre-dissolved (A) PVP, (B) SOL, (C) SA and (D) EC of different concentrations.

2.4.3 Effect of lipids on the LLPS of IDM

The LLPS onset concentrations for IDM were 72 ± 5 μg/mL, 119 ± 1.5 μg/mL, and 171 ± 8 μg/mL in the presence of 320 μg/mL, 800 μg/mL, and 1440 μg/mL of PL, respectively (Figure 2.3A and Table 2.1). The delayed LLPS onset was correlated with increasing PL concentration. G48 also delayed the LLPS of the IDM supersaturated solution as a function of carrier concentration, but with a weaker effect than observed for PL (Figure 2.3B and Table 2.1). The C_{LLPS} values of IDM in the presence of ATO were comparable with that in pure water, similar to the findings for the insoluble polymer EC. The C_{LLPS} values of IDM in the presence of individual polymers and lipids are summarized in Table 2.1. A one-way ANOVA test was conducted to compare the differences between LLPS values.

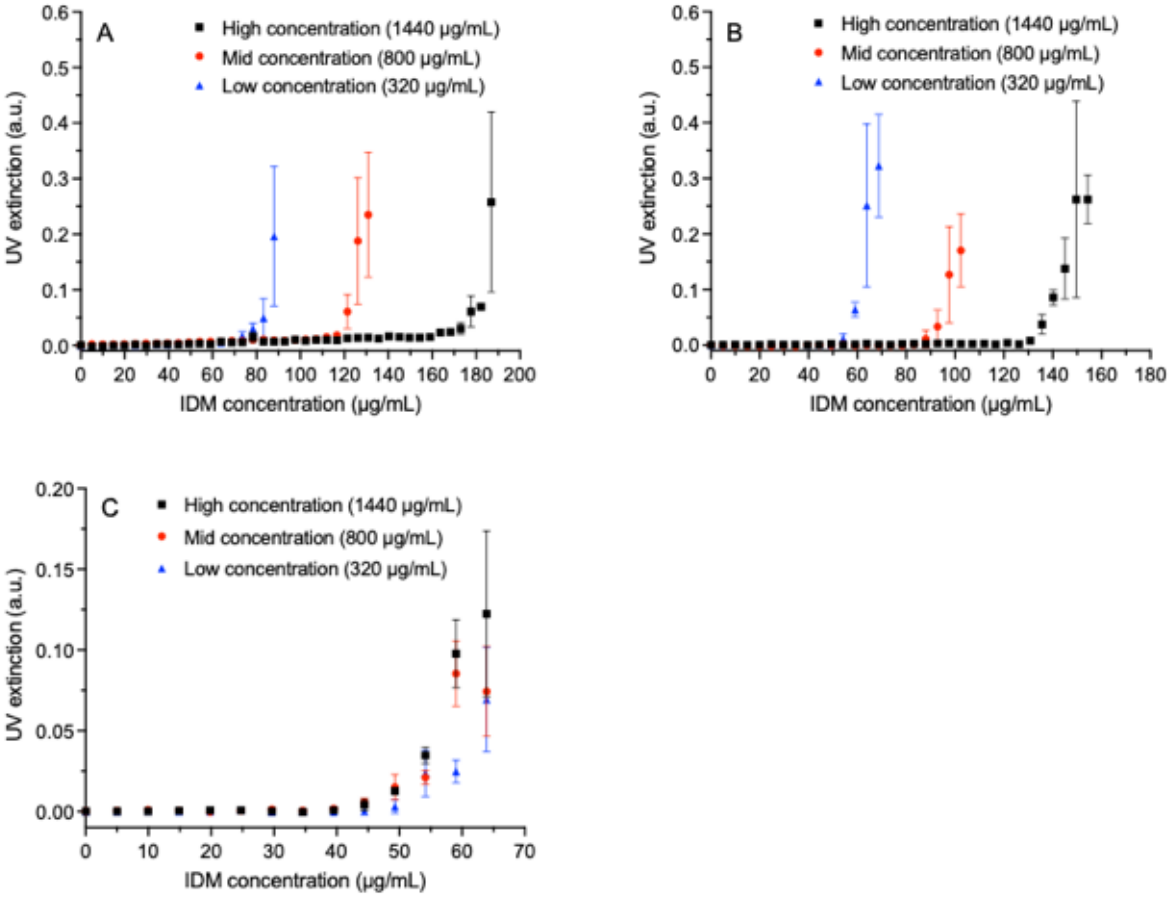

Figure 2.3. UV extinctions at 450 nm for IDM solutions with pre-dissolved (A) PL, (B) G48 and (C) ATO of different concentrations.

Table 2.1. LLPS concentration (C_{LLPS}, μg/mL) of IDM in the presence of different drug carriers.

Excipient Concentration [E] → / **Excipient (E) ↓**	**C_{LLPS} ([E] = 320 μg/mL)**	**C_{LLPS} ([E] = 800 μg/mL)**	**C_{LLPS} ([E] = 1440 μg/mL)**
PVP	47.6 ± 1.1	47.7 ± 1.5	48.5 ± 1.6
SOL	> 200**	> 200**	> 200**
SA	143 ± 3**	184 ± 2**	> 200**
EC	45.2 ± 0.6	44.9 ± 0.8	46 ± 3
PL	72 ± 5**	119 ± 1.5**	171 ± 8**

G48	54.4 ± 0.5**	88 ± 5**	133 ± 2**
ATO	45.3 ± 1.1	47.2 ± 1.5	44.1 ± 0.4

Note: C_{LLPS} of IDM in pure water was 46 ± 2 μg/mL. *$p < 0.05$ and **$p < 0.01$ between C_{LLPS} values of IDM in water and excipient solutions (n=3, mean ± SD).

2.4.4 Effect of polymer-lipid combinations on the LLPS of IDM

When PVP and PL were co-dissolved in water with a 1:1 weight ratio, a synergistic effect on the stabilization of LLPS of IDM was observed at each tested excipient concentration. C_{LLPS} values of IDM were higher than that for PVP or PL alone and showed a positive correlation with PVP-PL concentration (Table 2.2). Different from the synergism observed for PVP-PL combination, an averaged C_{LLPS} was observed for the PVP-G48 combination at each tested carrier concentration. The C_{LLPS} value increased with higher concentrations of PVP-G48. The LLPS onset of IDM in the presence of PVP-ATO was essentially unchanged when compared with that for PVP in all determined concentrations The C_{LLPS} values of IDM with different combinations of polymer and lipid ASD carriers at the concentrations of interest are summarized in Table 2.2. A one-way ANOVA test was conducted to compare the differences between LLPS values.

Table 2.2. LLPS concentration (C_{LLPS}, μg/mL) of IDM in the presence of polymer-lipid combinations.

Excipient Concentration [E] →	**C_{LLPS}**	**C_{LLPS}**	**C_{LLPS}**
Excipient (E) ↓	**([E] = 320 μg/mL)**	**([E] = 800 μg/mL)**	**([E] = 1440 μg/mL)**
PVP-PL	85.5 ± 1.5**	141 ± 7**	> 200**
PVP-G48	52.2 ± 1.6*	73 ± 4**	92 ± 3**
PVP-ATO	50.7 ± 1.7	50 ± 3	51 ± 2
SOL-PL	> 200**	> 200**	> 200**
SOL-G48	> 200**	> 200**	> 200**
SOL-ATO	> 200**	> 200**	> 200**
SA-PL	112 ± 4**	159 ± 5**	> 200**

SA-G48	100 ± 0.8**	143 ± 5**	170 ± 10**
SA-ATO	119 ± 5**	159 ± 0.9**	179 ± 6**
EC-PL	59 ± 5*	75 ± 3**	105 ± 13**
EC-G48	49 ± 3*	54 ± 3*	79 ± 4**
EC-ATO	46 ± 3	47 ± 4	45 ± 2

Note: C_{LLPS} of IDM in pure water was 46 ± 2 µg/mL. *$p < 0.05$ and **$p < 0.01$ between C_{LLPS} values of IDM in water and excipient solutions (n=3, mean ± SD).

For SOL-lipid combinations at all concentrations, no LLPS of IDM could be observed within the tested range of 200 µg/mL. The effects seen for the individual lipids on the LLPS of IDM (Figure 2.3) were overweighed by the strong stabilizing effect (i.e. solubilization) of SOL. All combinations of SA and lipid demonstrated an averaged effect on the LLPS of IDM compared to SA and the individual lipids alone. The C_{LLPS} values showed a positive correlation with carrier concentration for all SA-lipid combinations. No synergistic or antagonistic effect on the LLPS of IDM was observed for these combinations. The LLPS behaviors of IDM in the presence of EC-lipid combinations were governed by the properties of corresponding lipids. For EC-PL and EC-G48 of all concentrations, an averaged C_{LLPS} value was observed with regard to EC and individual lipids. For the substrates pre-treated with EC-ATO, C_{LLPS} values of IDM were essentially the same as that in water.

2.4.5 LLPS of APX in pure water

The UV extinctions of APX in pure water at both absorbing and non-absorbing wavelengths are shown in Figure 2.4. The UV absorbance at 330 nm showed a linear increase until a break point and started to lose its linearity afterwards. At the non-absorbing wavelength of 450 nm, the UV extinction remained close to the baseline until reaching a break point and increased substantially afterwards. The LLPS onset of APX in pure water was determined to be 291 ± 7 µg/mL.

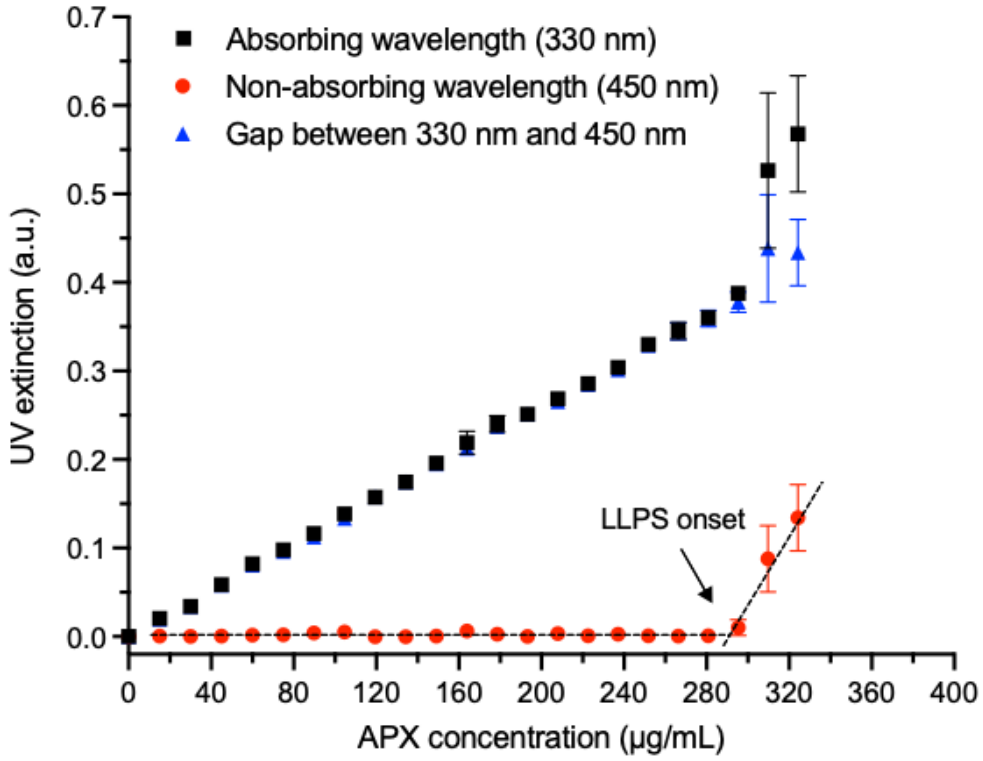

Figure 2.4. UV extinctions at different wavelengths for APX solutions in water.

2.4.6 Effect of polymers on the LLPS of APX

The LLPS behavior of APX was influenced by polymer carriers in different manners, as shown in Figure 2.5. In the presence of PVP of 320 μg/mL, 800 μg/mL, and 1440 μg/mL, the LLPS onset of APX was 397 ± 15 μg/mL, 425 ± 10 μg/mL, and 420 ± 8 μg/mL, respectively, which were significantly higher than that in pure water (291 ± 7 μg/mL). No obvious difference was observed for PVP solutions at the two higher concentrations from that obtained at 320 μg/mL. SOL had a significant stabilizing effect for APX where LLPS could be observed for APX within the tested drug concentration range up to 600 μg/mL in the presence of SOL. The absence of distinct LLPS point was similar to the case of IDM, while for APX there was no continuous increase in UV extinction with regard to drug concentration. SA has a small effect in delaying the LLPS of APX. The C_{LLPS} of APX was 313 ± 9 μg/mL, 320 ± 20 μg/mL and 319 ± 4 μg/mL from low to high SA concentration, which were comparable between different SA concentrations. This was different from its strong stabilizing

effect on supersaturated IDM solutions. The LLPS behavior of APX was essentially unchanged in the water substrate pre-treated with EC, again similar to the finding for IDM.

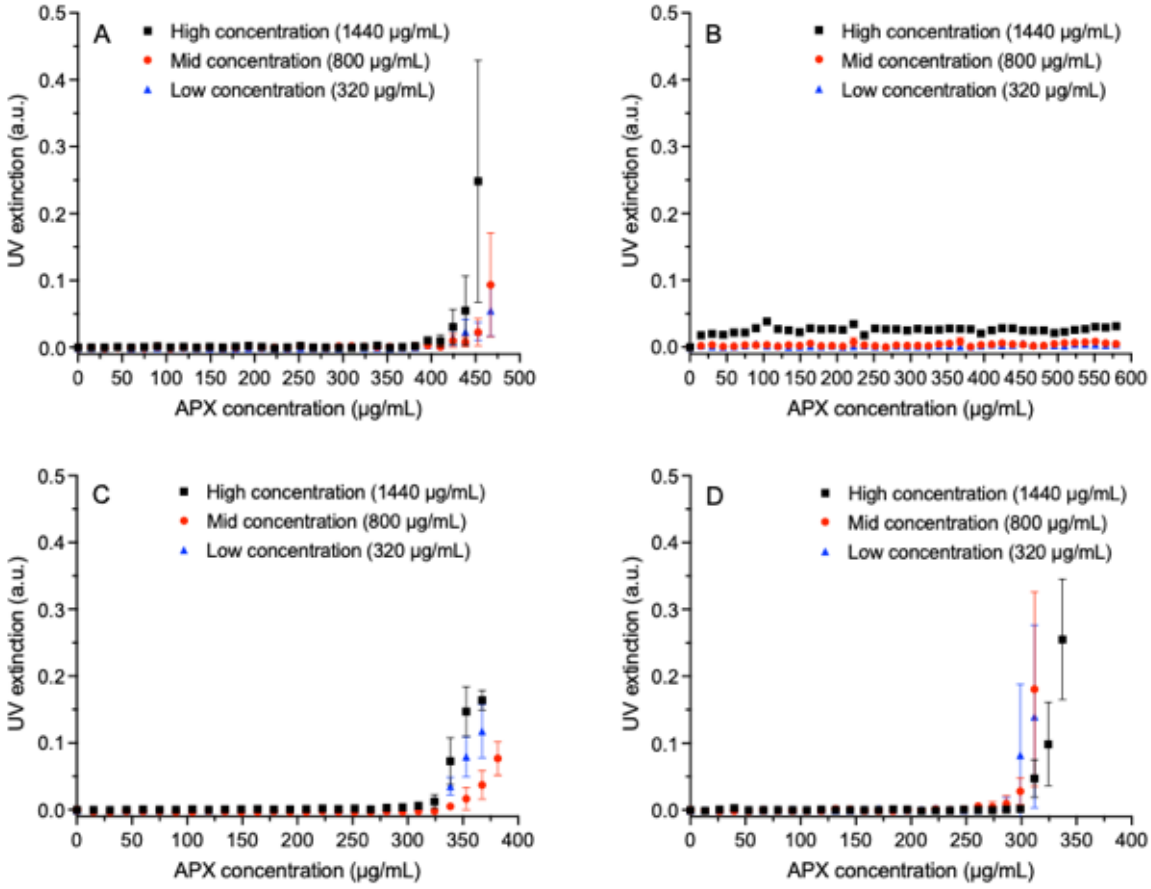

Figure 2.5. UV extinctions at 450 nm for APX solutions with pre-dissolved (A) PVP, (B) SOL, (C) SA and (D) EC of different concentrations.

2.4.7 Effect of lipids on the LLPS of APX

Significantly different for the IDM/PL system, PL was seen to promote LLPS of APX, as shown in Figure 2.6. The LLPS onset concentrations of APX were 272 ± 8 µg/mL, 266 ± 6 µg/mL, and 251.0 ± 0.4 µg/mL in the presence of 320 µg/mL, 800 µg/mL, and 1440 µg/mL of PL, respectively. If we recall section 2.4.3 LLPS for IDM was delayed by increasing amount of PL. G48 was also seen to promote LLPS of APX supersaturated solution with a positive correlation with G48 concentration (Figure 2.6B). The C_{LLPS} was determined to be 270 ± 20 µg/mL, 264 ± 5 µg/mL and 265 ± 14 µg/mL, respectively (Table 2.3). UV extinctions at 450 nm before LLPS remained close to

the baseline without obvious increase. The C_{LLPS} values for APX in the water pre-treated with ATO were essentially unchanged from that for pure water. The C_{LLPS} values of APX in the presence of individual polymers and lipids were summarized in Table 2.3. A one-way ANOVA test was conducted to compare the differences between LLPS values.

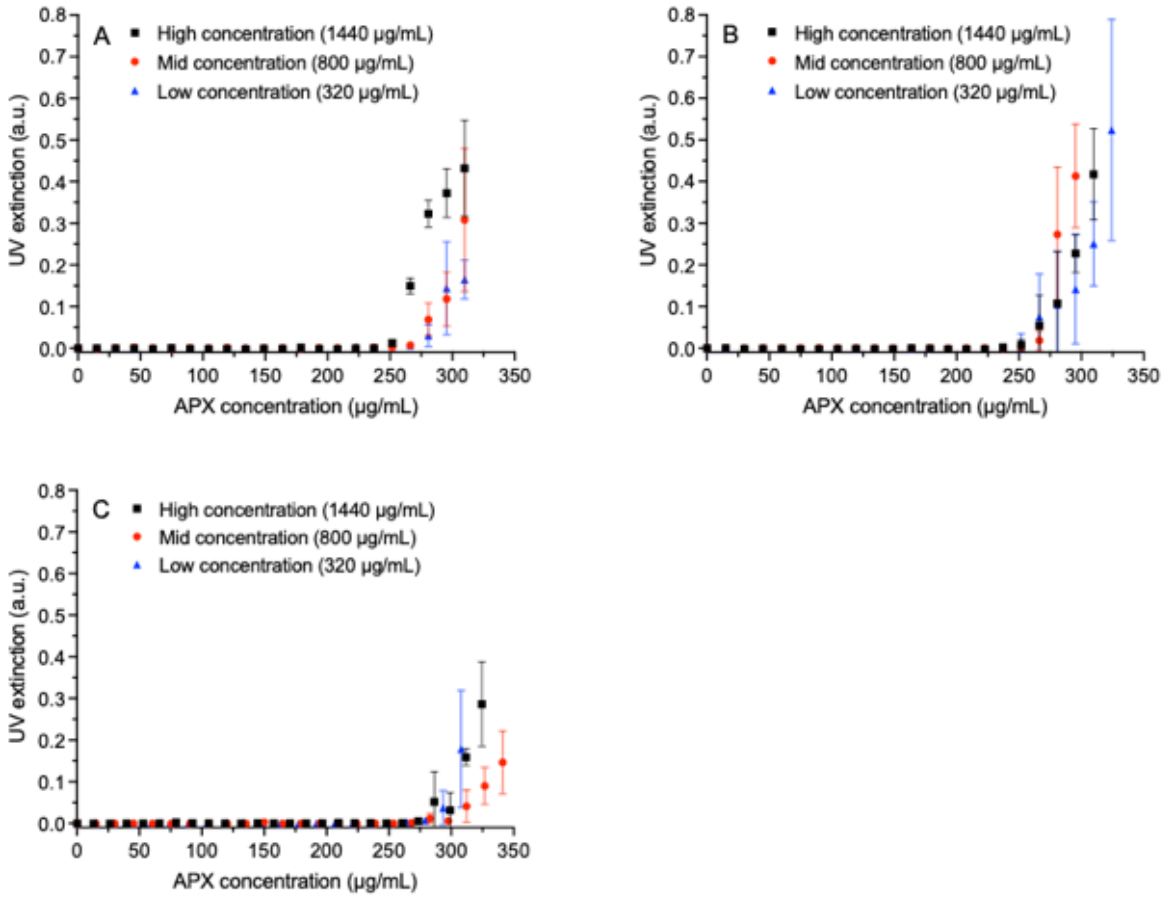

Figure 2.6. UV extinctions at 450 nm for APX solutions with pre-dissolved (A) PL, (B) G48 and (C) ATO of different concentrations.

Table 2.3. LLPS concentration (C_{LLPS}, μg/mL) of APX in the presence of different drug carriers.

Excipient Concentration [E] → / **Excipient (E) ↓**	**C_{LLPS} ([E] = 320 μg/mL)**	**C_{LLPS} ([E] = 800 μg/mL)**	**C_{LLPS} ([E] = 1440 μg/mL)**
PVP	397 ± 15**	425 ± 10**	420 ± 8**
SOL	> 600**	> 600**	> 600**
SA	313 ± 9	320 ± 20	319 ± 4**
EC	289 ± 6	289 ± 8	299.0 ± 1.3
PL	272 ± 8	266 ± 6*	251.0 ± 0.4**
G48	270 ± 20	264 ± 5*	265 ± 14
ATO	281 ± 7	294 ± 5	290 ± 13

Note: C_{LLPS} of APX in pure water was 291 ± 7 μg/mL. *$p < 0.05$ and **$p < 0.01$ between C_{LLPS} values of APX in water and excipient solutions (n=3, mean ± SD).

2.4.8 Effect of polymer-lipid combinations on the LLPS of APX

The combination of PVP and PL had an intermediate (or average) effect on the LLPS of APX as compared with individual excipients (Table 2.4). The overall effect of the PVP/PL combination appears to be governed by PVP, as C_{LLPS} values were closer to those obtained for PVP alone rather than for PL alone. This is in contrast to the synergistic effect observed for the PVP/PL combination on the LLPS of IDM. The PVP-G48 showed similar behaviours where the measured C_{LLPS} for APX for the PVP/G48 combination was between those for PVP and G48 alone with values being closer to those for G48. The LLPS onset of IDM in the presence of PVP-ATO was delayed to a degree similar to PVP alone. The addition of insoluble ATO did not bring change to the PVP system that delayed the LLPS of APX.

For SOL-lipid combinations of all concentrations, no LLPS of APX could be observed up to 600 μg/mL. The strong inhibition of LLPS is comparable to that seen for SOL alone as well as to results obtained for IDM (Section 2.4.4).

Table 2.4. LLPS concentration (C_{LLPS}, µg/mL) of APX in the presence of polymer-lipid combinations.

Excipient Concentration [E] →	**C_{LLPS}**	**C_{LLPS}**	**C_{LLPS}**
Excipient (E) ↓	**([E] = 320 µg/mL)**	**([E] = 800 µg/mL)**	**([E] = 1440 µg/mL)**
PVP-PL	400 ± 20**	396 ± 13**	416 ± 8**
PVP-G48	344 ± 13**	336 ± 12**	360 ± 20*
PVP-ATO	423 ± 7**	411 ± 13**	429 ± 10**
SOL-PL	> 600**	> 600**	> 600**
SOL-G48	> 600**	> 600**	> 600**
SOL-ATO	> 600**	> 600**	> 600**
SA-PL	299 ± 6	280 ± 20	281 ± 16
SA-G48	303 ± 13	312.9 ± 1.2**	312 ± 3
SA-ATO	306 ± 4*	305.4 ± 0.6*	312 ± 3*
EC-PL	265 ± 13*	262 ± 5*	272 ± 17
EC-G48	294 ± 16	282 ± 10	281 ± 5
EC-ATO	290 ± 6	296 ± 4	293 ± 5

Note: C_{LLPS} of APX in pure water was 291 ± 7 µg/mL. *$p < 0.05$ and **$p < 0.01$ between C_{LLPS} values of APX in water and excipient solutions (n=3, mean ± SD).

Similar effects were observed for both the SA-lipid combinations and the EC-lipid combinations, where polymers combined with PL were observed to promote LLPS of APX (i.e. C_{LLPS} decreased compared to that for water alone) and only to average the effect for the polymers combined with G48. Values determined for the EC-lipid combinations were comparable to those observed for the lipids alone. Neither EC nor ATO appear to affect the LLPS of APX.

2.4.9 Viscosity of solutions of ASD carriers

The viscosities of solutions of ASD carriers were determined to facilitate the analysis of the LLPS mechanism, as shown in Table 2.5. SA was observed to substantially increase the viscosity as compared to water alone. PL slightly increased the viscosity from 0.787 ± 0.006 mPa·s for pure water to 1.108 ± 0.018 mPa·s with increasing PL concentration. Solutions of the other individual carriers had viscosity values that were essentially the same as water. For polymer-lipid combinations containing SA and PL viscosities increased to different degrees. Other combinations again had viscosities comparable to the viscosity of water. No synergistic or antagonistic effect was observed for any combination.

Table 2.5. Viscosity (mPa·s) of ASD carrier solutions of different concentrations.

Excipient Concentration [E] →	**Viscosity**	**Viscosity**	**Viscosity**
Excipient (E) ↓	**([E] = 320 µg/mL)**	**([E] = 800 µg/mL)**	**([E] = 1440 µg/mL)**
PVP	0.88 ± 0.04*	0.924 ± 0.014**	0.953 ± 0.006**
SOL	0.877 ± 0.008**	0.785 ± 0.018	0.794 ± 0.014
SA	2.243 ± 0.010**	3.49 ± 0.05**	5.635 ± 0.007**
EC	0.764 ± 0.008	0.764 ± 0.016	0.768 ± 0.009
PL	0.908 ± 0.014**	0.935 ± 0.017**	1.108 ± 0.018**
G48	0.811 ± 0.019	0.811 ± 0.011	0.800 ± 0.010
ATO	0.795 ± 0.017	0.78 ± 0.03	0.766 ± 0.010
PVP-PL	0.85 ± 0.03	0.90 ± 0.02**	1.033 ± 0.018**
PVP-G48	0.820 ± 0.015*	0.819 ± 0.009*	0.818 ± 0.010*
PVP-ATO	0.777 ± 0.019	0.876 ± 0.005**	0.860 ± 0.008**
SOL-PL	0.80 ± 0.06	0.865 ± 0.019**	0.931 ± 0.004**
SOL-G48	0.862 ± 0.014**	0.928 ± 0.007**	0.801 ± 0.002*
SOL-ATO	0.86 ± 0.02*	0.799 ± 0.012	0.773 ± 0.016

SA-PL	1.77 ± 0.04**	2.465 ± 0.006**	4.05 ± 0.03**
SA-G48	1.70 ± 0.03**	2.415 ± 0.017**	3.654 ± 0.014**
SA-ATO	1.74 ± 0.03**	2.33 ± 0.03**	3.435 ± 0.006**
EC-PL	0.78 ± 0.03	0.812 ± 0.014	0.976 ± 0.010**
EC-G48	0.79 ± 0.02	0.76 ± 0.03	0.773 ± 0.011
EC-ATO	0.77 ± 0.02	0.784 ± 0.012	0.792 ± 0.004

Note: Viscosity of pure water was 0.787 ± 0.006 mPa·s. *$p < 0.05$ and **$p < 0.01$ between viscosity values of water and excipient solutions (n=3, mean ± SD).

2.4.10 Surface tension of excipient solutions

The surface tension values of solutions of different ASD carriers were also determined in order to aid in the analysis of the LLPS mechanism (Table 2.6). Solutions of the hydrophilic polymer PVP at different concentrations showed a reduced surface tension regardless of PVP concentration. Solutions of the amphiphilic polymer SOL had a significantly reduced surface tension to approximately 43 mN/m. Solutions of the ionizable polymer SA showed a moderate reduction in surface tension to 61-62 mN/m. Samples containing the insoluble polymer EC had the same surface tension as for water. The amphiphilic lipid PL significantly reduced the surface tension from 36.2 mN/m to 29.1 mN/m when concentration was increased from 320 µg/mL to 1440 µg/mL. Amphiphilic G48 also effectively reduced the surface tension from 37.9 mN/m to 37.2 mN/m when concentration increased from 320 µg/mL to 1440 µg/mL. As for EC, the insoluble lipid ATO did not change the surface tension from that obtained for pure water. The surface tension values for solutions of the polymer-lipid combinations were generally between those for individual polymers and lipids at the corresponding concentration. As expected for combinations containing surface-active components, the surface tension values were reduced. No synergistic or antagonistic effect on surface tension was observed for any polymer-lipid combination.

Table 2.6. Surface tension (mN/m) of ASD carrier solutions of different concentrations.

Excipient Concentration [E] → **Excipient (E) ↓**	**Surface tension** **([E] = 320 µg/mL)**	**Surface tension** **([E] = 800 µg/mL)**	**Surface tension** **([E] = 1440 µg/mL)**
PVP	64.0 ± 0.7**	63.6 ± 0.7**	63.5 ± 0.9**
SOL	43.1 ± 0.4**	43.2 ± 0.6**	42.8 ± 0.3**
SA	60.85 ± 0.05**	60.3 ± 0.4**	62.0 ± 0.5**
EC	69.9 ± 0.2	69.5 ± 0.5	71 ± 2
PL	36.2 ± 0.8**	30.6 ± 0.2**	29.1 ± 0.4**
G48	37.9 ± 0.5**	36.34 ± 0.11**	37.2 ± 0.3**
ATO	69.8 ± 0.5	70.4 ± 0.2	69.78 ± 0.10
PVP-PL	45.30 ± 0.13**	46.3 ± 0.5**	46.3 ± 0.6**
PVP-G48	38.79 ± 0.08**	39.55 ± 0.18**	38.0 ± 0.5**
PVP-ATO	63.6 ± 0.7**	62.4 ± 0.3**	63.0 ± 0.7**
SOL-PL	38.6 ± 0.3**	42.4 ± 0.6**	41.8 ± 0.6**
SOL-G48	40.1 ± 0.7**	38.9 ± 0.6**	38.7 ± 0.5**
SOL-ATO	44.2 ± 0.4**	43.4 ± 0.6**	43.4 ± 0.5**
SA-PL	43.05 ± 0.12**	48.1 ± 0.4**	47.1 ± 0.3**
SA-G48	40.5 ± 0.5**	40.0 ± 0.7**	38.9 ± 0.4**
SA-ATO	60.84 ± 0.04**	61.3 ± 0.7**	63.0 ± 1.0**
EC-PL	36.5 ± 1.0**	30.7 ± 0.6**	29.21 ± 0.10**
EC-G48	37.25 ± 0.10**	36.27 ± 0.03**	36.48 ± 0.09**
EC-ATO	68.6 ± 0.9	69.4 ± 0.2	69.77 ± 0.10

Note: Surface tension of pure water was 69.5 ± 0.4 mN/m. *$p < 0.05$ and **$p < 0.01$ between surface tension values of water and excipient solutions (n=3, mean ± SD).

2.5 Discussion

In this chapter we determined that the LLPS behavior of IDM and APX could be influenced by polymers and lipids differently depending on the properties of the polymers or lipids themselves but also on properties of mixtures of polymer and lipid. Generally, insoluble ASD carriers (EC or ATO) did not influence the LLPS of drugs, while soluble polymer or lipid carriers could show effects for a given drug that were completely opposite of those observed for another. The combinations of polymers and lipids could show either synergistic or an averaged effect on LLPS compared to the individual polymer or lipid carrier. The underlying mechanisms for the various observations are discussed below.

2.5.1 Effect of polymers on the LLPS of IDM

The results showed that the LLPS onset for IDM could be delayed depending upon the polymer carrier and its concentration. Soluble polymers, including PVP, SOL and SA, influenced the LLPS of IDM in different manners according to different mechanisms. PVP did not result in an obvious change to the phase separation onset of IDM, although it has been suggested to improve the supersaturation of different hydrophobic drugs (including IDM) by inhibiting drug crystallization through the formation of in-solution hydrogen bonding between PVP and a drug according to different studies [186–188]. Comparing the experimental observations for this study and previous studies, it can be speculated that drug recrystallization was stabilized through slowing crystal growth, instead of any effect on LLPS and nucleation. While viscosity has been suggested to slow droplet coalescence that leads to phase separation in a liquid environment, the slightly increased viscosity of the PVP solutions did not appear to delay or stabilize (i.e. prolong the duration) the LLPS for IDM [189–191]. The decreased surface tension of PVP solutions also did not appear to affect the LLPS for IDM. It should however be noted that the surface tension characterized in this study describes the interfacial tension between a solution and air, which is different from the interfacial tension between two liquid phases that are involved in the LLPS. Based on the assumption that the formation of a detectable drug-rich amorphous phase in a continuous solution phase would have a phase correlation similar to the coalescence of liquid droplets in an air phase, the correlation between solution-air surface tension and liquid-liquid interfacial tension can be obtained by Young's equation:

$$\gamma L2 = \gamma L1L2 + \gamma L1 \cos\theta \qquad \textbf{Equation 2.1}$$

where γL1 is the surface tension of liquid L1, γL2 is the surface tension of liquid L2 that is wetted by LI, γL1L2 is the interfacial tension between L1 and L2, and θ is the contact angle between L1 and L2. Young's equation requires that the system is at equilibrium, the surface of L2 is planar and no chemical reaction occurs between L1 and L2 [192]. For the LLPS theory, the drug-rich phase (L2) is treated as a nanosized liquid that exists in a metastable equilibrium with the water-rich phase (L1) for a transient period. The contact angle between the drug-rich phase and water-rich phase is close to zero given that the two liquid phases are highly miscible during LLPS. The surface tension between L2 and air is a constant as it is determined by the intrinsic properties of the amorphous drug. Therefore, a higher surface tension between air and the excipient solution corresponds to a lower interfacial tension between the drug-rich phase and water-rich phase, which facilitates the fusion of drug-rich droplets that corresponds to the coalescence of droplets in an water-air system [193]. Given that the essentially unchanged C_{LLPS} values of IDM with PVP, the effects of viscosity and surface tension can be considered to be weak and the in-solution hydrogen bonding between IDM and PVP should be the determinant factor for the LLPS of IDM.

The strong stabilizing effect of SOL on the LLPS of IDM could be a result of both in-solution hydrogen bonding and the ability of SOL to form micelles capable of incorporating IDM molecules. Similar to PVP, SOL also is able to take part in hydrogen bonding with hydrophobic drugs, inhibiting the molecular mobility and nucleation of drug molecules in an aqueous environment [194,195]. Amphiphilic SOL can also effectively incorporate drug molecules within micelles if the SOL concentration is above its critical micelle concentration of 1.9 μg/mL at 37 °C [161]. In such a system, the drug can partition such that a portion of the IDM molecules are found in the micellar phase slowing LLPS separation of the drug- and water-rich phases. As previously mentioned, a gradual increase in UV extinction at the non-absorbing wavelength 450 nm was observed without a distinct breakpoint for samples containing SOL, in contrast to samples containing PVP, where UV extinctions remained close to zero. We attribute this behaviour to the presence of SOL micelles since the SOL concentration in all cases was more than 150 times its CMC; the increase in extinction with increasing IDM concentration resulting from changes in micelle structure as IDM is incorporated into the micelles. In such a case there is no formation of a new phase as would occur if LLPS occurred; nevertheless light scattering from the solution can detect drug incorporation into the SOL micelles. This is confirmed since UV absorbance at 318 nm increases linearly with IDM concentration following the Beer-Lambert law during the whole titration process, suggesting that IDM was in a

dissolved or solubilized state and did not undergo LLPS hence the observed delay in or lack of LLPS. We do not consider the viscosity of SOL solutions as a contributor for the stabilization of LLPS as the viscosity values were essentially the same as water. The significantly reduced surface tension, and therefore the increased interfacial tension between drug aggregates (if present) and the bulk SOL solution, could potentially maintain drug-rich droplets from becoming a bulk liquid phase; however it is more likely that drug-rich droplets do not form at these high concentrations of SOL. Previous studies demonstrated that the combination of IDM and SA was a successful drug-polymer pair for the development of an SA-based ASD [170,171]. Here we considered that it is the pH activity of SA as a significant factor for the delayed phase separation of IDM solutions, since IDM is a weak acid drug showing pH dependent solubility profiles. By comparing the IDM LLPS onset values with IDM crystalline solubilities in the presence of SA at the same concentrations we found that the LLPS/solubility ratio remained constant between 2.0 to 2.3. A constant amorphous solubility/crystalline solubility ratio would be expected for a drug undergoing pH-induced ionization that follows the Henderson-Hasselbalch law where any pH-induced change in amorphous solubility or crystalline solubility of the drug would be the same [196,197]. Additionally, the large increase in viscosity of SA solutions may also contribute to the stabilization of LLPS. The contributions of pH-induced ionization and viscosity to the stabilization of LLPS will be further analyzed by examining the effect of SA on the LLPS for the non-ionizable drug APX (discussed below); theoretically, the pH effect should be weakened or not present for non-ionized APX while the viscosity effect would be unchanged. The LLPS of IDM was not influenced by the insoluble polymer EC, as seen by the C_{LLPS} values equal to that in pure water. Most EC molecules should be removed from water substrate during the preparation of carrier solution due to the low solubility of EC. The remaining EC in water was considered to have negligible effect on the phase behavior of dissolved drug. Although an insoluble material can have a very limited solubility value in water it can still have a measurable impact on both viscosity and surface tension of a solution. For the EC-IDM system viscosity and surface tension were determined to be equal to those of water indicating that there is no driving force for EC to impact LLPS for IDM.

2.5.2 Effect of lipids on the LLPS of IDM

The effects of lipids to stabilize the LLPS of IDM were mainly a result of the amphiphilic properties of PL and G48. Like the amphiphilic copolymer SOL, PL and G48 could potentially interact with IDM by incorporating IDM in the core of PL or G48 micelles or by facilitating the

aggregation of IDM molecules through in-solution hydrophobic interactions. Since the LLPS of IDM was stabilized with PL and G48 and the low surface tension values are consistent with micelle formation for both, it is clear that IDM is localized within the micelle phase for both lipids. As seen for SOL, small changes in viscosity for the PL and G48 systems are consistent with such a mechanism, although solution viscosity was increased slightly more for PL compared to G48, which explain the PL having a slightly better ability to stabilize the LLPS of IDM. ATO did not present obvious changes to the viscosity, surface tension and LLPS of IDM, as expected given its insoluble nature.

2.5.3 Effect of polymer-lipid combinations on the LLPS of IDM

The combination of PVP with the different amphiphilic lipids used in our study were observed to behave synergistically for PL, while having an intermediate effect for G48 on the LLPS of IDM. The UV extinction pattern of IDM did not only show a delayed LLPS onset, but also maintained its linearity for a wider concentration range after the occurrence of LLPS by the PVP-PL combination, describing a prolonged duration of the LLPS. This could be a result of an improved ability of the system to maintain large nanodroplets due to the flexibility of the PL vesicles being able to grow and incorporate larger amounts of IDM. A recent study showed that the addition of a polymer additive could destabilize the balance of attractive and repulsive forces in multilayered vesicle structure and reduce the rigidity of PL vesicles, resulting in an expansion in the vesicle size [198]. For PVP-G48, the UV extinction profile of IDM at 450 nm after the LLPS onset did not show prolonged duration or improved linearity, indicating that the drug incorporation properties of G48 micelles remained unchanged by the addition of PVP, which was different from the case of PVP-PL. The average effect of PVP-G48 on the LLPS of IDM was considered to be a result of the smaller amount of dissolved G48, as compared with G48 alone. C_{LLPS} values equivalent to those seen for water alone indicated that no in-solution interaction occurred for the combination of PVP-ATO. To help confirm the hypothesis that the addition of PVP allowed for an increase in PL vesicle size we attempted to monitor the change in particle size for the PL and PVP-PL systems upon IDM titration using dynamic light scattering (DLS). A high degree of polydispersity was observed for the PL concentrations used in this study and useful data could not be obtained. We suspect that when LLPS occurs the sizes of drug-rich nanodroplets or PL vesicles could not be distinguished and the aggregates are very heterogeneous in size, making it difficult to measure the size change of PL vesicle during LLPS. These phenomena were noted for future reference.

Similar to the case for SOL alone, LLPS was not observed for IDM in the presence of SOL-lipid combinations consistent with the incorporation of IDM into mixed SOL-lipid aggregates regardless of lipid type. The effects of SA-lipid combinations on the LLPS of IDM were also determined by the amount of SA without showing a synergistic or antagonistic effect due to carrier combination. The effects of EC-lipid combinations to that observed for the lipids alone but with a lesser effect (due to the lesser amount of lipid present in the equivalent mass of 1:1 mixture).

To help confirm or refute our analysis of the mechanism(s) of LLPS stabilization of IDM for the excipients described above, we carried out the same study but replacing IDM with APX which is non-ionizable and has a different solution behaviour from IDM. If the ability of the excipients to stabilize APX is similar it will serve to help confirm our interpretation presented above.

2.5.4 Effect of polymers on the LLPS of APX

Generally, the LLPS behavior of APX was influenced by polymer carriers but with several different observations from those for IDM. Contrary to what was seen for IDM a clear stabilization of the LLPS of APX was demonstrated as a function of PVP concentration, which was likely a result of strong in-solution hydrogen bonding between APX and PVP. The different effects of PVP on IDM and APX demonstrate the importance of understanding the nature of drug-polymer interactions when selecting a polymer as an ASD carrier. For SOL, similar to IDM a strong stabilization of LLPS was observed for APX, suggesting that specific drug polymer interactions were less important for the stabilization of LLPS than the presence of the micelles formed by SOL regardless of the drug. For both drugs the absence of LLPS is due to solubilization of the crystalline drug. The possible formation of a supersaturated drug solution will be testified in the next chapter. In contrast, the effect of ionizable SA on drug LLPS was not the same for IDM and APX. As we expected, the ionization of SA and associated pH-modifying effect did not influence non-ionized APX, and therefore the C_{LLPS} of APX did not increase as seen for IDM. The increase in C_{LLPS} could be attributed to the weak APX-SA interaction and viscosity of SA solution. Insoluble EC did not alter the phase behavior of the solution, and therefore the LLPS of APX was essentially unchanged, in agreement with our results for IDM.

2.5.5 Effect of lipids on the LLPS of APX

Interestingly, in the presence of amphiphilic PL and G48, the LLPS of APX was destabilized to different degrees, contrary to what was seen for IDM. According to previous analysis, the effect of

PL and G48 on drug LLPS was based on the competition of their effects to facilitate drug aggregation or incorporate drug into micelle structures. The promotion of the LLPS of APX indicated that the ability of the lipid to incorporate APX into the micelles was not effective enough to load the small drug aggregates that form through the aggregation of molecularly dissolved drug in solution. For recrystallization to occur in a molecularly dissolved solution, where particle size is seen smaller than 1 nm, a prerequisite is that solute molecules aggregate to form clusters larger than the critical nucleus size, which could range from 1 to 5 nm [199,200]. Nuclei and aggregates smaller than the critical nucleus size are expected to incorporate into micelles through hydrophobic interactions. APX has a larger topological polar surface area (111 $Å^2$) than that for IDM (68.5 $Å^2$), possibly resulting in a less effective partitioning in the hydrophobic micelle cores composed of hydrocarbon chains of PL and G48. Because of this, the overall process of phase separation could be facilitated. The fact that an ASD carrier has such completely different effects on different drugs suggests that the LLPS was not influenced by the excipient according to the same mechanism. This suggested a possibility that carrier effects could induce different dissolution and supersaturation behaviors of IDM and APX under non-sink conditions, which will be evaluated in the following chapter. The lack of effect of ATO on the LLPS of APX with ATO agreed with observations for IDM and that the insoluble carrier did not interfere with solution phase behavior.

2.5.6 Effect of polymer-lipid combinations on the LLPS of APX

PVP-PL did not demonstrate a synergistic effect on the LLPS of APX, as observed for IDM. We can examine the PVP-PL/APX system using the mechanism presented above for the PVP-PL/IDM system. The synergistic effect of PVP-PL on IDM LLPS was based on the incorporation of nanodroplets with larger sizes being facilitated by the PVP's effect on PL vesicles allowing them to be more flexible to grow in size. If we consider that the incorporation of APX is less efficient than for IDM as described in the previous section, then the effect of PVP making PL vesicles more flexible would be less pronounced since the root cause of this effect, the drug incorporation into PL vesicles, was less effective in the case of APX. Therefore, the LLPS behaviour of APX is governed by the properties of PVP. The same phenomenon was observed for PVP-G48, further suggesting that the overall effect of PVP-G48 on the LLPS of APX was determined by the amount of dissolved PVP. For PVP-ATO, the averaged effect on the LLPS of APX was determined by the amount of PVP as ATO did not interfere with the solution phase behavior.

In the presence of all SOL-lipid combinations, no LLPS of APX could be observed within the tested range, corresponding to the strong stabilizing effect of SOL. The observations were also aligned with those for IDM, suggesting that the stabilizing effect of SOL was not selective between different drugs. The averaged effect on the LLPS of APX provided by SA-lipid combinations indicated that the phase behavior was determined by the individual properties of SA and the corresponding lipid, without the occurrence of strong SA-lipid interactions that were able to bring synergistic or antagonistic change to the system. Due to the inert property of EC in supersaturated APX solutions, the LLPS of APX was determined by the properties of corresponding lipid materials. This agreed with observations for IDM.

2.6 Conclusion

In this chapter, the LLPS behaviors of IDM and APX in the presence of polymer and lipid carriers were successfully characterized by the double wavelength UV extinction method. The LLPS behaviour of APX was revealed for the first time. The onset and duration of LLPS of both drugs is influenced by polymer and lipid carriers in different manners, depending on one or more of mechanisms: in-solution hydrogen bonding, drug aggregation facilitated by amphiphilic agents, micelle/vesicle incorporation, and ionization induced solubility enhancement. Viscosity and surface tension of ASD carrier solutions were characterized and considered as minor determinants for the LLPS of IDM and APX. Polymer or lipid carrier can modify LLPS behaviour in completely different ways depending upon the nature of the PWSD, in this case IDM or APX. The effects of polymer-lipid combinations on the LLPS of both drugs in most cases corresponded to average of the effects of the individual carrier compounds. The combination of PVP and PL had a synergistic effect that delayed the onset and prolonged the duration of LLPS of IDM by stabilizing large nanodroplets due to the ability of PVP to alter the vesicle properties of PL. Whether and how LLPS properties correlate to the dissolution and recrystallization behaviors of IDM and APX will be evaluated in the following chapters. The methodology is expected to serve the LLPS investigations of more types of drugs and excipients. Our work suggests that drug-excipient combinations must be analyzed on a case by case basis, given the fact that an ASD carrier can behave markedly differently for different drug compounds.

Chapter 3
Effect of polymers and lipids on the stabilization of supersaturated solutions of IDM and APX

3.1 Abstract

The supersaturation effect of an ASD carrier in an aqueous environment is expressed by its ability to maintain the concentration of a supersaturated drug solution at an improved level and for a prolonged period. The purpose of this chapter was to evaluate the supersaturation effects of polymer and lipid ASD carriers on IDM and APX under non-sink dissolution conditions using a solvent-shift method. The supersaturation behaviors of IDM and APX were analyzed based on the previously identified (Chapter 2) LLPS properties. Results showed that the supersaturation behaviors of IDM and APX were influenced by individual ASD carriers in different manners by mechanisms that include in-solution hydrogen bonding, pH-induced solubility change, solubilization, and reduced crystal growth rate. The recrystallization behaviors of IDM and APX did not necessarily align with the LLPS results. LLPS properties were considered to influence the early stage of recrystallization behaviors of IDM and APX, and the overall recrystallization process was a sum result of LLPS and crystal growth rate modified by polymer and lipid carriers. All polymer-lipid combinations showed an averaged effect on the supersaturation evolution of IDM and APX, with no evidence of the synergistic effect that was observed for LLPS results. The recrystallization results revealed in this chapter will be used to analyze the dissolution and supersaturation behaviors of ASDs for IDM and APX prepared with different carriers.

3.2 Introduction

The supersaturation properties and precipitation kinetics of a drug in aqueous media are important information for the formulation design of ASD based SDDS. The ability of dissolved excipients to prevent the precipitation of poorly water-soluble drugs is recognized as a critical factor for the supersaturation performance of an ASD. With this effect, the high thermodynamic activity (i.e. proportional to the ratio of drug concentration and drug solubility) of supersaturated drug can be maintained for a longer time to enhance the absorptive flux across gastrointestinal membrane. The solvent-shift or pH-shift method are commonly used to achieve supersaturation in aqueous media for the assessment of drug precipitation due to recrystallization. For a typical solvent-shift process, the

poorly water-soluble drug is dissolved in a water miscible organic solvent that provides higher solubility for the drug. Examples include ethanol, methanol, dimethyl sulfoxide, dimethylformamide, polyethylene glycol, etc. The drug solution in organic solvent can be prepared by heating to increase drug solubility in order to achieve a high drug concentration required for the experiments. The drug solution is then added to water instantly or gradually to induce supersaturation at a desired induction rate as a result of solubility difference. As an alternative approach, for the pH-shift method, an ionized drug is dissolved in aqueous media with a pH value providing high solubility and then added to the dissolution media to initiate supersaturation.

After the generation of the supersaturated solution, the precipitation kinetics are expressed by the decrease in drug concentration over time. At pre-determined time intervals, the drug concentration in aqueous media can be determined after the separation of the solid phase, which requires immediate filtration or centrifugation of the withdrawn samples. Both methods have limitations that need to be considered for our study as amphiphilic carriers that affect drug solubilization/concentration will be used. For a supersaturated drug solution sample, in the presence of excipients that can solubilize the drug the measured concentration could be higher than the "real supersaturation" defined as the amount of molecularly dissolved drug that exceeds the drug solubility. This is because drug loaded micelle/vesicle structures enabled by common amphiphilic drug carriers could pass through commonly used 0.22 μm syringe filters used for dissolution testing due to their small size relative to the filter pore diameter. Ultracentrifugation could be more effective in separating molecularly dissolved drug from the micellar complexes; however, several issues must be considered regarding application in dissolution testing. An effective ultracentrifugation process capable of sedimenting large micelle structures could take 20-30 min or longer, or be completely impractical for micelles with a smaller size, such as the 11 nm micelles for the G48 excipient [178]. During centrifugation for a long time, drug recrystallization can continue for aliquot samples, and therefore the determined drug concentration in supernatant could be lower than that in the original state. In this regard, a small amount of polymer could be added to samples upon centrifugation to prevent drug recrystallization. However, whether and how these additives interact with drug-loaded micelle/vesicle structures and influence the sedimentation efficiency could be a question. Reviewing the suitability of different approaches, we selected the solvent-shift method. We conducted a filtration process for all aliquot samples using 0.22 μm syringe filters. In this regard, the determined supersaturation degree for a sample was seen as "apparent supersaturation" consisting of both molecularly dissolved part and

solubilized part provided by amphiphilic drug carriers. The effects of polymers, lipids, and their combinations on the supersaturation evolution of IDM and APX were evaluated based on this principle. These behaviors were correlated with the revealed LLPS results and used to predict the dissolution behaviors of ASDs for IDM and APX formulated with these carriers.

3.3 Materials and methods

3.3.1 Materials

Indomethacin (IDM, purity > 97.5%) and ethyl cellulose were purchased from Fisher Scientific (Hampton, NH, USA). Apixaban (APX, purity > 99%) was purchased from HuiRui Chemical Technology Co., Ltd (Shanghai, China). Poly (vinylpyrrolidone) (PVP) K90 and phospholipid were purchased from Sigma-Aldrich (Mississauga, ON. Canada). The phospholipid used in this study (Sigma-Aldrich catalog no. P3644) contains 55% phosphatidylcholine, 25% phosphatidylethanolamine and other phospholipids, with an average molecular weight of 776 g/mol. Polyvinyl caprolactam-polyvinyl acetate-polyethylene glycol graft co-polymer (Soluplus®, SOL) was a gift from BASF (Ludwigshafen, Germany). Sodium alginate (CAS number: 9005-38-3) was obtained from Acros Organics (USA). PEG-32 stearate (Gelucire® 48/16, G48) and glyceryl behenate (Compritol® 888 ATO) were a gift from Gattefosse (Saint-Priest, France). Ethanol and dimethyl sulfoxide (DMSO) of high-performance liquid chromatography (HPLC) grade were purchased from Fisher Scientific (Hampton, NH, USA). Water used in this study was obtained from a Millipore Milli-Q system.

3.3.2 Determination of solubilization effect of ASD carriers on crystalline IDM and APX

The dissolution profiles of crystalline IDM in the presence of ASD carriers were determined using a Vision Classic 6 dissolution system (Teledyne Hanson Research, USA) at 37 ± 0.2 ˚C with a paddle speed of 150 rpm. 20 mg of crystalline IDM was added to 250 mL of water containing 80 mg of pre-dissolved ASD carriers, corresponding to the non-sink condition (SI=0.1) described in the previous section. Insoluble ASD carriers were stirred in water for 2 hrs and filtered through a filter paper of grade 41. The collected liquids were used as dissolution media. During dissolution, 2 mL of samples were withdrawn at predetermined timepoints and replaced by the same amount of dissolution medium. Samples were filtered through a 0.22 μm PES syringe filter. The IDM concentration in the

filtrate was determined using a UV 2100 spectrometer at 318 nm based on a linear Beer-Lambert calibration curve for IDM (r^2=0.9991). All experiments were carried out in triplicate.

For APX, 90 mg of crystalline APX was added to 250 ml water containing 360 mg of pre-dissolved ASD carriers, corresponding to the SI index of 0.1. Other experimental procedures were the same as for IDM. The APX concentration in the filtrate was determined using a UV 2100 spectrometer at 280 nm based on a linear Beer-Lambert calibration curve for APX (r^2=0.9993). All experiments were carried out in triplicate.

3.3.3 Determination of the ability of ASD carriers to maintain supersaturated solutions of IDM and APX

The ability of the ASD carriers to maintain IDM and APX at a supersaturated concentration was evaluated by a solvent-shift method under non-sink dissolution condition. For IDM, a highly concentrated IDM stock solution of 20 mg/mL was prepared by dissolving 100 mg of crystalline IDM in 5 mL of ethanol. 1 mL of IDM stock solution was added as a single dose to 250 mL water containing the drug carrier of interest to give an initial concentration of 80 µg/mL IDM (10 × IDM solubility). 2 mL samples were withdrawn at predetermined timepoints and filtered through a 0.22 µm PES syringe filter. The filtrate was properly diluted and processed using the same method as section 3.3.2. All experiments were run in triplicates.

For APX, the stock solution of 90 mg/mL was prepared by dissolving 450 mg of crystalline APX in 5 mL of DMSO at 90 °C. 1 mL of APX solution was added as a single dose to 250 mL dissolution media to initiate a supersaturation of 360 µg/mL. The APX concentration was determined by UV at 280 nm. Other procedures were kept the same.

3.4 Results

3.4.1 Effect of ASD carriers on the solubilization of crystalline IDM and APX

The solubilization and supersaturation maintenance effect of different polymers and lipids were investigated in this section. Solubilization effects of polymeric carriers for crystalline IDM and APX are shown in Figure 3.1. The dissolution rate and concentration of IDM in the presence of PVP was essentially the same as for pure IDM. In the presence of SOL, IDM showed a similar dissolution rate to pure IDM, with a slightly higher equilibrium concentration of 10.1 ± 0.5 µg/mL at 24 hrs

(Figure 3.1A). SA provided a significant improvement in IDM dissolution, achieving a free drug concentration of 46.2 ± 0.4 µg/mL within 6 hrs, and an equilibrium concentration of 57.1 ± 0.2 µg/mL at 24 hrs. The dissolution rate and solubility were not changed by the addition of EC.

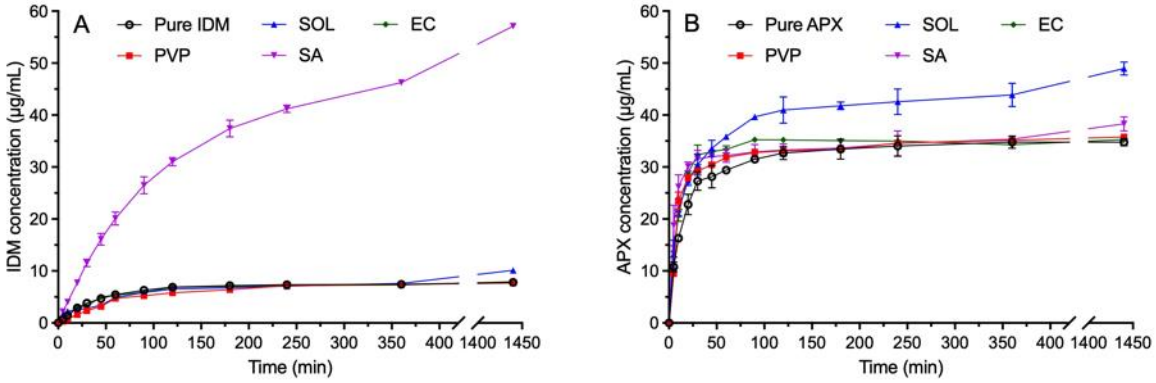

Figure 3.1. Dissolution of crystalline (A) IDM and (B) APX in the presence of pre-dissolved polymer carriers.

As shown in Figure 3.1B, PVP, SA and EC had minimal effect on the dissolution rate APX, with the APX concentrations at each timepoint being the same within experimental error. The equilibrium APX concentrations at 24 hr with PVP and EC were 35.8 ± 0.3 µg/mL and 35.3 ± 0.2 µg/mL, which were essentially the same as APX alone while SA slightly improved the equilibrium APX concentration to 38 ± 1 µg/mL. The solubilization effect of SA for weak acid IDM was distinctly more obvious than that for non-ionized APX, similar to its different effects on the LLPS of both drugs observed in the previous chapter (section 2.4.2 and 2.4.6). In the presence of SOL, both dissolution rate and the concentration of APX were increased, which can be attributed to the combined effects of increased wetting of APX particles (i.e., reduction in surface or interfacial tension) and the formation of micelles. The APX concentration reached 35.9 ± 0.1 µg/mL within 60 min, and further increased to 49 ± 1 µg/mL at 24 hrs, providing a 40% improvement in APX equilibrium concentration.

Lipids carriers including PL and G48 provided an improvement in both dissolution rate and crystalline solubility for both drugs, as shown in Figure 3.2. PL provided an IDM concentration of 10.3 ± 0.3 µg/mL at 60 min, which was 1.9-fold as that for IDM alone. The final concentration at 24 hr plateaued at 12.5 ± 0.4 µg/mL, equal to a 60% increase in solubility. For G48, the IDM

concentration was seen to further increase to 11.8 ± 0.2 µg/mL at 60 min, and 14.2 ± 0.2 µg/mL at 24 hrs. For APX the drug concentration at 24 hr was improved to 62 ± 4 µg/mL and 55 ± 2 µg/mL by PL and G48, respectively. In the presence of the insoluble lipid ATO, no change in dissolution was observed for both drugs. The concentration levels of IDM and APX dissolution will be used as baseline to evaluate the supersaturation performance of corresponding ASD carriers. The free drug concentration achieved beyond these measured solubilities (in the presence of pre-dissolved carrier) will be seen as a supersaturated concentration enabled by the amorphous solid mixture of drug and carrier.

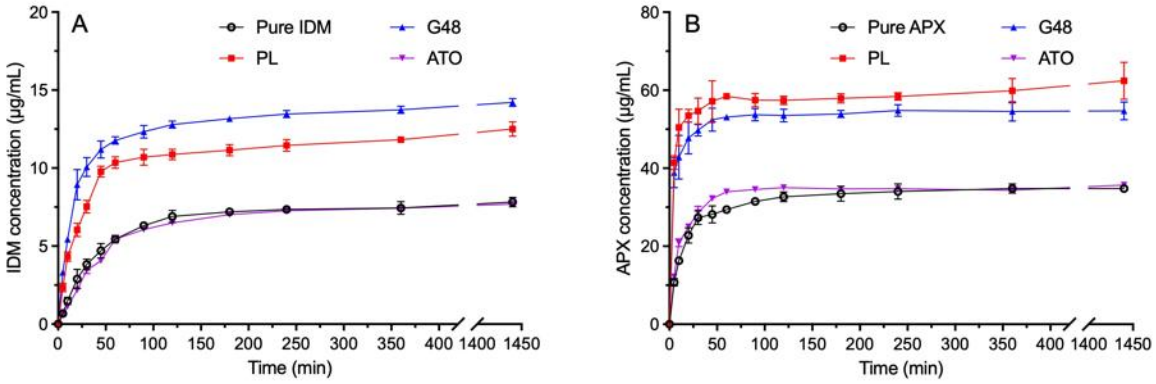

Figure 3.2. Dissolution of crystalline (A) IDM and (B) APX in the presence of pre-dissolved lipid carriers.

3.4.2 Effect of ASD carriers on the stability of supersaturated solutions of IDM and APX

The concentration-time profiles for a supersaturated solution of IDM and APX in the presence of different pre-dissolved polymer carriers are shown in Figure 3.3. Pure IDM showed a fast recrystallization in pure water, decreasing from an IDM concentration from 80.0 µg/mL (10 times the IDM solubility in water; used as a "standard" supersaturated concentration) to 11.4 ± 0.4 µg/mL within 90 min (Figure 3.3A). After a 24-hr equilibration, the IDM concentration returned to 8.4 ± 0.2 µg/mL, comparable to the endpoint for the dissolution of crystalline IDM (7.8 ± 0.2 µg/mL, see section 3.4.1). This was considered to be the equilibrium concentration of a supersaturated solution of IDM under non-sink condition without additives. In the presence of PVP, a slight increase in IDM concentration was observed at all time points, also demonstrating a longer equilibration time where

IDM concentration decreased from 37 ± 3 µg/mL (at 30 minutes) to 20.5 ± 0.2 µg/mL (at 360 minutes). As a comparison, drug concentration was 10.0 ± 0.2 µg/mL at 240 min for IDM in the absence of added carrier. In the PVP solution IDM concentration gradually decreased to an equilibrium concentration of 16.4 ± 0.5 µg/mL at 24 hr, approximately twice the concentration of 8.4 ± 0.2 µg/mL for IDM alone. Complete recrystallization of IDM to the concentration observed for water alone was not observed within 24 hrs due to PVP's ability to act as a solubilizer.

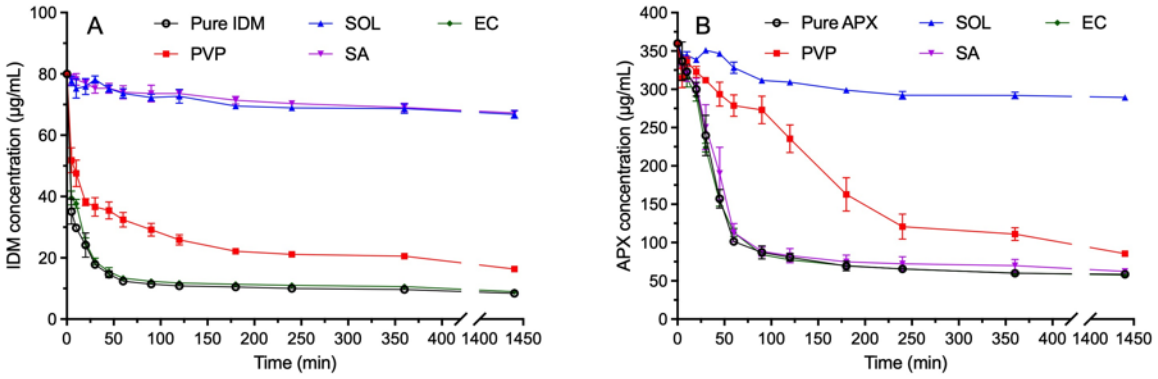

Figure 3.3. Recrystallization of (A) IDM and (B) APX in the presence of pre-dissolved polymer carriers.

SOL demonstrated a significant ability to maintain a supersaturated concentration for dissolved IDM. The IDM concentration maintained an equilibrium concentration of 67 ± 1 µg/mL at 24 hrs. The equilibration concentration obtained through the recrystallization process was significantly higher than that obtained for the solubilization test with SOL, suggesting that only partial recrystallization at 24 hrs. In the presence of SA, IDM also showed a high degree of supersaturation over 24 hrs. The IDM concentration was observed to be 67.3 ± 0.3 µg/mL after 24 hrs, which was slightly higher than the 57.1 ± 0.2 µg/mL for the solubilization test. The difference between equilibrium concentrations determined from the solubilization versus recrystallization tests describes an incomplete recrystallization of IDM, with the greatest degree of supersaturation observed for SOL, with weaker effect observed for SA and PVP. For the insoluble EC, the supersaturation profile of IDM was essentially unchanged with an IDM concentration of 8.98 ± 0.15 µg/mL (compared to 8.4 ± 0.2 µg/mL obtained in the absence of any carrier), with no significant ability to maintain supersaturation for IDM.

For APX, in pure water, drug concentration rapidly decreased from the initial concentration of 360 µg/mL to 81 ± 4 µg/mL within 120 min followed by a more gradual decrease to 58.5 ± 0.4 µg/mL at 24 h (Figure 3.3B). The addition of pre-dissolved PVP to the system resulted in APX concentrations that were higher than that in pure water at each timepoint. At 90 minutes the APX concentration in the PVP solution was 240 ± 30 µg/mL (a 2.0-fold improvement as compared with that in pure water). Afterwards, a more rapid decrease in APX concentration was observed, falling from 240 ± 30 µg/mL to 75 ± 4 µg/mL at 360 min. This was followed by a gradual decrease to an equilibrium concentration of 71 ± 4 µg/mL at 24 hrs, giving a 97% improvement in APX solubility. The SOL copolymer was even more effective at maintaining supersaturated APX concentration. The APX concentration decreased only gradually from 360 µg/mL to 289 ± 2 µg/mL over a period up to 24 h, demonstrating a 7-fold improvement in APX solubility. In contrast, neither SA nor EC had any significant impact on the recrystallization behavior of APX from a supersaturated solution.

Lipid carriers influenced IDM supersaturation in different manners based on their individual properties, as shown in Figure 3.4A. PL showed a moderate ability to maintain a supersaturated concentration of IDM similar to that observed in the previous section for PVP. At each timepoint, the IDM concentration was higher than that for IDM alone. A short plateau stage was observed for the first 20 min, where the IDM concentration was maintained at a high level of 74 ± 2 µg/mL. After the plateau the IDM concentration decreased to 42 ± 1 µg/mL at 60 min, with an equilibrium concentration of 19.0 ± 0.4 µg/mL after 24 hrs; this equilibrium concentration is approximately 2.3 times as the aqueous IDM solubility. This concentration was 50% higher than the crystalline solubility of IDM in the presence of a same amount of PL, suggesting that the IDM recrystallization process was not completed.

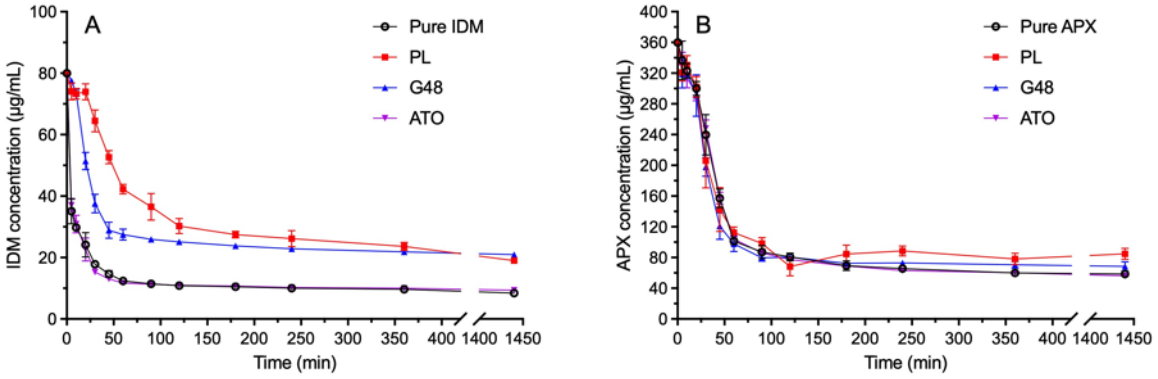

Figure 3.4. Recrystallization of (A) IDM and (B) APX in the presence of pre-dissolved lipid carriers.

G48 provided a similar degree of stability with respect to maintaining a supersaturated IDM concentration as was observed for PL. A large difference in IDM concentration was observed at 60 min for the G48 vs PL curves, 28 ± 2 μg/mL for the G48 system and 42 ± 1 μg/mL for PL; however, the same sharp decrease in concentration was observed between 0 to 60 min. Afterwards, a slow continuous concentration loss was observed until reaching 21.0 ± 0.2 μg/mL at 24 hr. Similar to PL G48 reached an equilibrium concentration of 21.0 ± 0.2 μg/mL at 24 hr, approximately 220% higher than that observed for the solubilization test (Figure 3.2A), indicating that IDM recrystallization was not completed after 24 hrs. The insoluble lipid ATO had a negligible effect on IDM recrystallization under non-sink conditions, reaching an endpoint concentration that was close to that for the solubilization test, suggesting a completed IDM recrystallization. This phenomenon was similar to that observed above for the insoluble polymer EC. As shown in Figure 3.4B, the recrystallization profiles of APX in the presence of lipid carriers were essentially the same as that in pure water, regardless of lipid type where at each timepoint prior to 24 hrs, the APX concentrations were all comparable. The improvement in drug equilibrium concentration by PL (45%) and G48 (17%) was likely a result of lipid solubilization and incomplete drug recrystallization.

PVP-lipid combinations, including PVP-PL, PVP-G48 and PVP-ATO, showed an averaged effect on the stabilization of an IDM supersaturated solution with the concentration curve lying between the curves obtained for PVP and the individual lipids (see Figure 3.5). The APX concentrations at 60 min and 24 hrs were summarized in Table 3.1.

Table 3.1. IDM and APX concentrations (μg/mL) at different time points with different excipients.

Drug →	**IDM**		**APX**	
Excipient ↓	**60 min**	**24 hr**	**60 min**	**24 hr**
Pure drug	12.4 ± 0.8	8.4 ± 0.2	101 ± 3	58.5 ± 0.4
PVP	32 ± 2**	16.4 ± 0.5**	279 ± 11**	85.6 ± 1.5**
SOL	74 ± 2**	66.8 ± 1.2**	328 ± 6**	289 ± 2**
SA	74 ± 2**	67.3 ± 0.3**	113 ± 10	62.3 ± 1.4*
EC	13.4 ± 0.2	8.98 ± 0.15*	108 ± 3	57.7 ± 0.8
PL	42.2 ± 1.3**	20.6 ± 0.8**	113 ± 6	85 ± 6**
G48	27.5 ± 1.5**	21.0 ± 0.2**	98 ± 8	69 ± 5*
ATO	11.3 ± 0.5	8.8 ± 0.3	104 ± 6	56.3 ± 1.3
PVP-PL	30 ± 2**	17.4 ± 0.3**	224 ± 12**	88 ± 5*
PVP-G48	30.5 ± 0.9**	17.0 ± 0.5**	180 ± 13**	64 ± 3
PVP-ATO	27.0 ± 1.3**	15.1 ± 0.2**	221 ± 10**	63 ± 3
SOL-PL	70.7 ± 1.0**	66 ± 2**	322 ± 4**	282 ± 6**
SOL-G48	69.2 ± 1.1**	64.0 ± 1.0**	323 ± 3**	287 ± 2**
SOL-ATO	69.7 ± 1.1**	68.8 ± 1.1**	313 ± 4**	276 ± 5**
SA-PL	71 ± 2**	62.6 ± 1.3**	104 ± 5	72.2 ± 1.4**
SA-G48	72 ± 2**	64.8 ± 1.6**	108 ± 3	63.7 ± 0.7**
SA-ATO	74.1 ± 0.8**	66.4 ± 0.4**	108 ± 2*	63 ± 3
EC-PL	30.4 ± 1.0**	12.1 ± 1.1**	110 ± 3*	62.3 ± 1.5*
EC-G48	19.2 ± 1.0**	17.4 ± 0.4**	98.6 ± 1.1	63.5 ± 1.4**
EC-ATO	11.0 ± 0.3	8.6 ± 0.3	101 ± 6	59.3 ± 1.0

Note: *$p < 0.05$ and **$p < 0.01$ between concentrations of IDM/APX in water and excipient solutions (n=3, mean ± SD).

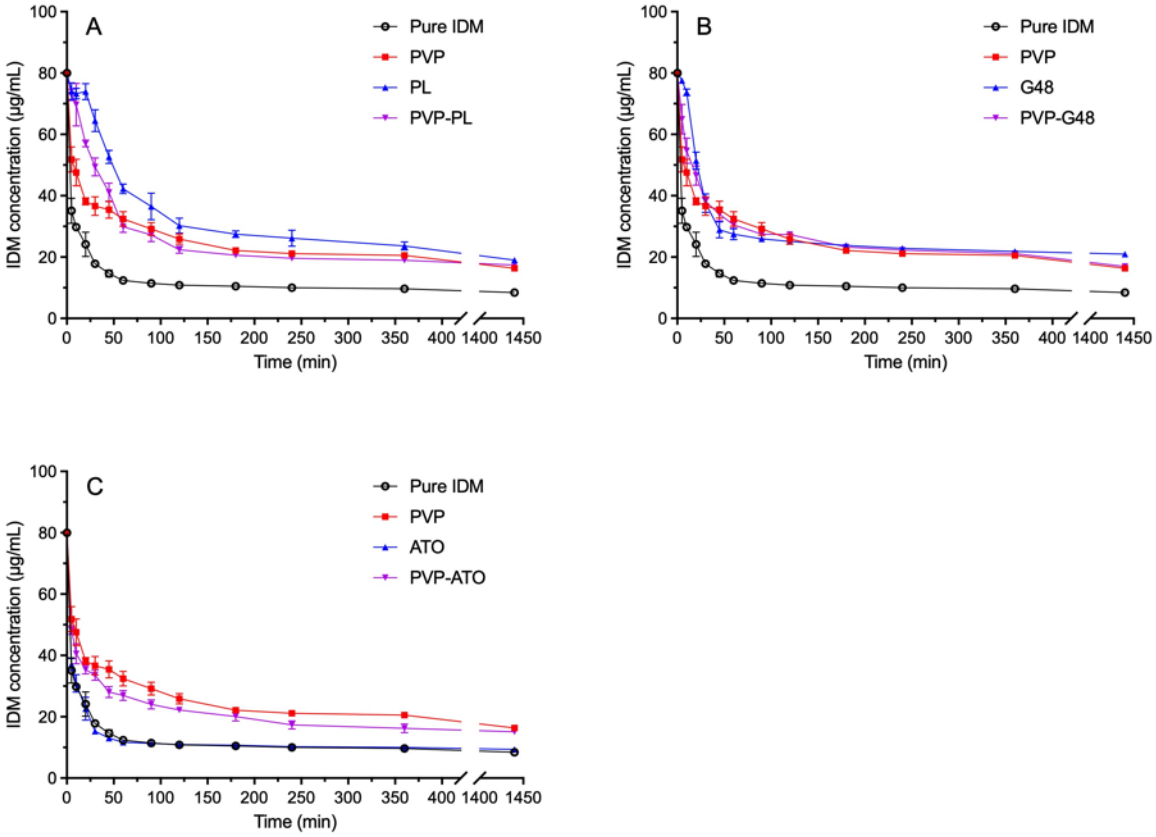

Figure 3.5. Recrystallization of IDM in the presence of pre-dissolved (A) PVP-PL, (B) PVP-G48 and (C) PVP-ATO.

SOL-lipid combinations presented a stabilizing effect for the IDM supersaturated solution similar to SOL alone, regardless of lipid type (Figure A-1 in appendix). The strong stabilizing effect of SOL on the supersaturated IDM solution was not compromised due to the combination with other excipients. SA-lipids combinations also presented a stabilizing effect for IDM supersaturated solution similar to SA alone (Figure A-2 in appendix). For all combinations, the IDM concentration was effectively maintained over 62.6 ± 1.3 μg/mL for up to 24 hrs. Combinations of EC with lipids provided stabilizing effects for IDM supersaturated solutions depending on the lipid type (Figure A-3 in appendix). For EC-PL and EC-G48, the stabilization of the IDM supersaturated solution was lying between EC and the individual lipid, which was determined by the stabilization ability of the lipid components. For EC-ATO, the IDM recrystallization profile was essentially the same as IDM alone.

For APX, PVP-lipid combinations showed an average effect on its recrystallization profile with regard to PVP and individual lipids (Figure 3.5). For PVP-PL, the APX concentration was maintained above 325 ± 10 μg/mL within the first 10 min followed by a rapid decrease to 107 ± 4 μg/mL at 120 min after which the rate of the decrease in APX concentration was approximately constant reaching an equilibrium APX concentration at 24 h of 88 ± 5 μg/mL, suggesting a near completion of recrystallization of APX. Comparable results were obtained for the PVP-G48 and PVP-ATO systems, where APX concentrations decreased to 64 ± 3 μg/mL and 63 ± 3 μg/mL, respectively.

The recrystallization profiles of APX in the presence of SOL-lipid combinations were governed by the solubilization abilities of SOL. The APX concentration was effectively maintained over 300 μg/mL level for 6 hrs, and the general shape of the concentration-time profiles were comparable with that for SOL alone. The equilibrium APX concentrations for SOL-PL, SOL-G48 and SOL-ATO at 24 hrs were 282 ± 6 μg/mL, 287 ± 2 μg/mL, and 276 ± 5 μg/mL, respectively (Table 3.1). SA-lipid combinations generally presented APX recrystallization profiles highly comparable with those for individual SA and lipids. No obvious change in APX recrystallization rate or extent was induced by the combination of SA with different lipids. The equilibrium APX concentration at 24 hrs with SA-PL combination was 72.1 ± 0.8 μg/mL, which was lower than the 85 ± 6 μg/mL for individual PL. The reduced concentration was corresponding to the decreased PL amount. A similar phenomenon was observed for the SA-G48 case; the equilibrium APX concentration was determined to be 63.7 ± 0.7 μg/mL as compared with the 69 ± 5 μg/mL for G48 alone. The equilibrium APX concentration for APX-SA-ATO was similar to that for APX-SA and APX-ATO.

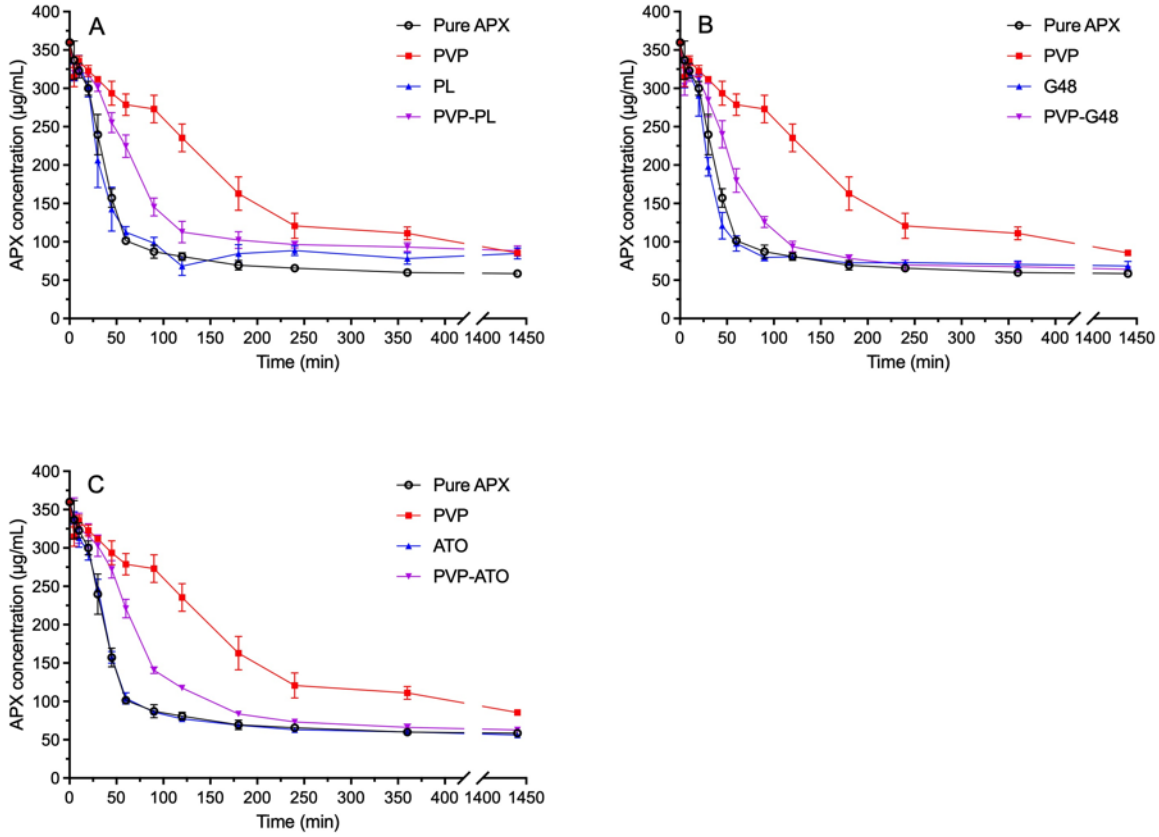

Figure 3.6. Recrystallization of APX in the presence of pre-dissolved (A) PVP-PL, (B) PVP-G48 and (C) PVP-ATO.

3.5 Discussion

In this section, it was revealed that the stability of supersaturated solutions of IDM and APX were influenced by polymer and lipid ASD carriers in different manners and these effects also are seen to depend on the properties of the drug compound itself.

3.5.1 Effects of polymer carriers on the stability of supersaturated solution of IDM and APX

Within the category of polymer ASD carriers, SOL showed the most substantial effect on both IDM and APX solutions, which is attributed to an ability to delay the onset of LLPS for both drugs. This can be observed from the recrystallization studies where a 6.95-fold improvement was achieved for the equilibrium concentration of IDM after a 24-hr recrystallization, and a 3.95-fold improvement was achieved for APX. The ability to maintain drug concentration exceeding crystalline

solubility by such large amounts indicated that SOL functions by delaying the precipitation of the dissolved drug, rather than by enhancing the dissolution of the drug. In the previous chapter (Chapter 2), we concluded that drug incorporation into SOL micelles was the main contributor for the stabilization of LLPS of IDM and APX. Here we see that the solubilization effect of SOL on crystalline IDM and APX appears to be weak. The large concentration gap between the solubilization and recrystallization endpoints for both IDM and APX (see Figure 3.7) also suggests that drug partitioning into a SOL micelle was more effective for the dissolved drug than the crystalline drug. As a result, SOL significantly improved the supersaturation of IDM and APX in the absence of obvious solubilization effects. These phenomena suggest that SOL could serve as an effective excipient for maintaining supersaturation concentrations for the ASD formulations of IDM and APX.

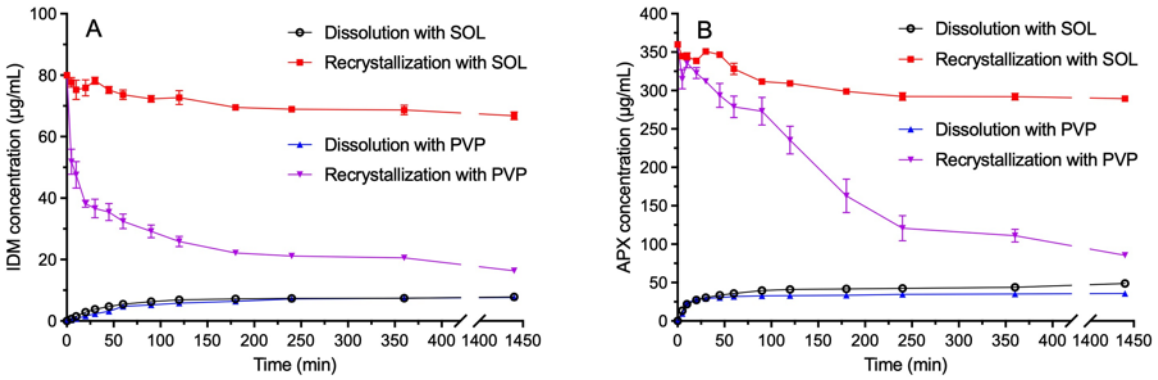

Figure 3.7. Comparison of dissolution and recrystallization profiles for (A) IDM and (B) APX in PVP and SOL solutions.

In comparison, PVP was only moderately effective at maintaining supersaturation of IDM, but had a strong effect for APX. For the case of IDM, the stabilizing effect of PVP on drug supersaturation did not align with its effect on the LLPS of the drug. It was possible for the supersaturated IDM solution to undergo a direct recrystallization process without passing the LLPS stage. The onset of LLPS for IDM was essentially unchanged by PVP indicating that phase separation of the IDM solution was not stabilized, and the formation of small crystalline clusters during LLPS experiment (Section 2.4.2) suggested the occurrence of nucleation upon stirring. The improved stability of IDM supersaturated solution upon recrystallization was considered as a result of inhibited growth rate of small crystals. Hydrogen bonding between IDM and PVP in solution could possibly

compete with self-association of IDM molecules during crystal growth process according to previous literature [95,201]. The carboxylic acid hydrogen of IDM bonded to the PVP carbonyl group reduces the formation of carboxylic dimer of IDM and therefore weakens the IDM aggregation [88]. The PVP amides also compete with IDM amides to bond to IDM carboxylic acid to weaken the IDM self-association. However, this mechanism was not effective enough to maintain the metastable state and LLPS of IDM. The slightly increased viscosity of PVP solution may also slow crystal growth. For APX, the ability of PVP to strongly stabilize both LLPS and supersaturation of APX that agreed with each other. Considering the absence of micelle in the PVP solution and similar viscosity when used for different drugs, the strong LLPS inhibition and supersaturation maintaining effect were seen as a result of APX-PVP hydrogen bonding. Similar to IDM, the APX amide could possibly bond to the PVP carbonyl group to attenuate APX nucleation. Such interaction should be more effective than the IDM-PVP interactions in terms of weakening phase separation and nucleation tendency, thereby placed different effects on different drugs. The selective interaction of a polymer with different drugs could be a determinant for the stabilization of drug supersaturation.

Similar to PVP, different behaviors were seen for the effect of SA on IDM and APX, where the stability of IDM supersaturated solution was significantly improved by SA, but no improvement was seen for APX. Given the ionic nature of IDM it is likely that the increased pH of dissolution medium induced by the dissolving of SA gives rise to both improved crystalline solubility and the large degree of stabilization of supersaturated solutions of IDM. The hydrogen bonding between IDM carbonyl group and SA hydroxyl group and alkyl-π interactions between SA methylene group and aromatic rings of IDM could also be positive factors for maintaining supersaturation. The alkyl-alkyl hydrophobic interactions of methylene of SA and methoxy group of IDM and the repulsive interaction between the IDM carboxyl group and SA carboxylate could negatively influence supersaturation maintaining. In this regard, the positive interactions between IDM and SA were seen to overweigh the negative ones. This can be seen by comparing the gap between recrystallization equilibrium and solubility of IDM with different excipients. The observed difference between the equilibrium IDM concentrations obtained for the solubilization (57.1 ± 0.2 μg/mL) and recrystallization tests (67.3 ± 0.3 μg/mL) in the presence of the same amount of SA was much smaller than that for SOL (10.1 ± 0.6 μg/mL vs 66.8 ± 1.2 μg/mL). This meant that a significant portion of supersaturated IDM concentration with SA was built upon the increased crystalline solubility, while SOL improved IDM supersaturation based on essentially unchanged drug solubility. The

solubilization effect of SA should be a result of ionic interaction with IDM, considering the alkaline property of SA and weak acid property of IDM. Therefore, the ionic interaction between SA and IDM was considered as a major contributor to the highly supersaturated IDM solution. The improvement in LLPS onset, crystalline solubility, and supersaturation maintenance for IDM were in agreement with each other. Higher concentrations of SA (as compared to those used for IDM) having much greater viscosities which in theory could aid in the stabilization of supersaturated solutions were also not effective for APX, indicating that viscosity did not contribute significantly to the stability of supersaturated IDM or APX solutions.

EC did not alter the crystalline solubility or stability of supersaturation solutions of IDM and APX due to its insoluble nature, consistent with it having no impact on the LLPS of IDM and APX. In spite of this observation, several studies have shown that small amounts of drug supersaturation could be achieved for EC-based ASD [95,202]. Based on our findings in this section, it is likely that this is the result of gradual release of amorphous drug payload, and that any supersaturation seen is results from the intrinsic properties of the drug molecules rather than any stabilizing effect from EC.

3.5.2 Effects of lipid carriers on the stability of supersaturated solution of IDM and APX

Amphiphilic PL and G48 improved the stability of supersaturated IDM solutions, while they showed no effect on the stabilization of APX supersaturated solutions. The increased crystalline solubility of IDM (Section 3.4.1) was considered as the first reason for PL and G48's ability to improve IDM supersaturation. The increased crystalline solubility, as expressed by the equilibrium IDM concentration from the solubilization test, constantly decreased the supersaturation degree and Gibbs free energy of IDM solutions at each timepoint during recrystallization test. Both nucleation and crystal growth rate could be slowed by the net decrease in the gap between drug solubility and supersaturated concentration. The gap between endpoint concentrations of the solubilization and recrystallization tests for G48 was small, suggesting IDM recrystallization is the main mechanism by which the solution decreases its free energy. In comparison, the large concentration gap observed for PL suggested that an additional contribution arising from the supersaturation of dissolved IDM in addition to solubility enhancement gave rise to the stability of the system. This contribution is attributed to the stabilized LLPS of IDM by PL. The metastable state was prolonged by PL and solute concentration was maintained during the early stage of recrystallization test. Therefore, PL could

provide a greater stabilizing effect on IDM supersaturation. In contrary to the obvious improvement in IDM supersaturation, when PL and G48 were used to stabilize supersaturated APX solutions, the weak ability of these excipients to maintain supersaturation is attributed to their facilitating LLPS. Although PL and G48 increased the crystalline solubility of APX, the LLPS state was not stabilized and APX recrystallization kinetics were essentially unchanged. The stability of a supersaturated drug solution under non-sink condition was observed to rely on the specific drug-lipid interactions and a prolonged metastable LLPS state.

ATO did not influence the recrystallization rate of IDM or APX due to its insoluble nature resulting in negligible to no change in solution properties including drug solubility or recrystallization rate. Here it is noted that for an excipient defined as insoluble it may have a reported solubility representing the scarce amount that dissolves in water; pharmaceutically this is defined as 1 part of solute dissolving in 10,000 or more parts of solvent. Such a minimal amount of a dissolved hydrophobic solute could potentially facilitate the aggregation of other solutes through hydrophobic interactions; the results in this section indicate that this did not occur in the presence of ATO in agreement with the LLPS results in Chapter 2. Therefore, the drug release profile from ATO-based ASDs during dissolution is considered as a reflection of the normal drug release behavior and the intrinsic recrystallization rate for the drugs themselves.

3.5.3 Effects of polymer-lipid combinations on the stability of supersaturated solution of IDM and APX

Generally, the effect of the combination of a polymer and a lipid on the supersaturation stability of IDM and APX was observed to be between the effects seen for the corresponding individual components. Interestingly, for the PVP-PL combination that had a synergistic effect on the LLPS stabilization of IDM, its effect on the stability of an IDM supersaturated solution did not show the same synergism. A possible mechanism for this difference could be the removal of nanodroplets by filtration during the sample preparation process commonly used for dissolution testing. Reviewing the experimental procedures of LLPS determination, the solution properties are reflected by the UV absorption and extinction upon titration of drug stock solutions, and no filtration is carried out due to the limited size of sample (100 μL) for each UV measurement. The formation of nanodroplets of any size will be seen as a change in UV extinction. In comparison, commonly used dissolution test protocols are coupled with HPLC-UV quantification methods requiring that samples are in a fully

dissolved state. A filtration process with 0.22 μm or 0.45 μm filter membrane is required to treat dissolution aliquot samples, meaning that nanodroplets with a size greater than the pore diameter could possibly be removed. The major peak size of unfiltered PL vesicles was determined in our work to be 886 ± 109 nm according to dynamic light scattering, corresponding to the large size of C18:0 phospholipid vesicle. After filtration with 0.45 μm PES membrane, the major size of PL was determined to be 347 ± 5 nm, corresponding to the size of C16:0 phospholipid vesicle. While the vesicles themselves are a dynamic structure such that filtration through a narrow pore size will decrease the overall size of vesicles without a net loss of material, it is also possible that, given these droplet sizes, a certain amount of vesicles containing drugs could theoretically be removed by the filtration step. This would result in the drug concentration determined from dissolution tests would be lower than the concentration in the original (unfiltered) solution. In such a case any stabilizing effect of PVP-PL on the LLPS of IDM could be masked by this mechanism. Additionally, LLPS was considered to influence the early stage of drug recrystallization since it is the step prior to nucleation and crystal growth. The later stages of drug recrystallization profile relied more on the inhibition of crystal growth and an enhanced crystalline solubility. This could result in recrystallization kinetics for PVP, PL and PVP-PL combination that are all comparable. All other PVP-lipid combinations with either IDM or APX resulted in effects on recrystallization that were comparable to the effect observed for the individual PVP and lipid excipients.

SA-lipid combinations presented IDM recrystallization profiles governed by SA, regardless of lipid type. This was a result of the strong ability of SA to maintain supersaturation of IDM as a result of ionic interactions, even with a decreased amount of SA in the binary SA-lipid carriers. With APX, the SA-lipid combinations did not change the drug recrystallization profile due to a lack of interaction between the ionic SA and the non-ionic APX.

Combinations of EC with lipid demonstrated weaker effects on the recrystallization of IDM than observed for the lipids alone, likely because of the reduced amount of amphiphilic lipid present in the binary EC-lipid mixtures. This observation is consistent with the LLPS results for IDM that showed the EC-PL and EC-G48 provided an LLPS stabilization that was an average of the effect observed for EC, PL, and G48 alone. The moderate inhibition of IDM recrystallization within first 10 min could be the result of LLPS stabilization of IDM by EC-PL or EC-G48, with the increased recrystallization observed at later times being consistent with this since LLPS stabilization mainly has an effect on the early stage of the recrystallization process. EC-lipid combinations did not result in

any change to the APX recrystallization profile as no synergistic or antagonistic effect was induced by the combinations.

3.6 Conclusion

In this chapter, it was observed that polymer and lipid carriers produced different stabilizing effects on supersaturated solutions of IDM and APX. These effects were considered to result from different mechanisms including in-solution hydrogen bonding, incorporation of drug in excipient micelles and pH-induced solubility change. Generally, the supersaturation and recrystallization behaviors of IDM and APX were not correlated with their LLPS behaviors in the presence of same ASD carriers, as LLPS only influenced the early stage of recrystallization. The overall kinetic solubility profiles of IDM and APX were more governed by the inhibition of drug crystallization by excipients after the occurrence of LLPS and nucleation, which was determined by the mentioned mechanisms. All polymer-lipid combinations showed an averaged effect on the stabilization of supersaturated drug solutions for IDM and APX, without generating synergistic or antagonistic effects. The previously revealed synergistic effect of PVP-PL combination on the LLPS of IDM (Chapter 2) did not convert to better maintained supersaturated concentrations of IDM, as the concentration of IDM in separated nanodroplets was not counted as supersaturated concentration following the experimental condition of dissolution testing. The information revealed in this chapter will be used to facilitate the analysis of dissolution and supersaturation behaviors of ASDs of IDM and APX prepared with different carriers.

Chapter 4
Fluorescence techniques to determine drug amorphization and miscibility between drug and ASD carriers

Portions of this chapter have previously been published in the Canadian Journal of Chemistry:

Huang J, Chen PX, Wettig S. Fluorescence-based techniques to assess the miscibility and physical stability of a drug–lipid complex. Canadian Journal of Chemistry. 2019;97(6):496-503.

Experimental studies of this chapter were planned by me in consultation with Dr. Wettig. All experiments were carried out by me at the University of Waterloo. I was responsible for data analysis of the results and created the initial draft of the manuscript. Dr. Peter X Chen provided assistance in the analysis of fluorescence spectra results. Dr. Wettig edited the various drafts of the manuscript and contributed to the discussion of the experimental results and to the overall conclusions that resulted.

4.1 Abstract

The purpose of this chapter was to evaluate the feasibility of using fluorescence-based techniques to assess the drug-excipient miscibility for indomethacin (IDM) and apixaban (APX) under solvent-free conditions. The miscibility results were used as an indication of the degree of drug amorphization in ASD carriers. Thin film ASD systems for IDM and APX with different drug loadings were prepared with selected polymer and lipid excipients and characterized by fluorescence spectroscopy and fluorescence microscopy based on the autofluorescent properties of the drug molecules. Spectral parameters including peak shape, peak intensity and peak wavelength were used to analyze drug-excipient miscibility and physical state of IDM and APX in ASD systems. Distribution of fluorescence intensity and birefringence properties of fluorescence microscopy were also used to analyze the drug-excipient miscibility. The miscibility between drug and ASD carriers varied with carrier type. Both amorphous-amorphous phase separation and amorphous-crystalline transformation could be identified and used to assess the drug amorphization state in an ASD formulation.

4.2 Introduction

Various techniques have been used to evaluate the drug-excipient miscibility and physical state of a drug in an ASD formulation. Differential scanning calorimetry (DSC) and powder X-ray diffraction (PXRD) are the most common techniques used to evaluate these properties based on the change in thermal profile and diffractogram induced by drug amorphization and loading in ASD carriers. For DSC, when the characteristic endothermic peaks of two individual components show obvious peak elimination, new peak emergence, change in peak shape, or onset after complexation, different levels of miscibility can be concluded. PXRD is used to evaluate the crystallinity of ASD formulations based on changes in position and intensity of characteristic peaks that result from the crystalline drug. These techniques have limitations for the characterization of lipid based ASDs. The thermal motion of lipids induced by the ramping temperature during DSC characterization may change the physiochemical properties of the formulations. Drug payloads can partially dissolve in the melting lipids when the temperature reaches the phase transition temperature for lipid that is lower than the melting point of loaded drug, thus altering the formulation properties during characterization. A disadvantage of the PXRD method is that it may be ineffective to detect the amorphous-amorphous separation that occurs in the early stage of phase separation, as no crystallinity is expected for this state. Scanning electronic microscopy (SEM) and transmission electronic microscopy (TEM) have been employed to evaluate drug-excipient miscibility through visualization and can effectively achieve a high spatial resolution; however, these techniques cannot chemically identify different phases. Identifying components in different phases by SEM or TEM is often based on the known morphology of the component unit(s) (i.e., shape and structure). The identification may be less effective if two phases are without highly organized structures or clear shape boundaries such as the early stage of amorphous-amorphous separation. Raman spectroscopy is another technique that can be used to assess the miscibility between different components and enables the chemical identification of different phases, but it often requires long experiment time. Additionally, IR spectroscopy and solid state nuclear magnetic resonance spectroscopy have been employed to evaluate the drug-excipient miscibility.

Fluorescence spectroscopy and fluorescence microscopy have been used for decades with great success in many fields across a broad range of physical, chemical, biological, and medical sciences. They enable non-destructive characterizations based on the specific localization of fluorescent molecules, mainly in solutions. Of late, fluorescence spectroscopy has been employed to

characterize the active pharmaceutical ingredients in tablets and distinguish the solid forms (solvate, cocrystal, amorphous, and polymorph) of insoluble drugs. These advances allow for new quality assessment methods for solid dosage forms whose physiochemical properties are influenced by amorphization through pharmaceutical processes, including milling, granulation, compaction, freeze-drying, etc. More recently, the crystallization of amorphous drug in polymer-based solid dispersions has been successfully investigated using solid-state fluorescence techniques.

In this chapter, we investigated the feasibility of using fluorescence-based techniques to evaluate the drug-excipient miscibility for IDM and APX with various excipients including lipid carriers. Previous studies have demonstrated that APX has detectable fluorescence intensity in aqueous media and so we also sought to expand the application of fluorescence spectroscopy and fluorescence microscopy techniques to the miscibility assessment of APX solid formulations based on the hypothesis that APX was autofluorescent under a solid state. The proposed methods are expected to distinguish between two types of phase separation, namely amorphous-amorphous separation and amorphous-crystalline transformation, for accurately evaluating the drug amorphization and drug loading in ASD carriers. Crystal shape can be a factor that identifies different phases. The chemical identification of different domains is also based on their different fluorescence behaviors, including peak position for fluorescence spectroscopy and fluorescence intensity distribution for fluorescence microscopy, that correspond to the varying fluorophore property in different chemical environments. Fluorescence-based techniques are expected to combine with conventional techniques to provide more accurate information about drug-excipient compatibility, benefiting both quality assessment and formulation design.

4.3 Materials and methods

4.3.1 Materials

Indomethacin (IDM, purity > 97.5%), ethanol (HPLC grade), methanol (HPLC grade), ethyl acetate (HPLC grade) and ethyl cellulose were purchased from Fisher Scientific (Hampton, NH, USA). Apixaban (APX, purity > 99%) was purchased from HuiRui Chemical Technology Co., Ltd (Shanghai, China). Poly (vinylpyrrolidone) (PVP) K90 and phospholipid were purchased from Sigma-Aldrich (Mississauga, ON. Canada). The phospholipid used in this study (Sigma-Aldrich catalog no. P3644) contains 55% phosphatidylcholine, 25% phosphatidylethanolamine and other phospholipids, with an average molecular weight of 776 g/mol. Polyvinyl caprolactam-polyvinyl

acetate-polyethylene glycol graft co-polymer (Soluplus®, SOL) was a gift from BASF (Ludwigshafen, Germany). Sodium alginate (CAS number: 9005-38-3) was obtained from Acros Organics (USA). PEG-32 stearate (Gelucire® 48/16, G48) and glyceryl behenate (Compritol® 888 ATO) were a gift from Gattefosse (Saint-Priest, France). Water used in this study was obtained from a Millipore Milli-Q system.

4.3.2 Preparation of drug-ASD carrier thin film samples

Thin films of drug and ASD carriers were prepared using a drop casting method. IDM and the excipient of interest were dissolved in organic solvents at different weight ratios (0:10, 1:9, 2:8, 3:7, 4:6, 5:5, 6:4, 7:3, 8:2, 9:1, 10:0) to produce a solution with a total concentration of 10 mg/mL. Ethanol was used to dissolve IDM with PVP, SOL, EC, PC, and G48. SA does not dissolve in ethanol or other organic solvents commonly used for ASD preparation, as such the prepared samples were suspensions where IDM fully dissolved, and SA existed as solid particles suspended in the solvent. Ethyl acetate at 90°C was used to dissolve the IDM/ATO samples. Other than those containing SA, all samples were determined to be fully dissolved state based upon visual inspection. The same weight ratios were used to prepare APX samples, but at a total concentration of 1 mg/mL due to the low solubility of APX in the organic solvent. DMSO can provide a solubility of more than 10 mg/mL for APX; however, it is not suitable for the drop casting method due to a slow evaporation rate. Methanol was used to prepare APX stock solutions with carriers including PVP, SOL, SA, EC, PC, and G48 and a binary solvent of methanol: ethyl acetate (1:1 v/v) was used to dissolve APX with ATO at 90 °C.

4.3.3 Methodology development for fluorescence spectroscopy

The objective of fluorescence spectroscopy in this study is as a means to evaluate the polarity of the environment of the drug payload in an ASD thin film using characteristics of the emission peaks. The emission peak wavelength of a fluorescent substance is a constant value regardless of the excitation wavelength applied; however, drugs formulated in ASD films can exist in both crystalline and/or amorphous states, which can have different emission peaks. Although the emission peak wavelengths for crystalline and amorphous drug do not vary with excitation wavelength, the separation of these signals relies on the selection of a suitable excitation wavelength due to possible overlap of the signal components. According to our preliminary experiments, the emission signal in a spectrum can be affected by different phenomena including 2nd order transmission, Raman signal and

sample thickness. These parameters are rarely investigated in related studies and need to be optimized for the fluorescence spectra experiment for IDM and APX.

320 nm, 335 nm, and 355 nm were used as excitation wavelengths to obtain the emission spectra of crystalline IDM and IDM-PL (10% w/w) on a SpectraMax M5 plate reader (Molecular Devices, LLC., USA). Fluorescence emission signal was recorded from 250 nm to 850 nm with a step size of 1 nm. The emission spectra of blank 96-well plate under these same excitation conditions were measured as a baseline. During our preliminary experiments, we also found that the thickness of the sample could influence the emission spectrum of the tested drug by altering the baseline signal. This effect was also observed for non-fluorescent materials, and therefore it was accounted for by including 60, 120, or 180 μL of pure water added to the blank plate and the fluorescence emission spectra were recorded from 420 nm to 700 nm with λ_{ex} =355 nm.

4.3.4 Fluorescence spectroscopy to determine drug-ASD carrier miscibility

Samples for fluorescence spectroscopy were prepared by dropping 60 μL of the solution of interest into a well of a 96-well plate and left to dry under ambient conditions for 8 h. Samples were further dried overnight in a vacuum oven at room temperature to remove any residual solvent. The emission spectra of IDM-ASD carrier thin films were recorded over the range of 420-600 nm, with an excitation wavelength of 355 nm and a step size of 1 nm. The emission spectra of APX-ASD carrier thin films were recorded over the range of 400-508 nm with an excitation wavelength of 280 nm and a step size of 1 nm.

4.3.5 Fluorescence microscopy to determine drug-ASD carrier miscibility

For fluorescence microscopy measurements, 10 μL of the solution of interest was dropped onto a glass slide cover and left to dry under ambient condition for 8 h. Samples were further dried overnight in a vacuum oven at room temperature to remove any residual solvent.

The miscibility and phase separation of IDM and APX thin films were assessed using an EVOS fluorescence microscope. IDM films were assessed on an Alexa 488 GFP (green fluorescent protein) channel, and APX films were assessed on a DAPI (4′,6-diamidino-2-phenylindole) channel based on the emission spectra obtained in the fluorescence spectroscopy studies described above. All samples were assessed on day 0, day 7, day 14, and day 21 after preparation. The thin films were stored under vacuum at 40 °C when not being measured.

4.4 Results

4.4.1 Illustration of baseline signal components of an emission spectrum

An emission scan (250 nm to 850 nm) of a blank plate with an excitation wavelength of 355 nm is shown in Figure 4.1. The large peak at 355 nm corresponds to the excitation signal that is coupled with a 2nd emission signal at 710 nm due to the 2nd order transmission of the excitation signal. As shown in Figure 4.1 (B), an asymmetric shape is observed for the excitation peak, and the tailing signal extended to 480 nm region resulting from the overlap of the Raman diffusion and excitation signals. The wavelength relationship between excitation, Raman diffusion, and 2nd order emission is shown in Figure 4.2 [203].

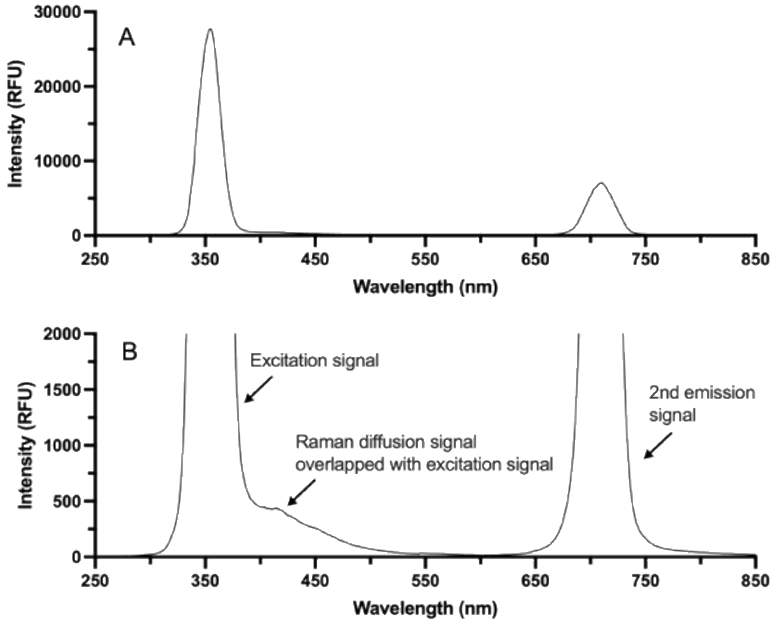

Figure 4.1. Excitation and emission signal of a blank 96-well plate in (A) full scale and (B) zoom-in view.

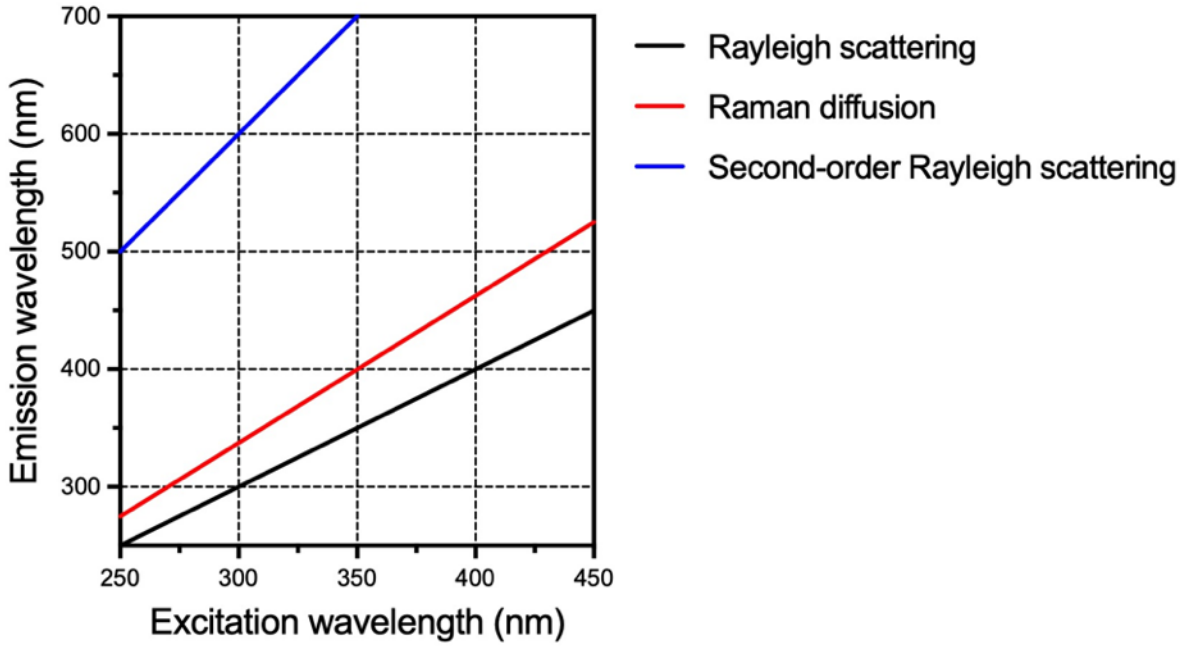

Figure 4.2. Wavelength relationship between excitation, Rayleigh scattering, Raman diffusion and second-order emission.

Our preliminary measurements showed that the emission peak for crystalline IDM occurs at 460 nm with the blue shoulder of the emission peak beginning between 430 nm to 440 nm. The emission peak of amorphous IDM occurs at 508 nm. In order to observe the changes in emission associated with different degrees of amorphization of the drug, it is necessary to select an excitation wavelength where its Raman diffusion signal has minimal overlap with the blue shoulder (430 nm) of the drug emission peak. Similarly, the blue shoulder of the 2nd emission peak should have minimal overlap with the emission peak of amorphous IDM (508 nm). For excitation wavelengths of 320 nm, 335 nm and 355 nm, the 2nd order emission peak wavelengths were 640 nm, 670 nm, and 710 nm, respectively. The Raman signal moved with the excitation wavelength and overlapped with the excitation signal in different amounts, as shown in Figure 4.3. Based on the desired minimal signal overlapping, 355 nm was selected as excitation wavelength and emission spectra were obtained from 420 nm to 600 nm.

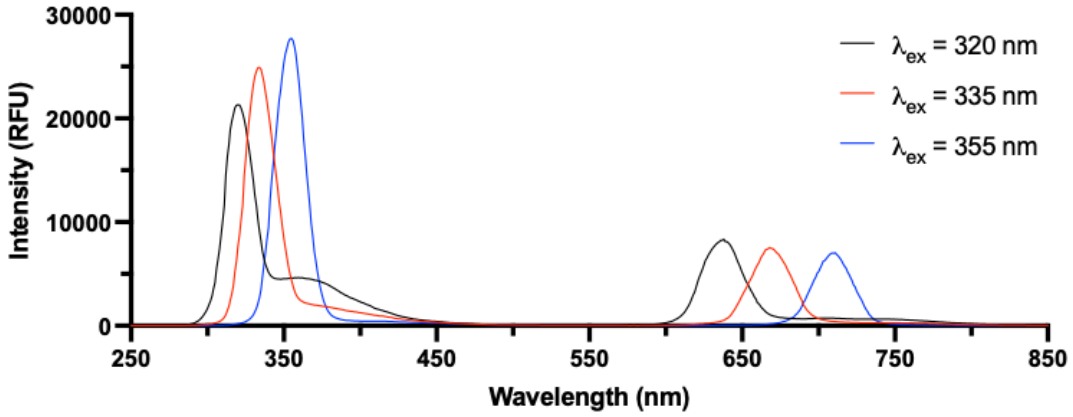

Figure 4.3. Excitation and emission signal of a blank 96-well plate with different excitation wavelengths (λ_{ex}).

After optimizing the excitation wavelength, we noticed that a thicker sample gave rise to a higher fluorescence intensity at 420 nm, and the blue shoulder of the 2nd emission peak observed at lower wavelengths with higher intensities. The emission spectra of volumes of water (corresponding to different thicknesses of sample) are shown in Figure 4.4. The observed emission peaks could result from the trace amount of organic impurities and/or the formation of reactive oxygen species, particularly hydroxyl radicals, when water is exposed to ultraviolet excitation during measurement [204]. Water samples had an obviously higher fluorescence intensity compared to the blank plate. 120 μL and 180 μL samples showed similar profiles, which might be the limit of thickness influence. The thickness effect brought certain considerations for the spectra processing method used in our study. Variation of the drug-excipient weight ratio can result in thin films of different thickness since the two components of the mixture will have different contributions to the overall film thickness due to different packing densities. Therefore, the subtraction of the emission spectrum obtained for the pure excipient (which should not emit in our experimental emission range) from that obtained for the sample could give rise to an experimental artifact at different drug excipient ratios. As a result, the blank plate signal was subtracted from the fluorescence spectra obtained in this study.

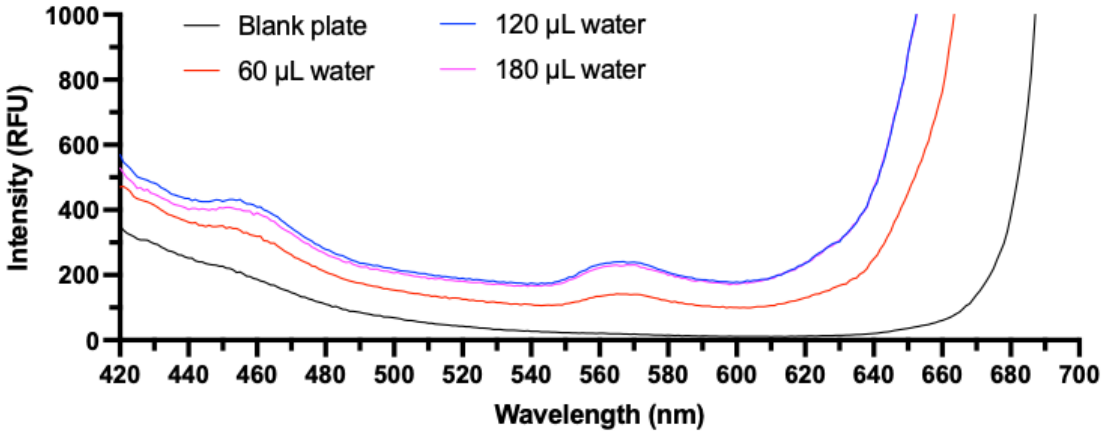

Figure 4.4. Emission signal of water samples with an excitation wavelength of 355 nm.

Based on these considerations, the fluorescence spectra of IDM samples were measured from 420 nm to 600 nm with an excitation wavelength of 355 nm. The fluorescence spectra of APX samples were measured from 400 nm to 510 nm with an excitation wavelength of 280 nm. A step size of 1 nm was used for both drugs. All spectra were subtracted with blank plate signal that was obtained for the corresponding excitation wavelength.

4.4.2 IDM amorphization and miscibility between IDM and ASD carriers

The change in the local polarity of a fluorescent probe is reflected by the change in its emission spectra, and this characteristic is used in this chapter to evaluate the extent of amorphization and the drug-excipient miscibility of IDM ASD systems. As shown in Figure 4.5, the spectrum of pure crystalline IDM has an emission peak at 464 nm, while amorphous IDM (loaded in SOL carrier) has an emission peak wavelength at 508 nm, red-shifted relative to pure IDM. The emission peak of 464 nm is an intrinsic characteristic of crystalline IDM, and the red shift of the emission profile can be explained by the polarity difference between the two samples. Crystalline IDM corresponds to a homogeneous drug-rich phase in which all IDM probes share a polarity environment consisting of the same IDM molecules. In contrast, for an IDM ASD sample with low drug loading, IDM is expected to uniformly disperse in the drug carrier to form a homogeneous solid solution, in which IDM is surrounded predominantly by excipient molecules; i.e., IDM in an amorphous phase. The local

environment of IDM is considered less polar in a crystalline phase, while the polarity of the IDM-excipient mixture is larger due to the hydrophilicity of the drug carrier structures and of IDM in its amorphous state. The results confirmed that the emission signal of IDM is sensitive to the local environment and IDM could be used as a probe to assess the phase distribution of IDM ASDs without the addition of another fluorescence probe.

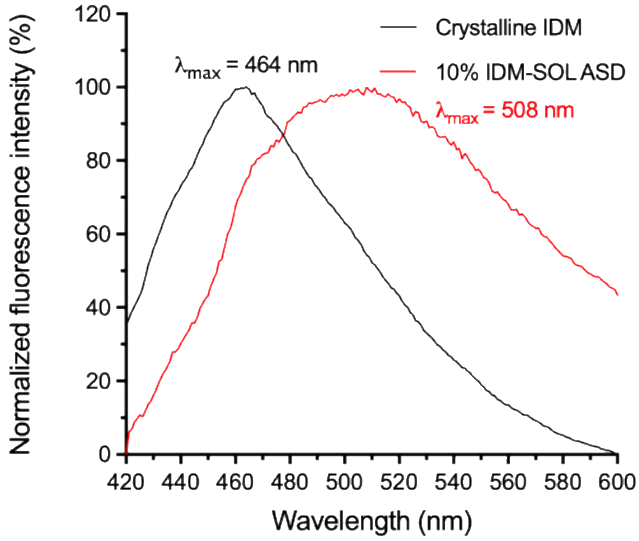

Figure 4.5. Fluorescence emission spectra of crystalline IDM and 10% (w/w) IDM-SOL ASD with an excitation wavelength of 355 nm.

(a) IDM-PVP miscibility

The fluorescence spectra of IDM-PVP films showed a large emission peak in the region of 508 nm for the drug loading amounts of 10% to 90% (Figure 4.6). The overall fluorescence intensity of a sample was proportional to the drug content. Additionally, beginning at drug loading amounts of 50% a tiny separation in emission peak was observed between the 470 nm and 510 nm region.

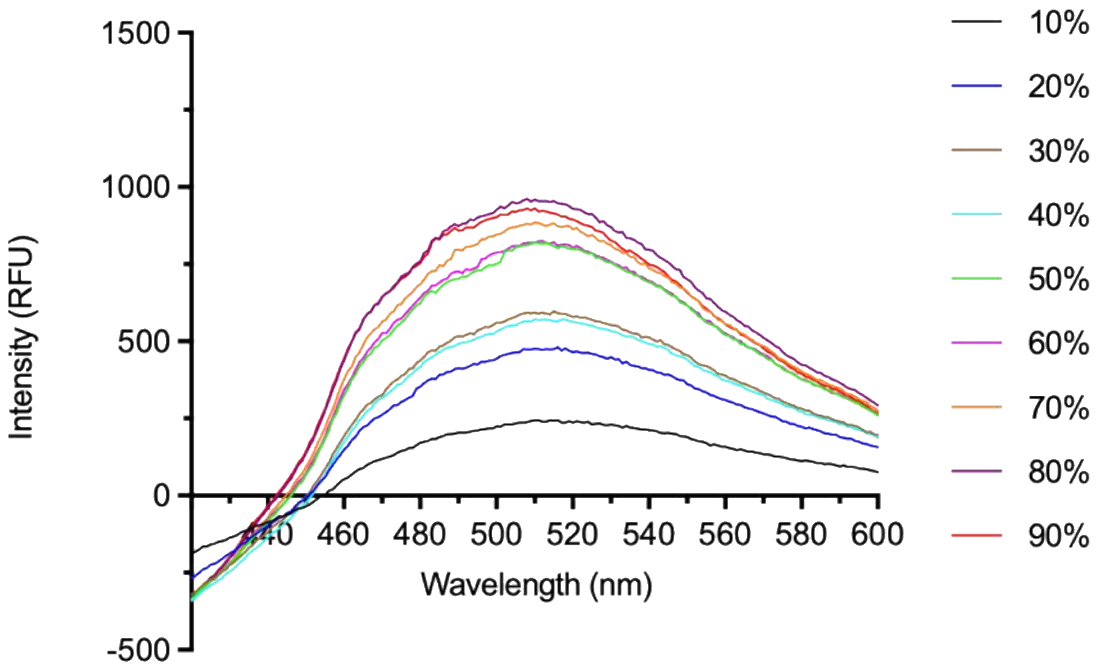

Figure 4.6. Fluorescence emission spectra of IDM-PVP ASDs. Percentage refers to drug loading degree (w/w).

Fluorescence imaging results were used to facilitate the analysis of drug-excipient miscibility (see Figure 4.7). For IDM-PVP with 10% and 20% (w/w) drug loading, a homogeneous fluorescence was observed from the prepared samples. For samples with a drug loading from 30% to 50%, non-homogeneous fluorescence was revealed by the appearance of small round-shape regions. These regions presented similar fluorescence intensity to the bright background and showed distinguishable edges with lower fluorescence intensity. With a further increasing drug loading, the density of these non-homogeneous fluorescent regions increases, corresponding to a larger amount of immiscible IDM content. The immiscible regions showed clear boundaries and embedded domains with lower fluorescence intensity; however, no needle-shaped domains corresponding to crystalline IDM could be observed for samples exhibiting the immiscible phases.

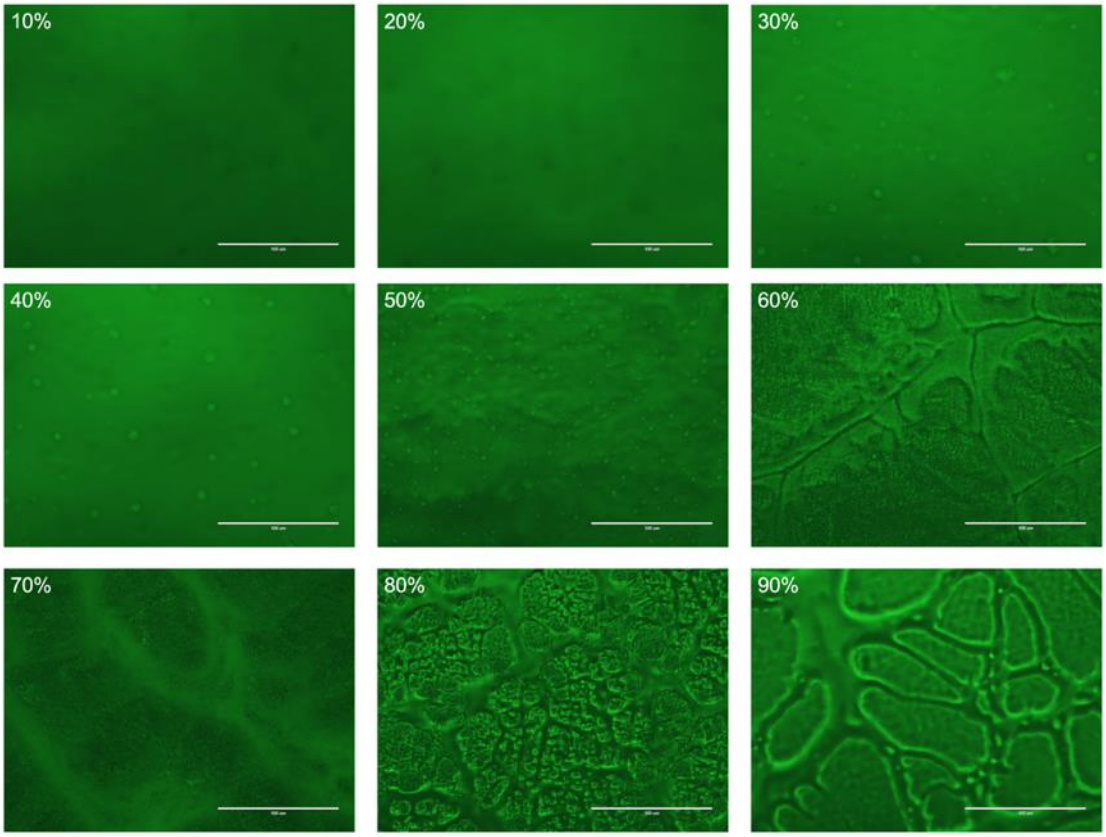

Figure 4.7. Fluorescence images of IDM-PVP ASDs after preparation. Percentage refers to drug loading degree (w/w). Scale bar is 100 μm.

After storage at 40 °C for 1 week, the sample with 10% drug loading still showed a homogeneous fluorescence distribution as initial measured; however the non-homogenous fluorescence patterns attributed to immiscibility were now observed at 20% drug loading instead of at 30% as initially measured. Again, no crystalline characteristics could be observed in any of the samples. After 2 weeks, the 10% drug loading sample also started to exhibit the bright dots associated with immiscibility describing the development of amorphous-amorphous phase separation as a function of time. Samples that initially showed immiscibility continued to remain in an amorphous-amorphous phase separated state without developing obvious crystalline domains. The IDM-PVP miscibility was weakened by increasing drug content and storage time. Additional figures for the 1, 2, and 3 week images are provided in Figure B-1 to B-3 in Appendix.

(b) IDM-SOL miscibility

IDM-SOL showed increased fluorescence intensity for samples with higher drug loading, but the fluorescence intensities for drug loading over 40% became more similar, as shown in Figure 4.8. Fluorescence spectra for all samples showed the broad peak centered in the 508 nm region characteristic of amorphous IDM, as obtained for IDM-PVP. IDM-SOL films with 10% to 30% drug loading were again observed to be homogeneous in nature (see Figure 4.9). An increasing amount of immiscible domain could be observed beginning with the 40% sample, with similar fluorescence intensity to the homogeneous background. At 50%, the immiscible domains began to show a nonhomogeneous fluorescence distribution and birefringence properties. In contrast to the IDM-PVP system the miscibility for all samples was compromised under the accelerated storage condition of 40 °C. After storage for 1 week, tiny separations could be observed for samples with low drug loading of 10% and 20% in contrast to IDM-PVP where the 10% was unchanged after 1 week. Other samples showed an increase in both density and size of immiscible domains. All samples showed a further development in phase separation after heating for 2 weeks. After 3 weeks, the 80% drug loaded sample showed not only amorphous domains, but the first observation of separated clusters with a needle shape that is characteristic of IDM crystal formation (see Figure 4.10). Figures for the 1 and 2 week samples stored at 40°C are provided in Figure B-4 to B-5 in Appendix.

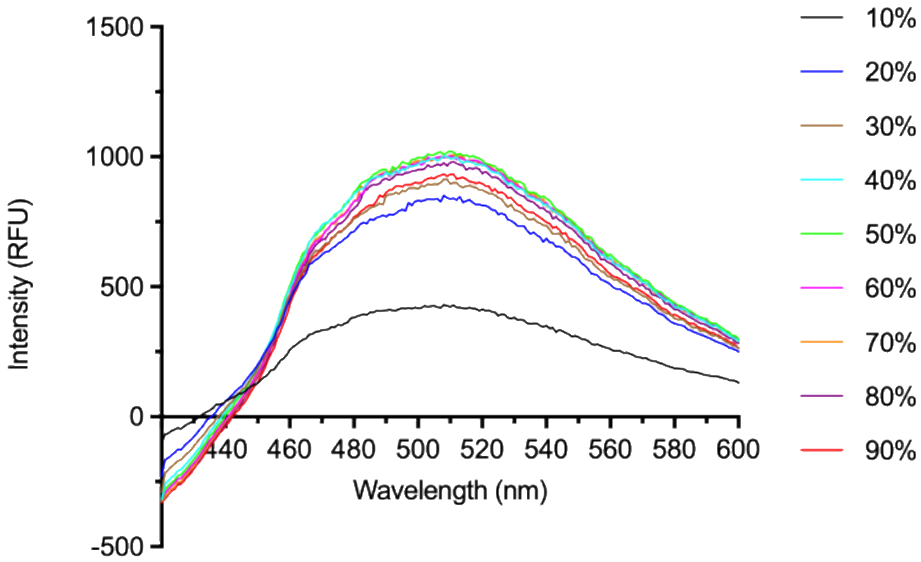

Figure 4.8. Fluorescence emission spectra of IDM-SOL ASDs. Percentage refers to drug loading degree (w/w).

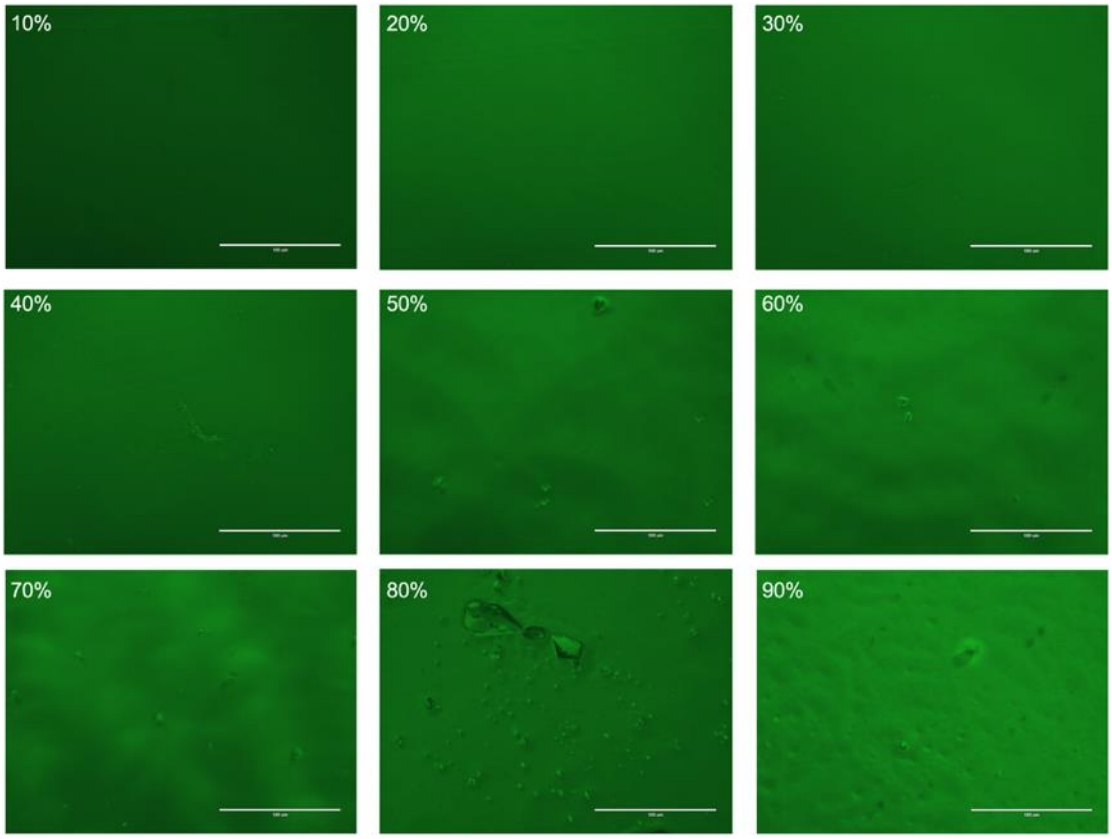

Figure 4.9. Fluorescence images of IDM-SOL ASDs after preparation. Percentage refers to drug loading degree (w/w). Scale bar is 100 µm.

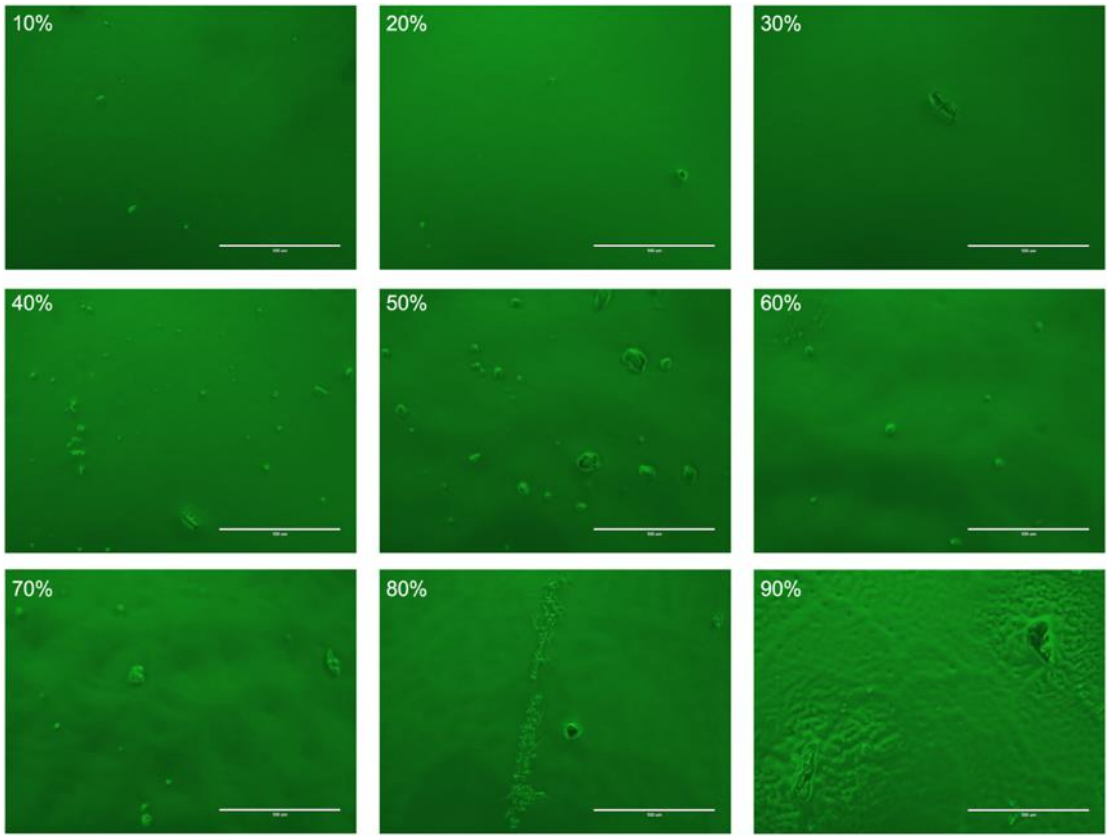

Figure 4.10. Fluorescence images of IDM-SOL ASDs after 3-week heating. Percentage refers to drug loading degree (w/w). Scale bar is 100 μm.

(c) IDM-SA miscibility

The fluorescence spectra obtained for the IDM-SA ASD system exhibited a shoulder peak at approximately 464 nm that increased with increasing drug loading, markedly different from spectra obtained for IDM-PVP and IDM-SOL (Figure 4.11 vs Figures 4.6 and 4.7). All samples continued to have the broad emission peak at 508 nm characteristic of amorphous IDM. Possible reasons for the appearance of the shoulder at 464 nm will be discussed later in the chapter.

Fluorescence microscopy results showed immiscibility for all IDM-SA samples (Figure 4.12). Immiscible domains could be observed for samples starting with 10% drug loading, showing both birefringence characteristics for crystalline clusters and halo shapes for amorphous-amorphous phase separation. The phase separation and recrystallization of IDM-SA samples developed continuously under the accelerated storage condition. After heating for 3 weeks, the immiscible

domains showed a significantly higher fluorescence as compared to the homogenous background. Figures for the 1, 2, and 3 week samples at 40°C are provided in Figure B-6 to B-8 in Appendix.

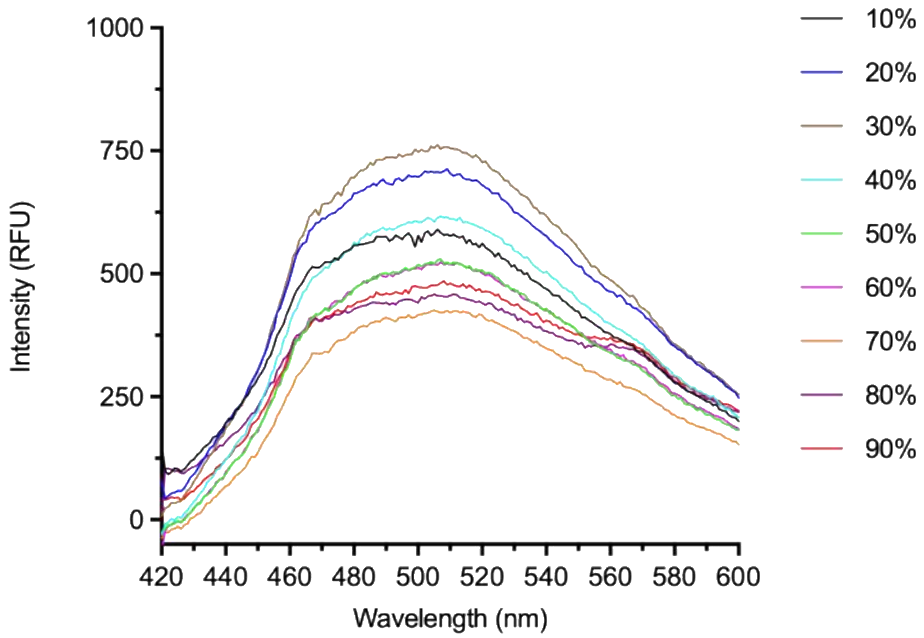

Figure 4.11. Fluorescence emission spectra of IDM-SA ASDs. Percentage refers to drug loading degree (w/w).

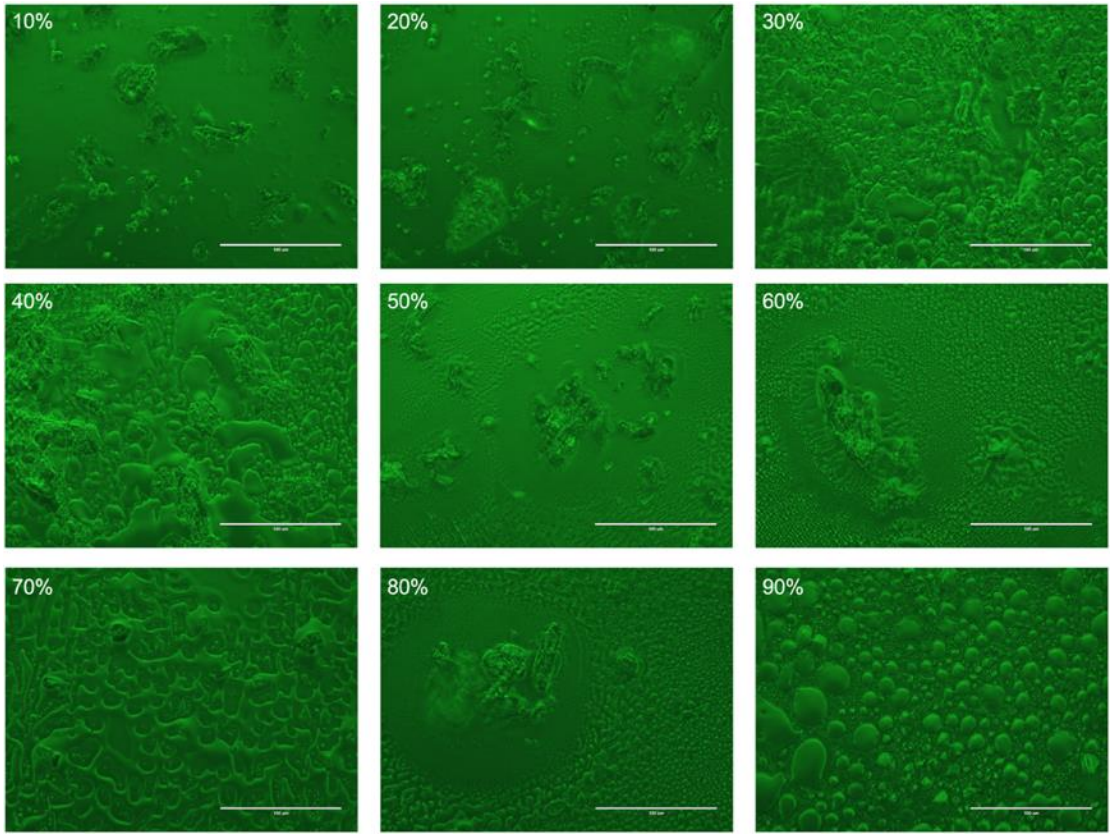

Figure 4.12. Fluorescence images of IDM-SA ASDs. Percentage refers to drug loading degree (w/w). Scale bar is 100 μm.

(d) IDM-EC miscibility

As seen for the IDM-PVP samples the spectra for IDM-EC samples generally showed an increase in fluorescence intensity with increasing drug loading (Figure 4.13) with a broad emission peak at 508 nm again consistent with IDM being in an amorphous state. A slight peak separation in emission spectra could be observed for samples with drug loading more than 70%, corresponding to a non-homogeneous distribution of IDM molecules in these ASD samples.

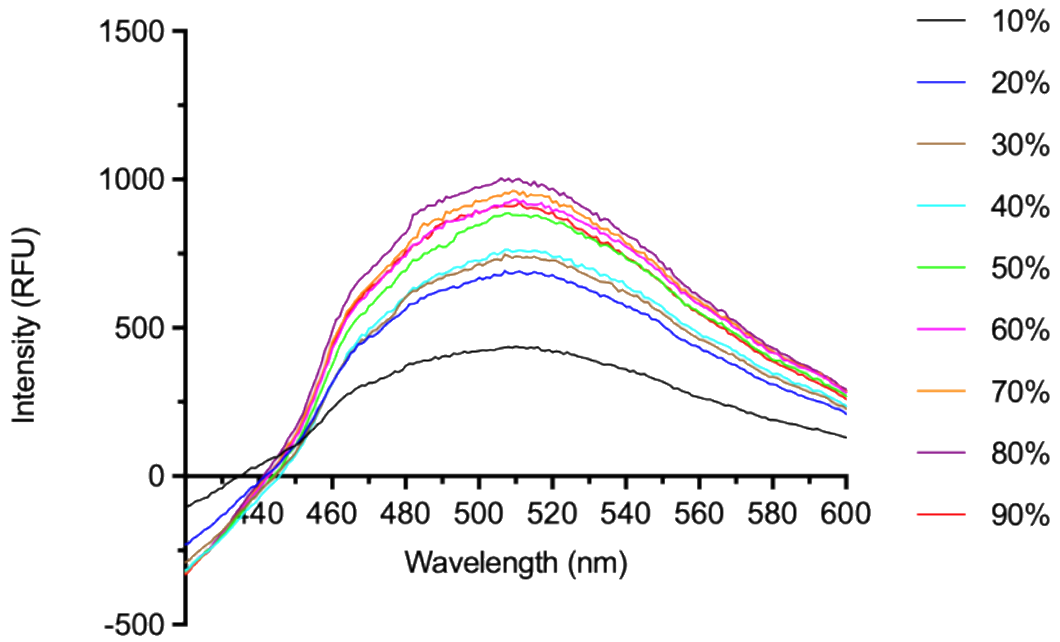

Figure 4.13. Fluorescence emission spectra of IDM-EC ASDs after preparation. Percentage refers to drug loading degree (w/w).

Interestingly in contrast to the fluorescence spectra an amorphous-amorphous phase separation was observed for all samples based upon the fluorescence imaging results (see Figure 4.14). Immiscible domains could be observed that had higher fluorescence intensity compared to the background, suggesting an increased concentration of IDM within these domains. The amorphous-amorphous phase separation became more obvious with increasing drug amount. Starting with 30% drug loading, birefringence properties could be observed for some of these domains, indicating the crystalline nature of these domains. The size, density, and birefringence properties of these domains did not exhibit any obvious change over 3 weeks when stored at 40 ºC. Images for the 1, 2, and 3 week samples are provided in Figure B-9 to B-11 in Appendix.

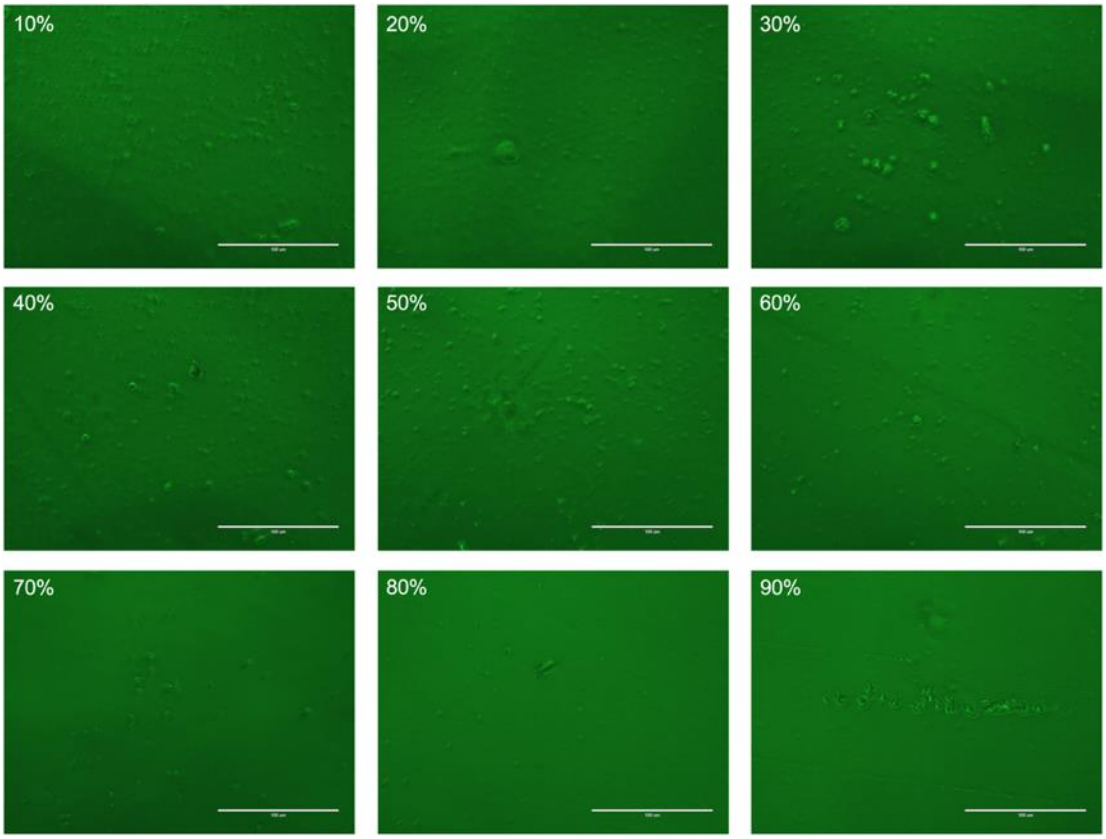

Figure 4.14. Fluorescence images of IDM-EC ASDs. Percentage refers to drug loading degree (w/w). Scale bar is 100 μm.

(e) IDM-PL miscibility

As shown in Figure 4.15, spectra obtained for the IDM-PL samples showed a different fluorescence emission as compared to the IDM-polymer samples. For samples with a drug loading of 10% and 20%, the expected broad single emission peak was observed at 508 nm. Starting at 30% drug loading, a second peak became clear at 464 nm that exhibited a blue shift with increasing drug concentration. As expected, the intensity of fluorescence emission increased as the drug concentration increased. Possible reasons for the appearance of the shoulder at 464 nm will be discussed in Section 4.5.2.

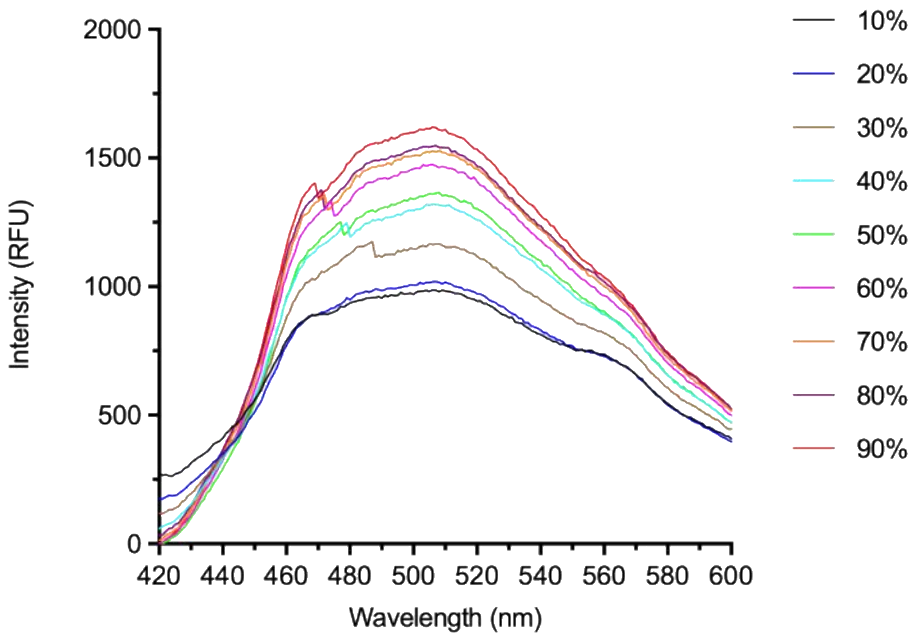

Figure 4.15. Fluorescence emission spectra of IDM-PL ASDs after preparation. Percentage refers to drug loading degree (w/w).

Figure 4.16 shows the fluorescence microscopy results obtained for the IDM-PL samples. At low drug concentrations of 10% and 20% a homogeneous fluorescence background was observed. For samples with drug concentrations of 30% to 60%, immiscible domains became more obvious, increasing in both number and size. These domains showed a greater fluorescence intensity along the edge of the domain and lower intensity for inner regions, again different from the domains observed for the IDM-polymer systems. At 70% drug loading, phase separation was obvious and isolated domains were observed with crystalline characteristics, including birefringence and needle-like shape. Phase transitions of the immiscible domains were observed to occur during storage at 40°C. After 1 week, 10% and 20% IDM-PL samples remained as a homogeneous film with uniform fluorescence intensity. The immiscible domains in the 30% IDM sample began to exhibit crystalline characteristics, suggesting a transition from an amorphous to a crystalline state (see Figure 4.17); these crystalline structures became more obvious for samples with higher drug loadings. After 2 weeks, the 10% and 20% IDM samples also began to show immiscible regions with non-homogeneous fluorescence intensity. Crystalline clusters could be observed for samples with drug loading of 30% and higher. After 3 weeks the crystalline features could be seen in the 20% IDM-PL

sample. The amorphous-crystalline transformation gradually developed during storage under heating, compromising the miscibility between IDM and PL. Figures for week 2 and week 3 samples are provided in Figure B-12 to B-13 in Appendix.

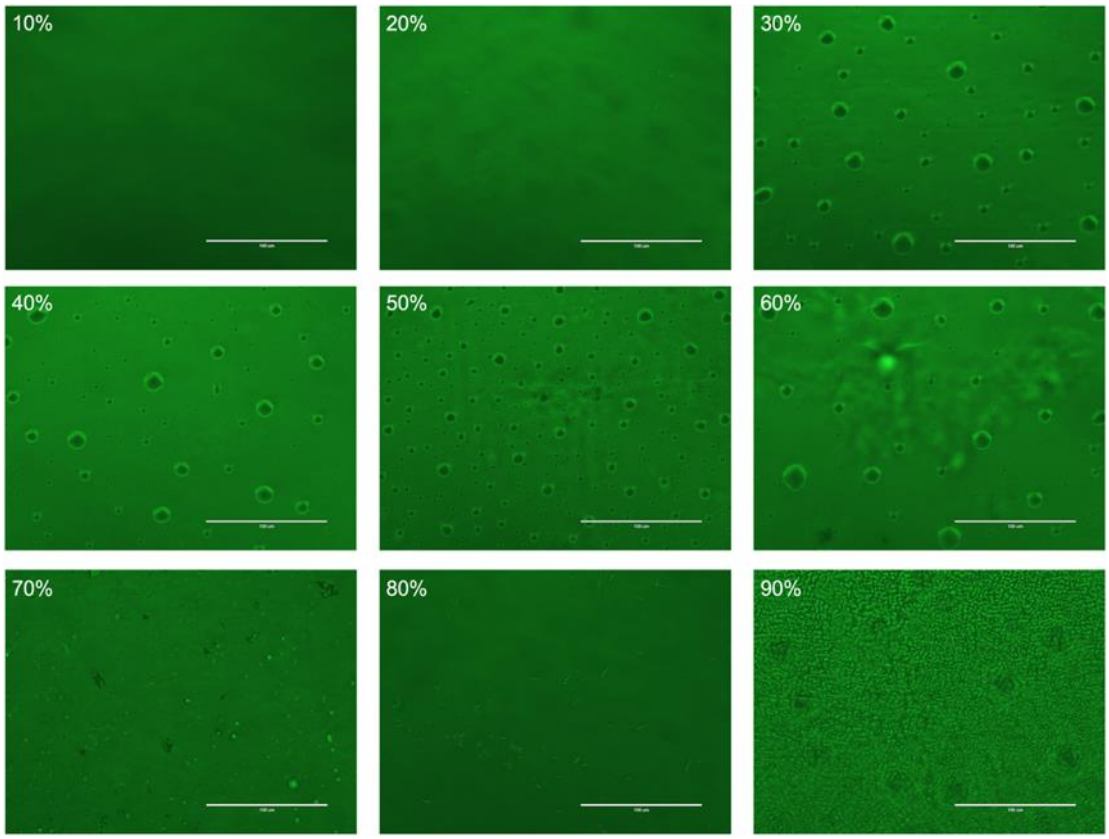

Figure 4.16. Fluorescence images of IDM-PL ASDs after preparation. Percentage refers to drug loading degree (w/w). Scale bar is 100 μm.

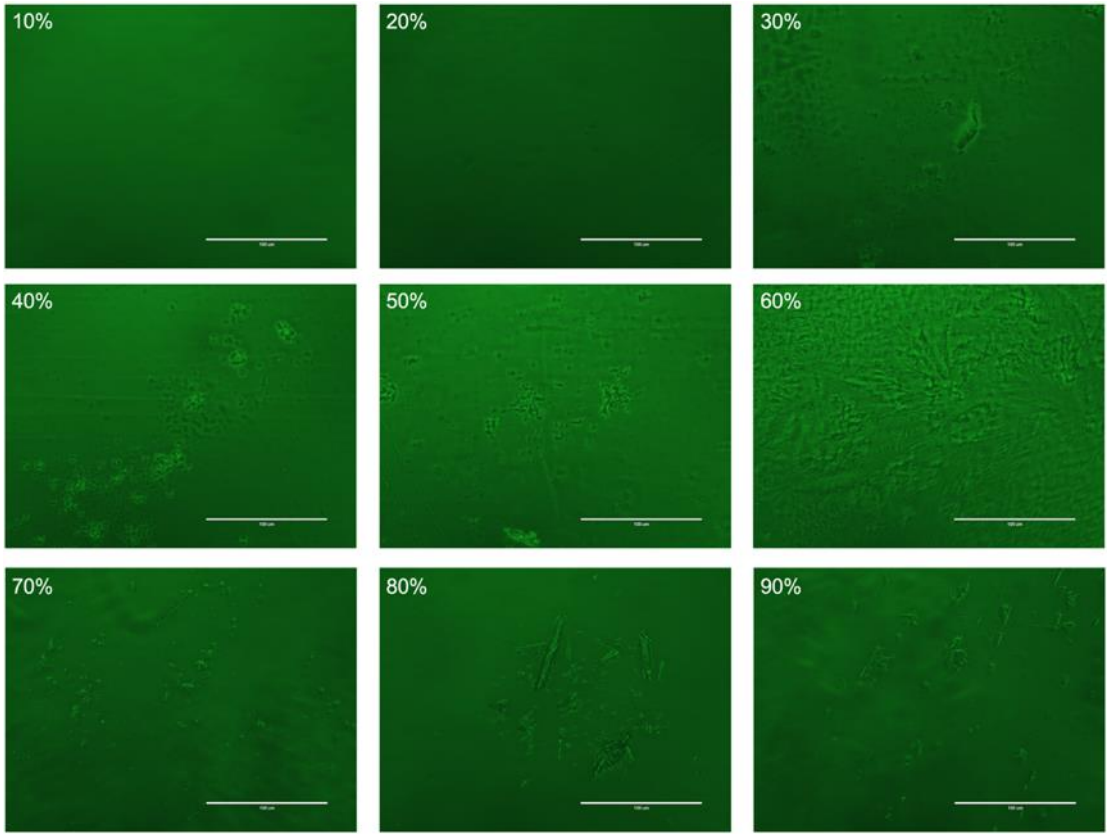

Figure 4.17. Fluorescence images of IDM-PL ASDs after 1-week heating. Percentage refers to drug loading degree (w/w). Scale bar is 100 μm.

(f) IDM-G48 miscibility

The fluorescence spectra of IDM-G48 films varied significantly with IDM drug loading, as presented in Figure 4.18. 10% and 20% drug loading samples showed a generally low fluorescence intensity with the peak intensity in the 508 nm region. Starting at an IDM drug loading of 30% a strong emission peak at 464 nm was observed, and its fluorescence intensity was significantly higher than that at 508 nm seen in all other IDM samples characteristic of amorphous IDM. The overall fluorescence intensity increased with increased drug concentration.

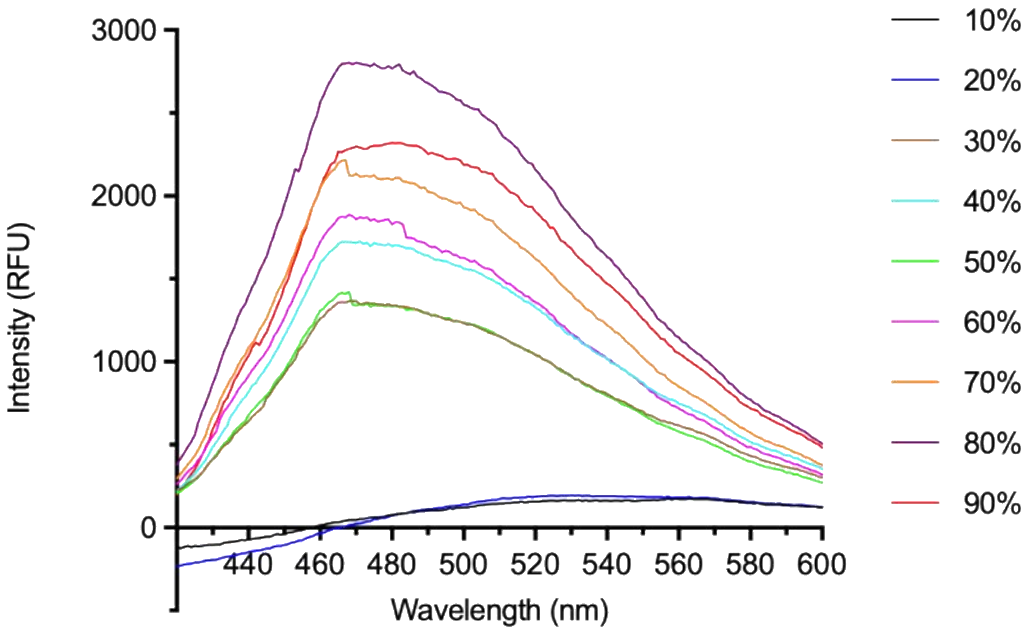

Figure 4.18. Fluorescence emission spectra of IDM-G48 ASDs. Percentage refers to drug loading degree (w/w).

Figure 4.19 shows the fluorescence microscopy images for the IDM-G48 samples. Again at an IDM concentration of 30% large immiscible and separated domains could be observed. Interestingly, the contrast between immiscible domains were lower than those for previously discussed systems (i.e. the fluorescence intensities of immiscible domains were similar to background). For samples with drug loadings of 40% to 80%, immiscible domains showed more obvious birefringence properties and clear fan-like crystal growth shape (Figure 4.20). 90% sample showed a high density of immiscible domains which mixed more uniformly, with less obvious fan-like crystalline features. After storage at 40 °C for 1 week, the 20% sample now showed the appearance of immiscible crystalline domains while samples with IDM concentrations of 30% and higher exhibited long needle-like crystals with increased numbers. After heating for 3 weeks, the appearance of the IDM-G48 samples were similar to those for week 2. Figures for week 2 and week 3 are provided in Figure B-14 to B-15 in the Appendix.

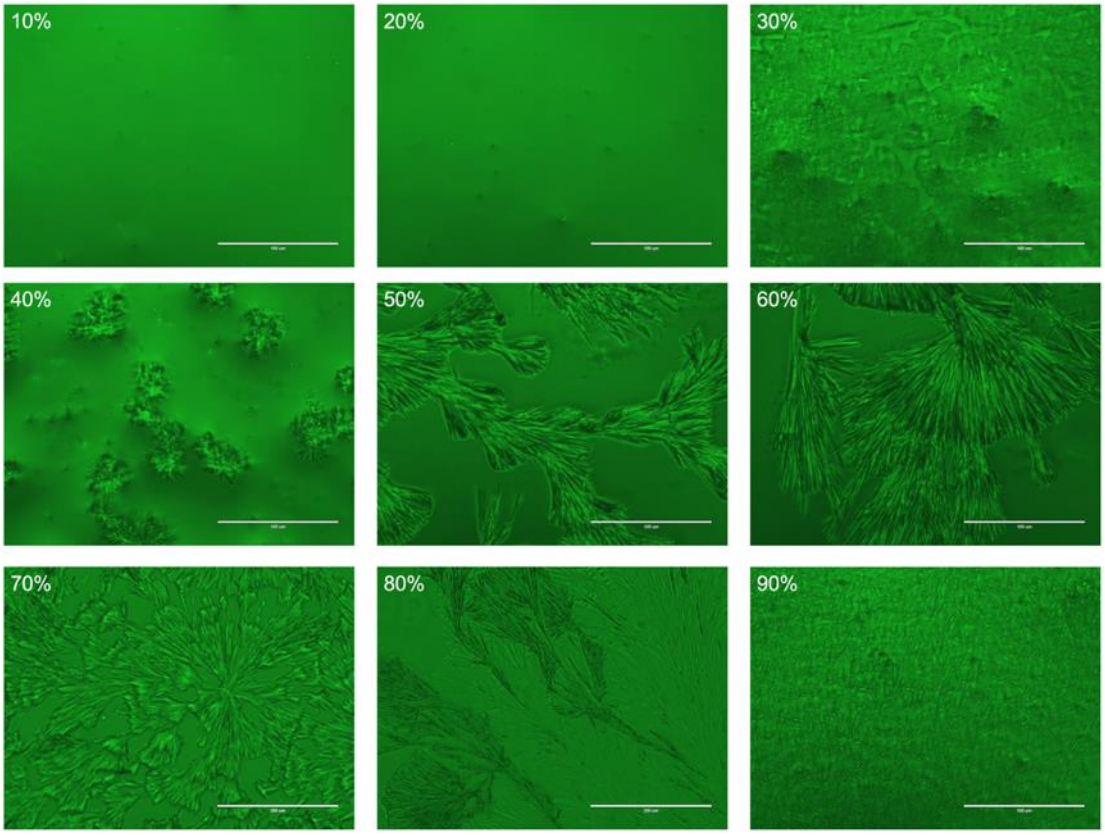

Figure 4.19. Fluorescence images of IDM-G48 ASDs after preparation. Percentage refers to drug loading degree (w/w). Scale bar is 100 μm.

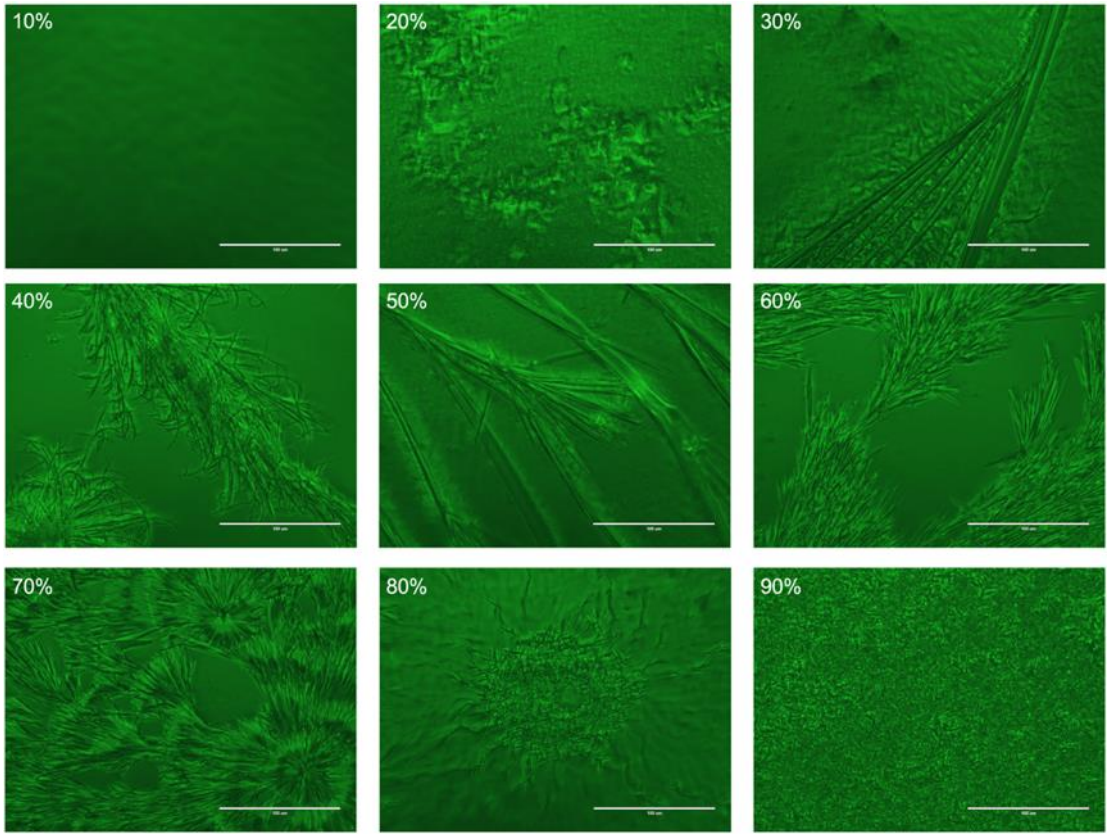

Figure 4.20. Fluorescence images of IDM-G48 ASDs after 1-week heating. Percentage refers to drug loading degree (w/w). Scale bar is 100 μm.

(g) IDM-ATO miscibility

IDM-ATO films had the characteristic peak at 508 nm for amorphous IDM (Figure 4.21). When IDM content did not exceed 70%, the fluorescence spectrum showed a single a single broad peak without any obvious shoulder peak. For samples of 80% and 90% IDM a shoulder peak at lower wavelength was clearly evident.

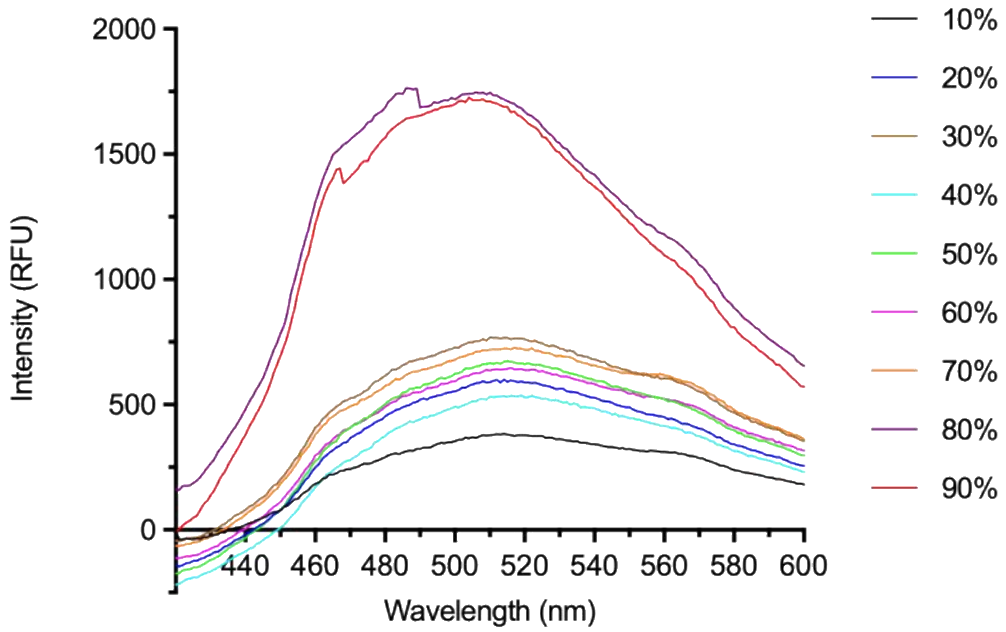

Figure 4.21. Fluorescence emission spectra of IDM-ATO ASDs. Percentage refers to drug loading degree (w/w).

The fluorescence microscopy results for IDM-ATO samples showed that phase separation occurred in the samples at all drug loadings (Figure 4.22). Immiscible domains were observed to fill a large portion of the viewing field. For samples with 10% to 70 % IDM loading, separated domains were characterized with lower fluorescence intensity for inner structures and higher fluorescence intensity for boundaries. For 80% and 90% IDM loaded samples, the inner structures of the immiscible domains increased in fluorescence intensity. After storage at 40 ^{o}C for 1 week, samples at higher IDM concentrations had an increasing number of immiscible domains with increased fluorescence intensity for inner structures, in contrast to initial observations (Figure 4.23 as compared to Figure 4.22). This phenomenon was especially obvious for 70% to 90% IDM samples where significantly higher fluorescence intensity was observed for the inner structures. After 3 weeks the images remained similar to those obtained at week 1. Figures for week 2 and week 3 are provided in Figure B-16 to B-17 in Appendix.

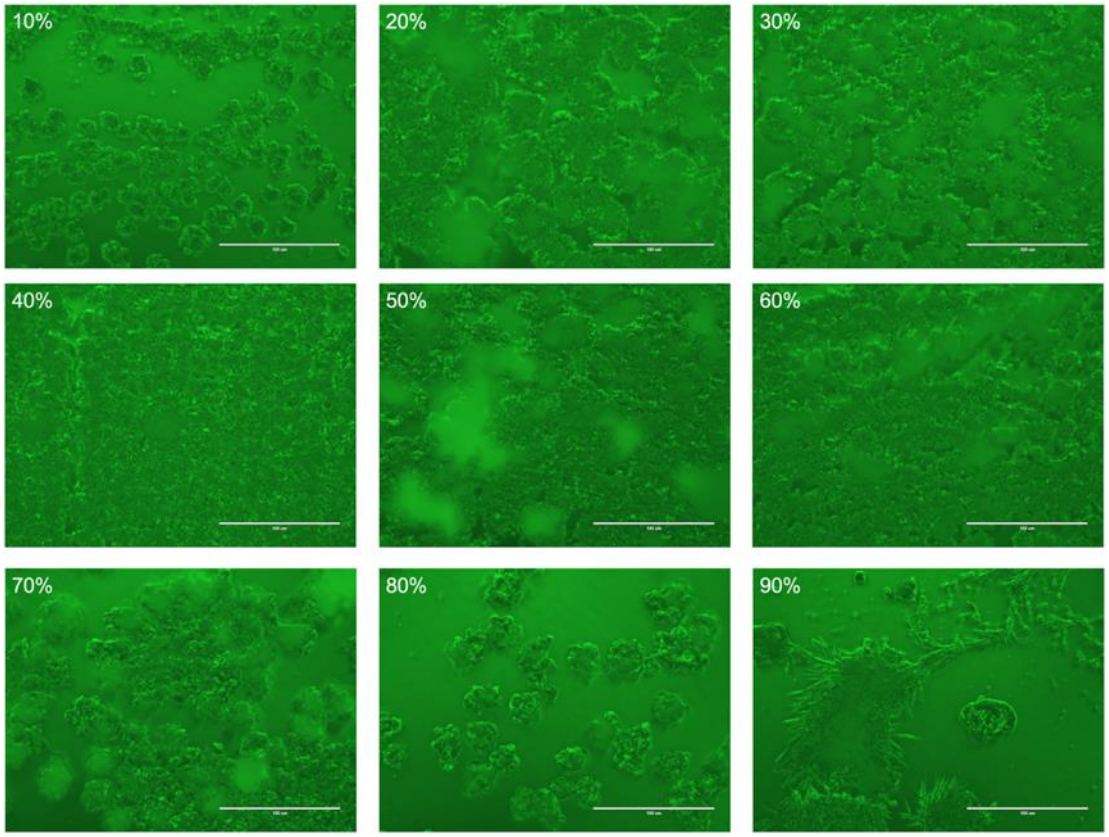

Figure 4.22. Fluorescence images of IDM-ATO ASDs after preparation. Percentage refers to drug loading degree (w/w). Scale bar is 100 µm.

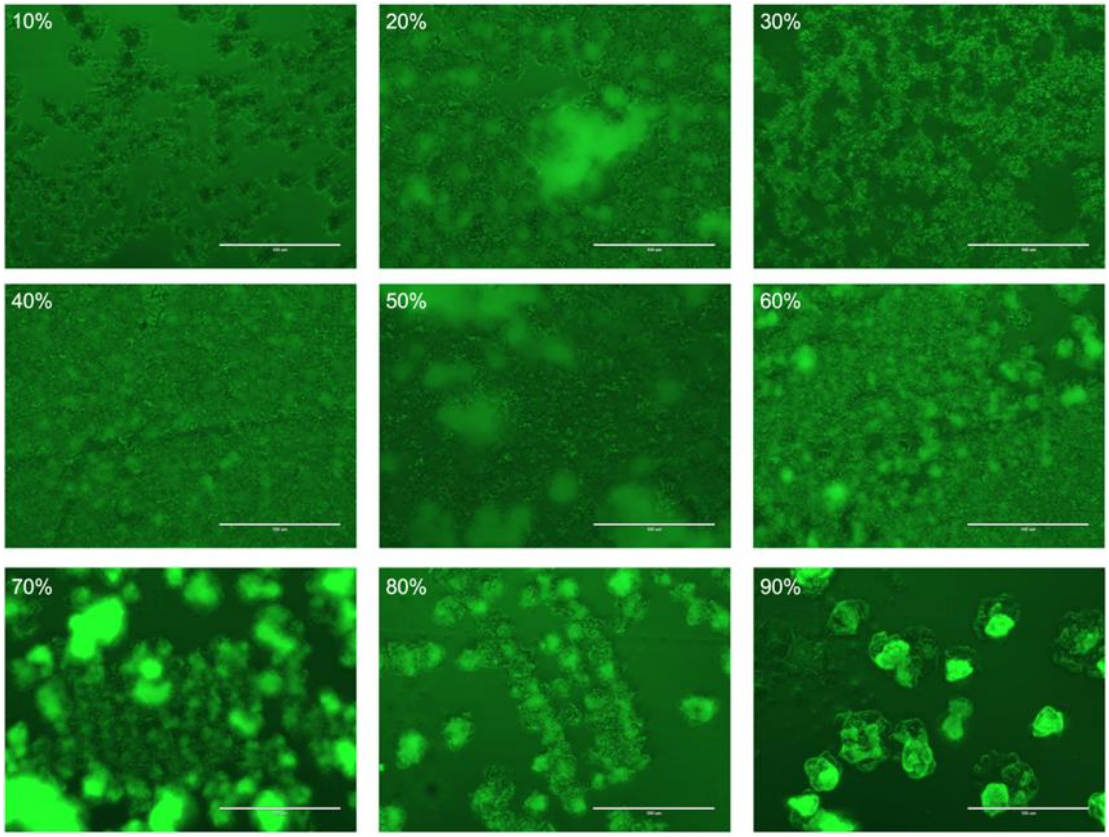

Figure 4.23. Fluorescence images of IDM-ATO ASDs after 1-week heating. Percentage refers to drug loading degree (w/w). Scale bar is 100 μm.

4.4.3 APX amorphization and miscibility between APX and ASD carriers

As shown in Figure 4.24, the spectrum of pure crystalline APX has an emission peak at 416 nm, while amorphous APX loaded in the PVP carrier has an emission peak at 460 nm, red-shifted compared to that for pure APX. The emission peak of 416 nm is an intrinsic characteristic of crystalline APX, and the red shift of the emission profile can be explained by the polarity difference between the two samples. For an APX ASD sample with low drug loading, APX is expected to uniformly disperse in the drug carrier to form a homogeneous solid solution, in which APX is surrounded predominantly by excipient molecules (i.e. APX is in an amorphous state). The results confirmed that the emission signal of APX is sensitive to the local environment and APX could be used as a probe to assess the phase distribution of APX ASDs without the addition of another fluorescence probe.

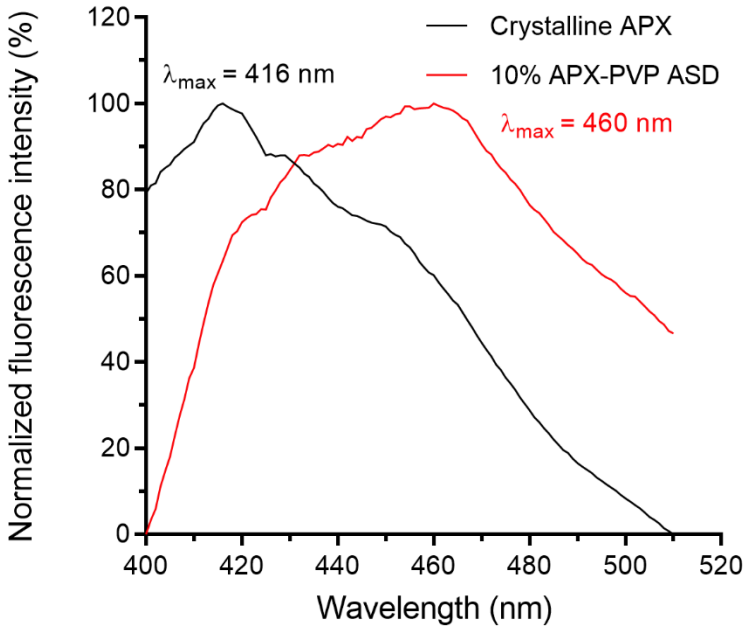

Figure 4.24. Fluorescence emission spectra of crystalline APX and 10% (w/w) APX-PVP ASD with an excitation wavelength of 280 nm.

(a) APX-PVP miscibility

The fluorescence spectra of APX-PVP films showed a large emission peak in the region of 465 nm for the drug loading amounts of 10% to 90% (Figure 4.25). A peak separation could be observed for all samples in the 416 nm region. The overall fluorescence intensity of a sample was disproportionate to the drug content.

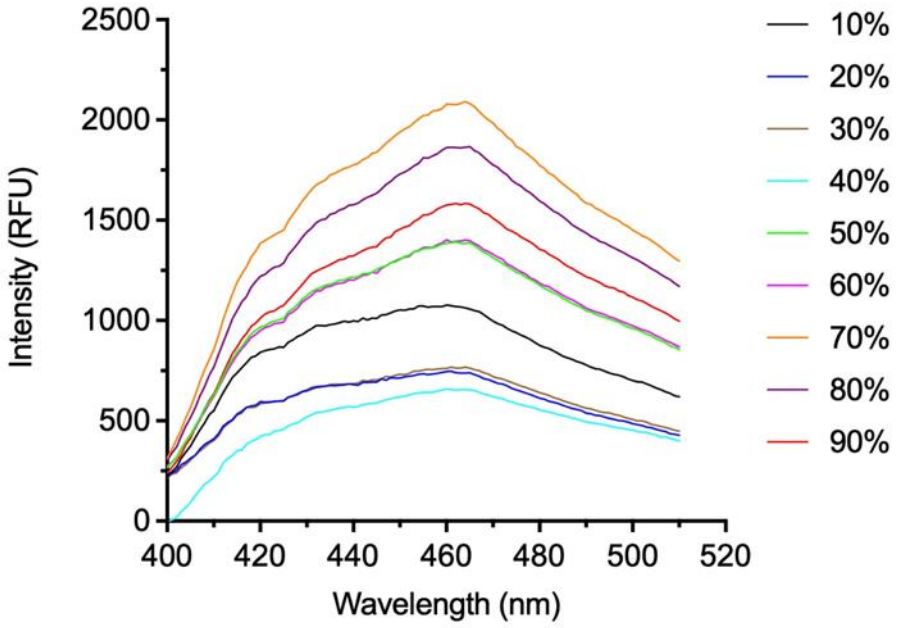

Figure 4.25. Fluorescence emission spectra of APX-PVP ASDs. Percentage refers to drug loading degree (w/w).

According to fluorescence microscopy results, 10% drug loading APX-PVP showed a homogeneous fluorescence in most of the viewed regions (see Figure 4.26). Only scarce immiscible domains with higher fluorescence were observed. No birefringence properties were presented for these regions. For the samples with 20% to 80% drug loading, separated domains were observed with high fluorescence intensity and halo characteristic without presenting crystalline shape or birefringence property. The density of these non-homogeneous fluorescent regions increases, corresponding to a larger amount of immiscible APX content. Birefringence property corresponding to crystalline APX was observed for the 90% loading sample.

After storage at 40 °C for 1 week, the sample with 10% drug loading sample started to show an increasing amount of immiscible regions with higher fluorescence intensity than background, while still without birefringent property. For samples with drug loading from 20% to 40%, the immiscible patterns showed aggregations with irregular shapes without crystalline characteristics. Starting the drug loading of 50%, several immiscible regions could be observed with birefringent property, describing the amorphous-crystalline transformation as a function of time. After storage for 2 weeks, birefringence property was observed at 30% drug loading instead of 90% as initially

measured. The separated domains with different physical states could be observed for some samples, such as for the 50% and 60% drug loading samples (see Figure 4.27 for comparison). After heating for 3 weeks, the samples with 10% and 20% drug loading remained in their amorphous-amorphous separation state, while other samples showed increasing amounts of crystalline domains to different degrees. Additional figures for week 1 and week 3 were provided in Figure B-18 to B-19 in Appendix.

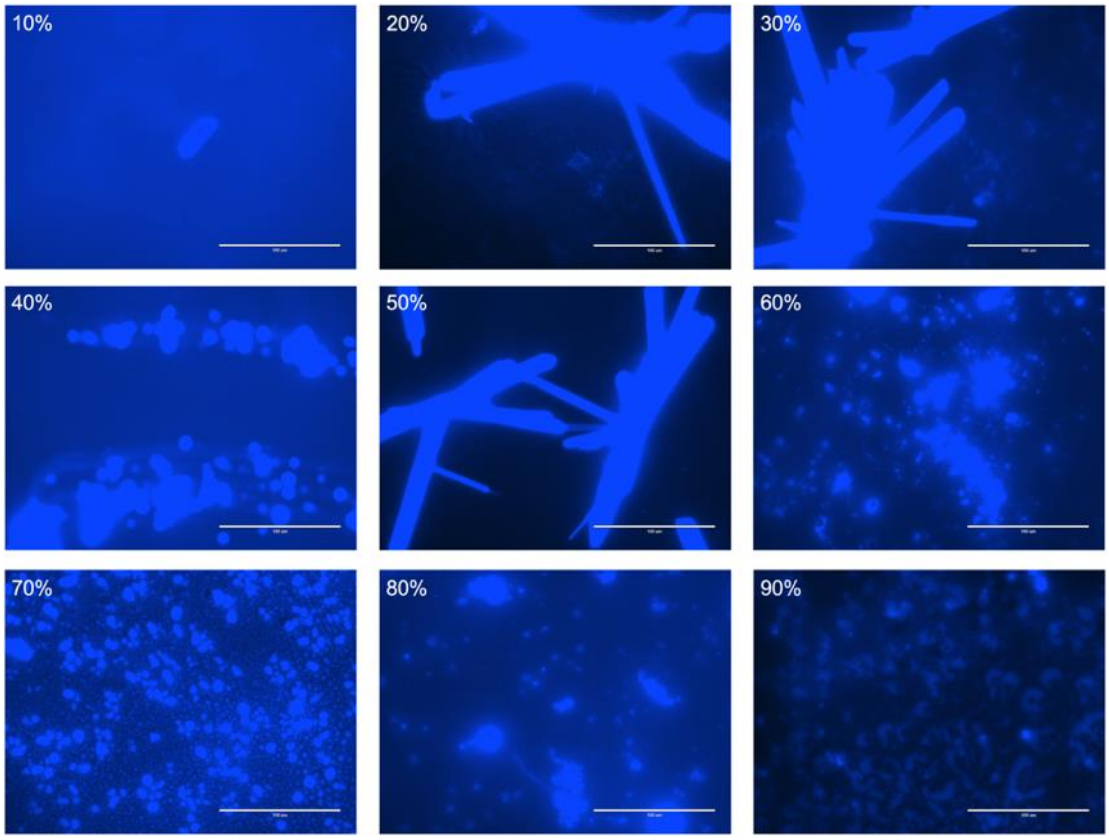

Figure 4.26. Fluorescence images of APX-PVP ASDs after preparation. Percentage refers to drug loading degree (w/w). Scale bar is 100 μm.

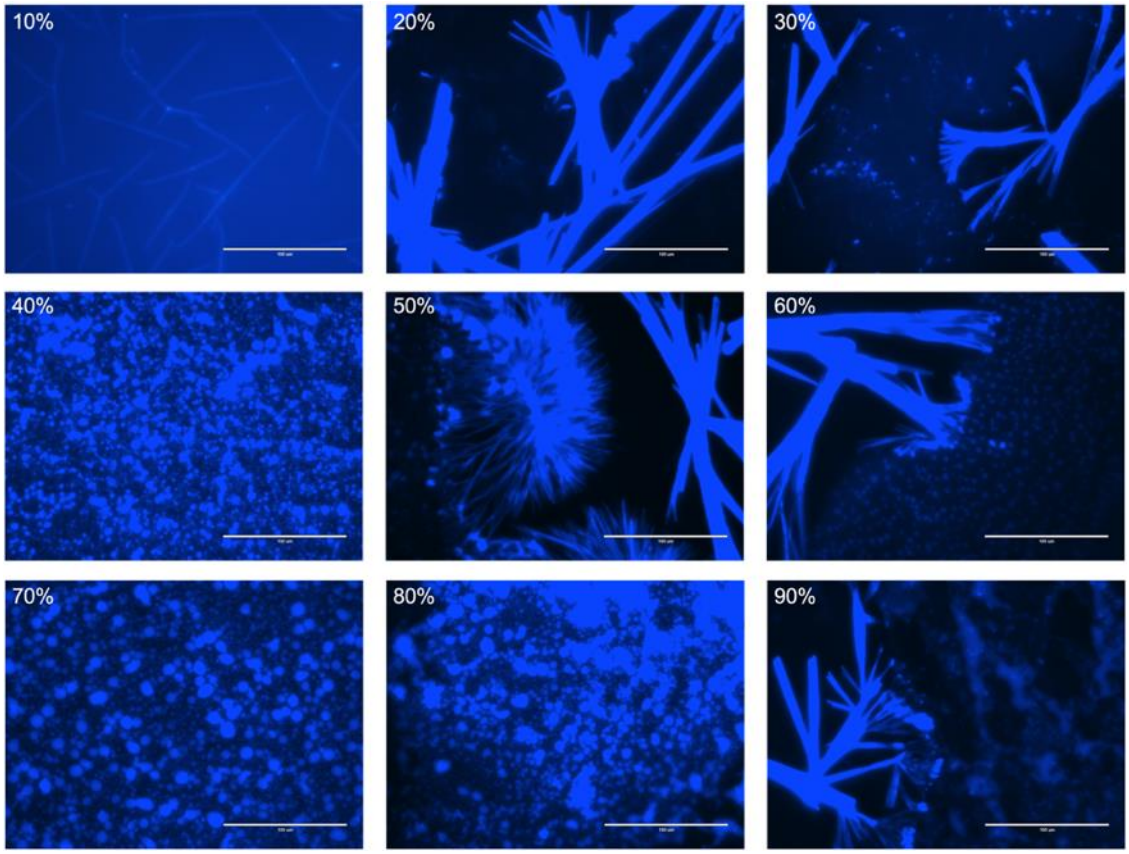

Figure 4.27. Fluorescence images of APX-PVP ASDs after 2-week heating. Percentage refers to drug loading degree (w/w). Scale bar is 100 μm.

(b) APX-SOL miscibility

The fluorescence spectra of APX-SOL films showed a large emission peak in the region of 465 nm for the drug loading amounts of 10% to 90% (Figure 4.28). No obvious peak separation was observed for all samples. The overall fluorescence intensity of a sample showed a general decreasing trend with regard to drug content. APX-SOL films with 10% to 30% drug loading showed a highly homogeneous fluorescence intensity, with only scarce bright dots observed in the viewing field. Staring with 40% drug loading, there was an increase in the number of immiscible regions with higher fluorescence intensity than the surrounding environments for all samples (Figure 4.29). After storage under 40 °C for 1 week, phase separation was observed for all samples from 10% to 90% drug loading. The density of immiscible regions further increased with heating time for 2 weeks, describing a further development of phase separation. Samples with drug loading not less than 60%

started to present trace birefringent properties, which is a characteristic of the formation of crystalline APX. After storage for 3 weeks, phase separation became more obvious, and birefringent properties for crystalline clusters could be observed for samples with drug loading not less than 30%. Figures were provided in Figure B-20 to B-22 in Appendix.

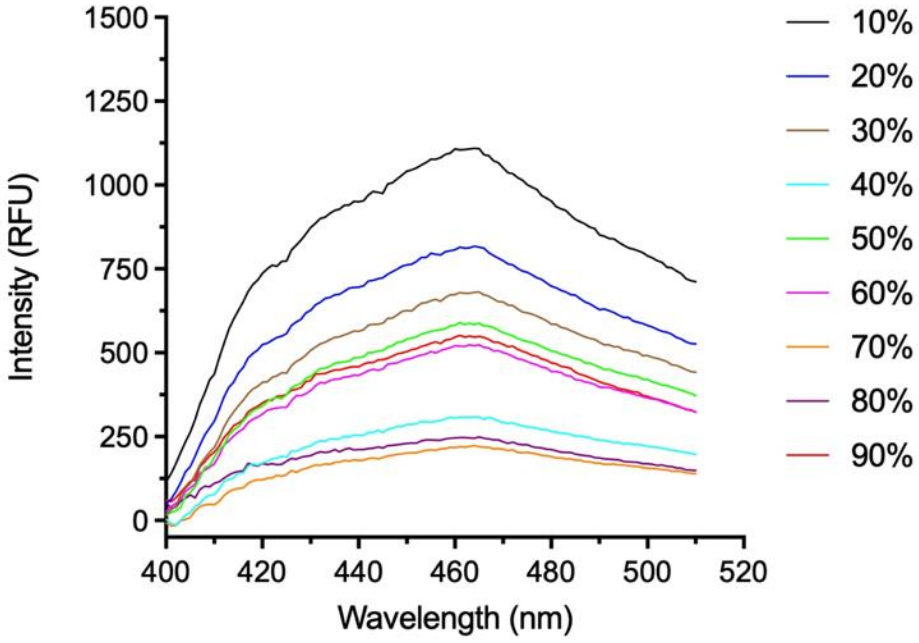

Figure 4.28. Fluorescence emission spectra of APX-SOL ASDs. Percentage refers to drug loading degree (w/w).

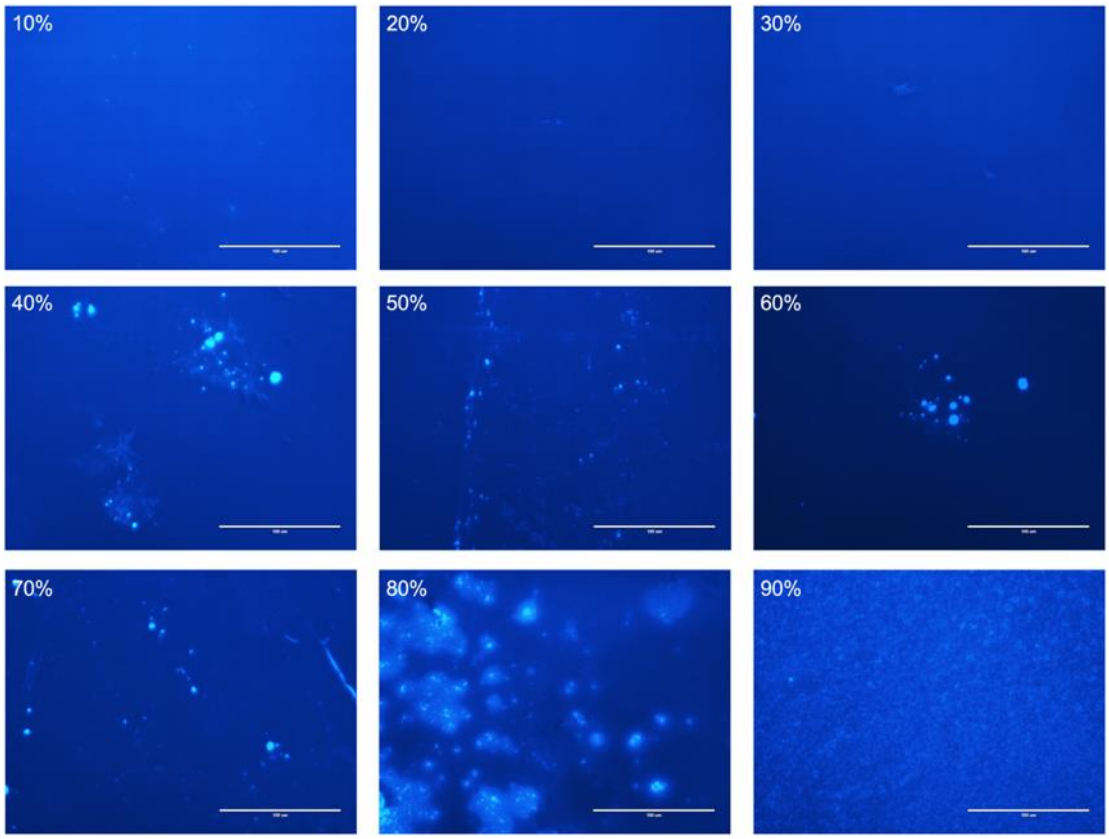

Figure 4.29. Fluorescence images of APX-SOL ASDs after preparation. Percentage refers to drug loading degree (w/w). Scale bar is 100 µm.

(c) APX-SA miscibility

The fluorescence spectra of APX-SA samples showed a large emission peak in the region of 465 nm for the drug loading amounts of 10% to 90% (Figure 4.30). No obvious peak separation was observed for all samples. The fluorescence intensity of a sample overall decreased with drug content. APX-SA samples of all drug loadings showed immiscible domains without birefringent property in the fluorescence images after preparation (Figure 4.31). APX was concentrated in these regions as suggested by the significantly higher fluorescence intensity. After storage for 1 week, no amorphous-crystalline transformation for these domains were observed. After heating for 2 weeks, birefringent property was observed for samples with drug loading at 60%, describing an amorphous-crystalline transformation for APX. The fluorescence properties for all samples did not present further change after heating for 3 weeks. Figures were provided in Figure B-23 to B-25 in Appendix.

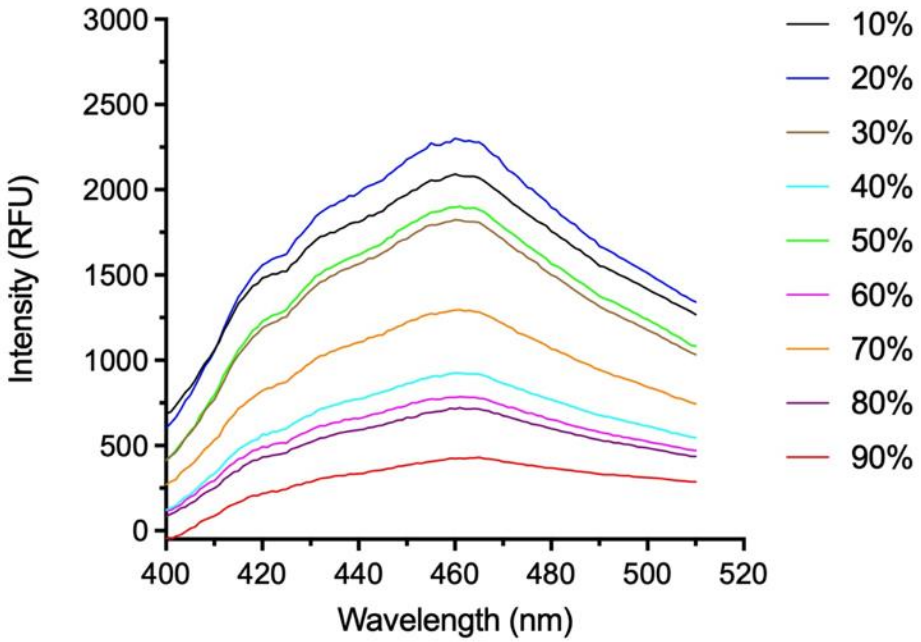

Figure 4.30. Fluorescence emission spectra of APX-SA ASDs. Percentage refers to drug loading degree (w/w).

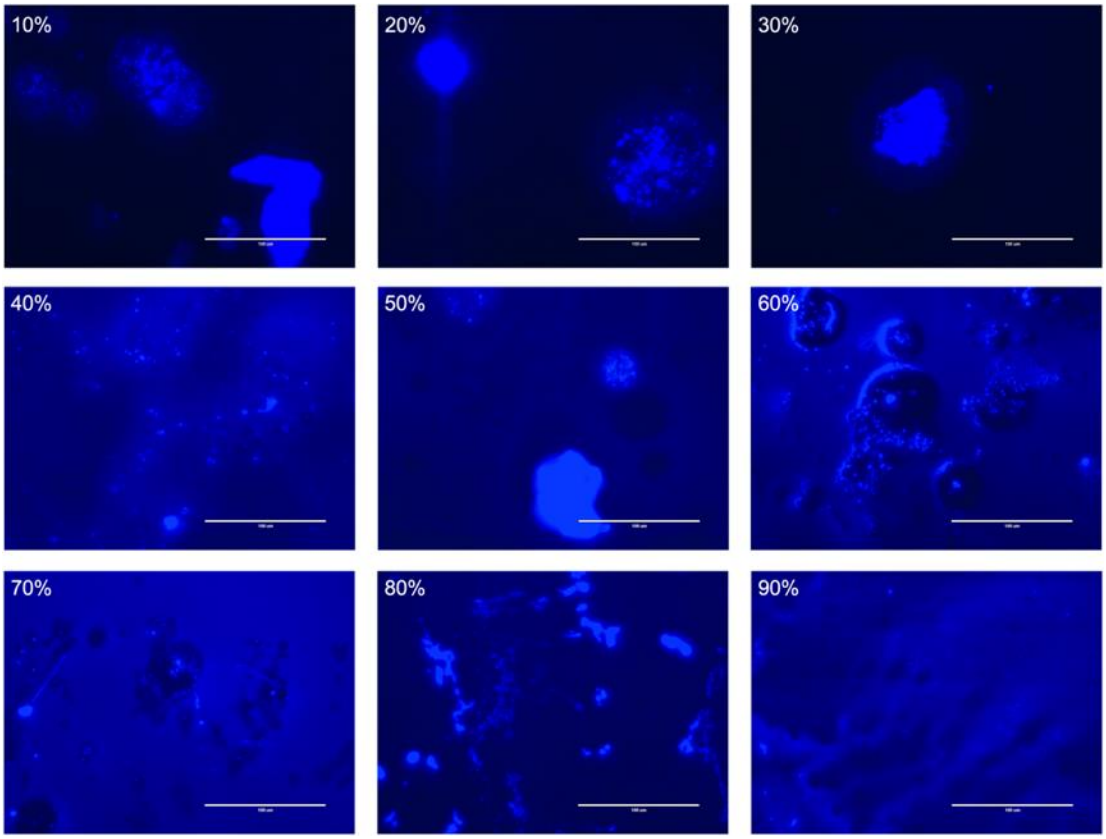

Figure 4.31. Fluorescence images of APX-SA ASDs after preparation. Percentage refers to drug loading degree (w/w). Scale bar is 100 µm.

(d) APX-EC miscibility

The fluorescence spectra of APX-EC films showed a large emission peak in the region of 465 nm for all drug loadings (Figure 4.32). No obvious peak separation was observed. The fluorescence intensity of a sample overall decreased with drug content. A homogeneous fluorescence intensity for APX-EC system could only be maintained when the drug loading was 10% (Figure 4.33). With a higher drug loading, the system showed immiscible regions with higher fluorescence intensity free of birefringent property, suggesting the amorphous nature of isolated regions. After storage under heating for 3 weeks, immiscible domains could be observed for all samples without birefringent property, similar to the initial findings. Figures were provided in Figure B-26 to B-28 in Appendix.

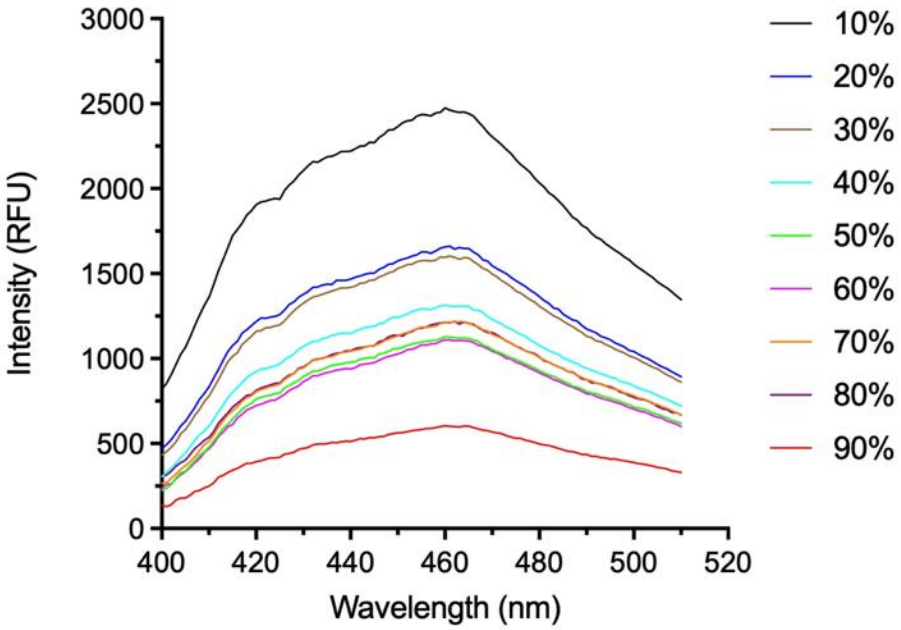

Figure 4.32. Fluorescence emission spectra of APX-EC ASDs. Percentage refers to drug loading degree (w/w).

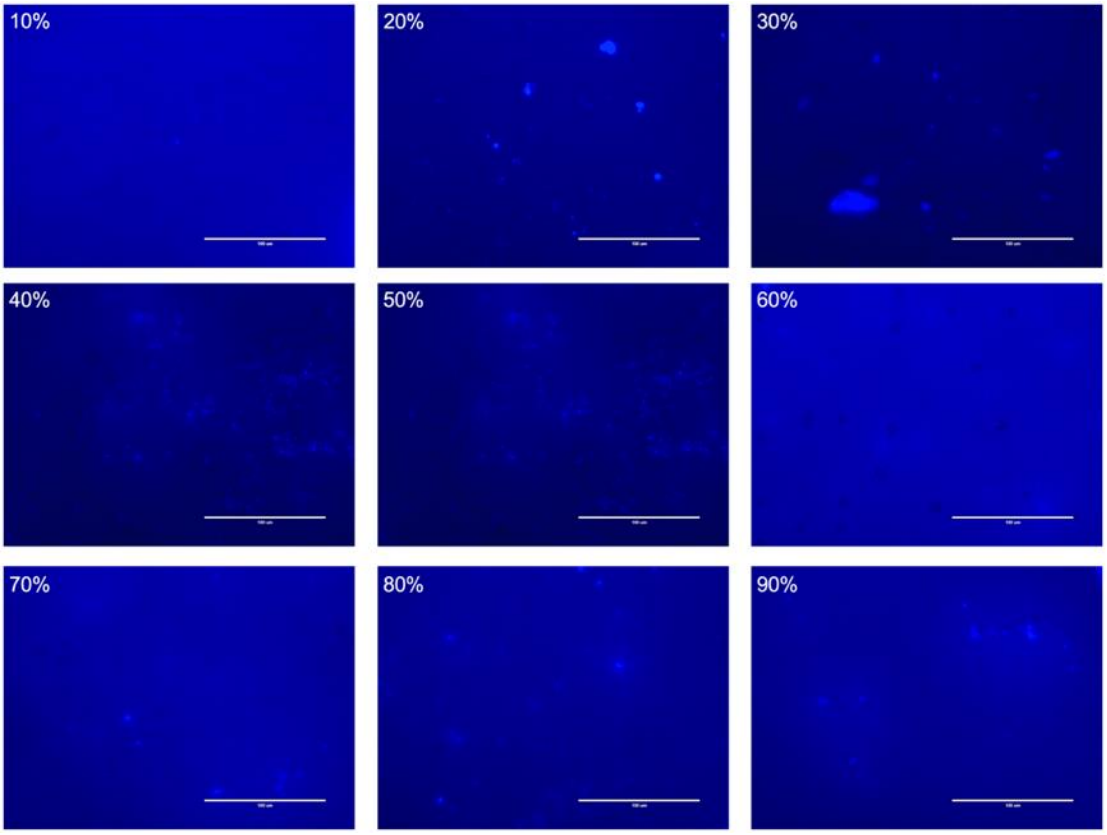

Figure 4.33. Fluorescence images of APX-EC ASDs after preparation. Percentage refers to drug loading degree (w/w). Scale bar is 100 μm.

(e) APX-PL miscibility

The fluorescence spectra of APX-PL films showed a large emission peak in the region of 465 nm with a tiny peak separation in the 420 nm region for all drug loadings (Figure 4.34). The fluorescence intensity of a sample was not proportional to drug content. 10% APX-PL showed scattered immiscible domains with higher fluorescence intensity than background, suggesting an increased concentration of APX in these domains (Figure 4.35). Samples with drug loading not less than 20% showed either increased amount or size in immiscible regions. No crystalline characteristics were observed for all samples. After storage with heating for 1 week, no change was observed for all samples in terms of amorphous-crystalline transformation. After 2 weeks, 60% to 90% APX-PL started to present birefringent regions, suggesting the occurrence of recrystallization of APX under solid state. Other samples remained in an amorphous state with phase separation. After 3 weeks,

samples showed similar profiles to those for 2 weeks without further recrystallization or crystal growth. Figures were provided in Figure B-29 to B-31 in Appendix.

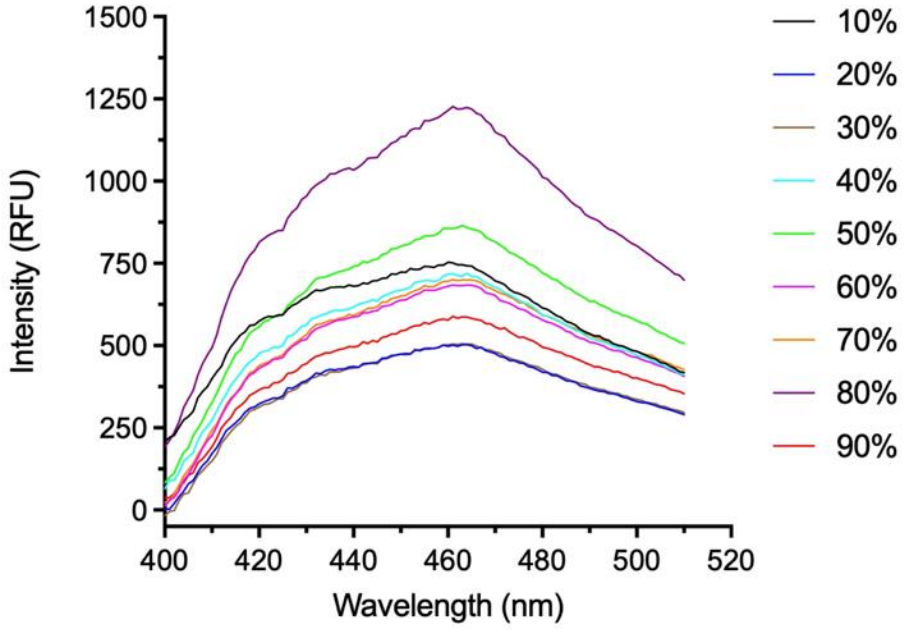

Figure 4.34. Fluorescence emission spectra of APX-PL ASDs. Percentage refers to drug loading degree (w/w).

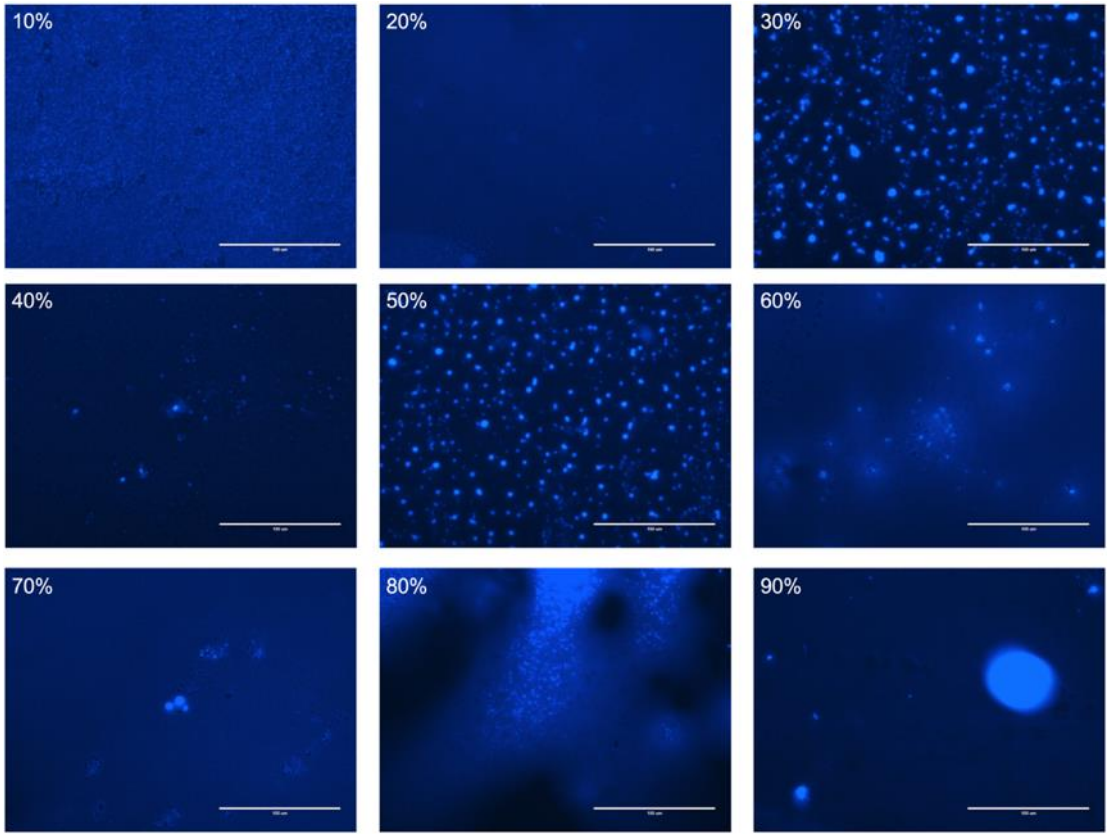

Figure 4.35. Fluorescence images of APX-PL ASDs after preparation. Percentage refers to drug loading degree (w/w). Scale bar is 100 µm.

(f) APX-G48 miscibility

The fluorescence spectra of APX-G48 samples showed a large emission peak in the region of 465 nm with a tiny peak separation at 420 nm region for all drug loadings (Figure 4.36). The fluorescence intensity of a sample was not proportional to drug content.

Immiscibility could be observed for samples with a drug loading starting at 10%. The separated domains showed higher fluorescence intensity due to the concentration of APX molecules. 20% to 40% drug loading samples showed similarly immiscible patterns with increasing density and size of APX clusters and presented non-crystalline characteristics. Starting with a drug loading of 50%, crystalline APX was observed as seen by the defined edges and birefringence properties (Figure 4.37). After storing under heating for 1 week, amorphous-crystalline transformation was observed for all samples (see Figure 4.38 for comparison). Crystalline domains were observed with clearer edge

and birefringent properties. The density of crystal aggregations increased with drug loading degree. After 2 weeks and 3 weeks, all samples showed separated crystalline and amorphous phases similar to week 2 (figures provided in Figure B-32 to B-33 in Appendix).

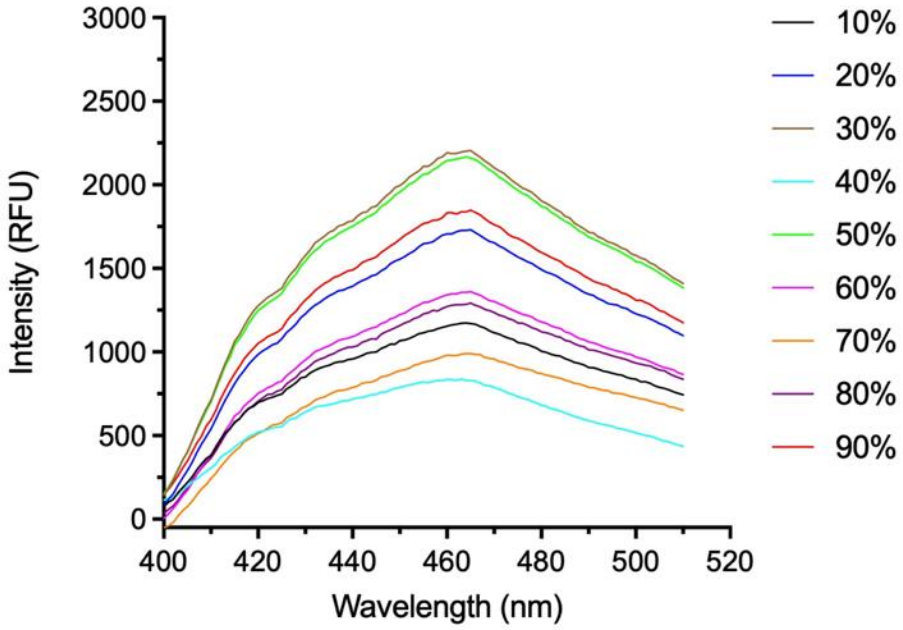

Figure 4.36. Fluorescence emission spectra of APX-G48 ASDs. Percentage refers to drug loading degree (w/w).

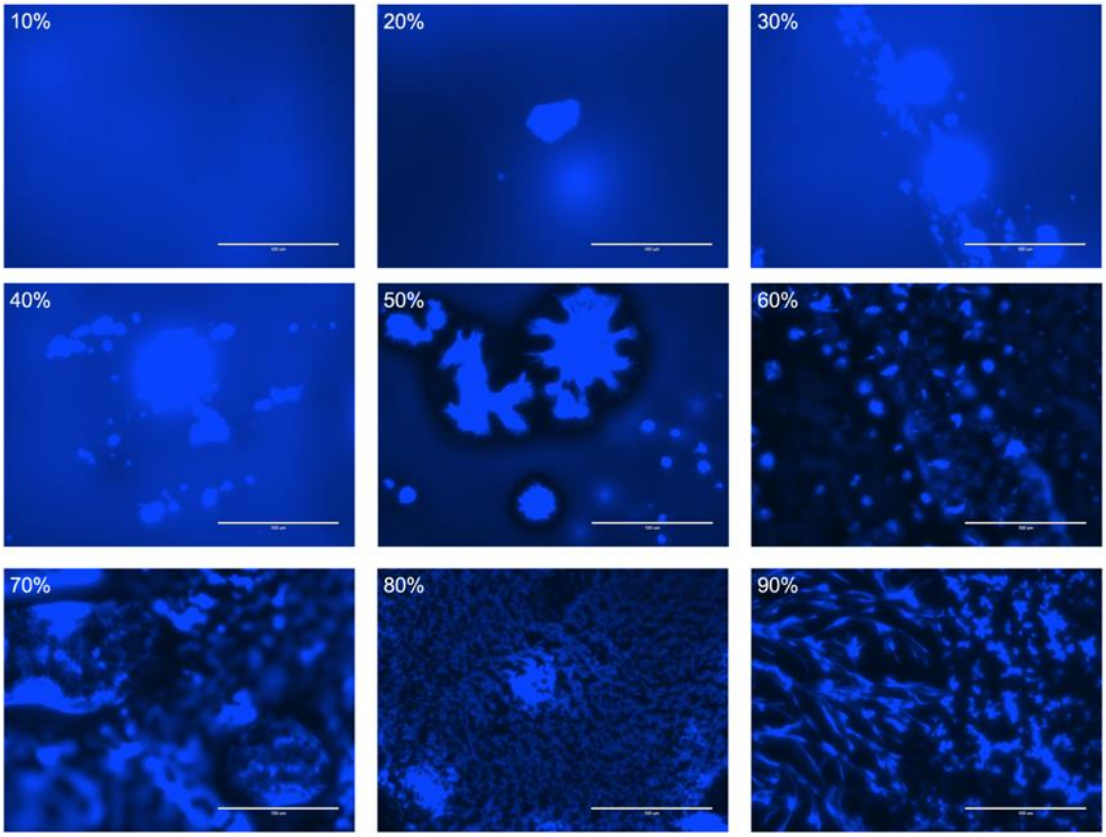

Figure 4.37. Fluorescence images of APX-G48 ASDs after preparation. Percentage refers to drug loading degree (w/w). Scale bar is 100 μm.

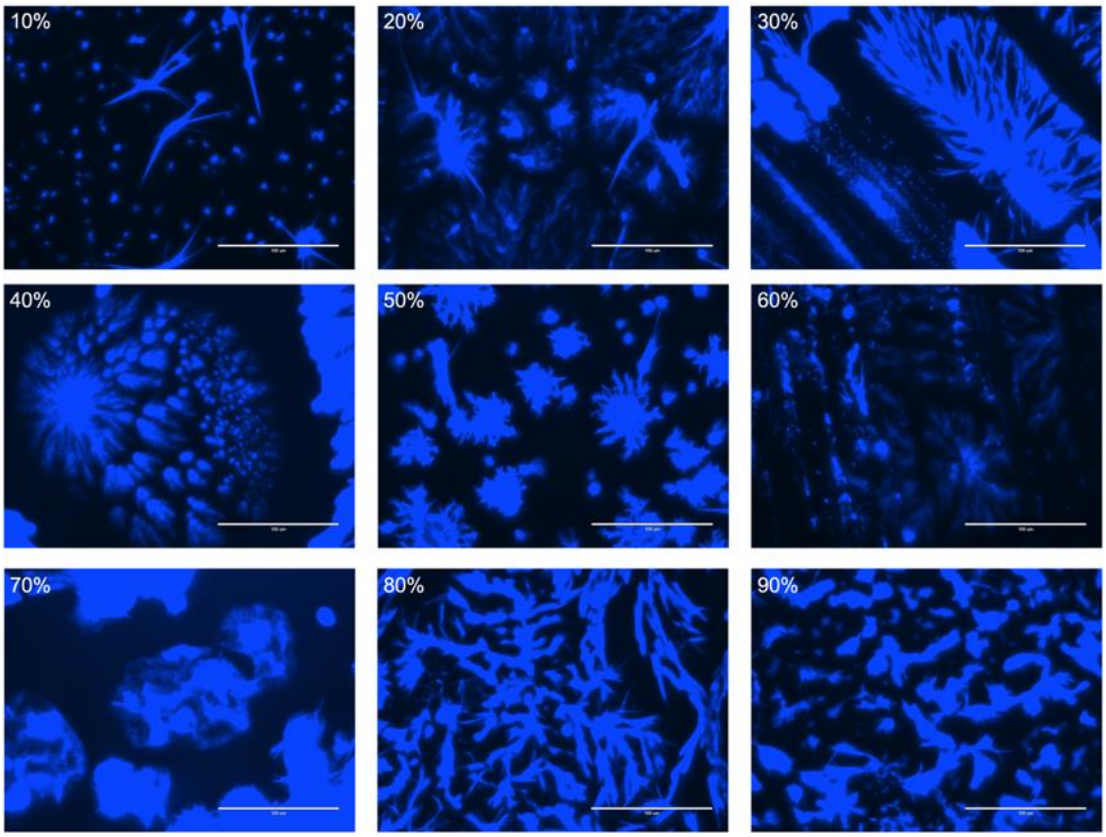

Figure 4.38. Fluorescence images of APX-G48 ASDs after 1-week heating. Percentage refers to drug loading degree (w/w). Scale bar is 100 µm.

(g) APX-ATO miscibility

The fluorescence spectra of APX-ATO samples showed a large emission peak in the region of 465 nm with an obvious peak separation in the 420 nm region for all drug loadings (Figure 4.39). The fluorescence intensity of a sample was not proportional to drug content. APX-ATO samples with all drug loading degrees showed a poor drug-excipient miscibility with a significant number of separated domains (Figure 4.40). The sample with 10% drug loading showed an amorphous-amorphous phase separation where both amorphous drug with high fluorescence intensity and ATO domains with lower fluorescence intensity were observed to mix with each other. No birefringence property was observed for this sample. Samples with a drug loading from 20% to 90% showed significant phase separation where several immiscible domains were observed with birefringence property, suggesting the occurrence of APX recrystallization after ASD preparation. After heating for

different time periods, most of the separated domains for all samples showed halo property with higher fluorescence intensity. Certain regions could be observed with birefringence properties. Figures were provided in Figure B-34 to B-36 in Appendix.

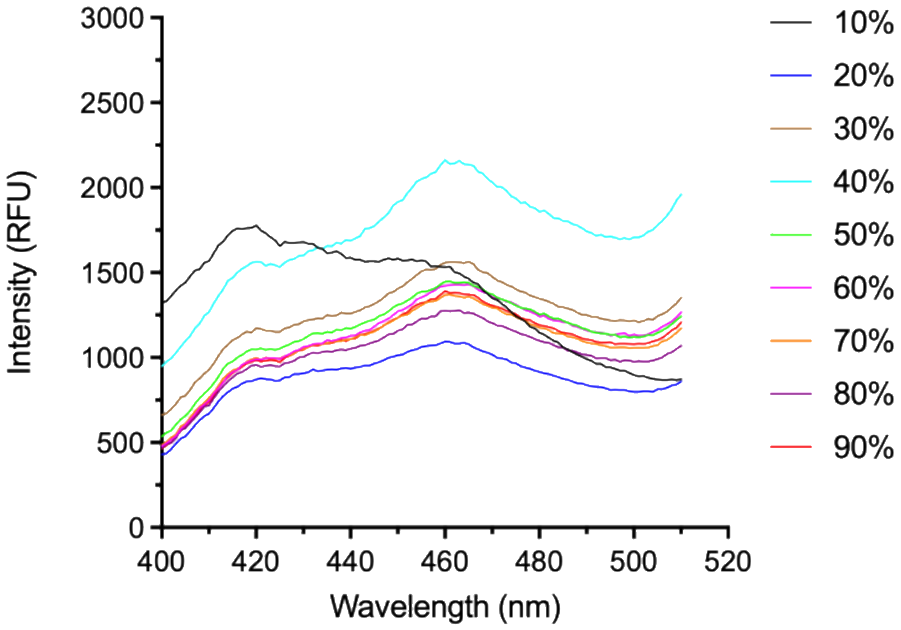

Figure 4.39. Fluorescence emission spectra of APX-ATO ASDs. Percentage refers to drug loading degree (w/w).

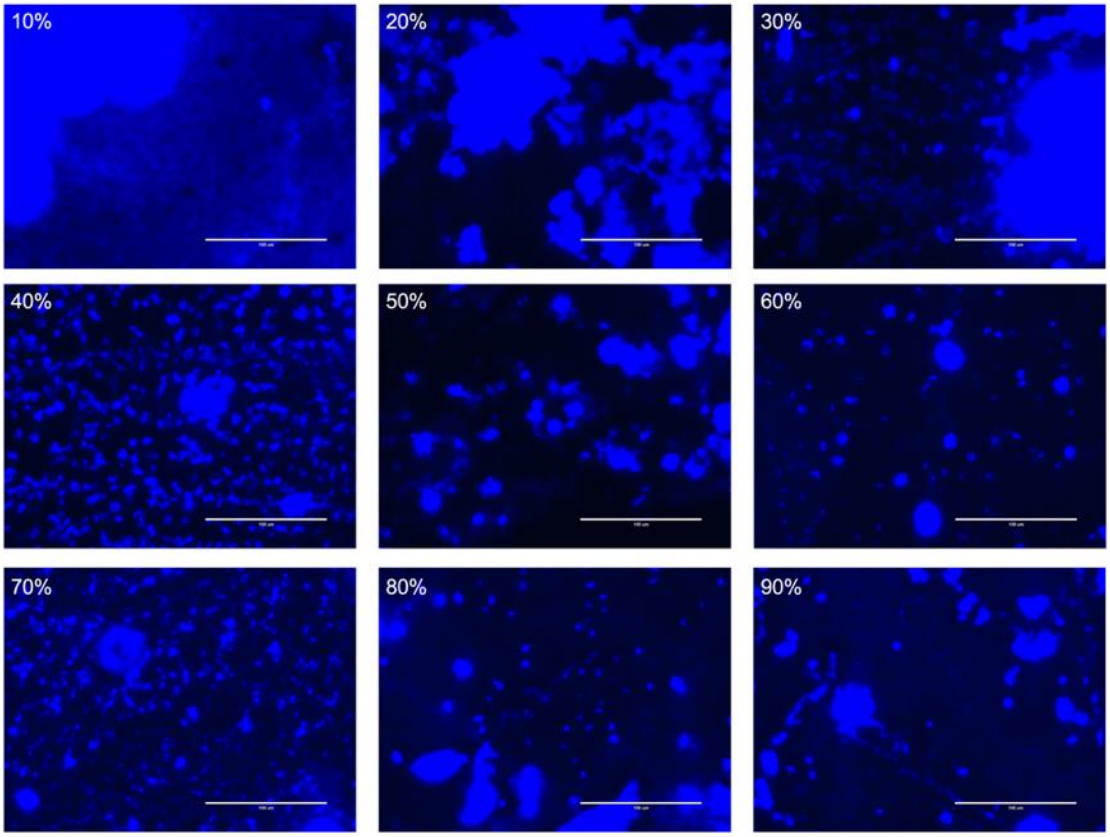

Figure 4.40. Fluorescence images of APX-ATO ASDs after preparation. Percentage refers to drug loading degree (w/w). Scale bar is 100 μm.

4.5 Discussion

4.5.1 Fluorescence emission spectra

Comprehensively viewing the fluorescence spectra for different drug-excipient systems, we consider the different parameters that are useful for analysis when using fluorescence methods to assess drug-excipient miscibility and drug amorphization for an ASD system. The wavelength of the emission peak maximum intensity is the first and most common parameter to consider as it can be used to indicate the local polarity of the fluorescent drug molecules. For IDM samples, the existence of an amorphous drug was reflected by the 508 nm peak. Phase separation and/or recrystallization were indicated by the shoulder peak close to the 460 nm region. For the APX samples, amorphous

drug and phase separation were indicated by the 460 nm peak and the 416 nm peak, respectively. The wavelengths were used to indicate the local polarity of drug molecules in different states.

The second parameter is the overall intensity of the fluorescence emission spectrum. In the case of IDM, the overall intensity of IDM-excipient samples generally increased with increased drug loading, except for the IDM-SA system. Comparing different APX systems, while all samples used the same drug-excipient ratio system as the case of IDM, they showed arbitrary change in fluorescence intensities which could be a sign of fluorescence quenching. Detailed discussions will be provided later.

A third parameter is the overall shape of fluorescence spectrum. A flat curve shape of the emission peak means that no obvious overlap occurs between the interested peak and other peaks, and most drug molecules in this sample share a similar polarity environment. As introduced, the polarity environment of IDM is determined by the crystallinity of other surrounding IDM molecules. Therefore a flat curve shape indicates that drug molecules are either in amorphous or crystalline state (depending on peak wavelength), instead of being a mixture of amorphous and crystalline domains with detectable difference in fluorescence shape. IDM-PVP, IDM-SOL, IDM-SA and IDM-EC showed this type of spectra with a broad single peak at 508 nm, suggesting that most IDM molecules were located in a high-polarity environment due to the surrounding of amorphous IDM. In contrast, IDM-PL showed a main peak at 508 nm associated with divided peaks at different wavelengths, suggesting two environments with distinctly different polarities. Fluorescence microscopy results for IDM-PL clearly showed large amounts of phase separation for samples with high drug loading, which agreed with the fluorescence spectra results that showed peak separation. Therefore, the peak separation in the emission spectra was considered to be an indication of poor miscibility and high degrees of phase separation as seen for IDM-PL and IDM-ATO systems [135,205]. This type of profile was also seen for IDM-G48 system where samples with high drug loading showed a fixed peak at 460 nm with high intensity, indicating that a large portion of IDM was in a crystalline state. Different shapes for emission peaks could also be observed for ASD systems containing APX, and no correlation between the general fluorescence intensity and drug loading was observed. In this regard, the emission spectra for ASD systems of IDM and APX will be analyzed based on peak shape, peak wavelength, relative intensity of different peaks, and corresponding information provided by fluorescence microscopy.

4.5.2 Drug amorphization and drug-excipient miscibility for IDM

(a) IDM-PVP miscibility

The increasing fluorescence intensity as a function of drug loading suggested that there was no obvious fluorescence quenching due to the increasing amount of IDM, which can be obtained by analyzing the fluorescence quenching mechanism. Fluorescence quenching can occur when the distance between fluorescent molecules was less than a critical value (i.e. several nanometers, depending on the properties of fluorescent molecules) [206–208]. Following this mechanism an IDM solution showed a much lower fluorescence intensity than solid IDM, as the molecule distance in a solution is less than 2 nm [205,209]. IDM was in a finely dispersed state in the PVP carrier whereby the fluorescence efficiency was not limited by close contact due to aggregation. With drug loading of 10% and 20%, IDM showed a high miscibility with PVP as indicated by the single emission peak at 508 nm and homogeneous fluorescence distribution of fluorescence images. The homogeneous fluorescence distribution of these samples suggested a uniform dispersion of IDM in an amorphous state through-out the PVP carrier. The emission spectra indicated phase separation of IDM from PVP beginning at an IDM concentration of 40% while fluorescence microscopy showed evidence of phase separation beginning for concentrations of 30%, From the fluorescence spectra, the slight peak separation between 460 nm and 508 nm region indicated that a portion of IDM molecules dispersed in an environment with smaller polarity. According to fluorescence microscopy, immiscible dots presented a similar fluorescence intensity to the bright background and were without needle shape or birefringence properties for crystalline IDM, suggesting that these regions were mostly amorphous in nature [205]. For 60% to 90% drug loading samples, the reduced uniformity of fluorescence intensity and birefringence properties were possibly due to the partial recrystallization of IDM. Upon heating, samples with lower drug loading started to gain these characteristics, describing the recrystallization evolution for IDM. While the investigation of long-term stability of ASD systems was beyond the scope of this study, the change in sample appearances upon heating could help us better identify the physical state of separated domains. The inhibited amorphous-crystalline transformation of IDM could be a result of solid-state hydrogen-bonding and Van der Waals force between IDM and polymeric chains of PVP [147,205]. Based on the experimental observations, the 20% drug loading IDM-PVP that we used for dissolution studies likely corresponds to an amorphous solid dispersion as theorized. The amorphous nature of IDM in IDM-PVP sample was expected to improve the dissolution and supersaturation buildup rate for IDM.

(b) IDM-SOL miscibility

The fluorescence spectroscopy results indicated that IDM-SOL with a drug loading of 10% to 30% had a high-degree of molecular miscibility supported by the fluorescence imaging results. Amorphous IDM dispersed uniformly throughout the SOL carrier. While samples with higher drug loadings also showed a main peak in the 508 nm region with negligible peak separation, immiscibility could be clearly observed by fluorescence spectroscopy results. Immiscibility was also inferred from the irregular change in fluorescence spectroscopy intensity starting at 40% drug loading. It is possible that fluorescence quenching could be induced between fluorescent molecules with a distance less than 30 nm. In the ASD drug aggregates could form if the drug content exceeds the loading capacity of the carrier material and these aggregates would be expected to contain a significant amount of amorphous drug. The distance between chromophores of a drug in its crystalline form depends on the crystalline lattice composed of fixed lengths and angles of lattice edges, whereas for a drug in its amorphous form, the distance between chromophores is no longer restricted because of the absence of the crystal lattice. As such it is possible that the overall emission efficiency of a drug could be attenuated by self-quenching if the distances in the amorphous drug are short enough to allow for such quenching. The high fluorescence density and weak birefringence properties of separated domains for immiscible IDM-SOL samples indicate that these domains are mostly amorphous IDM. These systems were considered to undergo amorphous-amorphous phase separation without obvious recrystallization, corresponding to the fluorescence spectra with single emission peak at 508 nm [205]. From this case, it was found that samples with amorphous-amorphous separation may still show single emission peak whereby peak divergence was not obvious. Therefore, a single emission peak does not necessarily mean a good miscibility between drug and excipient. Fluorescence microscopy results should be combined to accurately analyze the miscibility between IDM and polymer.

(c) IDM-SA miscibility

The changes in fluorescence emission intensity from IDM in the IDM-SA system (Figure 4.11) clearly suggest that there is increased quenching of the emission with increasing IDM concentration for IDM concentrations greater than 40%. The FM images also show the presents of phase separation and aggregation which indicates that the decrease in emission intensity is the result of IDM aggregation - most likely through self-quenching. Reviewing the solvent evaporation and film casting method used to prepare solid dispersions, a good solvent is often selected to dissolve the drug

and carrier to form a molecular solution so that both components can co-precipitate from solution to enable strong drug-excipient interactions such as hydrogen bonding and Van der Waals force. For the IDM-SA samples, IDM could not finely disperse in the SA carrier due to SA's insolubility in organic solvents and therefore showed an asynchronous precipitation behavior. Such preparation method would result in a weak solid-state interaction between IDM and SA. A large amount of IDM molecules was expected to adsorb onto the surface of SA and existed in the form of aggregates. The concentrated fluorescence intensity and weak birefringence properties of immiscible domains of IDM-SA suggested that most drug aggregates existed in an amorphous state. This being said, trace crystallinity of IDM was suggested by the existence of regions with birefringence properties for all samples. By comparing the fluorescence images of IDM-SA at day 0 and week 3, it was suggested that the drug domains at the early stage were governed by the amorphous feature. Comprehensively correlating these analyses, the IDM-SA was considered as a biphase ASD system composed of aggregates of amorphous IDM and small amount of crystalline IDM. The spectral properties were governed by the dominant amount of amorphous IDM, with weak expressions of crystalline properties at 464 nm region. The crystalline properties of IDM-SA samples were more effectively revealed by the fluorescence microscopy. The 20% IDM-SA that we used for other sections was considered a semi-crystalline ASD with weak crystallinity. Such property will be taken into consideration when analyzing the dissolution behaviors and supersaturation properties of IDM-SA ASD in the following chapter.

(d) IDM-EC miscibility

The IDM-EC series showed a fluorescence spectroscopy profile similar to that for IDM-PVP and IDM-SOL system. No severe fluorescence quenching was suggested by the monotonic increase in fluorescence intensity as a function of drug loading, except for the 90% drug loading sample. This corresponded to the few immiscible domains revealed by fluorescence microscopy. The major emission peak at 508 nm governed by amorphous IDM suggested a high-degree of miscibility between IDM and EC. The slight peak divergence in the 490 nm region depicted a slight immiscibility, matching the conclusions reached by fluorescence imaging. The small number of immiscible domains were with birefringence properties, suggesting the existence of crystalline IDM clusters. But this did not bring obvious peak divergence for the fluorescence spectra, possibly due to the different sensitivities of the two techniques. The maintained fluorescence microscopy properties under heating suggested an effective maintenance of amorphous IDM due to restricted molecular

mobility provided by EC polymer chain. EC has been recognized as an effective ASD carrier to load amorphous drug through the formation of hydrogen bonding between drug molecules and the cellulose hydroxyl groups. The 20% IDM-EC formulation that we use is expected to release the drug in the amorphous state. Its dissolution and supersaturation behaviors are established based on the successful amorphization and loading of IDM.

(e) IDM-PL miscibility

The fluorescence emission spectrum for IDM-PL mixtures was highly dependent on drug loading. The single emission peak centered at 508 nm for the 10% and 20% IDM samples suggested that the fluorescent probes in each sample share a local environment with uniform polarity, indicating that IDM molecules homogeneously dispersed in the phospholipid carrier. The homogeneous distribution of fluorescence across the entire viewing field in fluorescence microscopy images for the 10% and 20% IDM-PL samples support this conclusion. A high miscibility resulting from the strong molecular interactions between drug and excipient was suggested for these samples [87,210,211]. The appearance of the second peak at shorter wavelengths observed first at 30% IDM loading is a sign of a non-homogeneous distribution of IDM molecules within the PL carrier. The main emission peak remains fixed at 508 nm indicating that a large amount of IDM remains in an amorphous state as previously discussed for the IDM-polymer systems. The continuous blue shift of the secondary peak as a function of increasing IDM concentration indicated a gradual change in the polarity of the environment that the IDM molecules experience, most likely due to the mixing of IDM molecules in different states. The distribution of intensities observed across the immiscible domains suggests that IDM molecules are clustered at the interface between the miscible and immiscible domains and excluded from the interior when the drug content exceeds the drug loading capacity of PL. As introduced, the environmental polarity of a drug molecule in an ASD is determined by the physical state of other drug molecules surrounding it. The polarity of an IDM molecule in an immiscible region is provided by the mixture of IDM (either amorphous or crystalline) and PL, which is lower than that in a fine dispersion provided by pure amorphous IDM molecules [205,212]. Therefore, for the immiscible domains observed by fluorescence imaging, a significant amount of IDM molecules should locate in an environment with reduced polarity provided by the mixture of PL and IDM. Accordingly, a shoulder peak with smaller wavelength was observed for the fluorescence spectra of these samples. With a further increasing drug loading, certain immiscible regions showed crystalline properties, whereby certain IDM molecules shared a local environment with lower polarity as they

were surrounded by crystalline IDM which has lower polarity than amorphous IDM. This explained the further decreased wavelength of shoulder peaks for samples with higher drug loadings due to the increasing crystallization. Lastly, the overall fluorescence intensity level showed a constant increase as a function of IDM amount without severe fluorescence quenching. Given the fact that IDM aggregates in both amorphous and crystalline states were clearly observed, the correlation between fluorescence quenching and drug aggregation should be summarized as follow: the quenching of fluorescence intensity indicates the existence of drug aggregates, but the absence of fluorescence quenching cannot rule out the possibility of drug aggregation. The 20% IDM-PL that we used for other sections was considered with good IDM amorphization and high IDM-PL miscibility. An illustration of immiscible profiles of IDM-PL was shown in Figure 4.41.

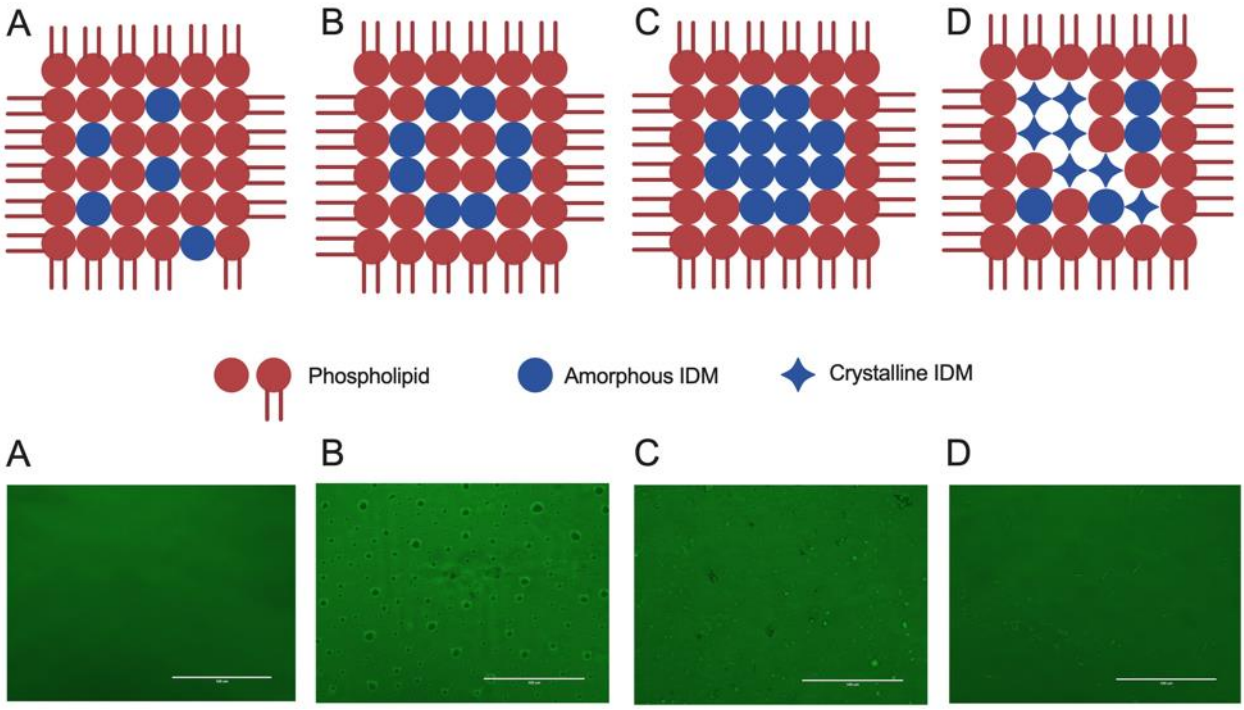

Figure 4.41. Schematic illustration and fluorescence imaging of IDM-PL in different states: (A) IDM uniformly disperses in PL carrier in an amorphous state; (B) small amount of amorphous IDM aggregates in PL carrier; (C) large amount of amorphous IDM aggregate into drug clusters; and (D) mixtures of amorphous and crystalline IDM aggregate into drug clusters.

(f) IDM-G48 miscibility

Generally, the IDM-G48 system presented a different way to express drug-excipient immiscibility. For the 10% and 20% drug loading samples, the fluorescence intensity at the 508 nm region was significantly lower than that for other systems as seen by the flat shape of the fluorescence spectra. The homogeneous fluorescence distribution was confirmed by the results of fluorescence microscopy. When drug loading exceeded 20%, a major emission peak was observed in the 464 nm region that represented crystalline IDM, masking the peak shape at 508 nm that represented amorphous IDM. No gradual change in wavelength was observed for the emission peak at 464 nm region, suggesting that the local polarity conditions of IDM molecules in these samples were highly comparable with that for crystalline IDM. Accordingly, the fluorescence microscopy results clearly showed the existence of immiscible domains with low fluorescence intensity and low contrast with regard to background. The low fluorescence intensity observed by microscopy corresponded to the low fluorescence intensity of 508 nm peak in the fluorescence spectra. The GFP channel of a fluorescence microscope optimally detects emission at 508 nm, and emission signal with smaller wavelengths could show a reduced contrast with regard to background due to attenuated fluorescence efficiency. This intensity attenuation mechanism was different from the fluorescence quenching induced by drug aggregation. Needle shape and birefringence properties could be observed for samples with drug loading larger than 20%, suggesting the presence of crystalline IDM in G48 carrier, corresponding to the pronounced 464 nm emission signal in fluorescence spectra. IDM-G48 samples upon heating did not gain fluorescence intensity or contrast, suggesting that the physical states of these samples were comparable with their earlier stages (i.e. crystalline state). The 20% IDM-G48 that we used for other sections was considered as an amorphous formulation after its preparation.

(g) IDM-ATO miscibility

For IDM-ATO, a single emission peak at 508 nm was observed for samples with drug loading from 10% to 70%, seemingly suggesting a miscibility between IDM and ATO for these samples. However, immiscible domains could be clearly visualized for these samples by fluorescence microscopy, contradicting the spectroscopy results. We think that the crystalline nature and poor film forming ability of ATO could be a reason for this deviation. For a fluorescence spectrum, ATO is not autofluorescent and emission signal is merely generated by the IDM molecules of different states. The

addition of ATO to drug molecules will not change the emission peak of IDM, supposed that IDM exists in the amorphous state. For fluorescence imaging, it is possible for the non-fluorescent crystalline ATO to be expressed as immiscible domains if certain amount of IDM, either crystalline or amorphous, is adsorbing on the surface of ATO. The immiscible regions for the samples with 10% to 60% drug loading had edges with higher fluorescence intensity and core areas with lower fluorescence intensity, suggesting that the large portion of these domains were nonfluorescent ATO carrier, and IDM aggregated at the boundaries of these regions. This profile was similar to the phase separation profile of IDM-PL with high drug loading, whereby inner structures of immiscible domains were nonfluorescent PL. The separation of amorphous IDM may not present a divergence in emission spectra due to the similar polarity environment of IDM molecules, as discussed before. In contrast, 70% to 90% drug loading samples presented a higher fluorescence intensity and birefringence properties for the core areas of immiscible domains, suggesting that these domains contained more drug aggregates. The drug aggregates were identified as crystal based on the birefringence properties observed, corresponding to the blue-shifted emission peak in the fluorescence spectra. The heating-induced change in appearance of IDM-ATO samples also supported this conclusion. The exhibition of high fluorescence intensity in the core areas of separated domains started to occur for samples with lower drug loadings after heating for different time periods, describing the aggregation of both amorphous and crystalline IDM.

From the case of IDM-ATO, it was seen that a single large emission peak at 508 nm region did not necessarily indicate a good miscibility between IDM and ATO. The separated amorphous drug may not bring change to the wavelength and integrated shape of the main emission peak. The fluorescence distribution of immiscible domains could be different for different IDM-carrier systems. Fluorescence spectroscopy and microscopy need to be combined to accurately assess the physical state of IDM-ATO.

The miscibility between IDM and polymers or lipids under solid state was characterized by fluorescence spectra and fluorescence microscopy methods. The spectral parameters including peak shape, peak wavelength, and general intensity could vary for different systems. The individual properties of an ASD carrier, such as crystallinity and film forming ability, need to be considered when interpreting the IDM fluorescence spectra results, for without such considerations the spectra results could be misleading due to the different ways of expression for immiscibility. Fluorescence spectroscopy and fluorescence microscopy are suggested to be conducted simultaneously to assess the

miscibility between IDM and ASD carriers. Comparisons between samples with different drug loadings are suggested, since viewing the spectrum for specific samples may be insufficient to obtain an accurate assessment.

4.5.3 Drug amorphization and drug-excipient miscibility for APX

Most APX-polymer and APX-lipid systems presented a similar type of fluorescence spectra with regard to drug loading. The presence of a large emission peak at 460 nm region for all samples could be due to the existence of a large amount of amorphous APX in the corresponding formulations. This suggested that APX recrystallization under solid state was slow, even without effective recrystallization inhibition effect provided by the ASD carriers after phase separation. For APX-PVP, fluorescence microscopy revealed the phase separation of APX for samples with drug loading more than 20%, but this did not bring obvious change to the spectral properties of different samples. Besides, most separated APX domains were with condensed fluorescence intensity free from birefringence properties, indicating that most of these aggregates were amorphous APX, which contributed to the high intensity of 460 nm emission peak. Similar indications could be obtained for other systems including APX-SOL, APX-SA, APX-EC, APX-PL and APX-G48. APX-EC was the only system showing a different type of fluorescence spectra, whereby the shape of the 420 nm emission peak was more obvious. For the 10% drug loading sample, the fluorescence intensity of the 420 nm peak was higher than that for the 460 nm peak, which could indicate that 10% APX-ATO was with poorer miscibility between APX and ATO following the previously summarized rule. However, we do not think that APX-ATO with a lower drug loading should provide a microenvironment with lower polarity as a larger ratio of carrier and drug amount should be with better loading ability for amorphous drug. The higher fluorescence intensity of 420 nm peak should be a result of higher fluorescence efficiently of crystalline APX than amorphous APX. As discussed, fluorescence quenching could occur due to drug amorphization and shortened distance between chromophores. The amount-normalized fluorescence efficiency of recrystallized APX could be higher than that for the large amount of amorphous APX in the 10% drug loading sample, and therefore the 420 nm peak could be more obvious. With a higher drug loading, the increasing amount of APX mainly existed in an amorphous state that contributed to the fluorescence intensity of the 460 nm peak. The 420 nm low-polarity peak did not effectively gain intensity since redundant APX did not effectively recrystallize according to the microscopy results. The fluorescence microscopy results for all APX-ATO samples revealed that only a small number of immiscible domains were with birefringence

property, and most regions were with non-crystalline optic properties. Given the dominant amount of amorphous APX, the higher fluorescence intensity at 420 nm was considered as result of higher fluorescence efficiency of crystalline APX. For the fluorescence spectra of APX-carrier systems, the dominant intensity and integrated shape of 460 nm emission peak were attributed to the existence of amorphous APX, but did not indicate a good APX-carrier miscibility.

Given the similarity in spectral characteristics of different systems, fluorescence microscopy results should be used to facilitate the analysis of the APX physical state. A uniform distribution of fluorescence density was a straightforward indicator for good APX-carrier miscibility, which aligned with the assessment principle for IDM systems. The birefringence property of a separated domain was an indicator for the crystalline nature of this region. The shape also needed to be considered to accurately evaluate the physical state of these immiscible domains. Taking the 20% APX-PVP at day 0 as example, the immiscible domains showed a stripe shape of crystalline substance with regularity of edges and a nonbirefringent property for amorphous material. Based on both shape and optic properties, we think this domain was composed of both crystalline and amorphous APX, which was also corresponding to the peak divergence of fluorescence spectrum. As shown in Figure 4.42, the 90% APX-PVP at week 1 was an example simultaneously showing fiber-like crystal shape (right part), birefringent property (right part), nonbirefringent property (middle large domain), and more homogeneous dispersion of APX molecules (left part), describing the different evolution stages for phase separation and recrystallization of APX. Similar phenomena could be also seen from the previously shown Figure 4.27.

Figure 4.42. Fluorescence image of 90% APX-PVP after 1-week heating.

The 50% APX-G48 at day 0 showed spiky aggregates with condensed fluorescence intensity in their core areas and slight birefringent properties for their edges. We considered that this was another type of amorphous-crystalline mixture of APX, for which the shape was determined by the spatial arrangements of different drug carriers. The 90% APX-G48 at day 0 was an example simultaneously presenting flocculent aggregates with birefringent properties and non-birefringent aggregates with less regularity in shape. After heating for different times, spiky and flocculent aggregates with birefringence properties became obvious for samples with lower drug loading. This comparison suggested that these morphology and optic properties were indicators for an advanced development stage of phase separation and transformation. By assessing the initial states of APX samples with these principles, the 20% APX-SOL that we used for other experiments was considered to be a high-degree amorphous formulation with good drug-polymer miscibility. Other APX formulations with 20% drug loading should contain mostly amorphous APX and small amount of crystalline APX.

4.6 Conclusion

In this chapter, fluorescence spectroscopy and fluorescence microscopy were successfully used to characterize the drug amorphization and drug-carrier miscibility for IDM and APX with

optimized experimental parameters. The solid-state fluorescence properties of APX dispersed in ASD carriers were revealed for the first time. Results showed that IDM and APX had varied miscibility levels with different polymer and lipid carriers. Immiscibility could be expressed as the separation of amorphous drug aggregates and/or recrystallized drug ASD carriers. The interpretations of fluorescence spectroscopy characteristics could be different based on the phenomena of different systems. The divergence in fluorescence spectra indicated an immiscibility between drug and carrier, but a single emission peak did not guarantee a good drug-carrier miscibility. Immiscible samples with amorphous drug aggregates may still present a single emission peak with negligible peak divergence. The overall intensity of a fluorescence spectrum could be attenuated by fluorescence quenching due to drug aggregation. The distribution of fluorescence density for fluorescence microscopy was a more effective criterion for the assessment of drug-carrier miscibility. The shape and birefringence properties of immiscible domains were also used to assess the physical state of drugs. The 20% drug loading IDM-PVP, IDM-SOL, IDM-PL and IDM-G48 used for future experiments were considered as amorphous formulations with uniform dispersion of IDM molecules, and the 20% IDM-SA, IDM-EC, and IDM-ATO were considered as amorphous formulations with the separation of amorphous IDM aggregates and trace amounts of crystalline IDM. The 20% drug loading APX-SOL was considered as amorphous formulation with uniform dispersion of APX molecules, while others were considered as amorphous formulations with amorphous APX aggregates. The drug amorphization state and drug-carrier miscibility revealed in this chapter will be used to analyze the dissolution and supersaturation properties of ASDs for IDM and APX prepared with different carriers that will be studied in following chapters. The presented methodology and assessment disciplines are expected to expand the application of fluorescence-bases techniques to the assessment of drug-excipient miscibility for more drugs and ASD carriers.

Chapter 5
Dissolution of IDM ASDs and APX ASDs prepared with polymer and lipid carriers

5.1 Abstract

In this chapter, ASDs for IDM and APX were prepared with polymers, lipids, and their combinations as carrier using both the solvent evaporation method and freeze-drying method. The physical state of IDM and APX was evaluated by differential scanning calorimetry and powder X-ray diffraction. The dissolution behaviors of the prepared samples were tested under non-sink conditions where LLPS and recrystallization were expected to occur for the released drug. The freeze-dried ASDs for IDM and APX were also assessed under two-stage dissolution conditions simulating the condition for the drug to transit from the gastric to intestinal environment. The dissolution and supersaturation parameters were analyzed based on previously investigated properties of carrier materials on the stabilization of LLPS and recrystallization results. For both IDM and APX, it was found that the dissolution parameters were greatly influenced by the carrier type in different manners. A given type of carrier could provide different effects when it was used to load different drugs. Preparation methods were found to induce inconsistent changes to different formulations. The disintegration, dissolution and dispersion of carrier materials were critical factors to assess the carriers' ability to generate and maintain supersaturated drug solutions. The correlations between carriers' effect on crystalline solubility, LLPS, recrystallization, and dissolution parameters could only be established when drug carriers could rapidly and completely dissolve or disperse in the dissolution media. The varied effects of polymer-lipid combination on the supersaturation evolution of drugs were based on the adjustment of solubility of carrier materials and therefore the in-solution properties of ASD carriers. To conclude, the effects of carrier materials on the amorphization, LLPS and recrystallization behaviors of PWSDs could effectively facilitate the analysis of supersaturation behaviors of ASD formulations and provide constructive directions to formulation adjustments. These properties could not be quantitatively correlated due to different solubility/dispersibility of carrier materials.

5.2 Introduction

Dissolution and drug release are important factors to evaluate the performance of an ASD formulation for both development and regulation purposes. Dissolution tests are commonly conducted on a dissolution apparatus where the volume of the dissolution media can be adjusted to provide both sink and non-sink conditions to assess different aspects of dissolution parameters. In chapter 3, we obtained the dissolution profiles of crystalline IDM and APX in the presence of different drug carriers, and concentration-time profiles of supersaturated IDM and APX solutions upon recrystallization under non-sink conditions on the basis of completely dissolved drug carriers. In this chapter, the dissolution profile of an ASD formulation will be seen as an overall result of drug amorphization during preparation, drug release from ASD carrier, solubilization effect of drug carrier on crystalline drug, and the evolution of supersaturated drug solution enabled by dissolved amorphous drug. A significant portion of analysis in this chapter will be based on the dissolution or dispersion of drug carriers, as it determines the drug release from drug carrier and associated supersaturation induction rate and evolution. The suitability of most commonly used drug release models for assessing the dissolution/dispersion of drug carriers for our experiment was reviewed.

1. The zero-order release kinetic refers to a process of constant drug release of a formulation that is controlled by the gradual drug release from the carrier material without being influenced by solute concentration [213]. It can be expressed as Equation 5.1:

$$F = F_0 + K_0 \cdot t \qquad \textbf{Equation 5.1}$$

where F is the amount of dissolved drug at a given time, F_0 is the initial amount of drug in solution, K_0 is the zero-order release constant, and t is time. This model describes the controlled release profile of a drug for which dosage form is a hindrance for dissolution. In the context of our experiment, the zero-order release profile within a period of time will indicate that the drug carrier is not instantly dissolved or dispersed in the dissolution media to release the amorphous drug.

2. The first-order release kinetic describes the situation where drug release is dependent on solute concentration, which is expressed by Equation 5.2 [213]:

$$\log C_t = \log C_0 - k_1 \cdot t/2.303 \qquad \textbf{Equation 5.2}$$

where C_t is the drug concentration at a given time, C_0 is the initial drug concentration, k_1 is the first-order drug release constant, and t is time. The equation proposes a first-order dependence on the

concentration gradient between the bulk solution phase and static diffusion layer next to solid surface. This model is used to describe the release of water-soluble drugs from porous matrices. For our application, a first-order release profile indicates that drug release is less restricted by the reservoir effect of the drug carriers.

3. The Higuchi model is a mathematical model proposed in 1963 to describe drug release from a matrix system, which is commonly used to study the release behaviors of poorly water-soluble drugs from solid and semi-solid matrices [214]. The model is expressed by Equation 5.3:

$$Q = A \cdot [D \cdot (2C - C_s) \cdot C_s \cdot t]^{1/2} \qquad \textbf{Equation 5.3}$$

Where Q is the amount of dissolved drug at a given time, A is the surface area of formulation, D is the diffusivity of the drug molecules, C is the initial concentration of drug, Cs is the equilibrium solubility of drug, and t is time. The simplified Higuchi model is expressed by Equation 5.4:

$$Q = KH \cdot t^{1/2} \qquad \textbf{Equation 5.4}$$

where KH is the Higuchi dissolution constant. This model is widely used to describe the drug release profile from the insoluble matrix, and therefore reflects the slow dissolution of carrier material.

4. The Hixson-Crowell cube root law was proposed to describe the dissolution rate of a drug that is normalized with the decrease in the surface area of solid carrier as a function of time, which is expressed by Equation 5.5 [215]:

$$Q_t{}^{1/3} = Q_0{}^{1/3} - K_{HC} \cdot t \qquad \textbf{Equation 5.5}$$

where Q_t is the remaining weight of solid formulation at a given time, Q_0 is the initial weight of the solid formulation, KHC is the dissolution rate constant, and t is time. This model is established based on the correlation that the surface area of a solid formulation with a uniform particle size decreases as the two-third power of its weight. The application of this model is claimed to be suitable for monodispersed solid materials for which all units have identical properties including size, shape, and surface characteristics. However, according to our experimental observations, several ASD formulations prepared by either the solvent evaporation method or the freeze-drying method showed different properties including particle aggregation and floating issue in the dissolution media. Therefore, drug release from different formulations will not depend on the uniform decrease in formulation size. This model will not be used to analyze the dissolution properties of drug carriers.

5. The Korsmeyer-Peppas model was proposed in 1983 to describe drug release from a polymeric system prepared with swelling or non-swelling material. The model is expressed by Equation 5.6 [216]:

$$\frac{M_t}{M_a} = K \cdot t^n \qquad \textbf{Equation 5.6}$$

Where M_t/M_a is the fraction of drug released at a given time, K is the dissolution rate constant, t is time, and n is the release exponent which can be effectively used to indicate the drug release mechanism through the polymer system. When the n value is not larger than 0.5, drug release follows a diffusion mechanism from the non-swellable matrix. When the n value is between 0.5 and 1.0, drug release is based on both diffusion and erosion of the polymer materials. The n value of 1.0 describes a zero-order release mechanism. The n value over 1.0 indicates that the drug release is governed by the erosion of polymer materials. However, linear regression using this model could not be conducted for dissolution data with the concentration decline profile. For several ASD formulations, the maximum drug concentration could be achieved within 5 min, generating insufficient amount of data points for regression analysis. As a result, this model is not suitable for the analysis of early stage of supersaturation buildup, thus it was not used in this study.

In this chapter, the dissolution and supersaturation properties of ASDs for IDM and APX will be correlated to the solid-state properties of loaded drugs, dissolution or dispersion of carriers, solubilization effect of carriers, and supersaturation maintaining effect of carriers. Model fitting of dissolution data within a specific period of time will be conducted to facilitate the analysis of dissolution or dispersion of drug carriers.

5.3 Materials and methods

5.3.1 Materials

Indomethacin (IDM, purity > 97.5%), ethyl cellulose and sodium dodecyl sulfate were purchased from Fisher Scientific (Hampton, NH, USA). Apixaban (APX, purity > 99%) was purchased from HuiRui Chemical Technology Co., Ltd (Shanghai, China). Poly (vinylpyrrolidone) (PVP) K90 and phospholipid were purchased from Sigma-Aldrich (Mississauga, ON. Canada). The phospholipid used in this study (Sigma-Aldrich catalog no. P3644) contains 55% phosphatidylcholine, 25% phosphatidylethanolamine and other phospholipids, with an average

molecular weight of 776 g/mol. Polyvinyl caprolactam-polyvinyl acetate-polyethylene glycol graft co-polymer (Soluplus®, SOL) was a gift from BASF (Ludwigshafen, Germany). Sodium alginate (CAS number: 9005-38-3) was obtained from Acros Organics (USA). PEG-32 stearate (Gelucire® 48/16, G48) and glyceryl behenate (Compritol® 888 ATO) were a gift from Gattefosse (Saint-Priest, France). Methanol, acetonitrile, and dimethyl sulfoxide (DMSO) of high-performance liquid chromatography (HPLC) grade, and tert-butanol (99%) were purchased from Fisher Scientific (Hampton, NH, USA). Anhydrous citric acid and sodium phosphate dibasic of ACS grade were purchased from VWR International (Radnor, PA, USA). Water used in this study was obtained from a Millipore Milli-Q system.

5.3.2 Preparation of ASDs for IDM and APX

5.3.2.1 Solvent evaporation method to prepare ASDs

IDM ASDs with a drug loading of 20% were firstly prepared by a solvent evaporation method. 450 mg IDM and 1800 mg of ASD carrier were added to 90 mL ethanol and stirred at 90 ˚C for 2 h. For IDM-ATO and IDM-polymer-ATO preparations, 90 mL ethyl acetate was used as solvent. The solvent was removed using a rotary evaporator under reduced pressure at 50 ˚C. The obtained samples were further dried in a vacuum oven at 40 ˚C overnight. The samples were removed from the round bottom flask and ground manually for 1 min using a pestle and mortar. The obtained powders were kept at 4 ˚C before further use.

For the preparation of APX ASDs, 400 mg of APX and 1600 mg of ASD carrier were added to 150 mL methanol and stirred at 90 ˚C for 2 h. For the preparation of APX-ATO and APX-polymer-ATO formulations, 225 mL methanol: ethyl acetate (3:1 v/v) binary solvent was used. Other procedures were kept the same.

For all experiments, ASD powder samples were not processed through sieves to control particle size, as some samples could not pass through sieve due to their specific physical properties (i.e. G48 based ASDs adhered to sieve pore due to wax-like property, PL based ASDs were in a semi-solid state with intermolecular complexation, etc). The effect of solid state of ASD powders will be taken into consideration for the analysis of dissolution data.

5.3.2.2 Freeze drying method to prepare ASDs

IDM ASDs with a drug loading of 20% were also prepared by a freeze-drying method. 200 mg of IDM and 800 mg of ASD carrier were added to 60 mL of tert-butanol and stirred at 70 ˚C for 2 h. The solution was then transferred to conical tubes and kept in a -80 ˚C freezer for 24 h. The frozen samples were lyophilized using a FreeZone Plus 2.5 freeze dryer (Labconco, MO, USA) at -85 ˚C under a reduced pressure of 0.090 mbar for 48 h. The obtained ASD powders were stored at 4 ˚C before further experiments.

For the preparation of APX ASDs, 350 mg of APX and 1400 mg of ASD carrier were added to 160 mL of a tert-butanol: methanol (7:1 v/v) binary solvent and stirred at 70 ˚C for 2 h. For APX-PVP, the solvent was 170 mL of tert-butanol: methanol: water (7:1:0.5 v/v) ternary solvent. The small quantity of water was added to reduce the swelling and improve the dissolution of PVP. Other procedures were kept the same. All samples were stored at 4 ˚C before further experiments.

5.3.3 Differential scanning calorimetry (DSC) for ASD samples

Thermograms of ASDs for IDM and APX were obtained using a Q2000 differential scanning calorimeter (TA Instruments, DE, USA). Approximately 5 mg of IDM sample was sealed in an aluminum pan and heated from 30 ˚C to 200 ˚C with a heating rate of 10 ˚C/min. The temperature range was 30 ˚C to 300 ˚C for APX samples. A nitrogen flow rate of 50 mL/min was maintained throughout the measurements.

5.3.4 Powder X-ray diffraction (PXRD) for ASD samples

X-ray diffraction patterns of ASDs for IDM and APX were obtained on a MiniFlex II X-ray diffractometer (Rigaku Corporation, Tokyo, Japan) using Copper K-α radiation at 30 kV and 40 mA. Diffractograms were recorded over a 2θ angle from 3° to 40° with a scanning rate of 2° per minute and a 0.05° step size for all samples.

5.3.5 In vitro dissolution study of ASDs for IDM and APX

5.3.5.1 Dissolution of IDM ASDs and APX ASDs in pure water

To investigate the dissolution behaviors of ASDs induced by their intrinsic properties, water without any buffer was initially used as dissolution medium. An SI index of 0.1 was used to select the dose for dissolution tests, corresponding to the previous supersaturation assessment for ASD carriers.

For the IDM section, ASD samples equivalent to 20 mg of IDM were added to 250 mL water maintained at 37 °C with a stirring rate of 150 rpm. The dose was 10 times IDM solubility in a 250-mL dissolution medium. At predetermined time intervals, a 2 mL sample was withdrawn, and a same amount of water was replenished. The samples were filtered through a 0.22 μm PES syringe filter. IDM concentration was determined by a UV spectrometer based on a Beer-Lambert calibration curve at 318 nm. For the APX ASD samples, an amount equivalent to 90 mg of APX was added to 250 mL of water to initiate dissolution testing. Other procedures were kept the same. The APX concentration was determined using a UV spectrometer based on a Beer-Lambert calibration curve at 278 nm. The dissolution tests were run for IDM ASDs and APX ASDs prepared by both the solvent evaporation method and the freeze-drying method.

5.3.5.2 Two-stage dissolution of freeze-dried IDM ASDs and APX ASDs

A two-stage dissolution condition was used to assess the dissolution behaviors of lyophilized IDM ASDs in two consecutive dissolution conditions which correspond to the pH environment of different gastrointestinal compartments. Generally, a change of pH from 2.2 to 5.0 is used to mimic the pH shift from the gastric environment to the upper intestine, and the change of pH from 2.2 to 6.8 was used for transition from the gastric to the main intestinal compartment. In our study, the range of pH 2.2 to pH 5.0 was selected as testing condition considering the pH-dependent solubility of IDM and the practical volume of dissolution medium. In pH 6.8 phosphate buffer, the IDM solubility shows a high solubility of 800.7 μg/mL at 37 °C, translating to a maximum dissolvable dose of 400 mg in a 500-mL dissolution medium. This would require a large dose of 4 g of IDM for the SI = 0.1 condition. Therefore, the 500-mL dissolution medium with a pH of 6.8 was a sink condition, which was a favorable condition, for the 20 mg IDM dose used in previous sections. No supersaturation or drug recrystallization was expected under such circumstance, and the dissolution behaviors of different formulations could not be correlated with the previously revealed supersaturation ability of polymer and lipid materials. In contrast, a pH of 5.0 is closer to the pKa of IDM and provides lower solubility, so that the condition is seen with higher non-sink degree suitable for the assessment of IDM supersaturation. Therefore, we selected pH 2.2 and pH 5.0 as two phases for the dissolution of IDM ASDs.

Dissolution media were prepared according to McIlvaine buffer compositions with modification [217]. The pH 2.2 McIlvaine buffer (referred to as stock A) was prepared by mixing 0.1

M citric acid solution and 0.2 M disodium phosphate solution with a volume ratio of 49:1. The 0.2 M disodium phosphate solution was referred as to stock B. For the acidic stage, 250 mL of stock A was used initially as the dissolution medium. Samples equivalent to 20 mg IDM were added to the dissolution media and stirred at 37 °C with a paddle speed of 75 rpm. At predetermined time intervals, 2 mL samples were withdrawn and replaced with the same volume of stock A. Filtered aliquots were diluted as required before ultra-performance liquid chromatography (UPLC) determination of IDM concentrations. At 60 min, 250 mL of stock B was added to stock A to achieve a 500-mL dissolution medium with a pH of 5.0. The dissolution parameters and sample processing method were kept the same.

For the APX section, dissolution buffers were also designed to correspond to available studies according to McIlvaine buffer compositions with modification. An alkaline buffer solution was prepared by dissolving 19.58 g of disodium phosphate, 18.46 g of sodium hydroxide, and 1.38 g of sodium dodecyl sulfate (SDS) in 2000 mL of water, referred to as stock C. ASD samples equivalent to 90 mg of APX was added to 250 mL of stock A to initiate dissolution at pH 2.2 with a paddle speed of 75 rpm at 37 ˚C. At 60 min, 650 mL of stock C was added to the dissolution vessel to initiate dissolution at pH 6.8. After mixing, the dissolution medium was a 0.05 M phosphate pH 6.8 buffer with 0.05% SDS, similar to compositions commonly used for dissolution media of APX products in previous studies [150,218]. 2 mL of sample was withdrawn at the predetermined time intervals and a same amount of dissolution medium was replenished. The APX concentration was determined using the UPLC method described in section 5.3.6.

5.3.6 UPLC method

The samples withdrawn from the dissolution vessels were filtered through a 0.22 μm PES syringe filter. Samples from the pH 2.2 stage were diluted with methanol to prevent drug recrystallization. Samples from the pH 6.8 stage were diluted with water to prevent the recrystallization of buffer salts. UPLC methods were developed to determine the concentration of the IDM and APX samples withdrawn from complexed media. All experiments were conducted on a Waters Acquity H plus UPLC system equipped with a quaternary pump, a diode-array detector, a degasser, and an autosampler. The separation was conducted on a BEH C18 column (1.7 μm, 2.1 × 50 mm) with a C18 VanGuard Pre-column (1.7 μm, 2.1 × 5 mm) both maintained at 40 ˚C. For IDM, the mobile phase consisted of 50% water and 50% acetonitrile (v/v). The injection volume was 10 μL and

the flow rate was 0.5 mL/min. The UV signal was collected over the 210 nm to 400 nm range and peaks were integrated at 318 nm by the Empower 3 software. The UPLC peak area was recorded for IDM solutions of 0.625 µg/mL to 20.0 µg/mL generated from a serial dilution. For APX, the mobile phase consisted of 60% water and 40% acetonitrile (v/v) with 0.1% triethylamine. The column temperature was maintained at 40 °C. The injection volume was 10 µL and the flow rate was 0.2 mL/min. The UV signal was collected over the 210 nm to 400 nm range and peaks were integrated at 280 nm by the Empower 3 software. The UPLC peak area was recorded for IDM solutions of 2.50 µg/mL to 30.0 µg/mL.

The accuracy of the UPLC method was assessed by a repeated injection of samples with known concentrations. IDM and APX solutions of different concentrations were injected for 3 times to record UPLC peaks areas. The recovery rates for these injections were calculated with regard to known concentrations. The precision was assessed by repeated injection of samples with known concentrations both intraday and interday.

5.4 Results

5.4.1 DSC

5.4.1.1 DSC thermograms of IDM ASDs

The DSC thermograms obtained for IDM and each ASD carrier were shown in Figure 5.1A. IDM showed a distinct melting peak at 160.9 °C, which is the characteristic of the IDM γ form. G48 and ATO showed a melting peak at 45.6 °C and 71.6 °C, respectively, describing the crystalline nature for these lipid carriers. PL exhibited endothermic signals at 175 °C, corresponding to the gel-to-liquid crystalline phase transitions of the hydrocarbon tails of PL [219]. Other carriers did not show any significant thermal behavior within the tested range consistent with their amorphous nature. PVP and SOL exhibited a broad endothermic curve at 120 °C and 70 °C, respectively, corresponding to their glass transition temperatures [220,221]. SA presented a wide endothermic curve at 170 °C, which was due to gelatinization and loss of non-freezing bond water [222]. EC presented a broad endothermic signal at 180 °C corresponding to its softening point [223]. The thermograms of solvent-based IDM ASDs based on PVP, SOL and EC were generally featureless suggesting that IDM existed in an amorphous state that was finely dispersed in ASD carriers (Figure 5.1B). A broad endothermic peak was seen for the IDM-PVP dispersion, with the peak position shifted to a lower temperature

(compared to PVP alone) due to the plasticizing effect provided by IDM. For IDM-SA, a tiny divergence in DSC curve without obvious peak shape was observed at 150 °C, which could possibly result from the trace crystalline IDM left in the formulation. The reduced peak intensity and changed peak position were indicators of drug amorphization molecular interactions between IDM and SA. For IDM-PL, the physical state of IDM could not be accurately analyzed due to the overlap of endothermic signals of the PL and IDM melting point from 155 °C to 175 °C. For IDM-G48, the shifted position and divergence of the G48 melting peak suggested the existence of strong interactions between IDM and G48 molecules. Although the melting peak of crystalline IDM at 160.9 °C disappeared for IDM-G48, it did not rule out the possibility that some crystalline IDM dissolved in the molten G48 carrier during measurement. This consideration also applied to IDM-ATO, whereby the melting point of the ATO carrier was lower than IDM. Nevertheless, for IDM-ATO, immiscible peaks at 130 °C and 152 °C were observed, suggesting the existence of remaining crystalline IDM in formulations. PXRD results need to be used to confirm whether crystalline IDM existed in IDM-PL and IDM-G48.

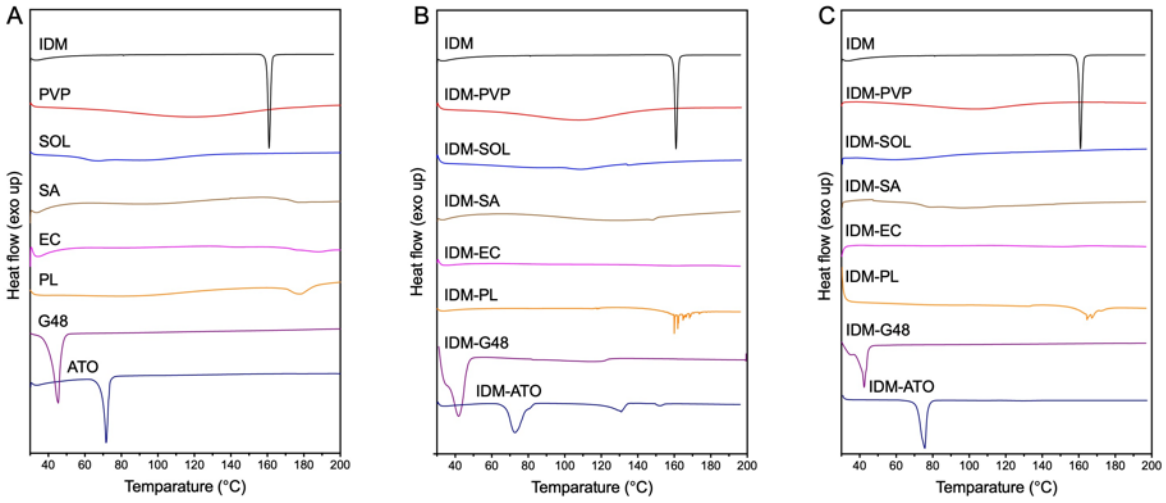

Figure 5.1. DSC thermograms of (A) ASD carriers, (B) solvent-based IDM ASDs and (C) freeze-dried IDM ASDs.

The thermograms of freeze-dried IDM ASDs were shown in Figure 5.1C. IDM existed in an amorphous state in all polymer-based formulations as revealed by the featureless thermograms. For

IDM-PL, small peaks could be observed at 160 °C region, which was lower than the characteristic phase transition region of PL. The peak intensity was significantly lower than the melting peak of IDM. While suggesting a good miscibility between IDM and PL after the freeze drying process, these indicators could not accurately confirm the crystallinity of IDM due to the overlapping signals of IDM melting and PL phase transition. For IDM-G48 and IDM-ATO, the physical state of IDM could not be obtained due to the presence of lipid melting at low temperatures, similar to the findings of solvent-based ASDs. PXRD results will be used to facilitate the analysis.

For solvent-based IDM ASDs prepared with polymer-lipid combinations, all samples did not show the characteristic melting peak of crystalline IDM at 160.9 °C (Figure C-1 in Appendix). Only endothermic signals of lipid components could be observed. The phase transition signal of the PL tail was not observed for samples using polymer-PL as binary carriers, suggesting a good miscibility between PL and these polymers. IDM-PVP-PL, IDM-SOL-PL and IDM-EC-PL showed an amorphous characteristic. As just mentioned, the physical state of IDM in formulations containing G48 and ATO could not be accurately determined due to the presence of melting behaviors of these formulations before the melting point of IDM. PXRD results will be used to analyze these samples.

Freeze-dried samples based on polymer-lipid combination carriers including PVP-PL, SOL-PL SA-PL and EC-PL showed featureless thermograms, indicating that IDM existed in an amorphous state finely dispersed in ASD carriers (Figure C-2 in Appendix). Other samples showed certain miscibility between different components as seen by the changed peak position, peak divergence and reduced intensity of lipid components. The physical state of IDM in these formulations will be analyzed based on the PXRD results considering the lipid melting at low temperatures.

5.4.1.2 DSC thermograms of APX ASDs

The thermograms of solvent-based APX ASDs and individual carriers were compared in Figure 5.2. Crystalline APX showed a distinct melting peak at 237 °C consistent with the characteristic of APX N-1 form [152]. Compared to the thermal properties between 30 °C and 200 °C revealed in the previous section, PVP, SOL, G48 and ATO did not show additional characteristic from 200 °C to 300 °C (Figure 5.2A). The exothermic signal of SA in the 230 °C to 270 °C region corresponded to the thermal decomposition of SA [222]. The wide endothermic peak at 235 °C for EC was a melting peak consistent with the semi-crystalline nature of EC [224]. The large endothermic signal at 265 °C for PL was a result of thermal decomposition [225]. APX-PVP and

APX-SOL presented thermograms similar to individual polymers, without characteristic of crystalline APX. APX-EC, APX-PL and APX-ATO showed a small endothermic peak at 237 °C, suggesting the existence of crystalline of APX in these formulations. The shapes of thermal signal for the decomposition of SA and the melting behavior of G48 were changed after the preparation of solid dispersions, which were due to the miscibility and strong interactions between APX and these carriers. Despite this, the physical state of APX-SA and APX-G48 will be further assessed by PXRD due to the overlapping of APX melting peak and SA decomposition signals, and melting of G48 at low temperature.

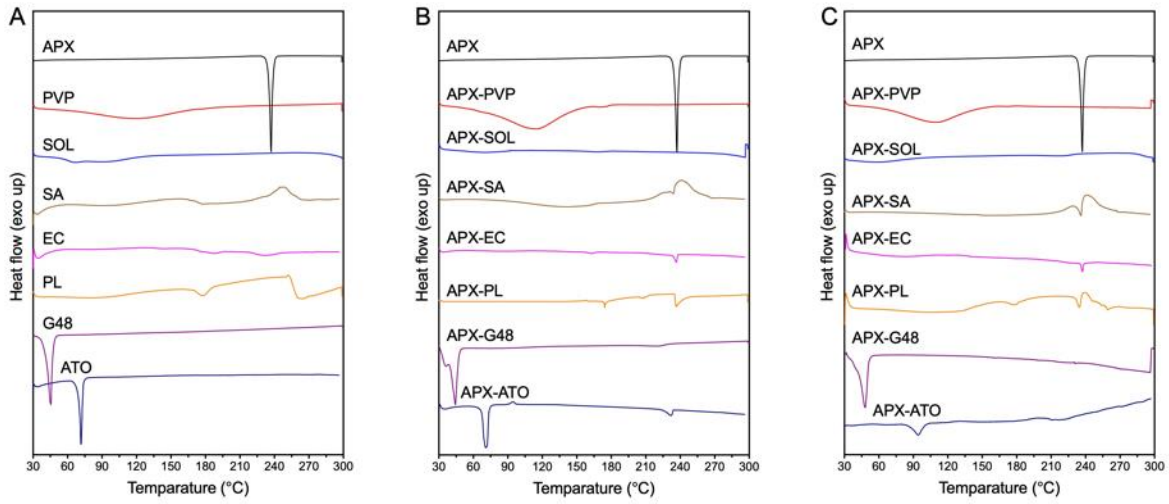

Figure 5.2. DSC thermograms of (A) ASD carriers, (B) solvent-based APX ASDs and (C) freeze-dried APX ASDs.

The thermograms of freeze-dried APX-ASDs were shown in Figure 5.2C. APX-PVP and APX-SOL presented a featureless thermogram that described their amorphous property. Crystallinity was confirmed by the small sharp endothermic peak at 237 °C for APX-EC. The physical state of other formulations will be confirmed by PXRD results due to signal overlap or lipid melting.

Solvent-based APX ASDs prepared with polymer-lipid combinations showed different miscibility levels according to the DSC results. APX-PVP-PL and APX-PVP-G48 showed a high-degree of miscibility between APX and carrier materials, without presenting the phase transition of PL or the melting of G48 (Figure C-3 in Appendix). The characteristic crystalline peak of APX at 237

°C was not observed, suggesting that APX existed in an amorphous state in these formulations. APX-SOL-PL was also considered as an amorphous formulation as seen by its featureless thermogram. In contrast, APX-SA-PL and APX-SA-ATO showed a distinct melting peak for APX, suggesting the existence of crystalline APX in these formulations. APX-SA-G48 presented a modified profile of SA decomposition, suggesting the existence of interactions between APX and binary carrier, but the physical state of APX needs to be confirmed by PXRD to rule out the possibility that crystalline APX is dissolved in molten G48. The small crystalline peak for APX could be observed for the thermograms of APX-EC-PL, APX-EC-G48 and APX-EC-ATO at 237 °C, confirming that a small amount of APX was loaded in the formulations in a crystalline state.

The thermograms of freeze-dried APX ASDs based on polymer-lipid combinations generally showed reduced characteristics of lipid components, resulting from the miscibility of formulation components after the freeze drying process (Figure C-4 in Appendix). APX-PVP-PL, APX-SOL-PL showed an amorphous profile. Crystallinity with reduced degree for APX was characterized for APX-SA-ATO, APX-EC-PL, APX-EC-G48 and APX-EC-ATO, suggesting the existence of crystalline APX in formulations due to recrystallization during or after sample preparation. The physical states of other formulations will be further assessed by PXRD due to signal overlap and lipid melting.

5.4.2 PXRD

5.4.2.1 PXRD diffractograms of IDM ASDs

PXRD diffractograms of IDM ASDs were obtained to further verify the physical state of IDM in the formulations, as shown in Figure 5.3. Pure IDM showed a high-degree of crystallinity as characterized by the sharp peaks at 11.96°, 17.32°, 19.92°, 22.12°, 24.32°, 26.92°, 27.80°, and 29.68°, associated with numerous small peaks. PVP, SOL, SA and PL showed an amorphous halo band over the investigated 2θ range, corresponding to their non-crystalline nature and consistent with the above DSC results (Figure 5.3A). EC showed a small peak at 11.94° consistent with its semi-crystalline nature, corresponding to the DSC results. Lipid G48 showed sharp peaks at 19.60° and 23.70°, and ATO showed sharp peaks at 21.62° and 23.94°, corresponding to their crystalline nature. The diffractograms of solvent-based IDM ASDs prepared with PVP, SOL, SA, EC and PL were essentially the same as individual carriers, suggesting that IDM was existing in an amorphous state in the formulations (Figure 5.3B). IDM-G48 showed peaks at 19.60° and 23.72° corresponding to the crystal property of G48 carrier with reduced intensity, and no characteristic peaks for IDM could be

observed. This suggested that the IDM loaded in the formulation was in an amorphous state, facilitating the analysis based on DSC thermograms. For IDM-ATO, a small peak was observed at 19.58°, additional to the characteristic peaks of ATO. A halo band was observed at 10° to 17° region, which did not align with the intrinsic property of ATO. The divided peak was mainly considered as an expression of a change in property of ATO carrier upon interacting with amorphous IDM. The characteristic crystalline peaks for IDM were not observed. IDM loaded in the ATO carrier was considered to exist in a mostly amorphous state. The diffractograms of freeze-dried IDM ASDs were shown in Figure 5.3C. All samples showed a high-degree of amorphous character whereby the observed peaks were assigned to the properties of the lipid carriers.

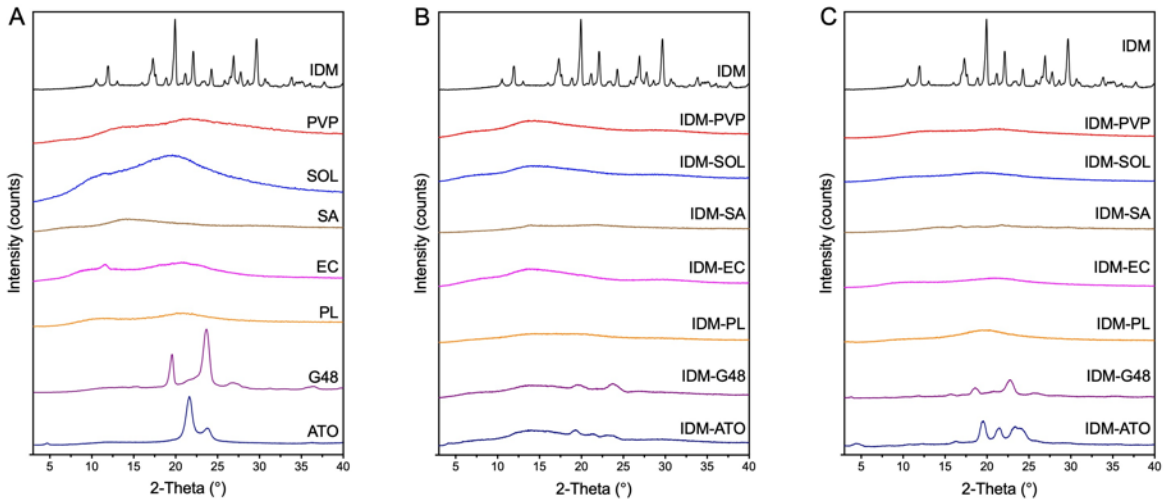

Figure 5.3. PXRD diffractograms of (A) ASD carriers, (B) solvent-based IDM ASDs and (C) freeze-dried IDM ASDs.

The diffractograms for solvent-based and freeze-dried IDM ASDs based on all polymer-lipid combinations showed an amorphous feature for loaded drug, whereby the observed peaks could be assigned to the properties of the lipid carriers (Figure C-5 and Figure C-6 in Appendix). The PXRD results further confirmed the physical state of IDM in ASD formulations on the basis of DSC results.

5.4.2.2 PXRD diffractograms of APX ASDs

The PXRD diffractograms of solvent-based and freeze-dried APX ASDs were shown in Figure 5.4. Pure APX showed a high-degree of crystallinity characterized with sharp peaks at 8.56°, 12.80°, 13.90°, 16.96° 18.40°, 19.60°, 21.60°, 21.90°, and 22.20°, associated with numerous small peaks. Solvent-based APX ASDs prepared with PVP, SOL, SA, EC and PL showed an amorphous diffractogram without sharp peaks (Figure 5.4B). For APX-G48, the large peak at 19.36° and 20.52° were consistent with the crystalline peak of the G48 carrier. The small peaks in the region of 11° to 17.5° with noticeable intensity suggested the existence of crystalline APX in APX-G48. No obvious crystallinity could be obtained from the diffractogram of IDM-ATO, but a halo band was observed from 10° to 17° which was different from the intrinsic property of ATO. This was considered as a sign of trace APX crystallinity as suggested by the above DSC result. The diffractograms of freeze-dried APX ASDs showed crystallinity to different degrees as shown in Figure 5.4C. APX-PVP, APX-EC and APX-ATO showed a high-degree of amorphous character as seen by the absence of characteristic crystalline peaks of APX. APX-SOL and APX-SA exhibited non-smooth diffractograms while without peaks with integrated shapes. This suggested that crystalline APX existed in the formulations in small amounts. APX-PL and APX-G48 showed more obvious diffraction peaks over the tested range, indicating that a significant portion of APX existed in a crystalline state after freeze drying process. Solvent-based samples prepared with PVP-lipid, SOL-lipid and EC-lipid combinations showed a high-degree of amorphous feature where small peaks were assigned to the characteristics of individual carriers (Figure C-7 in Appendix). Samples prepared with SA-lipid combinations presented non-smooth diffractograms with characteristics of crystalline APX. Freeze-dried samples prepared with polymer-lipid combinations including PVP-PL, PVP-G48, PVP-ATO, SOL-PL, SOL-G48, SA-PL, EC-PL and EC-G48 exhibited an amorphous feature whereby observed peaks could be assigned to the properties of the carrier materials (Figure C-8 in Appendix). Other freeze-dried samples showed small peaks consistent with the characteristic of crystalline APX, suggesting the existence of a significant amount of crystalline drug in the formulations.

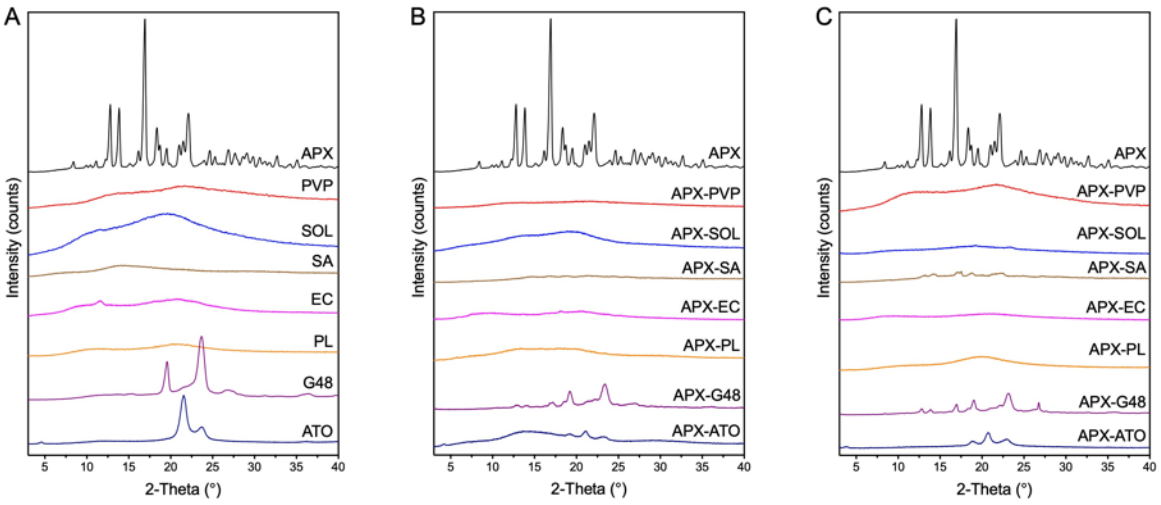

Figure 5.4. PXRD diffractograms of (A) ASD carriers, (B) solvent-based APX ASDs and (C) freeze-dried APX ASDs.

5.4.3 In vitro dissolution of IDM ASDs

5.4.3.1 Dissolution of solvent-based IDM ASDs in pure water

The dissolution profiles of IDM ASDs were characterized under non-sink conditions. The effects of polymer and lipid carriers on the dissolution behaviors of IDM were revealed, and the polymer-lipid combination effects will be analyzed according to properties of individual carriers. The dissolution behaviors were correlated with the effects of ASD carriers on the amorphization, LLPS, solubilization, and supersaturation of IDM that were investigated in previous chapters.

5.4.3.1.1 Dissolution of solvent-based IDM ASDs prepared with individual carriers

Figure 5.5 presents the dissolution profiles for IDM alone and for IDM formulated with individual polymer and lipid carriers. IDM alone showed a slow dissolution rate reaching an equilibrium IDM concentration of 7.8 ± 0.2 µg/mL after 24 hrs. The combination of IDM with SOL gave essentially the same dissolution profile (blue curve in Figure 5.5A) as IDM alone, reaching an equilibrium concentration of 10.3 ± 0.3 µg/mL after 24 hrs. The combination of IDM with PVP or with SA both gave an improvement in the dissolution profile, i.e. a more rapid dissolution, or in the equilibrium concentration. The profile obtained for the IDM-SA combination did not display any marked changes in concentration upon reaching a plateau of approximately 55 µg/mL or nearly 7

times the IDM solubility, indicating that recrystallization of IDM was prevented. PVP was also able to increase the solubility of IDM by approximately 4 times; however, the decrease in IDM concentration observed after approximately 250 minutes indicates that recrystallization was only delayed rather than prevented. EC was observed to inhibit the dissolution of IDM as a result of its own insoluble nature.

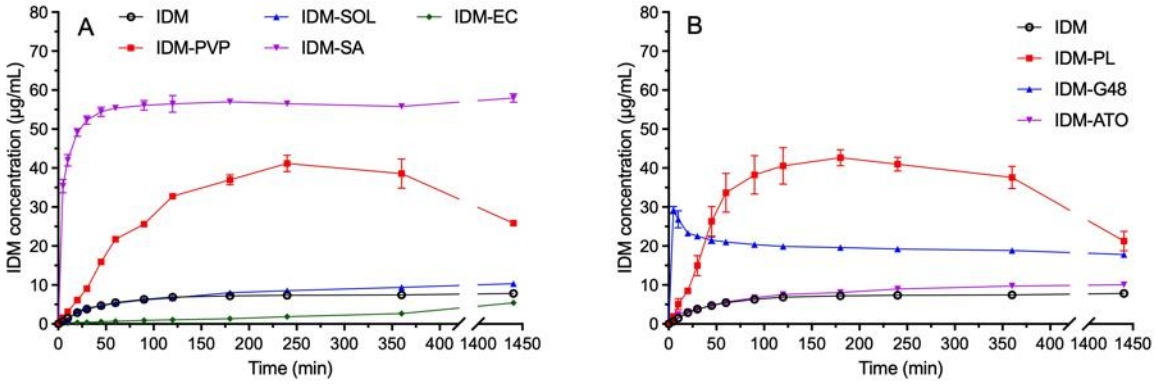

Figure 5.5. Dissolution of solvent-based IDM ASDs prepared with (A) polymer and (B) lipid carriers in water.

The dissolution profiles of IDM ASDs prepared by different lipids are shown in Figure 5.5B. IDM-PL generated a highly supersaturated state for IDM followed by slow concentration loss. The drug concentration continuously increased to its peak of 41 ± 4 μg/mL at 120 min due to facilitated wetting and release of amorphous IDM with higher Gibbs free energy. Afterwards, a slight drop of IDM concentration was observed due to recrystallization, reducing drug concentration to the endpoint concentration of 21 ± 2 μg/mL at 24 hrs. IDM-G48 showed a fast buildup of IDM supersaturation, reaching a peak concentration of 29.2 ± 0.7 μg/mL within a short dissolution time of 5 min. A fast decline in free drug concentration occurred immediately after the supersaturation buildup. IDM concentration decreased to an equilibrium of 17.8 ± 0.3 μg/mL after 24 hrs, which was slightly higher than the value (14.2 ± 0.2 μg/mL) for the solubilization test. IDM-ATO provided a dissolution profile which was highly comparable with pure IDM. The slightly higher endpoint concentration than pure IDM was a result of constant release of amorphous IDM with higher equilibrium solubility.

5.4.3.1.2 Dissolution of solvent-based IDM ASDs prepared with polymer-lipid combinations

Resulting from the individual effects of polymer and lipid, the dissolution behavior of IDM was altered by the combination of polymer and lipid as ASD carrier. The major changes were reflected by the drug release rate at the initial stage, maximum achievable concentration, and maintaining of supersaturation. As shown in Figure 5.6, IDM-PVP-PL showed a faster dissolution rate at the early stage of dissolution as compared with IDM-PVP and IDM-PL, achieving an IDM concentration of 47.1 ± 0.5 µg/mL at 60 min. Drug concentration was maintained at this plateau until 120 min, after which IDM concentration gradually decreased to 34 ± 3 µg/mL at 6 hrs due to slow recrystallization. The endpoint concentration at 24 hrs was 19.5 ± 0.6 µg/mL, which was similar to the values for IDM-PVP and IDM-PL. From the first 120-min dissolution data (Table 5.1) it could be seen that the dissolution of IDM-PVP-PL was less fitted to the Higuchi model that describes drug release from insoluble matrix, as compared with IDM-PVP and IDM-PL.

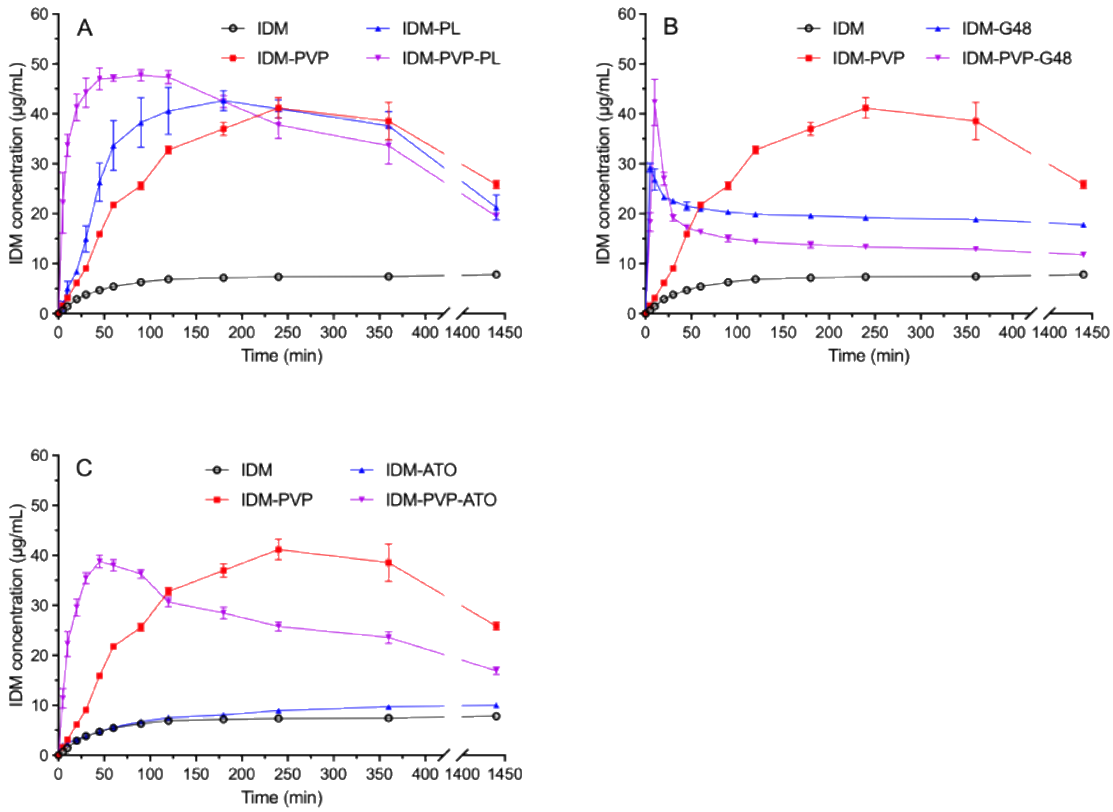

Figure 5.6. Dissolution of solvent-based IDM ASDs prepared with (A) PVP-PL, (B) PVP-G48 and (C) PVP-ATO carriers in water.

Table 5.1. Linear regression results of solvent-based IDM ASDs fitted to different dissolution models.

Dissolution model →	**Zero order**		**First order**		**Higuchi model**	
ASD name ↓	r^2	K_0	r^2	K_1	r^2	KH
IDM-PVP	0.971	0.898	0.990	0.006	0.887	7.773
IDM-SOL	0.709	1.055	0.984	0.028	0.950	9.666
IDM-SA	-1.255	1.244	0.982	0.177	0.293	12.414
IDM-EC	0.831	0.956	0.954	0.016	0.979	8.619
IDM-PL	0.891	1.017	0.972	0.013	0.895	8.977
IDM-G48	-2.948	0.927	0.861	3.933	-1.143	9.873
IDM-ATO	0.669	1.019	0.957	0.026	0.995	9.372
IDM-PVP-PL	-0.841	1.243	0.995	0.117	0.476	12.329
IDM-PVP-G48	-1.762	0.518	0.397	0.606	-0.850	5.869
IDM-PVP-ATO	-0.623	1.125	0.945	0.078	0.485	11.234
IDM-SOL-PL	0.561	1.115	0.987	0.036	0.918	10.376
IDM-SOL-G48	-0.528	1.231	0.994	0.093	0.615	12.101
IDM-SOL-ATO	0.684	1.070	0.988	0.030	0.948	9.835
IDM-SA-PL	0.852	1.012	0.964	0.016	0.890	8.995
IDM-SA-G48	-0.133	1.214	0.995	0.073	0.732	11.799
IDM-SA-ATO	0.116	1.131	0.978	0.060	0.872	10.804
IDM-EC-PL	0.007	1.131	0.986	0.070	0.829	10.853
IDM-EC-G48	-1.655	1.251	0.997	0.214	0.052	12.660
IDM-EC-ATO	0.896	0.917	0.989	0.012	0.969	8.178

IDM-PVP-G48 showed a fast buildup of IDM supersaturation, reaching a peak concentration of 42 ± 4 μg/mL at 10 min. The T_{max} was larger than that for IDM-G48, while the maximum

achievable concentration was effectively higher. Immediately after reaching peak concentration, a sharp decline in drug concentration to 16.3 ± 0.5 μg/mL was observed within 60 min, followed by a continuous decrease to 11.8 ± 0.5 μg/mL after 24-hr dissolution. The general supersaturation degree was between those for IDM-PVP and IDM-G48. The dissolution behavior showed minimal correlation with zero-order and Higuchi model, describing the free release of IDM from the formulation. IDM-PVP-ATO provided a different type of dissolution profile for IDM compared with those for IDM-PVP and IDM-ATO. A synergistic effect on IDM dissolution was observed for the early stage due to facilitated disintegration by ATO. Drug concentration reached its peak of 38.8 ± 1.0 μg/mL at 45 min, which was effectively faster than IDM-PVP. The maximum achievable concentration was slightly lower than that for IDM-PVP, which was possibly due to weakened supersaturation maintenance ability of the formulation with reduced amount of PVP. A faster recrystallization rate, as compared with IDM-PVP, was observed after the buildup of maximum supersaturation at 45 min. The dissolution profile was only fitted to the first order profile whereby drug release was limited by solute concentration, without being restricted by carrier dissolution.

IDM-SOL-PL presented an averaged dissolution profile between that for IDM-SOL and IDM-PL in terms of dissolution rate and supersaturation degree (Figure C-9 in Appendix). No decline in drug concentration was observed along the investigated timescale, which should be an overall result of low supersaturation degree achieved and SOL's ability to maintain IDM supersaturation. The averaged effect brought by the SOL-PL combination was different from the synergistic effect for the PVP-PL combination, suggesting a difference in disintegration when PL was added to different polymers. The first 120-min dissolution behaviors of SOL-PL showed good fitting with both the first-order model and the Higuchi model, indicating that drug release from binary carrier matrix could be a rate limiting factor for IDM dissolution. IDM-SOL-G48 also provided an averaged dissolution profile for IDM dissolution as compared with those for IDM-SOL and IDM-G48. Noticeably, the supersaturation degree of IDM after 45 min was higher than that for IDM ASDs prepared by individual polymer or lipid, and no concentration decline was observed due to recrystallization. These phenomena suggested that the supersaturation maintaining ability of formulation was enhanced by the dissolution of the SOL carrier due to facilitated disintegration induced by G48. The dissolution data of IDM-SOL-G48 was better fitted with the first-order model, and its correlation with Higuchi model was between those for IDM-SOL and IDM-G48. IDM-SOL-ATO showed a slightly improved dissolution profile over IDM-SOL and IDM-ATO in terms of dissolution rate and supersaturation

degree, which should be the result of facilitated disintegration of formulation that led to better release of stored amorphous drug. The maintenance of a higher supersaturation degree was also benefited from the dissolution of the SOL carrier. The dissolution behavior of IDM-SOL-ATO showed high similarity to both first order and Higuchi model.

IDM-SA-lipid samples showed averaged dissolution profiles for IDM as compared with IDM-SA and IDM-lipid (Figure C-10 in Appendix). This was mainly a result of the modified crystalline solubility of IDM in the presence of different amounts of SA. The dissolution behavior of IDM-SA-PL showed good correlation with the first order and the Higuchi model, which was similar to IDM-PL instead of IDM-SA. The linear regression results of IDM-SA-G48 were more similar to IDM-SA than IDM-G48, indicating that the release of IDM was less free than IDM-G48. The dissolution data of IDM-SA-ATO was more similar to IDM-ATO instead of IDM-SA.

IDM-EC-lipid samples also showed averaged dissolution profiles for IDM as compared with IDM-EC and IDM-lipid (Figure C-11 in Appendix). No drug concentration loss was observed due to the slow and gradual release of amorphous IDM. The first 120-min fitting results of IDM-EC-PL were similar to both IDM-EC and IDM-PL. IDM-EC-G48 showed a poor correlation with the zero order and Higuchi model. IDM-EC-ATO showed a dissolution profile more similar to IDM-EC than IDM-ATO as suggested by the linear regression results.

5.4.3.2 Dissolution of freeze-dried IDM ASDs in pure water

5.4.3.2.1 Dissolution of freeze-dried IDM ASDs prepared with individual carriers

As shown in Figure 5.7A, IDM-PVP showed a typical “spring and parachute” profile where drug concentration increased to the peak of 46.1 ± 1.0 μg/mL at 60 min, followed by a slow concentration decline to 40.0 ± 1.0 μg/mL after 6 hrs due to IDM recrystallization inhibited by the dissolved PVP. The dissolution rate was significantly faster than the solvent-based IDM-PVP at the early stage, possibly due to the reduced particle size for lyophilized powder. The peak IDM concentration was slightly higher than that for solvent-based IDM-PVP, suggesting that the supersaturation potential of IDM-PVP was benefited from the reduced particle size and faster dissolution of carrier material. The endpoint IDM concentration at 24 hrs was 28.2 ± 0.8 μg/mL, which was similar to that for solvent-based IDM-PVP due to drug recrystallization over long time.

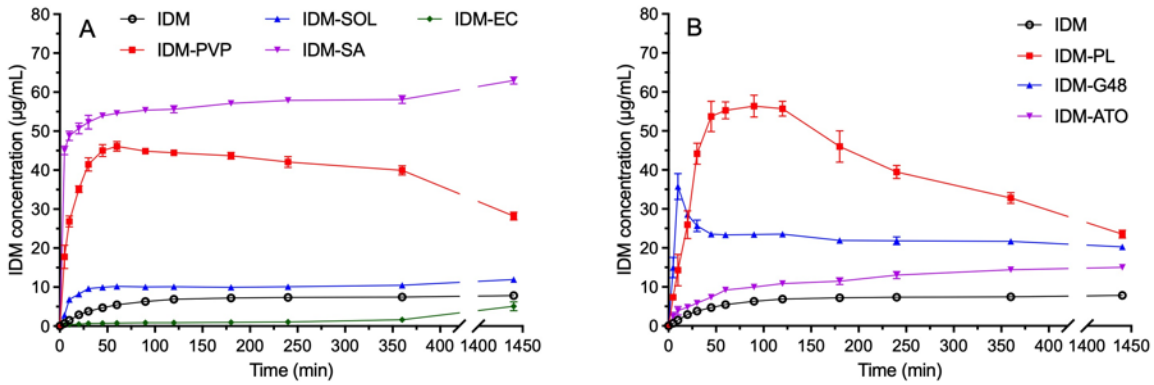

Figure 5.7. Dissolution of freeze-dried IDM ASDs prepared with (A) polymer and (B) lipid carriers in water.

IDM-SOL improved both dissolution rate and supersaturation degree as compared with pure IDM and solvent-based IDM-SOL. The drug concentration reached 10.2 ± 0.2 μg/mL within 60 min, which provided a 90% improvement for solvent-based IDM-SOL due to faster dissolution of the formulation with reduced particle size. With the low supersaturation degree achieved, no drug concentration loss was observed. IDM-SA showed an effective drug dissolution rate and supersaturation maintenance due to the improvement in IDM solubility. IDM-EC showed a slightly faster dissolution rate and higher concentration at each timepoint than its solvent-based counterpart, while the overall dissolution was still slower than IDM alone due to the sustained release effect.

The freeze-dried IDM ASDs based on lipid carriers show a faster dissolution rate than their solvent-based counterparts, associated with different supersaturation evolution profiles after achieving IDM supersaturation (see Figure 5.7B). IDM-PL achieved a peak IDM concentration of 55.7 ± 1.6 μg/mL within 120 min. The maximum supersaturation degree was higher than that for solvent-based IDM-PL, and the time required to achieve this state was 60 min shorter. Afterwards, IDM supersaturation remained at this level until 120 min, and showed a concentration decline to 32.8 ± 1.1 μg/mL at 360 min due to recrystallization. The freeze-dried IDM-G48 sample showed a dissolution profile similar to its solvent-based counterpart. A fast buildup of supersaturation to 36 ± 3 μg/mL was observed within 10 min, which was 33% higher than that for solvent-based IDM-G48 due to the more effective wetting of the G48 carrier. Due to the generation of high-degree supersaturation and poor supersaturation maintaining effect of G48, IDM concentration showed a fast drop to 23.6 ±

0.06 μg/mL within 45 min, and constantly decreased to 20.3 ± 0.3 μg/mL after dissolution for 24 hrs. The recrystallization profile was highly comparable with solvent-based IDM-G48, suggesting that no change in supersaturation maintaining ability was induced by the different preparation method. The freeze-dried IDM-ATO presented a dissolution profile with similar shape to its solvent-based counterpart, while with a higher IDM concentration at each timepoint due to the faster release of amorphous IDM from a formulation with smaller particle size and larger surface area.

5.4.3.2.2 Dissolution of freeze-dried IDM ASDs prepared with polymer-lipid combination carriers

The dissolution and supersaturation parameters including dissolution rate, maximum achievable concentration, supersaturation maintenance and equilibrium concentration were altered in different manners due to the combination of polymer and lipid carrier. Freeze-dried IDM-PVP-PL achieved a higher degree of drug supersaturation within a shorter time as compared with IDM-PVP and IDM-PL (Figure 5.8). The endpoint IDM concentration was determined to be 30.9 ± 1.8 μg/mL, which was slightly higher than the values for IDM-PVP and IDM-PL. The dissolution data of IDM-PVP-PL were poorly fitted with the Higuchi model as compared with IDM-PVP and IDM-PL, as indicated in Table 5.2.

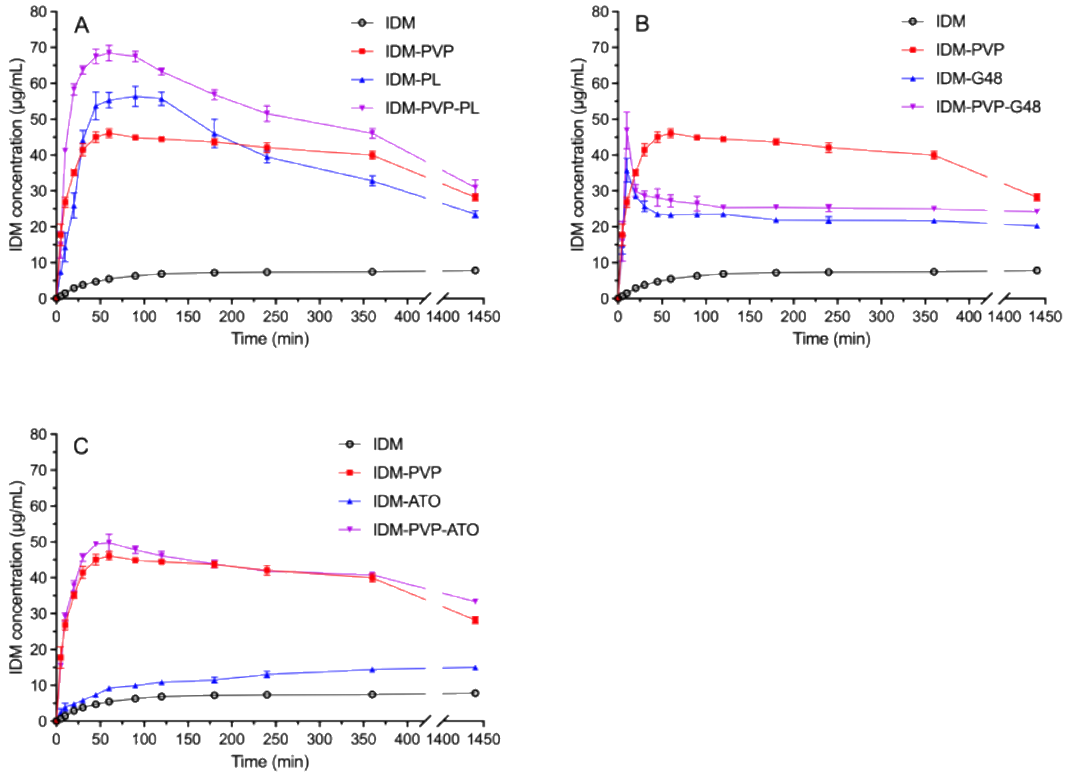

Figure 5.8. Dissolution of freeze-dried IDM ASDs prepared with (A) PVP-PL, (B) PVP-G48 and (C) PVP-ATO carriers in water.

Table 5.2. Linear regression results of freeze-dried IDM ASDs fitted to different dissolution models.

Dissolution model →	**Zero order**		**First order**		**Higuchi model**	
ASD name ↓	r^2	K_0	r^2	K_1	r^2	KH
IDM-PVP	-0.461	1.209	0.995	0.088	0.634	11.874
IDM-SOL	-0.404	1.233	0.986	0.090	0.620	12.119
IDM-SA	-1.927	1.257	0.989	0.346	-0.102	12.717
IDM-EC	0.206	1.150	0.975	0.051	0.899	10.936
IDM-PL	0.476	1.171	0.973	0.037	0.874	10.984
IDM-G48	-1.966	0.868	0.769	0.301	-0.491	9.082
IDM-ATO	0.604	1.062	0.973	0.030	0.982	9.835

IDM-PVP-PL	-0.362	1.205	0.979	0.084	0.605	11.882
IDM-PVP-G48	-1.774	0.746	0.647	0.317	-0.506	7.881
IDM-PVP-ATO	-0.420	1.193	0.992	0.084	0.620	11.744
IDM-SOL-PL	-0.493	1.171	0.972	0.110	0.647	11.433
IDM-SOL-G48	-1.580	1.213	0.986	0.192	0.044	12.317
IDM-SOL-ATO	0.647	1.056	0.993	0.031	0.960	9.750
IDM-SA-PL	-0.418	1.175	0.977	0.095	0.679	11.462
IDM-SA-G48	-0.779	1.228	0.984	0.121	0.523	12.125
IDM-SA-ATO	-0.293	1.201	0.982	0.081	0.726	11.682
IDM-EC-PL	0.214	1.130	0.972	0.054	0.894	10.740
IDM-EC-G48	-0.817	1.233	0.991	0.113	0.491	12.209
IDM-EC-ATO	-0.439	1.088	0.903	0.134	0.658	10.544

For IDM-PVP-G48, a synergistic effect in supersaturation buildup was observed as compared with IDM-PVP and IDM-G48. A highly supersaturated state of 47 ± 4 μg/mL was effectively achieved within 10 min, followed by an immediate drug concentration loss due to IDM recrystallization with insufficient supersaturation maintaining the effect rendered by the PVP-PL binary carrier. The IDM concentration after the occurrence of recrystallization was noticeably higher than that for IDM-G48 at each timepoint, attributed to the slightly improved supersaturation maintaining effect provided by PVP. The endpoint IDM concentration was between the values for IDM-PVP and IDM-G48. The linear regression results of IDM-PVP-G48 were similar to those for IDM-G48, with poor similarity to IDM-PVP. The fitting to the first order model showed a low r^2 value, suggesting that that drug release was not completed. IDM-PVP-ATO presented a dissolution profile similar to IDM-PVP in terms of dissolution rate, supersaturation degree and supersaturation maintenance. The slightly improved C_{max} could be due to the facilitated disintegration of PVP, and the moderate supersaturation maintaining effect was attributed to PVP in the binary carrier. The dissolution rate and supersaturation degree of freeze-dried IDM-PVP-ATO were both lower than its solvent-based counterpart. The dissolution data of IDM-PVP-ATO yielded a poorer fit with the Higuchi model as compared with IDM-PVP and IDM-ATO.

The freeze-dried IDM ASDs based on SOL-lipid combination also showed adjusted dissolution and supersaturation parameters including dissolution rate, supersaturation degree and supersaturation maintaining effect (Figure C-12 in Appendix). IDM-SOL-PL showed a faster dissolution rate than IDM-SOL and IDM-PL at the early stage, achieving an IDM concentration of 28.6 ± 0.4 μg/mL within 20 min. Afterwards, the drug concentration accumulation was less effective, whereby IDM concentration gradually increased to 36.0 ± 1.0 μg/mL at 6 hrs. No decline in IDM concentration was observed due to the slow rate of supersaturation generation. The endpoint IDM concentration was higher than the values for IDM-SOL and IDM-PL. This could be a result of improved IDM supersaturation due to the increasing amount of dissolved SOL from the binary carrier. The dissolution rate and supersaturation degree of freeze-dried IDM-SOL-PL were both higher than the solvent-based ASD. The linear regression results were similar to IDM-SOL. IDM-SOL-G48 also showed an averaged dissolution profile between IDM-SOL and IDM-G48, with an effectively stabilized supersaturation. The improved equilibrium concentration could be a result of stabilized supersaturation with facilitated dissolution of the SOL carrier. The linear regression results showed a decrease in Higuchi similarity with regard to IDM-SOL. IDM-SOL-ATO showed a faster dissolution rate than IDM-SOL and IDM-ATO without changing the profile shape. This phenomenon was similar to the profile of solvent-based IDM-SOL-ATO. No loss in drug concentration was observed. The dissolution data of IDM-SOL-ATO showed a high-degree of similarity to first-order and Higuchi model.

IDM-SA-PL, IDM-SA-G48 and IDM-SA-ATO did not change dissolution profile as compared with IDM-SA (see Figure C-13 in Appendix). The averaged supersaturation degree was to the decreased amount of SA that improved the solubility of crystalline IDM. No supersaturation prone to recrystallization was observed, masking the characteristics of IDM-PL and IDM-G48. Compared to its solvent-based counterpart, freeze-dried IDM-SA-PL presented a faster dissolution due to smaller particle size, while with a similar equilibrium IDM concentration determined by the alkalizing effect of SA. The dissolution profiles were similar for freeze-dried and solvent-based IDM-SA-G48, suggesting that particle size and disintegration were not limiting factors for dissolution. The overall supersaturation degree of IDM-SA-ATO was lower than its solvent-based counterpart, which could be a result of less effective drug amorphization and drug loading provided by the freeze-drying process. The dissolution data of IDM-SA-PL was similar to IDM-PL, but with a decreased r^2 value for the Higuchi model. IDM-SA-G48 showed an increase in the r^2 value for the Higuchi model,

suggesting an overall slower drug release than IDM-SA and IDM-G48. The first 120-min dissolution efficiency of IDM-SA-ATO was more similar to IDM-ATO than IDM-SA, indicative of a certain rate limiting effect brought by added ATO. Detailed analysis will be discussed in section 5.5.3.2.

IDM-EC-PL showed an altered dissolution profile that was different from both IDM-EC and IDM-PL, as shown in Figure C-14 in Appendix. The drug concentration effectively increased to its plateau of 35.0 ± 0.5 μg/mL within 120 min, followed by a continuous increase to its equilibrium of 36.7 ± 0.6 μg/mL at 24 hrs. The achieved IDM supersaturation was effectively maintained due to the slow supersaturation generation rate and constant release of amorphous IDM from the EC matrix. The overall supersaturation for this formulation was obviously higher than its solvent-based counterpart. The dissolution efficiency of first 120-min did not present obvious change with regard to IDM-EC and IDM-PL, as seen by the similar linear regression results. IDM-EC-G48 showed a first-order dissolution profile whereby drug concentration presented a gradual increase without concentration loss, masking the characteristic of IDM-G48. The equilibrium was higher than those for IDM-EC and IDM-G48, which could be a collaborative result of constant release of amorphous drug from EC matrix and maintained supersaturation with slow supersaturation induction rate. The Higuchi similarity of dissolution profile for IDM-EC-G48 was between those for IDM-EC and IDM-G48. IDM-EC-ATO showed a dissolution rate that was averaged between IDM-EC and IDM-ATO. In contrast to the solvent-based IDM-EC-ATO, the dissolution profile of the lyophilized sample was more governed by ATO, instead of EC. The Higuchi r^2 value for IDM-EC-ATO was lower than both IDM-EC and IDM-ATO, describing a slightly faster dissolution at the early stage.

5.4.3.3 Two-stage dissolution of freeze-dried IDM ASDs

5.4.3.3.1 Two-stage dissolution of freeze-dried IDM ASDs prepared with individual carriers

The concentration-time profiles of pure IDM and lyophilized ASDs formulated with polymer carriers were shown in Figure 5.9A. Pure IDM showed a slow dissolution within the acid stage, reaching a concentration of 1.20 ± 0.06 μg/mL at 60 min. After entering the pH 5.0 stage, which was favourable for IDM ionization and solubility, a larger IDM concentration was observed from 1.72 ± 0.07 μg/mL at 75 min to 9.0 ± 0.4 μg/mL at 6 hr. Ionization is expected for IDM in this environment as the pH was higher than the IDM pKa, so that the dissolution rate and equilibrium concentration of IDM were both improved. IDM-PVP provided a faster dissolution rate and supersaturated

concentration for IDM during acid stage, while not showing a typical "spring and parachute" profile, which was different from its behavior in pure water. After entering pH the 5.0 stage, IDM-PVP showed a continuous drug release and reached a peak concentration of 17.7 ± 0.3 µg/mL at 120 min upon further drug release from the formulation reservoir. Following, a slight concentration decay was observed, dropping to 16.5 ± 0.4 µg/mL for 6 hr and 13.8 ± 0.5 µg/mL for 24 hr. This behavior was similar to the slow desupersaturation observed for IDM-PVP in pure water due to IDM recrystallization. The endpoint IDM concentration was slightly higher than that for IDM alone, suggesting the existence of a low degree of supersaturation over a long time.

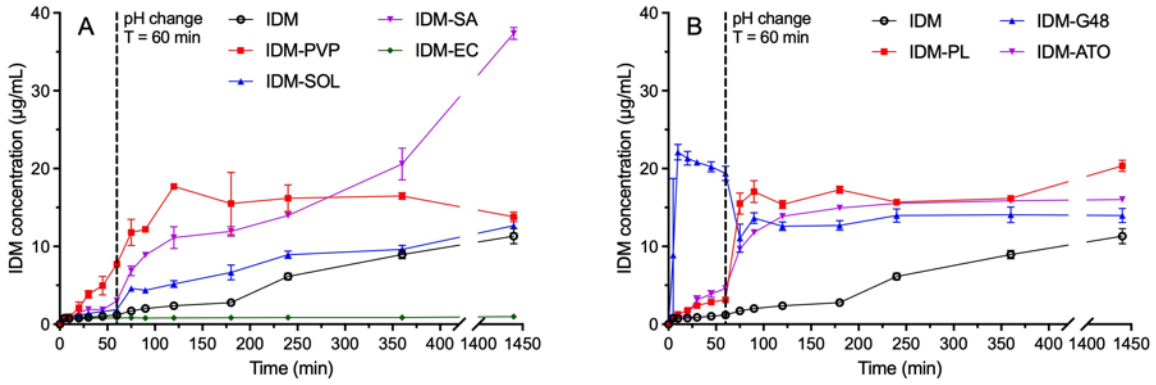

Figure 5.9. Two-stage dissolution of freeze-dried IDM ASDs prepared with (A) polymer and (B) lipid carriers.

IDM-SOL showed a slow dissolution rate in the acid stage similar to IDM alone, achieving an IDM concentration of 1.89 ± 0.07 µg/mL after a dissolution for 60 min. This behavior was similar to its behavior in pure water due to the formation of a SOL gel layer that increased the diffusion distance of IDM. After entering the pH 5.0 stage, IDM concentration increased more quickly than pure IDM, increasing from 4.61 ± 0.06 µg/mL to 12.7 ± 0.8 µg/mL from 75 min to 24 hrs. No obvious concentration decline was observed with low supersaturation degree achieved. IDM-SA presented a faster dissolution rate in the acid stage due to the increased ionization of IDM due to SA's alkalizing effect on the microenvironment of drug. The improvement in IDM dissolution was not as effective as that in pure water possibly because the alkalizing effect of SA was weakened in dissolution media with certain buffering capacity. When entering the pH 5.0 stage, the IDM

dissolution was further improved by the constant release from formulation. The dissolution efficiency was lower than that in pure water by a same mechanism of medium buffering capacity. No decline in drug concentration could be observed within the tested time range, corresponding to the supersaturation maintaining effect of SA on IDM. IDM-EC showed a typical diffusion-controlled dissolution profile resulting from the insolubility of drug carrier. The IDM concentrations at each timepoints in both stages were lower than those for IDM alone, similar to its behavior in pure water. The lyophilized IDM-EC existed in a sponge-like physical state with a poor wetting ability when exposed to the dissolution medium. The slow dissolution rate in both stages was a sum effect of high-degree IDM-EC complexation and poor wettability of the formulation.

As shown in Figure 5.9B, IDM-PL showed an effectively improved dissolution rate for IDM during the acid stage, achieving an IDM concentration of 3.12 ± 0.14 μg/mL at 60 min, which was 2.6-fold larger than that for pure IDM. However, the dissolution improvement was different from that for IDM-PL in pure water, where a fast buildup of highly supersaturated state was achieved within 60 min. The main reason for this deviation should be the protonation and electrostatic effect of PL under acid conditions which induced intermolecular complexation to delay drug release. After entering the pH 5.0 stage, where PL protonation was weakened by the increased pH, IDM concentration saw a burst increase to 15.5 ± 1.1 μg/mL at 75 min. This suggested that a significant part of IDM payload could enter water once the self-complexation of PL was weakened. Following, IDM concentration was effectively maintained over 20.4 ± 0.6 μg/mL for 24 hrs, which was 1.8-fold as that for pure IDM.

IDM-G48 presented a sharp increase in IDM concentration for the first 10 min in the acid stage and reached a peak at 22.1 ± 0.8 μg/mL that was approximately 30-fold higher than that for IDM alone. The effective improvement was aligned with the behavior of lyophilized IDM-G48 in pure water. Before stock B was added to initiate the second phase at 60 min, the IDM concentration was maintained at 19.4 ± 0.8 μg/mL, indicating the evolution of IDM recrystallization but to a lower extent than that in pure water. After entering pH 5.0 stage, the IDM concentration further increased from 11.1 ± 1.5 μg/mL at 75 min to 14.0 ± 0.7 μg/mL after dissolution for 24 hrs. The supersaturation maintenance ability of G48 was stronger at pH 5.0 than that in pure water due to lower non-sink degree achieved. IDM-ATO provided an effectively improved dissolution enhancement for IDM during acid stage, reaching a drug concentration of 4.6 ± 0.2 μg/mL at 60 min. Interestingly, as an insoluble lipid carrier, ATO provided a better dissolution enhancement than PL. This comparison was

different from the scenario in pure water. After entering the pH 5.0 stage, the increase in drug concentration remained constant, gradually reaching its plateau of 15.5 ± 0.11 µg/mL at 4 hrs and an endpoint concentration of 16.0 ± 0.2 µg/mL after dissolution for 24 hrs. The dissolution behaviors of IDM-ATO were similar in different stages and were comparable with that in pure water.

5.4.3.3.2 Two-stage dissolution of freeze-dried IDM ASDs prepared with polymer/lipid combinations

The dissolution behaviors of freeze-dried IDM ASDs could be altered by the combination of polymer and lipid carriers in different manners. PVP-PL provided a significantly synergistic effect in IDM dissolution in the acid stage, whereby drug concentration was higher than that for IDM alone at each timepoint (see Figure 5.10).

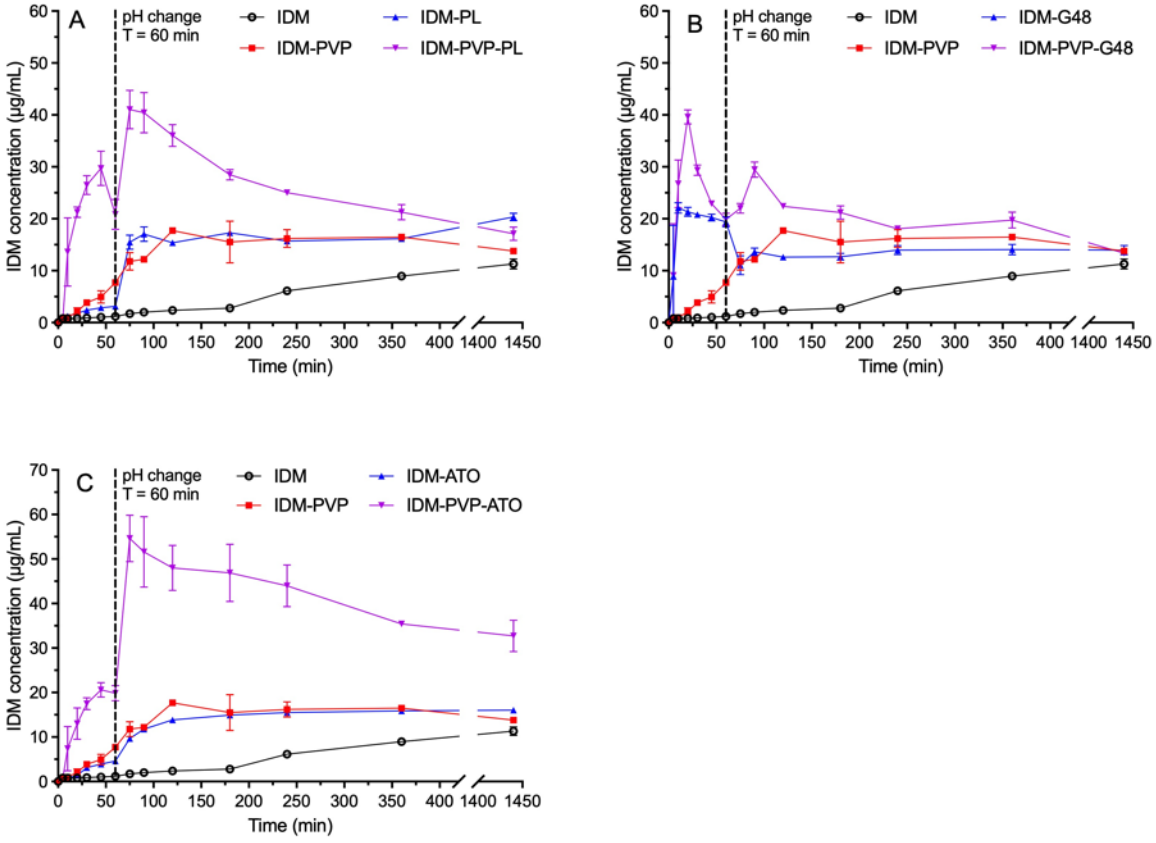

Figure 5.10. Two-stage dissolution of freeze-dried IDM ASDs prepared with (A) PVP-PL, (B) PVP-G48 and (C) PVP-ATO.

The IDM concentration effectively increased to its peak of 30 ± 3 μg/mL at 45 min, followed by a concentration decline to 21 ± 2 μg/mL at 60 min. After entering the pH 5.0 stage, a burst release was observed to achieve a peak IDM concentration of 41 ± 3 μg/mL at 75 min, followed by a gradual concentration loss to 17.1 ± 1.0 μg/mL after dissolution for 24 hrs. As shown in Table 5.3, IDM-PVP-PL showed a decrease in r^2 value for both the zero order and the Higuchi model, as compared with IDM-PVP and IDM-PL. This suggested a decreased restriction of drug release from the binary carrier. The synergistic effect of IDM-PVP-PL was in good agreement with its behavior in pure water.

IDM-PVP-G48 showed fast dissolution in the acid stage similar to the behavior of IDM-G48, achieving a drug concentration of 39.6 ± 1.1 μg/mL within 20 min. However, the drug concentration presented a fast decline after this timepoint, reducing to 19.9 ± 1.0 μg/mL at the end of the acid stage. After entering the pH 5.0 stage, the drug concentration presented another increasing period and leveled the drug concentration to 29.5 ± 1.2 μg/mL at 90 min. Again, IDM concentration decreased and returned to 19.8 ± 1.2 μg/mL at 6 hrs. The endpoint concentration was maintained at 13.4 ± 0.2 μg/mL. IDM-PVP-G48 showed a poor correlation with the Higuchi model, similar to IDM-G48, describing a free drug release process. IDM-PVP-ATO showed a synergistic effect on IDM dissolution during both stages. Drug concentration effectively increased to its peak of 20.6 ± 1.3 μg/mL at 45 min, followed by a concentration loss to 19.8 ±1.4 μg/mL at 60 min. The IDM concentration was significantly higher than those for both IDM-PVP and IDM-ATO at each timepoint.

Table 5.3. Linear regression results of two-stage dissolution of freeze-dried IDM ASDs fitted to different dissolution models.

Dissolution model →	**Zero order**		**First order**		**Higuchi model**	
ASD name ↓	r^2	K_0	r^2	K_1	r^2	KH
IDM-PVP	0.981	1.575	0.981	0.025	0.775	9.772
IDM-SOL	-0.113	1.982	0.826	0.069	0.921	13.354

IDM-SA	0.762	1.710	0.874	0.027	0.884	11.141
IDM-EC	-165.082	2.348	0.476	0.505	-60.173	16.876
IDM-PL	0.628	1.995	0.989	0.043	0.987	13.199
IDM-G48	-4.006	2.176	0.692	0.185	-0.864	15.572
IDM-ATO	0.947	1.799	0.961	0.009	0.829	11.385
IDM-PVP-PL	0.178	1.884	0.800	0.066	0.622	12.781
IDM-PVP-G48	-2.159	1.507	0.393	0.173	-0.613	11.145
IDM-PVP-ATO	0.711	2.051	0.945	0.038	0.856	13.438
IDM-SOL-PL	0.368	2.161	0.949	0.059	0.856	14.485
IDM-SOL-G48	-0.065	2.252	0.889	0.081	0.677	15.364
IDM-SOL-ATO	0.668	2.123	0.951	0.041	0.867	13.970
IDM-SA-PL	0.728	1.975	0.956	0.038	0.905	12.956
IDM-SA-G48	-0.062	2.226	0.841	0.082	0.635	15.193
IDM-SA-ATO	0.320	2.013	0.938	0.060	0.841	13.514
IDM-EC-PL	-0.227	2.066	0.915	0.073	0.876	13.995
IDM-EC-G48	-0.030	2.074	0.846	0.076	0.611	14.188
IDM-EC-ATO	-3.682	1.990	0.185	0.258	-0.304	13.715

After entering the pH 5.0 stage, the drug concentration showed another fast increase to its peak of 55 ± 4 μg/mL at 75 min, followed by a gradual concentration decline to 33 ± 3 μg/mL after dissolution for 24 hrs. The overall dissolution profiles in different pH environments were comparable with each other. The similarity between dissolution data of IDM-PVP-ATO and Higuchi model was not attenuated due to polymer-lipid combination as seen by the similar r^2 values.

A synergistic effect on IDM dissolution was also observed for IDM-SOL-PL in the acid stage as compared with IDM-SOL and IDM-PL (Figure C-15 in Appendix). The concentration of IDM reached 8.4 ± 0.3 μg/mL within 60 min, which was effectively higher than that for IDM-SOL and IDM-PC. Interestingly, after entering the pH 5.0 stage, the IDM concentration started to show a slow increase from 4.1 ± 1.6 μg/mL to 16.3 ± 1.1 μg/mL from 75 min to 24 hrs. The IDM concentrations

during this stage were similar to those for IDM-SOL, and were obviously lower than those for IDM-PL. As suggested by the r^2 values for different models, the dissolution of IDM-SOL-PL was still restricted by both solute concentration and drug release from the carrier material. The SOL-G48 combination provided an IDM release profile that was averaged between the profiles of IDM-SOL and IDM-G48. During the pH 2.2 stage, the IDM concentration increased to its plateau of 14.3 ± 1.6 μg/mL at 20 min, and effectively maintained at this level until 60 min. This was different from the recrystallization profile observed for IDM-G48. After entering pH 5.0 stage, the IDM concentration further increased to 18.9 ± 0.9 μg/mL at 75 min, and effectively maintained at this level thereafter. Drug concentrations at all timepoints were between those for IDM-SOL and IDM-G48. The Higuchi similarity of IDM-SOL-G48 was between those for IDM-SOL and IDM-G48. IDM-SOL-ATO showed an improvement in dissolution rate and extent as compared with IDM-SOL and IDM-ATO. During the pH 2.2 stage, IDM concentration increased to its plateau of 4.1 ± 0.5 μg/mL at 30 min, and effectively maintained at this level. After entering pH 5.0 stage, IDM concentration continued to increase to 26.0 ± 0.5 μg/mL at 120 min, followed by a slow increase to the endpoint concentration of 29.4 ± 0.2 μg/mL after dissolution for 24 hrs. Drug concentrations were effectively higher than those for IDM-ATO over long-time dissolution. The drug release from binary carrier was still a negative factor, as suggested by the similar r^2 values of Higuchi model for IDM-SOL-ATO, as compared with IDM-SOL and IDM-ATO.

IDM-SA-PL also provided an obvious synergistic effect on the IDM dissolution at both stages with regard to IDM-SA and IDM-PL (Figure C-16 in Appendix). During the pH 2.2 stage, the IDM concentration gradually increased to its peak of 10.8 ± 0.3 μg/mL at 60 min. After entering the pH 5.0 stage, the drug concentration showed a more gradual increase as compared with IDM-PL. The drug concentration increased from 15.8 ± 0.3 μg/mL to 30 ± 7 μg/mL from 75 min to 24 hrs. The first 60-min drug release restriction was not obviously improved by the binary carrier, as seen by the large Higuchi r^2 value similar to those for IDM-SA and IDM-PL. IDM-SA-G48 showed a generally averaged dissolution profile with regard to IDM-SA and IDM-G48. During the pH 2.2 stage, the IDM concentration showed a gradual increase to its peak of 19.1 ± 0.7 μg/mL at 45 min, followed by a slight decrease to 18.5 ± 0.5 μg/mL at 60 min. During this stage, IDM concentrations were between those for IDM-SA and G48. A different drug dissolution shape was observed thereafter. No further increase in IDM concentration was observed during pH 5.0 stage, describing a high-degree completion for drug dissolution. Drug concentration maintained in a narrow range of 13.0 ± 0.3

μg/mL to 14.2 ± 1.0 μg/mL from 75 min to 6 hrs. The endpoint drug concentration at 24 hrs was determined to be 16.6 ± 0.6 μg/mL, which was lower than the values for IDM-SA and IDM-G48. IDM-SA-G48 showed a slightly improved drug release from ASD carrier as seen by the smaller r^2 value for Higuchi model. IDM-SA-ATO provided a dissolution profile that was highly comparable with IDM-ATO, other than the endpoint drug concentration at 24 hrs. During the pH 2.2 stage, drug concentration showed a slightly faster increase rate than IDM-SA and IDM-ATO, reaching its peak of 4.84 ± 0.15 μg/mL at 45 min, followed by a slight decrease to 4.34 ± 0.14 μg/mL at 60 min. Once entering pH 5.0 stage, IDM concentration gradually increased from 9.7 ± 0.6 μg/mL to 16.1 ± 0.4 μg/mL from 75 min to 24 hrs. The endpoint concentration was lower than that for IDM-SA due to the reduced amount of SA dissolved. The dissolution at early stage was still limited by the dug release from ASD carrier, as seen by the similar r^2 values for Higuchi model using both individual and binary carrier.

IDM-EC-PL provided a synergistic effect on IDM dissolution during acid stage, as shown in Figure C-17 in Appendix. IDM concentration reached its peak of 5.9 ± 0.9 μg/mL at 45 min, followed by a slight decay to 5.5 ± 0.5 μg/mL at 60 min. IDM concentrations were higher than those for IDM-PL and IDM-EC, and a slight "spring and parachute" profile was generated by the combination of PL and EC. After entering the pH 5.0 stage, a drastic increase in IDM concentration to 9.7 ± 0.7 μg/mL was induced by the change in dissolution condition. Afterwards, IDM concentration maintained within the range of 6.7 ± 0.6 μg/mL to 8.2 ± 1.5 μg/mL from 90 min to 360 min. The endpoint IDM concentration was determined to be 11.5 ± 1.6 μg/mL at 24 hrs, which was between the values for IDM-EC and IDM-PL. The concentration level from 6 hrs was similar to that for IDM alone, without generating a supersaturated state. The carrier-controlled drug release profile was weaker than that for IDM-PL, as seen in Table 5.3. IDM-EC-G48 showed a dissolution profile that was the average of the dissolution profiles of IDM-EC and IDM-G48 in both dissolution stages. During the pH 2.2 stage, the T_{max} was longer than that for IDM-G48. Once entering the pH 5.0 stage, the IDM concentration maintained in the range of 10.6 ± 0.6 μg/mL and 11.0 ± 0.5 μg/mL from 75 min to 6 hrs. At each timepoint, IDM concentration was between those for IDM-EC and IDM-PL. As suggested by the linear regression result, binary carrier was more of a limiting factor for drug release than G48 alone. IDM-EC-ATO showed an averaged dissolution profile between IDM-EC and IDM-ATO. During the pH 2.2 stage, IDM concentration slowly increased to 1.13 ± 0.14 μg/mL at 60 min, which was essentially the same as that for pure IDM and IDM-EC. When entering pH 5.0 stage, drug

concentration gradually increased to 8.8 ± 0.8 μg/mL after 6 hrs, with a faster increasing rate than pure IDM and IDM-EC. The endpoint concentration at 24 hrs was determined to be 13.4 ± 1.5 μg/mL upon the continuous release of loaded amorphous IDM. The dissolution profile of IDM-EC-ATO did not correspond to the tested models.

5.4.4 In vitro dissolution of APX ASDs

5.4.4.1 Dissolution of solvent-based APX ASDs in pure water

The dissolution profiles of APX ASDs were characterized under non-sink conditions. Effects of polymer and lipid carriers on the dissolution and supersaturation behaviors of APX were determined, and the effects of polymer-lipid combinations will be analyzed according to the properties of individual carriers. The dissolution behaviors will be correlated with the effects of ASD carriers on the amorphization, LLPS, solubilization, and supersaturation of APX that were investigated in previous chapters. Besides, the effect of an ASD carrier on the supersaturation properties of IDM and APX will be compared to correlate with the previously hypothesized mechanisms.

5.4.4.1.1 Dissolution of solvent-based APX ASDs prepared with individual carriers

As shown in Figure 5.11A, APX ASDs based on individual polymer carriers showed different dissolution results, ranging from a highly supersaturated profile to a sustained-release profile.

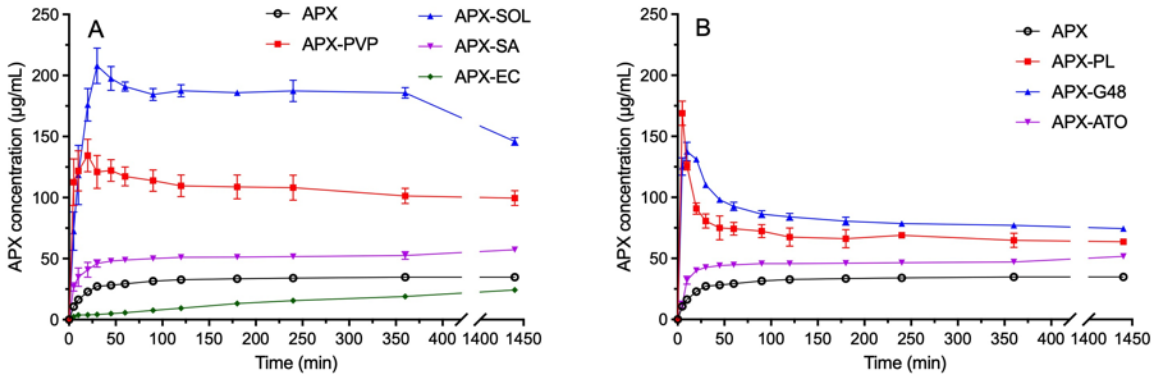

Figure 5.11. Dissolution of solvent-based APX ASDs prepared with (A) polymer and (B) lipid carriers in water.

Pure APX presented a slow dissolution rate, reaching 29.4 ± 0.2 μg/mL within 60 min, and gradually increased to its equilibrium of 34.8 ± 0.7 μg/mL after dissolution for 24 hrs. APX-PVP provided a significant improvement in both dissolution rate and extent for APX, and generated a "spring and parachute" profile where a slight drug concentration loss followed the achievement of a peak drug concentration. APX concentration effectively accumulated to its peak concentration of 134 ± 13 μg/mL at 20 min, which was 5.9 times that for APX alone. Afterwards, APX concentration slightly decreased to 117 ± 8 μg/mL at 60 min, and gradually reduced to its endpoint concentration of 100 ± 6 μg/mL at 24 hrs due to APX recrystallization.

APX-SOL showed an even faster drug release profile and higher supersaturation degree than APX-PVP. The system achieved a peak APX concentration of 208 ± 12 μg/mL at 30 min, followed by a slight concentration decline to 184 ± 4 μg/mL at 90 min. The APX concentration level was effectively maintained at this level for 6 hrs. The endpoint APX concentration at 24 hrs was 146 ± 3 μg/mL, which was still significantly higher than APX solubility. As a comparison, APX-SA showed a less effective improvement in dissolution rate and extent for APX, while without presenting concentration loss. The endpoint concentration at 24 hrs was determined to be 57.2 ± 1.0 μg/mL, which was 64% higher than pure APX. APX-EC showed a typical sustained release profile where drug concentration at each timepoint was lower than pure APX. The free drug concentration reached 5.6 ± 0.3 μg/mL within 60 min, which was approximately 19% of that for APX alone. The endpoint concentration increased to 24.3 ± 0.4 μg/mL upon the sustained release of APX, which was still lower than that for APX alone.

As shown in Figure 5.11B, APX-PL generated a highly supersaturated state followed by a sharp decline in APX concentration. The drug concentration reached 169 ± 8 μg/mL within a short time of 5 min, and then dropped to 67 ± 6 μg/mL after 120 min. Afterwards, APX concentration saw a more gradual decrease to its equilibrium of 63.7 ± 1.4 μg/mL after dissolution for 24 hrs. The supersaturation maintaining effect was weaker than that presented by polymer-based APX ASDs including APX-PVP and APX-SOL. APX-G48 also showed a fast buildup of APX supersaturation, while with a larger T_{max} and a lower C_{max} as compared with APX-PL. The formulation reached its peak concentration of 138 ± 6 μg/mL after dissolution for 10 min. Afterwards, a concentration decline to 93 ± 3 μg/mL was observed within 60 min, followed by a more gradual decrease to the equilibrium of 74.5 ± 1.3 μg/mL after dissolution for 24 hrs. The supersaturation maintaining effect

on APX concentration was more effective than that for APX-PL. APX-ATO provided a first-order dissolution enhancing profile for APX whereby no drug concentration decline was observed. The APX concentration slowly increased to 44.7 ± 1.4 µg/mL at 60 min, and gradually increased to 51.7 ± 1.2 µg/mL after dissolution for 24 hrs. The achieved drug concentration was effectively higher than pure APX.

5.4.4.1.2 Dissolution of solvent-based APX ASDs prepared with polymer-lipid combination carriers

The dissolution and supersaturation behaviors of APX were adjusted by the combination of polymer and lipid as ASD carrier. The changes were reflected by the dissolution parameters including T_{max}, C_{max}, maintaining of supersaturation degree, and general shape of concentration-time profile. APX-PVP-PL showed a fast supersaturation buildup rate which was similar to the behavior of APX-PL, and a supersaturation maintaining behavior similar to APX-PVP (see Figure 5.12).

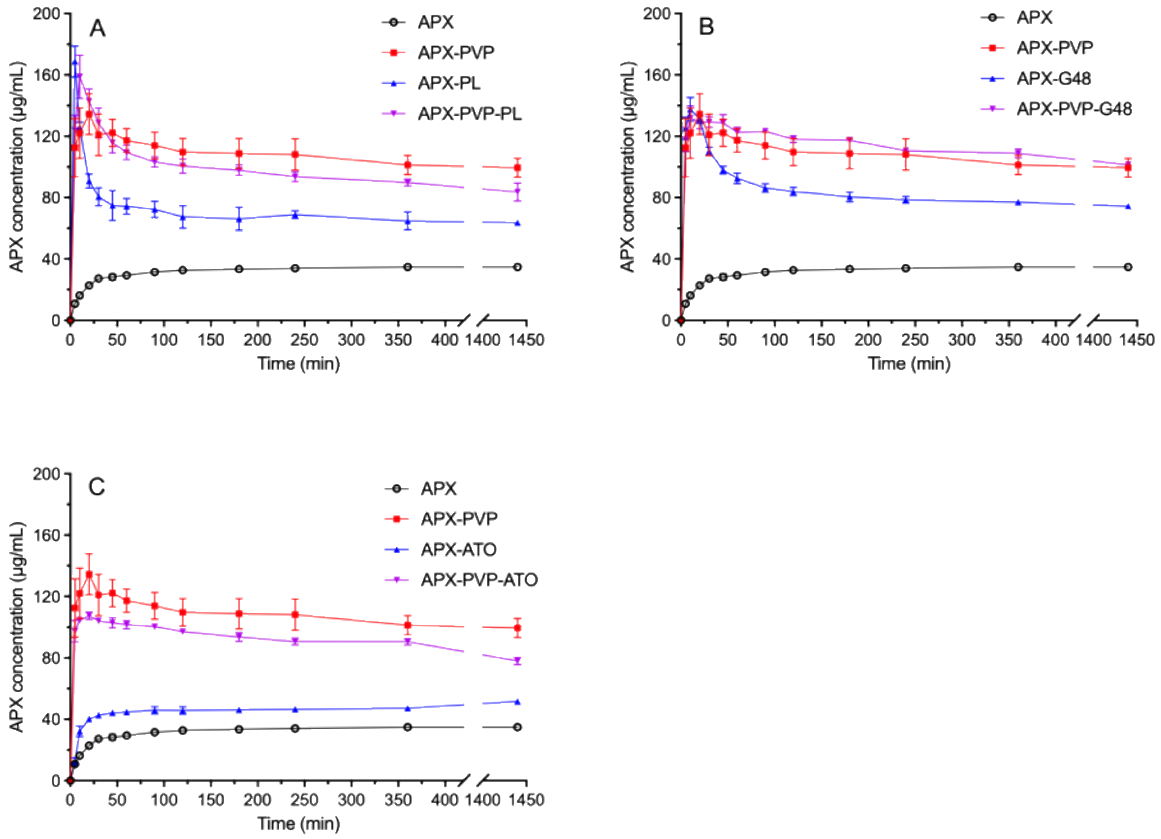

Figure 5.12. Dissolution of solvent-based APX ASDs prepared with (A) PVP-PL, (B) PVP-G48 and (C) PVP-ATO carriers in water.

No plateau was observed after the observation of C_{max}. A drug concentration decline to 101 ± 4 µg/mL was observed within 120 min upon APX recrystallization. APX concentration further decreased to its equilibrium of 84 ± 5 µg/mL after dissolution for 24 hrs, which was between the values for APX-PVP and APX-PL. The general desupersaturation rate was also sitting between those for APX-PVP and APX-PL. As shown in Table 5.4, the dissolution profile of APX-PVP-PL could not be fitted with the Higuchi model, suggesting that drug release from carrier was not a negative factor for dissolution.

APX-PVP-G48 showed a supersaturation buildup rate that was comparable with APX-PVP and APX-G48. The desupersaturation rate was more governed by the behaviors of APX-PVP than APX-G48. A mild concentration loss from the C_{max} to 101 ± 1.7 µg/mL was presented until 24 hrs. The low r^2 value for the Higuchi model suggested that drug release from carrier matrix was not a rate

limiting factor for APX dissolution. APX-PVP-ATO showed an averaged effect on the supersaturation degree of APX due to the combination of two carriers. At 20 min, APX concentration reached its peak of 107 ± 1.9 μg/mL, which was lower than that for APX-PVP. Drug concentration at each timepoint afterwards was lower than that for APX-PVP. The low r^2 value for Higuchi model suggested that drug release from carrier matrix was not a rate limiting factor for APX dissolution. APX-SOL-PL and APX-SOL-G48 presented dissolution and supersaturation properties highly similar to APX-SOL (Figure C-18 in Appendix).

Table 5.4. Linear regression results of solvent-based APX ASDs fitted to different dissolution models.

Dissolution model →	**Zero order**		**First order**		**Higuchi model**	
ASD name ↓	r^2	K_0	r^2	K_1	r^2	KH
APX-PVP	-2.703	1.108	0.971	0.56	-0.686	11.567
APX-SOL	-0.717	1.152	0.980	0.103	0.460	11.481
APX-SA	-0.864	1.220	0.979	0.133	0.486	12.059
APX-EC	0.639	0.946	0.852	0.023	0.954	8.679
APX-PL	-2.124	0.577	0.476	3.729	-1.114	6.432
APX-G48	-2.959	0.879	0.771	3.423	-1.250	9.601
APX-ATO	-0.461	1.237	0.980	0.098	0.587	12.181
APX-PVP-PL	-2.923	0.897	0.826	2.974	-1.108	9.660
APX-PVP-G48	-2.639	1.201	0.989	0.565	-0.621	12.461
APX-PVP-ATO	-2.624	1.204	0.993	0.607	-0.606	12.476
APX-SOL-PL	-2.454	1.253	0.999	0.541	-0.468	12.887
APX-SOL-G48	-0.693	1.225	0.982	0.109	0.555	12.078
APX-SOL-ATO	0.344	1.106	0.984	0.045	0.935	10.438
APX-SA-PL	-2.797	1.113	0.966	4.273	-0.838	11.587
APX-SA-G48	-2.185	1.210	0.987	0.293	-0.311	12.437
APX-SA-ATO	-0.737	1.218	0.970	0.121	0.548	11.989

APX-EC-PL	0.129	1.113	0.968	0.058	0.882	10.612
APX-EC-G48	0.409	1.125	0.992	0.043	0.928	10.588
APX-EC-ATO	0.471	1.093	0.995	0.039	0.947	10.242

The overall supersaturation degrees were higher than that for APX-PL and APX-G48. The low r^2 value of APX-SOL-PL for the Higuchi model suggested that drug release from carrier matrix was not a rate limiting factor for APX dissolution. The large r^2 value of APX-SOL-G48 for the Higuchi model suggested that drug release from carrier matrix was still a rate limiting factor for APX dissolution. APX-SOL-ATO also showed an averaged supersaturation profile in terms of supersaturation degree with regard to APX-SOL and APX-ATO. The shape of supersaturation profile was more comparable with APX-ATO than APX-SOL, as seen by the absence of concentration loss pattern. The large r^2 value for the Higuchi model suggested that drug release from carrier matrix was a rate limiting factor for APX dissolution.

APX-SA-PL showed an averaged supersaturation profile with regard to APX-SA and APX-PL, whereby a fast supersaturation buildup was followed by a concentration decline pattern, and the general supersaturation degree was between those for APX-SA and APX-PL (Figure C-19 in Appendix). The weakened desupersaturation kinetic was a result of slow buildup of lower supersaturation. The low r^2 value for the Higuchi model suggested that drug release from carrier matrix was not a rate limiting factor for APX dissolution. APX-SA-G48 and APX-SA-ATO also showed an averaged dissolution profile with regard to the IDM-SA and IDM-lipid samples, while no drug decline profile was observed. The general supersaturation pattern was similar to that for APX-SA. The low r^2 value of APX-SA-G48 for the Higuchi model suggested that drug release from carrier matrix was not a rate limiting factor for APX dissolution. The similar Higuchi r^2 value of APX-SA-ATO to that for APX-SA suggested that the drug release efficiency was not obviously improved by the addition of ATO.

APX-EC-PL showed a typical sustained release profile similar to IDM-EC, with a slower drug release rate than APX alone and no concentration decline process was observed (Figure C-20 in Appendix). The endpoint APX concentration was 36.3 ± 1.5 μg/mL at 24 hrs, which was similar to the crystalline solubility of APX. The dissolution characteristic of APX-PL was significantly masked. APX-EC-G48 and APX-EC-ATO both showed an averaged dissolution profile between APX-EC and

APX-lipid samples before 24 hrs due to the modified drug release from matrix carriers. The equilibrium APX concentration at 24 hrs was improved in both cases, which was likely a result of constant release of amorphous APX. For all APX ASDs based on EC-lipid combinations, the drug release efficiency from carrier matrices were governed by the characteristics of EC, as suggested by the similarly large r^2 values for Higuchi model.

5.4.4.2 Dissolution of freeze-dried APX ASDs in pure water

The dissolution and supersaturation characteristics of freeze-dried APX ASDs were characterized under non-sink conditions in pure water. Effects of polymer and lipid carriers on the supersaturation parameters of APX were characterized, and the effects of polymer-lipid combinations will be analyzed according to the properties of individual carriers. The supersaturation properties will be correlated with the effects of ASD carriers on the amorphization, LLPS, solubilization, and supersaturation of APX that were investigated in previous chapters. Comparisons will be conducted between the behaviors of solvent-based and freeze-dried APX ASDs.

5.4.4.2.1 Dissolution of freeze-dried APX ASDs prepared with individual carriers

In general, freeze-dried APX ASDs based on individual polymer carriers showed different dissolution results, ranging from a highly supersaturated profile with obvious “spring and parachute” characteristic to sustained-release profile, as shown in Figure 5.13. The dissolution and supersaturation properties of a composition could be different from those for its solvent-based counterpart. APX-PVP provided an obvious improvement in both dissolution rate and extent for APX, achieving a drug concentration of 59.9 ± 1.5 μg/mL within 30 min, followed by a gradually slow decrease to its endpoint concentration of 51.9 ± 1.7 μg/mL. The achieved supersaturation degree was considerably lower compared with its solvent-based counterpart.

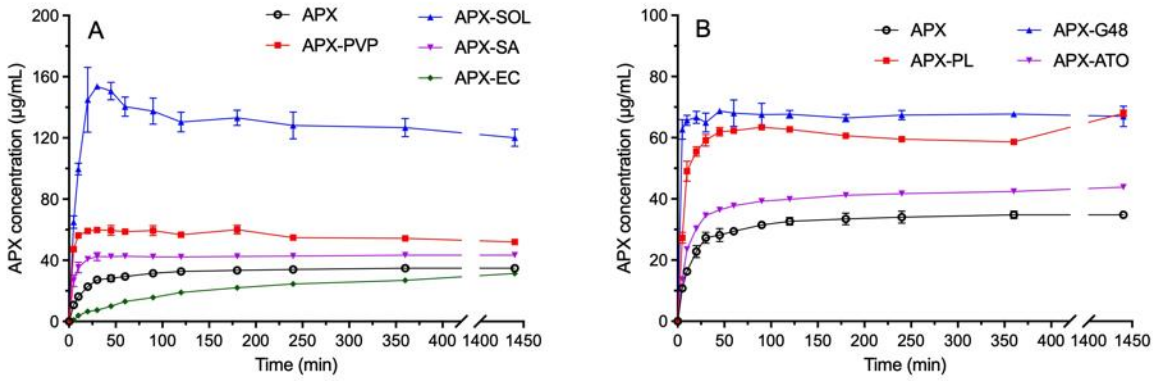

Figure 5.13. Dissolution of freeze-dried APX ASDs prepared with (A) polymer and (B) lipid carriers in water.

APX-SOL showed a significantly enhanced supersaturation buildup rate associated with obvious concentration loss upon drug recrystallization. The system achieved a peak APX concentration of 153.7 ± 1.6 μg/mL at 30 min, followed by a gradual concentration decline to the endpoint concentration of 120 ± 5 μg/mL. The overall supersaturation degree was much higher than that for APX-PVP, while was noticeably lower than the solvent-based APX-SOL. APX-SA showed a similar dissolution profile to APX-PVP, with a lower supersaturation degree achieved. APX concentration reached its plateau of 40.7 ± 1.4 μg/mL at 20 min, and effectively maintained at this level for 24 hrs. The general supersaturation degree was similar to that for solvent-based APX-SA. APX-EC showed a typical sustained release profile where drug concentration at each timepoint was lower than pure APX. The free drug concentration reached 13.1 ± 0.3 μg/mL within 60 min, which was approximately 45% of that for APX alone. The endpoint concentration increased to 31.4 ± 0.5 μg/mL upon the sustained release of APX, which was lower than the crystalline solubility of APX. The overall drug concentration level was higher than that for the solvent-based APX-EC.

The dissolution profiles of freeze-dried APX ASDs prepared with different lipids were shown in Figure 5.13B. APX-PL presented a gradual increase in drug concentration to the peak level of 63.4 ± 0.7 μg/mL at 90 min. Afterwards, APX concentration showed a slow decrease to 58.6 ± 0.6 μg/mL after 6 hrs. The endpoint concentration was determined to be 68.0 ± 0.9 μg/mL, which was 1.9 times as the crystalline solubility of APX. The overall supersaturation degree was lower than the solvent-based APX-PL. APX-G48 showed a similar supersaturation profile to APX-PL, with a faster supersaturation generation rate and a slightly higher supersaturation degree. The formulation reached

its plateau concentration of 68.7 ± 0.7 μg/mL after dissolution for 45 min. The endpoint concentration at 24 hrs was determined to be 67 ± 3 μg/mL, which was 1.9-fold as APX solubility. The supersaturation generation rate and overall concentration level were significantly lower than those for the solvent-based APX-G48. Similarly, APX-ATO provided a first-order dissolution enhancing profile for APX whereby no drug concentration decline was observed. The APX concentration slowly increased to 37.8 ± 0.2 μg/mL at 60 min, and gradually increased to 43.9 ± 0.5 μg/mL after dissolution for 24 hrs. The overall drug concentration was lower than that for solvent-based APX-ATO.

5.4.4.2.2 Dissolution of freeze-dried APX ASDs prepared with polymer-lipid combination carriers

The supersaturation evolution of APX could be adjusted by the combination of polymer and lipid as binary ASD carriers. The changes were reflected by the dissolution parameters including T_{max}, C_{max}, maintaining of supersaturation degree, and general shape of concentration-time profile.

A synergistic effect on the generation of APX superstation could be observed when PVP and lipids were combined as binary carrier, as shown in Figure 5.14. For APX-PVP-PL, at 45 min, a high-degree of supersaturation equal to 79.7 ± 1.2 μg/mL was achieved, which was approximately 30% higher than that for APX-PVP and APX-PL. Following, the APX concentration showed a gradual decline to the endpoint concentration of 70 ± 2 μg/mL after dissolution for 24 hrs. The overall supersaturation level was higher than APX-PVP and APX-PL. A similar phenomenon was observed for APX-PVP-G48. The peak drug concentration of 80.9 ± 1.0 μg/mL was observed at 30 min, followed by a slow concentration decline. The desupersaturation profile was similar to that for APX-PVP and APX-G48. The endpoint APX concentration was determined to be 68.6 ± 1.3 μg/mL after dissolution for 24 hrs, which was comparable with that for APX-G48. APX-PVP-ATO showed a more obvious synergistic effect on the supersaturation generation of APX. The C_{max} of 83.0 ± 1.6 μg/mL was achieved within 45 min, followed by a gradual concentration loss to 62 ± 3 μg/mL after dissolution for 24 hrs, which was higher than that for both APX-PVP and APX-ATO. As suggested by the r^2 values of these formulations fitted to the Higuchi model (Table 5.5), the first 120-min drug release efficiency was not limited by the matrices of binary carriers.

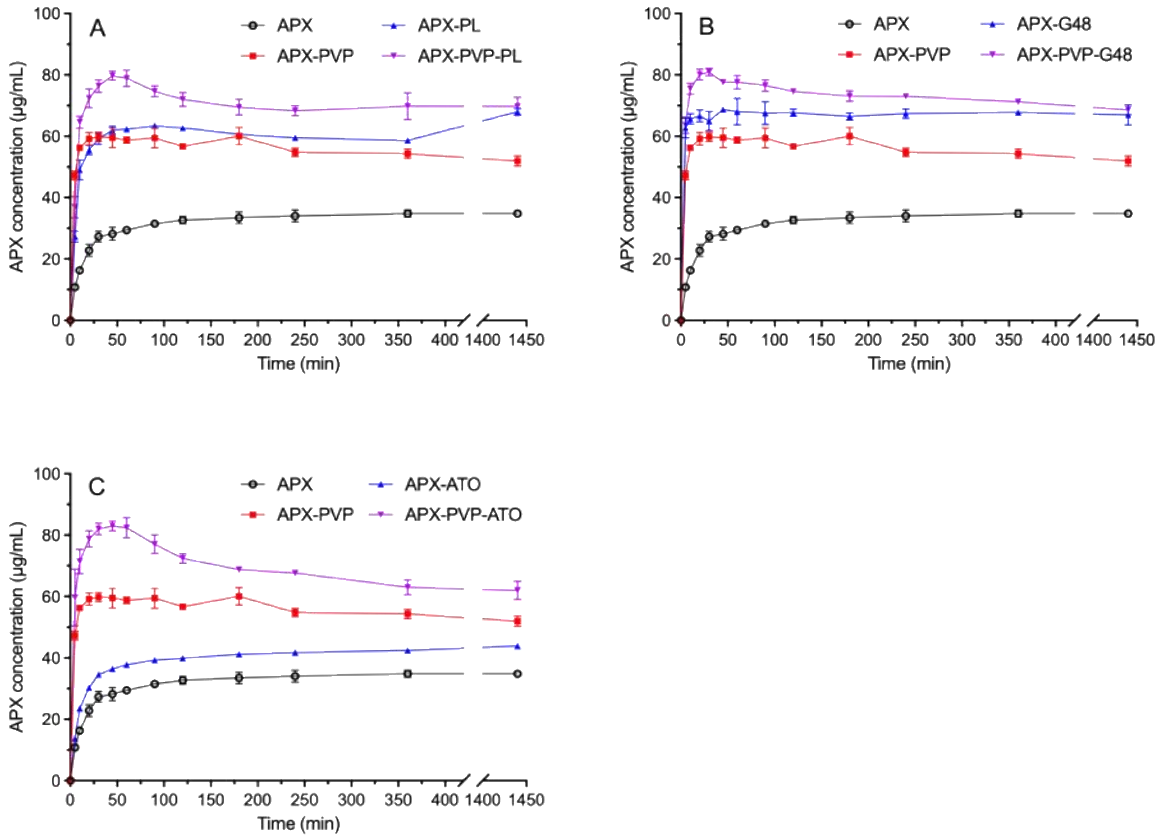

Figure 5.14. Dissolution of freeze-dried APX ASDs prepared with (A) PVP-PL, (B) PVP-G48 and (C) PVP-ATO carriers in water.

Both synergistic effect and averaged effect on the supersaturation evolution of APX were induced by different SOL-lipid combinations (Figure C-21 in Appendix). For APX-SOL-PL, drug concentration effectively increased to 191 ± 6 μg/mL within 10 min. The supersaturated APX solution presented a gradual concentration decline to 148 ± 0.6 μg/mL after dissolution for 24 hrs. The endpoint APX concentration was maintained higher than that for APX-SOL and APX-PL. Similarly, for APX-SOL-G48, the APX concentration effectively accumulated to the plateau level of 175 ± 7 μg/mL within 20 min. Afterwards, drug concentration effectively maintained at this level for 24 hrs with only mild concentration loss observed. As a comparison, APX-SOL-ATO showed an averaged supersaturation profile in terms of supersaturation degree with regard to APX-SOL and APX-ATO. Within a short time of 20 min, the system reached its C_{max} of 62 ± 2 μg/mL, which was between the values for APX-SOL and APX-ATO. An obvious concentration loss occurred after

reaching the peak concentration, decreasing the free drug concentration to 54 ± 2 μg/mL at 60 min. The endpoint APX concentration (52.2 ± 0.2 μg/mL) was approximately 45% higher than the APX solubility. As suggested by the r^2 values of these formulations fitted to the Higuchi model, the first 120-min drug release efficiency was not limited by the matrices of binary carriers.

The supersaturation properties of freeze-dried APX ASDs prepared with SA-lipid combinations were governed by the characteristics of lipid components. For all combinations, the concentration-time profile was highly comparable with that for APX-lipid in terms of supersaturation buildup rate and supersaturation maintenance (Figure C-22 in Appendix). As suggested by the r^2 values of these formulations fitted to the Higuchi model, the first 120-min drug release efficiency was not limited by the matrices of binary carriers of SA-PL and SA-G48. The larger r^2 value of APX-EC-ATO indicated a certain restriction of drug release from binary carrier.

Table 5.5. Linear regression results of freeze-dried APX ASDs fitted to different dissolution models.

Dissolution model →	**Zero order**		**First order**		**Higuchi model**	
ASD name ↓	r^2	K_0	r^2	K_1	r^2	KH
APX-PVP	-2.191	1.252	0.998	0.323	-0.277	12.820
APX-SOL	-1.163	1.146	0.985	0.131	0.234	11.612
APX-SA	-1.524	1.261	0.999	0.191	0.130	12.725
APX-EC	0.904	0.947	0.990	0.014	0.957	8.430
APX-PL	-0.884	1.242	0.992	0.13	0.438	12.347
APX-G48	-2.330	1.262	0.997	0.538	-0.385	12.909
APX-ATO	-0.301	1.202	0.994	0.085	0.708	11.709
APX-PVP-PL	-1.287	1.199	0.986	0.153	0.210	12.122
APX-PVP-G48	-2.302	1.217	0.995	0.340	-0.360	12.515
APX-PVP-ATO	-2.117	1.197	0.984	0.269	-0.231	12.302
APX-SOL-PL	-2.075	1.221	0.981	0.269	-0.252	12.533
APX-SOL-G48	-1.894	1.258	0.999	0.247	-0.093	12.806

APX-SOL-ATO	-1.317	1.121	0.903	0.167	0.053	11.455
APX-SA-PL	-1.161	1.238	0.984	0.165	0.291	12.382
APX-SA-G48	-1.893	1.263	0.999	0.263	-0.089	12.826
APX-SA-ATO	-0.800	1.236	0.985	0.123	0.511	12.217
APX-EC-PL	0.293	1.077	0.968	0.051	0.921	10.188
APX-EC-G48	0.248	1.172	0.998	0.051	0.880	11.156
APX-EC-ATO	-0.191	1.190	0.980	0.076	0.768	11.526

APX ASDs prepared with EC-lipid combinations showed an averaged dissolution profile with regard to individual behaviors of APX-EC and APX-lipids. All samples showed a slow and gradual increase in APX concentration, and the tendency preserved until the end of investigated timescale. At each timepoint, APX concentration was between that for ASDs prepared with EC and individual lipids (Figure C-23 in Appendix). As suggested by the large r^2 values of these formulations fitted to the Higuchi model, the first 120-min drug release efficiency was limited by the matrices of binary carriers.

5.4.4.3 Two-stage dissolution of freeze-dried APX ASDs

5.4.4.3.1 Two-stage dissolution of freeze-dried APX ASDs prepared with individual carriers

As shown in Figure 5.15A, pure APX showed a gradual increase in drug concentration to 28.4 ± 0.5 μg/mL at 60 min. After entering the pH 6.8 stage, APX concentration showed a continuous increase from 20.1 ± 0.4 μg/mL to the endpoint concentration of 29.6 ± 1.1 μg/mL. The apparent concentration decrease at 75 min was due to a change in the volume of dissolution media. APX-PVP provided a faster dissolution rate and supersaturated degree for APX during the pH 2.2 acid stage, while not showing a typical "spring and parachute" profile, which was corresponding to its behavior in pure water. The APX concentration gradually increased to 75 ± 2 μg/mL in acid stage within 60 min. After entering pH 6.8 stage, drug concentration effectively increased from 48.8 ± 1.1 μg/mL at 75 min to 51.6 ± 1.9 μg/mL at 6 hrs without seeing any obvious concentration decline or further

increase. The endpoint concentration at 24 hrs was determined to be 62.1 ± 1.6 µg/mL, which was approximately 2.1-fold as that for pure APX.

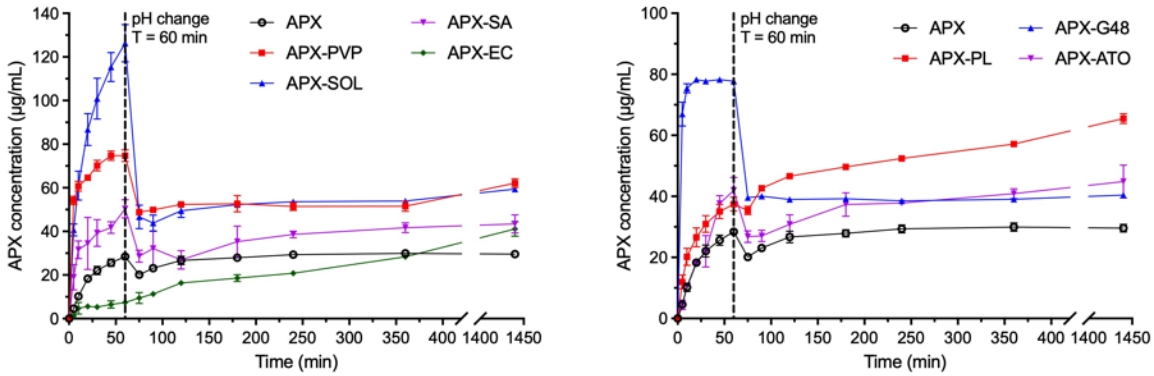

Figure 5.15. Two-stage dissolution of freeze-dried APX ASDs prepared with (A) polymer and (B) lipid carriers.

APX-SOL showed an even faster dissolution rate in the acid stage, achieving an APX concentration of 126 ± 8 µg/mL after dissolution for 60 min. The supersaturation generation period was without concentration decline. After entering the pH 6.8 stage, APX concentration showed a continuous increasing tendency from 47 ± 5 µg/mL at 75 min to 59.4 ± 1.0 µg/mL after dissolution for 24 hrs. APX-SA presented a slightly faster dissolution rate in acid stage, achieving a drug concentration of 50 ± 3 µg/mL at 60 min. When entering the pH 5.0 stage, APX concentration showed a constant increase from 29 ± 2 µg/mL to 43 ± 3 µg/mL at the end of dissolution. The general concentration-time profile was similar to that in pure water. APX-EC showed a typical diffusion-controlled dissolution profile. Before 6 hrs, APX concentrations at each timepoints in both stages were lower than those for IDM alone, similar to its behavior in pure water. Drug concentration was accumulated to 7.4 ± 0.6 µg/mL at 60 min, and further increased to 41 ± 3 µg/mL after dissolution for 24 hrs.

The two-stage dissolution results of freeze-dried APX ASDs prepared with lipid carriers were shown in Figure 5.15B. APX-PL showed a slight improvement in APX dissolution during acid stage, achieving a drug concentration of 37.5 ± 1.8 µg/mL at 60 min. The supersaturation buildup efficiency was drastically lower than that in pure water. After entering the pH 6.8 stage, APX concentration

showed a more effective increase from 35.4 ± 1.1 μg/mL at 75 min to 65.5 ± 1.3 μg/mL at 24 hrs. APX-G48 showed a fast supersaturation buildup rate during acid stage, which was similar to its behavior in pure water. Drug concentration accumulated to 78.3 ± 0.4 μg/mL at 20 min, and effectively maintained at this level without obvious concentration loss. Once entering pH 6.8 stage, APX concentration remained at approximately a 40 μg/mL level for 24 hrs without concentration loss or further increase. APX-ATO provided a slight improvement in APX dissolution during acid stage, showing a gradual increase in APX concentration to a 42 ± 4 μg/mL at 60 min. Once entering pH 6.8 stage, APX concentration continuously increased from 26.8 ± 1.9 μg/mL to the endpoint concentration of 45 ± 5 μg/mL at 24 hrs.

5.4.4.3.2 Two-stage dissolution of freeze-dried APX ASDs prepared with polymer-lipid combination carriers

As seen in Figure 5.16, APX-PVP-PL provided a synergistic effect on the supersaturation buildup of APX in the acid stage, achieving its peak concentration of 143 ± 15 μg/mL within 30 min, followed by a concentration loss to 128 ± 9 μg/mL after 60 min. The drug release showed a completed profile in the acid stage, and the overall drug concentration level was higher than both APX-PVP and APX-PL. After entering the pH 6.8 stage, APX concentration slowly increased from 42 ± 8 μg/mL to its endpoint of 56 ± 3 μg/mL after dissolution for 24 hrs. APX-PVP-G48 and APX-PVP-ATO also provided a synergistic effect on the supersaturation generation of APX to different degrees. APX-PVP-G48 effectively achieved a peak concentration of 97 ± 12 μg/mL within 5 min, followed by a slight concentration decline to 87 ± 4 μg/mL at the end of the acid stage. After entering the pH 6.8 stage, APX concentration gradually decreased from 50 ± 9 μg/mL to 45 ± 3 μg/mL. APX-PVP-ATO showed a gradual monotonic increase in APX concentration to 102 ± 2 μg/mL at the end of acid stage. After entering the pH 6.8 stage, APX concentration slowly declined from 48.3 ± 1.8 μg/mL to 40.9 ± 0.4 μg/mL from 75 min to 120 min. Following, APX concentration maintained at this level for up to 24 hrs. As suggested by the large r^2 values of these formulations fitted to the Higuchi model (Table 5.6), the first 60-min drug release efficiency was not limited by the matrices of binary carriers.

Freeze-dried APX ASDs based on SOL-lipid combinations showed both synergistic effect and averaged effect on APX dissolution in the acid stage (Figure C-24 in Appendix). APX-SOL-PL presented a rapid increase in drug concentration, reaching 180 ± 20 μg/mL at 20 min, followed by a

concentration loss to 146 ± 4 μg/mL at the end of the pH 2.2 stage. After entering pH the 6.8 stage, no obvious change in APX concentration was observed. A slight concentration decline to 52 ± 7 μg/mL was observed for 24 hrs. For APX-SOL-G48, APX concentration showed an even faster accumulation to 175 ± 12 μg/mL within 10 min, and maintained at this level until the end of pH 2.2 stage. Once entering the pH 6.8 stage, APX concentration did not show obvious change. As a comparison, APX-SOL-ATO showed an averaged dissolution profile with regard to APX-SOL and APX-ATO. A gradual and monotonic increase in drug concentration to 59 ± 3 μg/mL was observed during the pH 2.2 stage. Entering the pH 6.8 stage, APX concentration continuously increased from 37.6 ± 1.5 μg/mL to the endpoint concentration of 50 ± 2 μg/mL after 24 hrs. The endpoint concentrations of all samples were similar. As suggested by the large r^2 values of these formulations fitted to the Higuchi model (Table 5.6), the first 60-min drug release efficiency was not limited by the matrices of binary carriers including SOL-PL and SOL-G48. The matrix of SOL-ATO showed a restriction to the drug release of APX.

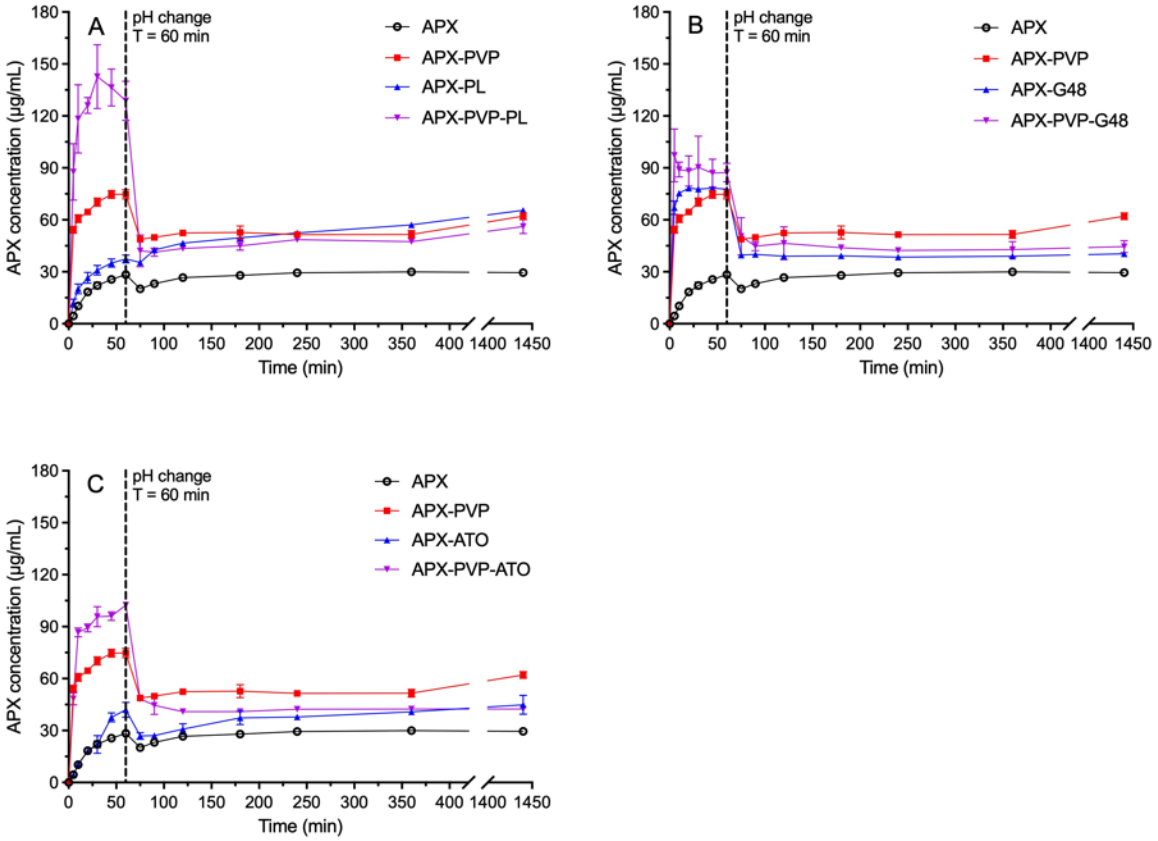

Figure 5.16. Two-stage dissolution of freeze-dried APX ASDs prepared with (A) PVP-PL, (B) PVP-G48 and (C) PVP-ATO.

Figure C-25 in Appendix showed that APX-SA-PL provided a slight improvement in APX dissolution with regard to APX-SA and APX-PL. Drug concentration monotonically increased to its peak of 63 ± 3 μg/mL at 45 min, followed by a slight concentration decline to 57 ± 2 μg/mL at 60 min. Drug concentration presented a continuous increase after entering pH 6.8 stage. The endpoint concentration was more similar to that for APX-PL than APX-SA. APX-SA-G48 showed a supersaturation evolution behavior that was essentially the same as APX-G48, rapidly achieving a peak drug concentration of 82 ± 6 μg/mL at 30 min and effectively maintained at this level until the end of the pH 2.2 stage. After entering pH 6.8 stage, drug concentration was without obvious further increase or concentration decline, which was similar to the behaviors of APX-G48. APX-SA-ATO showed a mild synergistic effect on APX dissolution. As suggested by the large r^2 values of these formulations fitted to the Higuchi model (Table 5.6), the first 60-min drug release efficiency was not

limited by the SA-G48 binary carrier. In contrast, APX-SA-PL and APX-SA-ATO showed good correlations with the Higuchi model, suggesting that the drug release was hindered to some degree.

Table 5.6. Linear regression results of two-stage dissolution of freeze-dried APX ASDs fitted to different dissolution models.

Dissolution model →	**Zero order**		**First order**		**Higuchi model**	
ASD name ↓	r^2	K_0	r^2	K_1	r^2	KH
APX-PVP	-17.0	2.300	0.717	0.258	-4.27	16.262
APX-SOL	0.140	2.060	0.979	0.064	0.959	13.860
APX-SA	-0.881	2.022	0.858	0.102	0.728	13.801
APX-EC	0.044	2.042	0.860	0.077	0.777	13.803
APX-PL	-0.048	2.100	0.981	0.072	0.920	14.200
APX-G48	-100.0	2.387	0.988	0.389	-36.0	2.108
APX-ATO	0.961	1.812	0.981	0.011	0.869	11.524
APX-PVP-PL	-11.1	2.215	0.921	0.210	-2.70	15.777
APX-PVP-G48	-225	2.188	0.000	3.579	-98.0	16.014
APX-PVP-ATO	-3.893	2.248	0.920	0.160	-0.274	15.754
APX-SOL-PL	-49.525	2.166	0.430	0.403	-19.657	15.883
APX-SOL-G48	-5.354	2.325	0.807	0.190	-1.078	16.520
APX-SOL-ATO	0.857	1.891	0.995	0.028	0.961	12.301
APX-SA-PL	0.159	2.006	0.929	0.059	0.908	13.488
APX-SA-G48	-40.010	2.312	0.812	0.318	-12.769	16.548
APX-SA-ATO	-0.338	1.961	0.815	0.085	0.845	13.271
APX-EC-PL	-162.335	2.249	0.000	3.079	-68.924	16.482
APX-EC-G48	0.326	2.059	0.923	0.053	0.947	13.763
APX-EC-ATO	0.701	2.004	0.995	0.040	0.956	13.196

As shown in Figure C-26 in Appendix, APX-EC-PL showed a strong synergistic effect on the release of APX as compared with APX-EC and APX-PL. Drug concentration effectively increased to the plateau level of 100 ± 9 μg/mL within 5 min and maintained at this level until 45 min. A concentration loss to 90 ± 5 μg/mL was observed at the end of the pH 2.2 stage. For the first 15 min at the pH 6.8 stage, APX concentration further decreased from 46.6 ± 1.1 μg/mL to 41 ± 4 μg/mL. Afterwards, drug concentration maintained at this steady level until 24 hrs. In contrast, APX-EC-G48 and APX-EC-ATO presented an averaged dissolution profile with regard to APX-EC and APX-lipids. According to the r^2 values of different formulations, EC-PL did not show a correlation with the tested models. EC-G48 and EC-ATO carriers showed a restriction for drug release at the early stage.

5.5 Discussion

5.5.1 Dissolution of solvent-based IDM ASDs and APX ASDs in pure water

5.5.1.1 Effect of individual polymer and lipid carriers on the dissolution of solvent-based IDM ASDs and APX ASDs

Overviewing the dissolution results obtained with IDM ASDs and APX ASDs prepared with individual polymers and lipids, supersaturation parameters including T_{max}, C_{max}, supersaturation degree, and supersaturation maintaining behaviors varied with carrier type, and a carrier could have different effects on the dissolution of both drugs. IDM-PVP and APX-PVP both generated a "spring and parachute" dissolution profile for which supersaturation was compromised by drug recrystallization after the achievement of peak concentration, while IDM-PVP had a larger T_{max} than APX-PVP. The achievement of a high-degree of supersaturation for both cases was due to the release of amorphous IDM or APX loaded in PVP carrier as found by fluorescence techniques, DSC and PXRD. The larger T_{max} for IDM-PVP had two reasons. The first reason was that IDM-PVP had a slower disintegration than APX-PVP, which can be seen by the comparison of linear regression results with different dissolution models. The second reason was that APX-PVP had a fast drug release due to the amorphous APX domains that were immiscible with PVP carrier, so that their release was not restricted by the polymeric carrier. This was in agreement with the characterization results obtained by fluorescence, DSC and PXRD. The presented stabilizing effect of PVP on IDM and APX solution agreed with PVP's moderate ability to inhibit the recrystallization of both drugs as revealed by the solvent-shift experiment. Considering that PVP did not obviously improve the LLPS

stability of IDM (see result in Section 2.4.2), the supersaturation maintaining effect for IDM-PVP formulation was considered as a result of inhibited crystal growth induced by dissolved PVP. As a comparison, the maintained APX supersaturation was a result of both delayed LLPS and crystal growth (see result of in Section 2.5.4 and Section 3.4.2) The expression of in-solution properties of PVP was based on the fast dissolution of the PVP carrier.

The use of SOL as ASD carrier suggested that drug release profile could be drastically different for different drugs. The slow dissolution of IDM-SOL could be contradicting to the common notion that SOL is an amphiphilic copolymer ASD carrier that facilitates drug dissolution. Although SOL has the good water solubility and dispersibility, gelation can occur at the surface of SOL formulations when SOL content is high in a formulation, especially with a high temperature [226,227]. The solution-gel transition of SOL is effectively facilitated by a temperature over 35 °C, which is close to the 37 °C commonly used for dissolution test that mimics body temperature [228]. According to different studies, a negative correlation between drug release rate and SOL content was observed using different preparation methods including freeze-drying, spray-drying, and powder homogenization [226,227]. The gelation of part of SOL molecules could delay the drug release by forming a physical barrier. In this regard, drug release should follow the diffusion-controlled mechanism which applies to insoluble carriers. The inhibition effect of dissolved SOL on the LLPS (Section 2.5.4) and recrystallization (Section 3.4.2) of IDM can be compromised if SOL cannot fully dissolve in water. The dissolution potential of amorphous IDM loaded in SOL was also masked by SOL gelation and slow dissolution. As a comparison, at room temperature, Dajun's study showed that a "spring and parachute" profile could be generated by IDM-SOL (20% w/w) in aqueous media under a non-sink condition with SI = 0.1, where the formulation and SI index were the same as this study [95]. The comparison suggested the important effect of temperature. Besides, due to the changing IDM solubility at different pH conditions, identical SI index and drug-excipient ratio require different drug dose and excipient amount for different dissolution media of a same volume. For Dajun's study, the experimental parameters required less than 10 mg SOL in a 250-mL dissolution medium with a pH of 1.2, which was less than the 80 mg of SOL for a 250-mL pure water dissolution medium. The larger amount of SOL is a negative factor for IDM dissolution at 37 °C as more SOL molecules could be trapped in the gel structure at the formulation surface. For another scenario in Dajun's study where the same formulation dissolved in the pH 7.4 buffer under a same non-sink level, an even larger amount of SOL was used, but a profile with a high-degree of supersaturation followed by drug

recrystallization could still be achieved at room temperature. This suggests that temperature is a more important factor to determine the release of IDM from SOL carrier. The first-order dissolution profile with a low drug concentration observed for solvent-based IDM-SOL suggested that the benefits of drug amorphization and supersaturation ability of SOL were completely masked by the gelation of SOL.

As a comparison, the drug release profile of APX-SOL was not negatively influenced by the gelation of SOL. This was likely due to the fast release of amorphous APX domains that were not fully miscible with SOL carrier as shown in Section 4.4.3. The gelled part of SOL should still occur as it was mainly controlled by temperature, but the amount of dissolvable part was expected to increase due to the larger contacting area of powder in dissolution media. Therefore, the supersaturation buildup rate was enhanced by the improved dissolution of SOL carrier. The comparison between dissolution of IDM-SOL and APX-SOL leads to the conclusion that a high drug-excipient miscibility is not necessarily a positive factor for supersaturation buildup.

For both IDM-SA and APX-SA, the achieved supersaturation levels were similar to the LLPS results recrystallization results. The effective expression of the in-solution property of SA suggested that drug release from carrier was not a restriction. The ionization effect discussed in Section 3.5.1 was considered as the core determinant for the more obvious enhancing effect of SA on the dissolution of IDM over APX. The solubility change for a drug under the ionization condition induced by a carrier should be taken into consideration for the evaluation of its dissolution profile, as it could place a more significant dissolution enhancing effect and supersaturation maintaining effect over drug amorphization.

The sustained release profile for both IDM-EC and APX-EC followed the diffusion-controlled mechanism due to the insoluble nature of EC. Considering that both IDM and APX existed in amorphous states in EC carriers which are supposed to dissolve fast, the slow drug release suggested a good drug-polymer miscibility whereby amorphous drug was mostly loaded in the EC matrix instead of being adsorbed on the carrier surface, so as to delay drug release. This suggestion was in agreement with the fluorescence results in Section 4.4.2 and 4.4.3 that characterized the immiscible amorphous domains of IDM and APX.

Among all lipids, PL provided the highest supersaturation degree for IDM, which was attributed to the good loading capacity of amorphous IDM and fast drug release. However, when

comparing with G48, the drug release for IDM-PL at early stage was considered to be hindered by the PL carrier to some degree. This could be the result of intermolecular complexation of PL molecules. PL is composed of C18:2 phosphatidylcholine and C18:2 phosphatidylethanolamine with a low phase transition temperature (T_m) of -57 °C and -40 °C, respectively. PL is difficult to formulate as fine powders under room temperature as the low T_m values and amorphous nature lead to sticky powders that are difficult to disaggregate [135,229]. Due to the cohesive or agglomerated state of PL, the wetting of the IDM-PL formulation can be compromised by the decrease in effective surface area contacting the dissolution medium. In this case, the overall drug release rate of IDM could be delayed to some extent, although amphiphilic materials were expected to facilitate the wetting and dissolution of drug particles. As such it could be understood that dispersed PL could facilitate drug wetting and solubilization by lowering interfacial tension, but the time required for PL to disperse in water plays an important role in determining overall drug release rate. As a comparison, the fast buildup of APX supersaturation indicated that the disintegration of APX-PL was more effective. Two possible mechanisms are considered. Firstly, the higher melting point of APX than IDM would make APX-PL more easily to be crushed into powder than IDM-PL during ASD preparation, resulting in a better disintegration when exposed to dissolution media. Secondly, a larger amount of PL was used in the formulation of APX-PL (360 mg, as compared with 80 mg for IDM-PL), so that more PL molecules were expected to disperse and release free APX. This mechanism is similar to the case of SOL gelation previously discussed. The supersaturated IDM solution was maintained better than APX, corresponding to the LLPS (Section 2.4.3 and 2.4.7) and recrystallization results (Section 3.4.2) found with the solvent-shift method. The slow supersaturation induction rate of IDM-PL could also be a reason for the better maintained supersaturation, as it was associated with lower recrystallization tendency. The constant release of amorphous IDM from PL carrier could also contribute to the supersaturation maintenance.

IDM-G48 and APX-G48 were without disintegration issue, attributed to the wetting and dissolution of G48 material. The PEGylated stearate has a large HLB value of 16 and a higher melting point of 48 °C than PL [178]. These properties enable the existence of G48 in a solid state that can be ground into fine powder and disperse fast when contacting water. The generated supersaturated solution of IDM and APX with high supersaturation degree were both vulnerable to concentration loss, which could be explained by the fact that G48 had a poor stabilizing effect on the recrystallization of both drug solutions.

ATO provided a similar slow release profile for both drugs due to its insoluble nature. However, the dissolution rates for both samples were faster than those combined with insoluble polymer EC. As revealed by fluorescence, DSC and PXRD, both IDM and APX had a lower miscibility with ATO than with EC. The amorphous drug domains immiscible with formulation were expected to dissolve faster than those loaded in the EC polymer chain uniformly. Similar to the case of IDM-SOL, these dissolution results again suggested that a good drug-excipient miscibility could be a negative factor for drug dissolution when carriers were insoluble. The absence of drug concentration loss was merely a result of the low drug concentration achieved.

From the above discussions it is concluded that the ASD carriers could have different effects on IDM and APX. The solubility and dispersibility of a carrier material play an important role in determining the kinetic-solubility profile of IDM and APX. For an instantly dissolved carrier the supersaturation behavior of loaded drug was highly dependent on the in-solution properties of carrier material, including the LLPS and the recrystallization inhibition ability. For an insoluble and slowly dissolved carrier drug dissolution was more dependent on the drug-carrier miscibility and drug amorphization. A slow dissolution of carrier material will delay or mask the expression of carrier's effect on the supersaturation of IDM. The dissolution profiles of IDM ASDs and APX ASDs in pure water were seen as fundamentals for their supersaturation behaviors in more complexed dissolution media. The effect of polymer-lipid combinations on the dissolution of both drugs will also be analyzed based on the changes in these parameters.

5.5.1.2 Effect of polymer-lipid combinations on the dissolution of solvent-based IDM ASDs

The synergistic effect of PVP-PL, PVP-G48 and PVP-ATO on the dissolution rate of IDM was considered a result of facilitated disintegration of both carriers. As discussed, PL exists in a semi-solid state with aggregation due to low T_m values. The intermolecular interactions of PL could be weakened by the combination with PVP, and the phase transition temperature of the binary carrier could be increased due to the higher glass transition temperature of PVP than PL. Therefore, the dissolution rate of IDM was faster than that for IDM-PL. The dissolution rate of IDM was also notably faster than that for IDM-PVP, which could possibly be due to weakened swellability of the formulation. Although PVP is well recognized as a hydrophilic carrier for increased drug dissolution, some opposing effects were reported by different studies [96,97]. A large amount of PVP in a solid

formulation, prepared either from a solvent evaporation method or a physical blending method, has been found to decrease the dissolution rate of drug payload due to PVP's swellability and large viscosity of the stagnant diffusion layer surrounding drug payload. These effects may hinder the release rate of drug payload to some degree, while not providing a slower rate than pure drug. This could be the reason for IDM-PVP not to generate a high-degree supersaturation within short time to provide a sharp shape on the concentration-time profile like that provided by IDM-G48. Therefore, the addition of PL may reduce the close contact of PVP molecules and provide a faster drug dissolution than formulation based on PVP alone.

The r^2 and constant values from linear regression results for different ASDs could facilitate the analysis on drug release behaviors. The significantly decreased r^2 value of IDM-PVP-PL fitted with the zero order model suggested that the release of IDM was less at a constant rate hindered by carrier. With a similarly high r^2 value (i.e. > 0.95) fitted with first order model as compared with IDM-PVP and IDM-PL, IDM-PVP-PL had a larger K_1 constant which suggested that the drug release rate at early stage had a higher rate and was less hindered by the carrier. Here it is suggested that constant values of different samples should only be compared when their r^2 values are high (i.e. the dissolution profiles of all samples had a good fit with a specific model). With a significantly reduced r^2 values fitted with a dissolution model, the analysis of drug release rate relying on constant values could lead to misleading results. The decreased r^2 values of IDM-PVP-PL fitted to Higuchi model also supported this analysis. According to the discussion of Section 2.5.3 and 3.5.3, although PVP-PL combination showed a synergistic effect on the stabilization of LLPS of IDM, it did not provide a better inhibition on the overall recrystallization process of IDM solution compared with PL due to the fact that stabilized LLPS only induced an effect on the early stage of dissolution, and large nanodroplets could be filtered during the preparation of the dissolution samples. Therefore, we considered that the improvement in IDM supersaturation before 180 min was simply attributed to the dissolution of a larger amount of amorphous IDM instead of any improvement in recrystallization inhibition. After this timepoint, the supersaturation profile of IDM-PVP-PL was comparable with those for IDM-PVP and IDM-PL, suggesting a similar maintaining effect on IMD supersaturation between different carriers.

As a comparison, the supersaturation generation rate of APX-PVP-PL was highly comparable with APX-PL, and the maintaining of supersaturated APX solution was more governed by the characteristics of APX-PVP. The r^2 value of APX-PVP-PL fitted with first order sat between those

for APX-PVP and APX-PL, suggesting an averaged drug release efficiency due to polymer-lipid combination. These phenomena suggested that the dissolution/dispersion of carrier materials was less of an issue to be solved by the combination of polymer and lipid, which was different from the observations for IDM-PVP-PL. As just discussed, the supersaturation profile of the drug is an expression of the in-solution properties of carrier material for a fast-disintegration formulation. In this case, the maintenance of APX concentration was based on dissolved PVP, which agreed with its ability to stabilize LLPS and inhibit the recrystallization of APX.

For IDM-PVP-G48, the fast release of IDM from G48 carrier was not compromised by the addition of PVP, and the peak concentration could benefit from the slowed recrystallization of IDM with co-dissolved PVP. The dissolution profile of IDM-PVP-G48 were poorly fitted with the first order and the Higuchi model, suggesting the drug release was not hindered by PVP-G48 carrier. This was an example where polymer and lipid carriers improved the weakness of each other (i.e. slow dissolution for PVP and poor supersaturation maintaining ability of G48). This effect was not maintained for a long time due to the smaller amount of PVP in IDM-PVP-G48 as compared with IDM-PVP. The general concentration loss profile was similar to that for IDM-G48, suggesting that IDM-PVP-G48 had difficulty maintaining the IDM supersaturation. The combination of PVP and G48 did not change the supersaturation buildup rate of APX since neither APX-PVP nor APX-G48 had disintegration issue. This was also seen by the similar r^2 values and K_1 constants of APX-PVP and APX-PVP-G48. The only difference induced by the combination was the compromised supersaturation maintaining ability of the formulation due to the smaller amount of PVP contained. In this case we again obtained that the dissolution and supersaturation behavior of a slow-disintegrating formulation could be effectively adjusted by the combination with disintegration facilitating material through the better expression of in-solution properties of carrier materials. The fact that PVP-ATO binary carrier significantly improved the dissolution rate of IDM at early stage but basically did not change that for APX could be explained by the same mechanism. The supersaturation profile of APX-PVP-ATO was less governed by the characteristics of APX-PVP, which was a result of relatively poor drug loading ability of ATO in the binary carrier. The more gradual supersaturation buildup and lower supersaturation achieved by APX-PVP-ATO than APX-PVP was associated with lower recrystallization tendency.

The combination of SOL-PL and SOL-G48 provided an averaged dissolution rate without the concentration loss characteristics of IDM-PVP and IDM-G48. The drug release behaviors of IDM-

SOL-PL and IDM-SOL-G48 at the early stage were considered to be more similar to IDM-SOL than IDM-lipids, as seen by the r^2 values and constants of IDM-SOL-PL and IDM-SOL-G48 fitted with the first order model that were similar to IDM-SOL. The r^2 values of IDM-SOL-PL and IDM-SOL-G48 were more similar to that of IDM-SOL than IDM-lipids for the Higuchi model. These results suggested a restricted drug release due to SOL's gelation, while the maximum achievable drug concentration was improved by the addition of lipid materials. The dissolution models of IDM-SOL-PL and IDM-SOL-G48 were more similar to IDM-SOL than IDM-lipids, masking the recrystallization characteristics of IDM-lipids. Since the in-solution properties (i.e. inhibited LLPS and recrystallization for IDM) of SOL was not expressed due to its insolubility, the absence of recrystallization was a result of slow supersaturation generation with low recrystallization tendency. As a comparison, the combinations of SOL-PL and SOL-G48 provided comparable dissolution profiles to APX-SOL, suggesting a dominant characteristics of APX-SOL. As previously discussed, the dissolved amount of SOL carrier was larger from APX-SOL than IDM-SOL, and therefore the in-solution properties of SOL could be expressed better. The maintenance of a higher drug concentration for APX-SOL-PL and APX-SOL-G48 than APX-lipids also indicated that the system benefited from the recrystallization inhibiting effect of dissolved SOL. The SOL-ATO combination did not bring an obvious change to the dissolution model of IDM with regard to IDM-SOL and IDM-ATO, whereby the slightly higher supersaturation could be a result of fast release of amorphous IDM domains that were not fully miscible with formulation. For APX, the supersaturation degree was obviously compromised by replacement of SOL carrier (with both supersaturation generating and maintaining ability) with insoluble ATO. As mentioned, the disintegration-facilitating effect of ATO would be useless when the disintegration of the formulation was not a significant rate-limiting factor.

The SA-lipid combinations provided dissolution profiles that sat between IDM-SA and IDM-lipids. The achieved supersaturation levels were due to the strong alkalizing effect of SA that increased IDM solubility, which overweighed the effects of lipid materials. This effect was fundamental for the improvement in crystalline solubility, LLPS stability and supersaturation maintenance of IDM in the water phase. The dissolution rate of IDM-SA-G48 was notably faster than IDM-SA-PL and IDM-SA-ATO before 180 min due to the fast dissolution of G48 carrier. The aggregation of PL did not only delay the drug release from binary carrier, but also slowed the dissolution of SA by which the pH increase effect was delayed. As such the supersaturation buildup of IDM could be less effective than other combinations. The combination of ATO to the formulation

could lower the drug-carrier miscibility as indicated by fluorescence, DSC and PXRD. Therefore, the dissolution of IDM-SA-ATO showed a more gradual drug release than IDM-SA. When used to formulate APX, SA-PL and SA-G48 both provided an averaged effect on the supersaturation profile of APX, which was simply a result of decreasing amount of PL and G48 in formulation. The pH-modifying effect of added SA did not influence the dissolution of nonionized APX corresponding to the LLPS and recrystallization result. By comparing the dissolution of IDM and APX with SA-lipid combinations it was concluded that the effect of ionized carriers was highly dependent on the ionization properties of loaded drugs.

All EC-lipid combinations provided an averaged dissolution profiles for both IDM and APX. The achieved supersaturation was maintained by slow supersaturation induction rate and constant release of IDM from EC matrix. The delayed effect on the release of IDM and APX induced by insoluble EC matrix was weakened by the addition of dissolvable and dispersible materials. The effects of adding lipid materials to insoluble polymer carrier were considered universal for both drugs through the adjustment of dispersibility of formulations. IDM-EC-PL showed a large r^2 value similar to IDM-EC and IDM-PL (i.e. >0.95) fitted with the first order model, and with an increased K_1 constant. The drug release from EC-PL carrier still followed the first order characteristics but was less hindered by carrier matrix. Here it should be noted that the increased K_1 constant described a faster drug release of a sample to reach its own maximum drug concentration within an investigated time range, but this did not mean the supersaturation degree achieved by it was higher. The reason for IDM-EC-PL to have a larger K_1 constant within 120 min was that its maximum achievable supersaturation level was much lower than IDM-PL. Therefore, linear regression results of r^2 value different constants should be combined with the absolute concentrations of a dissolution profile to accurately analyze the drug release behaviors of a sample.

In this section, we found that the change in the dissolution and supersaturation profiles of IDM induced by polymer-lipid combinations were mainly a result of facilitated disintegration, through which the in-solution properties of carrier materials could be expressed better. For formulations prepared by soluble carriers, the adjustment of supersaturation parameters of a drug through the addition of other carrier materials is based on the comprehensive expressions of in-solution properties of both carriers. By these mechanisms, the polymer-lipid combination effect on APX dissolution could be different from that for IDM, whereby the root cause was that individual carriers behaved differently for both drugs. The correlation between LLPS, recrystallization result and

dissolution behaviors could only be established for formulations which dissolved instantly. The solid-state characterizations helped us confirm that drug release hindrance for some formulations was controlled by carrier dissolution, excluding the possibility of a failed drug amorphization for ASD preparation. Lastly, it is recalled that the particle size of several formulations could not be reduced by passing through sieves due to their physical states that prevent their disaggregation. The dissolution results of freeze-dried IDM ASDs will be compared to analyze this factor.

5.5.2 Dissolution of freeze-dried IDM ASDs and APX ASDs in pure water

5.5.2.1 Effect of individual polymer and lipid carriers on the dissolution of freeze-dried IDM ASDs

The freeze-dried IDM ASDs based on most individual carriers provided a faster dissolution and supersaturation buildup rate than their corresponding solvent-based counterpart attributed to the improved wetting of formulations with smaller particle size and larger surface area. IDM-PVP stilled showed a “spring and parachute” profile based on the mechanism that supersaturation induction was faster while recrystallization inhibiting effect was not improved. The maximum supersaturation degree did not present any obvious change. This can be understood as that freeze-dried IDM-PVP provided a similar peak concentration in a more efficient manner, supporting the previous speculation that drug release from PVP carrier was hindered to some degree. For IDM-SOL, for which drug release was delayed by the gelation of carrier material, the lyophilized sample provided a faster dissolution and higher drug concentration. Gelation should still occur for both in-solution SOL molecules and for those on the surface of formulation by absorbing water. We hypothesized that gelation of in-solution SOL molecules did not negatively affect the drug release as this activity happened after the drug release process. The negative effect on drug release should be due to the gelation of SOL molecules on the surface of formulation, so that drugs at inner locations were less exposed to water due to the creation of this diffusion barrier. The gelation was not weakened for lyophilized sample, but an increasing portion of gelation process happened in solution phase due to faster dissolution of smaller SOL particles. This relieved the hindrance for drug release, but was not effective enough to achieve a high supersaturation degree as compared with other ASDs. The drug loaded in freeze-dried IDM-SOL was in an amorphous state as revealed by different characterization techniques, further justifying that slow drug release was not a result of failed drug amorphization.

As a comparison, freeze-dried APX-PVP and APX-SOL showed an obviously lower supersaturation degree than their solvent-based counterparts, which could be explained by two mechanisms. Firstly, the amorphization and drug loading process of APX could be less complete than solvent evaporation method due to drug precipitation during the pre-freezing process before freeze drying. The solubility of APX in organic solvents was highly dependent on temperature, and this was the reason that a high temperature of 90 °C was used to prepare solutions of APX and carriers. However, when samples were cooled in freezer, which was inevitable for freeze dry process, organic solutions containing APX and carriers could undergo drug precipitation with decreasing temperature. A part of APX would exist in a sedimentation state in a solution before the freeze-drying process. The obtained freeze-dried sample was expected to contain two solid phases, one of which was solid dispersion of APX in carrier material, and the other was a pure APX phase originated from precipitated part. The pure APX phase could exist in an amorphous form or nanocrystal form, considering that freeze-dried APX ASDs showed significantly reduced crystallinity as revealed by the DSC and PXRD (Section 5.4.1.2 and 5.4.2.2). Therefore, the overall supersaturation generation rate of freeze-dried APX ASDs could be compromised. Secondly, freeze-dried APX ASDs based on polymers, excluding SA, showed a physical state of porous scaffold that could float on dissolution media for a longer time than their solvent-based counterparts. Consequently, the supersaturation generation rate could be attenuated by the poorer wettability of these formulations. The effect of the first mechanism was considered to be dominant, since the freeze-dried IDM ASDs shared the latter mechanism but did not show attenuation in supersaturation generation. The better supersaturation maintaining behaviors of APX-PVP and APX-SOL than their solvent-based counterparts were a result of slower supersaturation induction rate.

For lyophilized IDM-SA, the reduced particle size only improved the dissolution rate of IDM at the early stage, but did not change the maximum achievable drug concentration and recrystallization inhibiting profile as these factors were determined by the absolute amount of SA in dissolution medium. For APX, unlike the significantly compromised dissolution efficiency for APX-PVP and APX-SOL induced by freeze-drying, the freeze-dried APX-SA showed a less influenced supersaturation generation rate. SA was insoluble in organic solvent and existed in a separated phase when using both preparation methods. Besides, different from the porous scaffold for APX-PVP and APX-SOL, freeze-dried APX-SA existed in a fine powder state without floating issue. As a result, the APX-SA yielded similar supersaturation profiles with different preparation methods.

The freeze-dried IDM-EC did not improve the dissolution rate of IDM, and no supersaturation was generated within 24 hrs, suggesting that particle size was not a limiting factor for the dissolution behavior of IDM-EC. Both formulations followed the diffusion-controlled drug release mechanism. In contrast, APX-EC presented a higher drug concentration than its solvent-based counterpart. For an ASD formulation prepared with insoluble polymer which followed a diffusion-controlled drug release mechanism, the precipitation of APX from organic solution could be a favorable factor as this part of drug could dissolve faster without being hindered by diffusion barrier of the EC matrix. This being said, the overall lower APX concentration than pure APX indicated that most APX molecules were loaded in the EC matrix. The achieved concentration was not a supersaturated state with regard to APX solubility. From this case it was observed that a poor solubility of drug in organic solvent used for ASD preparation could be a positive factor for drug dissolution.

The freeze-dried IDM ASDs prepared by lipid carriers showed a similar improvement in IDM supersaturation to polymer-based samples, whereby the maximum achievable concentration was improved by the freeze drying process for all samples. As discussed, the drug release efficiency from PL was limited by the aggregation of PL into large particles, which was a result of the reduced particle size. The reduced particle size also improved the supersaturation degree of IDM-G48 and IDM-ATO. After achieving peak drug concentration, the faster recrystallization rate of IDM-PL and IDM-G48, as compared with their solvent-based counterparts, could be a result of the higher recrystallization tendency associated with a higher supersaturation extent. The similar equilibrium concentrations for IDM-PL and IDM-G48 samples prepared with different methods were dependent on PL amount that determined the crystalline solubility of IDM, without being affected by preparation method. With a faster dissolution of PL and G48 carriers, the supersaturation parameters of IDM-PL and IDM-G48 corresponded to the LLPS and supersaturation results. The overall concentration-time profile of IDM-ATO was governed by the insolubility of ATO, which overweighed the effect of particle size.

As a comparison, the freeze-dried APX-PL and APX-G48 showed a lower supersaturation degree than corresponding solvent-based counterpart, which was also a result of APX sedimentation during freezing, as discussed for the polymer case. Here it is observed that a preparation method could have different effects on the supersaturation behavior of different drugs. The effective maintaining of supersaturated APX solution in these cases was considered to be the result of slow

supersaturation induction rate instead of a change in the recrystallization inhibiting ability of carriers. Unlike APX-PL and APX-G48, the dissolution profile of APX-ATO was less influenced by the freeze dry process as samples from both methods had poor drug-excipient miscibility. The dissolution of APX-ATO samples both follow the diffusion-controlled mechanism.

In this section, we observed that IDM ASDs and APX ASDs with individual carriers could be influenced by preparation methods in different manners. The reduced particle size affected supersaturation evolution by influencing peak concentration and T_{max}. Similar to the discussion of solvent-based samples, the dissolution and supersaturation characteristics of freeze-dried samples could be explained by the LLPS and recrystallization results revealed by solvent-shift experiment, but the change in excipient properties (mainly precipitation during freeze drying process) should be considered when analyzing dissolution profiles. The analysis of dissolution behaviors of freeze-dried ASDs prepared by polymer-lipid combinations will be based on the behaviors of individual material based ASDs prepared by the same method.

5.5.2.2 Effect of polymer-lipid combinations on the dissolution of freeze-dried IDM ASDs

The freeze-dried IDM-PVP-PL and IDM-PVP-G48 showed an obvious synergistic effect on early-stage dissolution rate and supersaturation degree, which was similar to the observation for solvent-based formulations, due to the improved disintegration of carrier material. IDM-PVP-PL showed similar r_2 values to IDM-PVP fitted with all tested models, suggesting a similar drug release behavior of IDM at the early dissolution stage. For the first order model, the K_1 constant of IDM-PVP-PL was slightly lower than that for IDM-PVP, describing a slower drug release for IDM-PVP-PL to achieve its maximum drug concentration within this range, which was a result of the higher maximum concentration that can be achieved by IDM-PVP-PL than IDM-PVP. The combination of PVP-PL was not a hindrance of drug release overall. IDM-PVP-G48 showed poor correlations with all tested models, indicating that drug release was not hindered by the combination of PVP and G48. Sharing a same mechanism, however, freeze-dried IDM-PVP-ATO showed a less effective synergistic effect. This could be explained by the different effects of insoluble lipid ATO on the formulations with different integration issues. For solvent-based samples, whereby IDM-PVP showed a large T_{max} value of 4 hrs due to disintegration issue, the buildup of drug supersaturation at early stage took the advantage of the facilitated disintegration observed with added ATO. Here it is recalled

that ATO itself did not provide an effective enhancement in drug dissolution, and the faster dissolution observed for solvent-based IDM-PVP-ATO was resulted from the earlier release of amorphous IDM stored in PVP carrier. As a comparison, for freeze-dried samples, the disintegration issue of IDM-PVP itself was relieved by the reduced particle size, allowing the release of amorphous IDM in a timely manner. Therefore, the addition of ATO could not further improve this parameter as significantly as in the case of solvent-based samples.

The synergistic effect on the supersaturation generation of APX-PVP-PL should be attributed to facilitated wetting. The insufficient wetting of PVP-based formulation due to the floating issue could be improved by the addition of PL, so that amorphous APX loaded in binary carrier could be released faster. APX-PVP-PL only showed a good correlation with the first order model, with a K_1 constant that averaged between APX-PVP and APX-PL. APX-PVP-PL took slightly longer time than APX-PVP to reach its own maximum concentration, which was due to the higher concentration level achieved by APX-PVP-PL, similar to the discussion in section 5.5.1.2. The observed drug concentration decline was due to APX recrystallization in the presence of weakened supersaturation maintaining effect when PVP amount was decreased in formulation. Nevertheless, the extent of desupersaturation was not increased significantly since C_{max} was not improved much, so that the recrystallization tendency of supersaturated APX solution should remain close to that for APX-PVP and APX-PL. This mechanism was believed to apply to APX-PVP-G48 and APX-PVP-ATO as well, as these lipid materials were expected to attenuate the highly organized porous structure of lyophilized powder created by PVP.

The averaged dissolution profiles of freeze-dried IDM-SOL-PL and IDM-SOL-G48 sitting between those for IDM-SOL and IDM-lipids shared a same mechanism of adjusted disintegration of SOL as discussed for solvent-based samples (section 5.5.1.2). The slightly synergistic effect of IDM-SOL-ATO was also aligned with its solvent-based counterpart, suggesting that the supersaturation adjustment mechanisms were not influenced by the parameters associated with preparation method (i.e. formulation particle size and floating issue for light scaffold). The facilitated disintegration effect of SOL-PL and SOL-G48 was more effective when formulating APX, which aligned with the comparison result between solvent-based IDM and APX samples. The combination of ATO with SOL showed an averaged supersaturation degree which was significantly lower than that for APX-SOL. The positive effect of facilitated wetting on supersaturation induction was overwhelmed by the negative effect of reduced amount of SOL carrier which showed better loading capacity for

amorphous APX. The decreasing amount of finely dispersed amorphous APX was likely to attenuate the supersaturation generation ability of the formulation. The negative effect of SOL-ATO carrier on APX dissolution was different from the synergistic effect brought by PVP-ATO carrier, although SOL and PVP were both soluble carriers in these dissolution scenarios. A plausible explanation could be obtained by analyzing the C_{max} achieved by individual carriers, whereby APX-PVP achieved a lower C_{max} (approximately 60 μg/mL) than that for APX-SOL (150 μg/mL). Indeed, the different intrinsic properties and abilities of two polymers should be the reason. But another way to describe this phenomenon was that a part of PVP carrier did not contribute to the generation of APX supersaturation. When the idle (i.e. ineffective in generating drug supersaturation) part of a carrier was replaced by another material that improved the disadvantageous factor (i.e. floating issue) of the whole formulation, the supersaturation generation efficiency of new system could be benefited. Following this mechanism, the supersaturation generation efficiency could be sacrificed by the replacement of SOL carrier with ATO, as the idle fraction of SOL was less than that for PVP in APX-PVP formulation as suggested by the comparison of C_{max} values. In this regard, the addition of ATO to polymer as a binary carrier could bring different effects to the supersaturation evolution of freeze-dried APX ASDs.

SA-lipid combinations also provided similar changes to the IDM ASD systems prepared by both methods. The dissolution and supersaturation profile of freeze-dried IDM-SA-PL were more governed by IDM-SA characteristics compared with the solvent-based case, as the aggregation issue of PL-containing formulation was weakened by the freeze dry process. The averaged supersaturation degrees of APX-SA-lipid formulations were considered as result of reduced amount of lipid carrier which had better supersaturation buildup efficiency. This also explained the similar behaviors of APX-SA-ATO to APX-SA and APX-ATO, as ATO did not provided a superior supersaturation ability over SA. The effective maintaining of APX supersaturation was due to the slow supersaturation induction rate associated with weak recrystallization tendency, since all involved carriers had poor supersaturation maintaining abilities. The effect of SA-lipid combinations on the supersaturation of both drugs were considered similar.

Freeze dried IDM-EC-PL and IDM-EC-G48 also exhibited changes similar to the IDM ASD systems comparable with solvent-based formulations. However, IDM-EC-ATO presented a dissolution profile similar to IDM-ATO, with a faster dissolution rate than IDM-EC, which was contrary to the observations for solvent-based sample set. The K_1 constant of APX-EC-ATO was

similar to APX-ATO and significantly higher than APX-EC. The faster release of IDM could be a result of compromised miscibility between ATO and EC carrier for freeze drying method. For the freeze-drying process, the drug solution was left to freeze for 24 hrs. During the cooling process, a part of ATO could precipitate before the solution was completely frozen as the solubility of ATO in organic solvent became significantly lower with decreasing temperature. After the freeze-drying process, this part of ATO was expected to be less miscible with EC and a portion of amorphous IDM adsorbed on the ATO surface could be more readily dissolved. This is different from the rotary evaporator based solvent evaporating process whereby all compositions precipitate together to form a highly miscible formulation. As such, freeze-dried IDM-EC-ATO provided a slightly faster dissolution rate. Above mechanisms could also be used to explain the averaged dissolution profiles of APX-EC-lipid combinations. The diffusion-controlled dissolution of EC matrix was weakened by the addition of lipid materials.

In this section, most freeze-dried IDM ASDs and APX-ASDs based on polymer-lipid combinations affected the dissolution and supersaturation behaviors of drug in a manner similar to what was found for solvent-based ASDs. Several compositions behaved differently when prepared by different methods. The adjustments in dissolution supersaturation parameters of IDM and APX were dependent on the changed dissolution of ASD carrier. It is believed that LLPS and solvent-shift recrystallization results should be qualitatively used to analyze dissolution behaviors of ASD formulations. Quantitative correlations between these in-solution properties and drug dissolution results could be inaccurate due to the varied dissolution rates of drug carriers.

5.5.3 Two-stage dissolution of freeze-dried IDM ASDs and APX ASDs.

5.5.3.1 Effect of polymer and lipid carriers on the dissolution of freeze-dried IDM ASDs and APX-ASDs

For IDM-PVP, the significant improvement in IDM dissolution rate in both phases resulted from the dissolution of amorphous drug loaded in PVP carrier. These behaviors were considered to inherit from the properties of IDM-PVP in pure water without being affected much by pH. The absence of a “spring and parachute” profile in the acid stage was considered to be a result of incomplete supersaturation evolution before the occurrence of net concentration loss, as IDM-PVP achieved its peak concentration at 60 min in pure water. After entering the pH 5.0 stage, the

maintaining of IDM supersaturation was a result of PVP's moderate ability to inhibit recrystallization, similar to the phenomenon in pure water.

For APX ASDs, the first phenomenon we noticed was that pure APX showed a higher solubility in acidic environment than in alkaline pH. The APX concentration achieved within 60 min in the pH 2.2 stage (28.41 ± 0.51 μg/mL) was only slightly lower than that achieved within 24 hrs in the pH 6.8 stage (29.58 ± 1.05 μg/mL). The equilibrium solubility in the alkaline stage was also lower than that of 34.79 ± 0.71 μg/mL in pure water. APX is commonly recognized as a non-ionizable compound with a pKa value of 13.12 and its solubility is expected to be unchanged at physiological pH range. However, different studies have found that APX solubility in acidic environment was higher than that in alkaline environment. A possible mechanism is that the weak interactions between the amine group of APX and protons in acid environment slightly improves the hydration and solubility of APX. This type of interaction is unstable and can be reversed by the increased pH, so that APX exhibited a solubility reduction in pH 6.8 medium. The further increase in APX concentration during pH 6.8 stage indicated that drug release was not completed in previous stage, and the non-sink level was relieved by the increasing amount of dissolution volume, so that drug release process could occur more effectively. The dissolution behavior and supersaturation profile of APX-PVP in acid stage was similar to those in pure water, suggesting that pH was not a major influencing factor for the performance of APX-PVP. The slightly higher concentration level could be a result of solubility change induced by pH as just discussed. Drug release process was incomplete in acid stage as suggested by the further increase in APX concentration in pH 6.8 stage. The overall APX concentration higher than APX alone was a combination of the effects induced by the constant drug release and supersaturation maintaining effect of dissolved PVP. The supersaturation evolution parameters were in good agreement with previously revealed properties of APX-PVP in pure water (Section 5.4.4.1.1).

The slow dissolution rates of IDM-SOL in both the pH 2.2 and pH 5.0 stages agreed with its performance in pure water, resulting from the delayed drug release due to SOL gelation. No change was observed with different pH conditions. The supersaturation performance was improved in the pH 5.0 stage, which was due to the increased volume dissolution medium. No concentration decline was observed in both phases, resulting from the low supersaturation degree achieved and supersaturation maintenance effect provided by dissolved part of SOL.

As a comparison, the supersaturation buildup efficiency of APX-SOL during the acid stage was significantly lower than that in pure water, whereby the “spring and parachute” profile changed to a monotonic increase profile. Considering that an acid environment improved APX solubility, the slow APX dissolution should be due to the lower paddle speed used for the experiments in this section. APX-SOL, which had superior supersaturation generation effect in pure water over APX-PVP, should be more vulnerable to the decreasing paddle speed as supersaturation buildup relies strongly on the disintegration of formulation. The drug release process was considered to be more complete than APX-PVP due to the following reason. The theoretical APX concentration at the moment of 60 min after the volume change of dissolution medium was calculated to be 20.76 μg/mL. A significant increase to 48.83 μg/mL was effectively achieved in the first 15-min dissolution in the pH 6.8 stage. In contrast, the APX concentration was 46.63 μg/mL at 75 min for APX-SOL, compared with the theoretical value of 35.08 μg/mL after the change in dissolution volume. A larger amount of APX was released from APX-PVP system than APX-SOL upon the attenuation of non-sink level. In pH 6.8 stage, APX concentrations were comparable for two cases, which should be attributed to the supersaturation maintaining abilities of two polymers and low supersaturation degree achieved. Based on the comparison between APX-PVP and APX-SOL, the more favorable dissolution condition of pH 6.8 stage was suggested to be less effective in discriminating APX ASD formulations.

IDM-SA showed a gradual increase in IDM concentration in the pH 2.2 stage and provided an incomplete drug dissolution within 60 min, which was obviously different from its behavior in pure water. Considering the enhanced dissolution of IDM by SA upon increasing the pH of the solution, this effect could be weakened by the buffering capacity of dissolution medium. Therefore, the supersaturation ability of SA determined in pure water could not be maintained in acidic buffer. The further increasing IDM concentration at pH 5.0 stage was due to the continuous dissolution of SA and leveled IDM solubility. The achieved drug concentration could be effectively kept from recrystallization due to the constantly improved crystalline solubility of IDM. These phenomena further supported the pH-modifying mechanism for SA-induced supersaturation. The gradual dissolution of APX-SA in both phases was corresponding to its behavior in pure water, without showing any change related to pH conditions.

Both IDM-EC and APX-EC showed a slower dissolution rate than pure drug in both stages due to the high-degree of diffusion-controlled drug release pattern from insoluble carrier. Regardless

of pH, the drug-EC miscibility and poor wetting of EC carrier (i.e. floating issue after freeze drying process) delayed the release of IDM and APX payload. This was also indicated by the incomplete drug release after 24 h for both cases.

IDM-PL showed a drastic change in dissolution and supersaturation behaviors in the pH 2.2 stage compared with those in pure water. The slow drug release was due to the facilitated aggregation of PL with strong intermolecular interactions in a more acidic environment. When the pH is close to the first pK value of PL, intermolecular acid-anion complexation could occur through strong hydrogen bonding between the protonated phosphatidic acid (P-OH) and deprotonated phosphatidic acid ($P\text{-}O^-$) groups [135,230]. The two major components of PL, phosphatidylcholine and phosphatidylethanolamine, have pKa values of 1.7 and 1.1, respectively, which are close to the environment pH of 2.2. Therefore, the aggregation of PL induced by intermolecular complexation was more favoured in lower pH. The previously revealed behaviors of PL in water phase, including supersaturation buildup and recrystallization inhibition, were not maintained in acid stage due to this change. Again, this was an illustration that the in-solution properties of an ASD carrier were masked if it could not rapidly dissolve in water. Nevertheless, the dissolution rate of IDM-PL was still faster than that for pure IDM, attributed to the dissolution of certain amount of amorphous IDM. The aggregation issue was relieved when entering the following phase with a higher pH, which was responsible for the fast release for the first 15 min in the pH 5.0 stage. However, it was noted that the achieved supersaturation at pH 5.0 stage was not with a high degree that was prone to recrystallization, which was different from the observation in pure water. This could be explained by the assumption that facilitated de-aggregation of PL by leveled pH was a gradual process with a starting state of large agglomeration. The recovered drug release from this state was expected to be slower than the case of IDM-PL dissolution in pure water, whereby the starting state was lyophilized powder with small particle size that was more readily dispersible. As a result, the supersaturation induction rate was low. The improved dissolution rate and extent of IDM in pH 5.0 environment were seen an overall effect of recovered drug release from PL carrier, supersaturation maintenance effect of dispersed PL, and solubilization effect of PL. Compared with pH 2.2 stage, the kinetic profile of IDM-PL at pH 5.0 stage was in more agreement with the PL performance in pure water. These mechanisms also applied to APX-PL.

Driven by the fast erosion and dispersion of G48 in aqueous environment, IDM-G48 and APX-G48 saw the similarly instant drug release in the pH 2.2 stage. The drug release performance of

nonionized G48 was not influenced by pH condition. Considering that G48 had poor supersaturation maintaining ability for both drugs, the steadier concentration level at pH 5.0 stage for both cases suggested that drug concentration reached an equilibrium between drug dissolution and recrystallization.

IDM-ATO provided a more effective dissolution enhancement than IDM-PL in the acid stage, which was different from the comparison in pure water. As discussed, although PL showed an improvement in IDM dissolution in the acid stage, drug release was still delayed by PL complexation. In comparison, the amorphous drug adsorbed on the surface of ATO was expected to dissolve fast once contacting water. This being said, there was still a significant portion of amorphous IDM that were loaded in ATO matrix, and the release of this part of drug should still be slow, following the diffusion-controlled mechanism. As an overall result, the dissolution of IDM-ATO was only slightly faster than IDM-PL in acid stage. At pH 5.0 stage, IDM-ATO showed a gradual increase in IDM concentration with a profile similar to previous stage, restating that its drug release mechanism was not influenced by pH. This also indicated that drug release was not completed in previous section. The achieved supersaturation was attributed to the constant dissolution of amorphous IDM. As a comparison, APX-ATO gave essentially same dissolution profile as APX-PL in acid stage. Although PL remained aggregated in this case, the larger amount of drug dose would result in a release of more drug from a formulation with poor dispersibility. In this regard drug release from immiscible domains of APX-ATO was not faster than APX-PL. Through the comprehensive comparison it is again suggested that the absolute amount of excipient could behave differently for different drug formulations with a same SI index.

To summarize, some freeze-dried IDM ASDs and APX ASDs based on individual polymers and lipids showed different dissolution and supersaturation behaviors in two-stage dissolution condition than in water. The deviations were resulted from the altered dissolution properties of carrier materials under different pH conditions. A carrier could have different effects on both drugs just as their behaviors in pure water. This emphasized our previous conclusion that the expression of carriers' ability to stabilize LLPS and drug supersaturation relies on their fast and through dissolution. The dissolution of carrier is one factor altered by polymer-lipid combinations to adjust the supersaturation characteristics of IDM.

5.5.3.2 Effect of polymer-lipid combinations on the dissolution of freeze-dried IDM ASDs

All PVP-lipid combinations showed a synergistic effect on IDM dissolution with regard to IDM-PVP and IDM-lipids due to the facilitated dissolution of drug carrier. The mixing of PVP and PL could weaken both swelling of PVP and aggregation of PL. The decreased r^2 values fitted with both the first order model and the Higuchi model suggested a less hindered drug release from the carrier. The concentration decline observed after 45 min suggested that the supersaturation buildup rate was enhanced to an extent that could not be effectively maintained. The sudden increase in drug concentration after entering the pH 5.0 stage suggested that the dissolution/dispersion of PVP-PL matrix was significantly facilitated by the increased pH and larger volume of dissolution medium. In both pH conditions, the combination of PVP and PL effectively changed the IDM release mechanism from diffusion-controlled profile to dissolution-controlled profile. These mechanisms also applied to APX-PVP-PL.

In contrast, a severer decrease in supersaturation was observed for IDM-PVP-G48 in the acid stage due to the higher supersaturation degree achieved and reduced amount of PVP in formulation which could inhibit recrystallization. After entering the pH 5.0 stage, drug concentration saw another increase trend until 90 min, followed by drug recrystallization until reaching steady state, describing a similar drug release mechanism in both phases. The concentration level at pH 5.0 stage was not improved due to the reduced amount of G48 with solubilization effect and PVP with supersaturation maintaining effect. As a comparison for APX-PVP-G48, the synergistic effect on supersaturation buildup was less effective, associated with a mild desupersaturation.

PVP-ATO provided an effective synergistic effect on the supersaturation generation of both IDM and APX, with a same mechanism as discussed for the PVP-PL combination. It was noted that the supersaturation enhancement of IDM-PVP-ATO under the pH 2.2 dissolution condition was more effective than that in pure water. Considering that the dissolve state of PVP and ATO was not influenced by the lower pH, and the volume of dissolution medium was smaller than that for pure water experiment, the disintegration and dissolution of binary carrier should not be improved by this condition. Therefore, the apparently higher supersaturation ability achieved in pH 2.2 stage should be mainly a result of larger mathematical ratio between achieved supersaturation over the smaller IDM solubility in acid environment. No pH-induced enhancement in carrier dissolution was considered for

IDM-PVP-ATO. No pH-induced change was considered for APX-PVP-ATO either given the similar degree of enhancement in supersaturation level in both dissolution tests.

The significantly enhanced supersaturation performance of freeze-dried IDM-SOL-PL in the pH 2.2 stage was also due to the facilitated disintegration of the binary carrier. As discussed, drug release was delayed by SOL by a mechanism of surface gel formation regardless of pH condition. The insertion of SOL and PC with each other may improve the wetting and disintegration of drug carrier by weakening the molecular interaction between individual materials. This phenomenon was different from its behavior in pure water, where the SOL-PL combination provided an averaged effect on IDM dissolution, because in pure water the problems induced by PL protonation and aggregation were much weaker. The facilitated disintegration effect was less effective in pH 5.5 stage as the aggregation issue of PL was reduced, and therefore the supersaturation properties were more governed by dispersed PL. These mechanisms also applied to APX-SOL-PL to provide a similar supersaturation enhancing profile.

For IDM-SOL-G48, the averaged effect on supersaturation generation in the acid stage was due to the high drug release efficiency of G48 carrier. The combination could not provide a faster supersaturation buildup than the sample with pure G48 carrier due to the gelation of SOL. The further increasing drug concentration at the early stage of pH 5.0 suggested that drug release was not completed in pH 2.2 stage, which was in good agreement with the dissolution profile in the pH 2.2 stage without desupersaturation. The maintenance of high supersaturation degree was considered to benefit from the dissolved SOL in formulation, given that G48 had a poor supersaturation ability for APX. The mechanisms also applied to APX-SOL-G48, whereby the only difference was that APX-SOL-G48 showed a more completed drug release in pH 2.2 stage, as seen by the essentially unchanged drug concentration for pH 5.0 stage.

IDM-SOL-ATO also benefited from the facilitated wetting mechanism, In contrast, this did not apply to APX-SOL-ATO which showed an averaged dissolution profile. The positive effect of improved wetting should be overweighed by the compromised drug loading effect due to reduced amount SOL. SOL's ability to stabilize LLPS and APX recrystallization could be a contributor, but the maintaining of a supersaturated APX solution during the pH 6.8 stage should be mainly due to the low supersaturation degree as this supersaturation level could also be maintained by other carriers with poor stabilization effect.

The facilitated disintegration also benefited the dissolution of IDM-SA-PL and APX-SA-PL, whereby the self-association of PL was reduced by the added SA. IDM-SA-G48 provided a more stabilized supersaturation generation without drug recrystallization, while compromising the maximum achievable concentration due to the decreased amount of G48 content. The endpoint drug concentration level was also determined by the absolute amount of SA in formulation. As a comparison, the combination with SA did not bring much change to the dissolution behavior of APX-G48, due to the strong supersaturation generation ability of G48 material and the weak effect of SA on the dissolution of APX. The slight promoting effect of IDM-SA-ATO on the buildup of IDM supersaturation was governed by the behavior of IDM-ATO, which was different from the observation for pure water test. This was a result of less dominant pH modifying effect of SA in acid stage than in water due to the buffer capacity. As for ATO, its supersaturation ability was testified to maintain in different pH conditions due to its nonionized property and the dissolution of IDM adsorbed on the ATO surface, thereby governing the supersaturation behavior of IDM-SA-ATO. For APX, without being influenced by SA, the combination of SA with ATO provided an advantage of facilitated disintegration by ATO.

IDM-EC-PL presented a synergistic improvement in IDM supersaturation degree at pH 2.2 stage followed by an averaged effect at pH 5.0 stage. The improvement was due to the attenuated self-association of PL and the floating issue of freeze-dried EC, and the averaged effect in the pH 5.0 stage was due to the recovered PL dispersion, so that supersaturation extent was proportional to the PL amount. The previously revealed supersaturation behaviors of IDM-EC-PL in pure water agreed with the observations in the pH 5.0 stage, while not for the pH 2.2 stage, restating the importance of dissolution/dispersion state of a carrier when determining drug supersaturation. The dissolution behaviors of APX-EC-PL aligned with these mechanisms. The averaged profiles of IDM-EC-G48 and APX-EC-G48 were a result of same mechanisms. But in these cases the supersaturation generation rates could not surpass pure G48 based formulations given the instant dissolution of G48 carrier and fast drug release. The averaged dissolution profile for IDM-EC-ATO and APX-EC-ATO were considered to share the same mechanism without being influenced by pH change, corresponding to their behaviors in pure water. The combination with insoluble lipid weakened the diffusion-controlled matrix of insoluble polymer EC.

5.6 Conclusion

In this chapter, we investigated the correlation between dissolution parameters of an ASD, the effect of drug amorphization within an ASD carrier, the effect of the carrier on LLPS of the drug, and the effect of the carrier on the recrystallization of supersaturated drug solutions. These properties were found to be highly dependent on the type of ASD carrier used in the formulation. For soluble carriers, both IDM and APX benefited from the rapid release of amorphous drug from carrier leading to supersaturated concentrations, while the ability to maintain the supersaturated concentration was determined by the effect that each carrier had on the recrystallization of each dissolved drug. For the case of insoluble carriers, drug release was dependent on the dissolution of the amorphous drug adsorbed on the surface of the carrier particles and the constant release of drug from within the carrier matrix through a diffusion process. For insoluble carriers, the induction of a supersaturated solution was dependent upon the rate of diffusion of the drug from the carrier matrix and therefore is a slow process. In such a case there is only a weak recrystallization tendency thus stabilizing the supersaturated condition. While some polymer and lipid carriers are well known for their classification as soluble or amphiphilic materials, other solution processes such as gelation, intermolecular complexation, poor wettability (related to preparation method), and pH-induced property changes could modify the ability of the material in its ability to solubilize a particular drug molecule. The expression of in-solution properties of these carriers were delayed or masked to different degrees during dissolution, and supersaturation evolution of ASD formulations based on these materials varied between dissolution-controlled and diffusion-controlled mechanisms. The polymer-lipid combinations resulted in either a synergistic or averaged effect on the supersaturation of IDM and APX depending upon the specific combination and inherent properties of each carrier.

Chapter 6
Conclusions and future directions

6.1 Summary of results

In this study, several in-solution and solid-state properties of polymer and lipid ASD carriers were studied. The effect of ASD carriers on LLPS, recrystallization, drug amorphization and dissolution behaviors of IDM and APX were investigated. In chapter 2, the LLPS behaviors of IDM and APX in aqueous solution in the presence of ASD carriers were characterized using the double wavelength UV extinction method. The onset and duration of LLPS for IDM and APX were influenced by ASD carriers in different manners a result of in-solution hydrogen bonding, drug partitioning into carrier aggregates such as micelles/vesicles, drug aggregation induced by the hydrophobic effect, and pH induced solubility change(s). For IDM, the combination of PVP-PL gave rise to a synergistic stabilization of LLPS as a result of the enhanced ability to incorporate separated nanodroplets of IDM due to the reduced rigidity and increased size of PL vesicle during LLPS. All polymer-lipid combinations showed an averaged effect on the stabilization of LLPS for both IDM and APX.

In chapter 3, whether and how LLPS behaviors of IDM and APX in the presence of different ASD carriers could transfer to increased stability of drug supersaturation were tested using recrystallization tests under non-sink dissolution conditions. In general, the recrystallization behaviour of IDM and APX were different in the presence of different ASD carriers. The LLPS and recrystallization behaviors of a drug did not necessarily align with each other due to the fact that the LLPS mechanism mainly affects the early stage of drug recrystallization. The different experimental parameters for LLPS determination and for the recrystallization tests are also responsible for the deviation between these results. The LLPS and recrystallization results were used to analyze the behaviors of supersaturated drug solutions enabled by ASD dissolution.

In chapter 4, the feasibility of using fluorescence spectroscopy and fluorescence microscopy to evaluate the drug-carrier miscibility and drug amorphization were successfully investigated. Several fundamental aspects of fluorescence spectroscopy involved in the parameter optimization and analysis of the emission signal, including the effect of Raman signal, 2^{nd} emission peak and sample thickness, were clarified. The characterization results showed that these techniques could be used for

all drug-carrier systems to assess the physical state of IDM and APX using different indicators. IDM and APX showed different degrees of miscibility with different ASD carriers. Different systems could have different ways to express drug-carrier miscibility and drug amorphization. The single peak shape in a spectrum could be a false negative indicator leading to a decision to exclude drug-carrier immiscibility. Samples undergoing amorphous-amorphous phase separation and trace crystallization may still show a single emission peak without obvious peak-shift due to the dominant intensity induced by an amorphous drug. A reduced overall intensity for emission spectra was considered to result from drug aggregation. Fluorescence intensity distribution and the identification of birefringence properties for fluorescence microscopy were more effective and accurate in confirming phase separation of an ASD system. The assessment principles obtained from pilot studies were optimized. The drug-carrier miscibility information was used to facilitate the analysis of drug release from ASD carriers.

In chapter 5, dissolution and supersaturation behaviors of IDM and APX prepared with polymer, lipid and binary carriers with different preparation methods were tested under different dissolution conditions. The dissolution characteristics of an ASD formulation were seen as a comprehensive expression of supersaturation buildup, maintenance, and attenuation that are determined by drug amorphization degree, drug release profile, and effect of carrier on the LLPS and recrystallization of dissolved drug. Our results suggested that correlations between these factors could be established when the drug carrier showed a fast and completed dissolution, emphasizing the importance of dissolution state of drug carriers. Such correlations were disconnected when an ASD carrier could not dissolve or disperse instantly, so that the in-solution properties of the carrier could not present effectively. The combinations of polymer and lipid changed the dissolution and supersaturation profiles of IDM and APX by adjusting the dissolution or dispersion of carrier materials and the associated supersaturation maintaining ability depending on the dispersing state of carriers. Overall, the results of all chapters explored the in-solution and solid-state properties of polymer and lipid carriers, and analyzed their roles in determining the dissolution and supersaturation properties of ASD formulations for IDM and APX prepared by them. The corresponding characterization methods were optimized, and their effects on the expression of experimental results were analyzed.

6.2 Significance of the study

With the percentage of insoluble drug compounds in the development pipeline showing a continuous increase, formulation scientists are tasked with designing formulation approaches to effectively deliver these compounds through oral administration which requires some level of solubility for a drug. Most ways in which solubility of a drug can be improved are established on the theoretical basis of the Whitney-Noyes equation through a reduction in drug particle size or by increasing the aqueous solubility of the drug using cosolvents and/or surfactants. The formation of ASDs is another tool that can enhance solubility and dissolution of poorly water-soluble drugs, doing so by achieving a supersaturated drug concentration in the gut with improved thermodynamic activity and flux across gastrointestinal membranes. The development of ASD formulations relies on the fundamental investigations into the properties of supersaturated drug solution, carrier functions and drug-carrier interactions, as these factors play a critical role in achieving and maintaining drug supersaturation. This study investigated the solid-state and in-solution properties of several polymer and lipid materials, as well as their combinations, and tested their behaviors as ASD carriers for model drug IDM and APX. For several materials, the properties mentioned above were firstly revealed in this study. The supersaturated properties of APX were also firstly reported in this study.

For chapter 2, LLPS is a relatively new mechanism to describe the metastable transient state of a drug before recrystallization, facilitating the analysis of drug recrystallization behavior during ASD dissolution. It is of great interest to characterize this behavior for a drug in the presence of different carrier materials, as such information could serve as fundamentals to direct the design of ASD formulations. For this study, the fact that LLPS of both IDM and APX were influenced by polymer and lipid carriers in different manners was within expectation. And the phenomena that a carrier could place different effects when used for different drugs suggested the necessity of evaluating LLPS for a specific drug-carrier pair for the development of ASD. Besides, the combinations of polymer and lipid could provide both synergistic and averaged effect on the stabilization of LLPS, suggesting that the suitability of an excipient for the use as LLPS stabilizer will depend on the specific drug-excipient interactions which are not universal. By conducting this series of experiment using a well-known drug model IDM, the obtained results could be used to correlate with the results of previous studies using IDM as model drug, benefiting the understanding of a carrier's properties. For example, that PVP not stabilizing the LLPS of IDM indicated that the moderate stabilizing effect of PVP on IDM supersaturation was a result of slowed crystal growth. The

strong stabilizing effect of SOL suggested that delayed nucleation was a significant contributor for SOL's ability to maintain IDM supersaturation. The investigation of novel carriers with few supersaturation studies, including SA, EC, PL, G48, and ATO, will enable comparisons between these carriers with well-known ones. For the second model drug APX, which is without LLPS or supersaturation data, the LLPS behaviors of APX in the presence of different carriers provided pilot information for its development as ASD formulations.

For chapter 3, the recrystallization kinetics of IDM and APX under non-sink condition were measured, in order to see whether and how the changed LLPS behaviors correlate to supersaturation evolution of drugs. In general, these behaviors did not necessarily align with each other, for which the deviations were considered to result from different reasons. As mentioned above, the first reason was that LLPS mainly placed effect on the early stage of recrystallization. PVP and PL are two types of example to illustrate this mechanism: PVP did not stabilize the LLPS of IDM but stabilized the recrystallization of drug; PL stabilized the LLPS of IDM, but could not stabilize the recrystallization of IDM on a long timescale. These comparisons supported the established theory of LLPS mechanism. Secondly, the deviation between LLPS and recrystallization kinetics of a sample could result from the different experimental parameters of our studies, which is considered to be a limitation of the study. This can be explained by the working principles of experimental approaches. LLPS is detected based on the formation of a new phase that can cause light scattering, which means that no substance should be removed from the liquid system before characterization. In contrast, the common techniques (UV and HPLC) to determine the concentration of a liquid sample require that the system is in a fully dissolved state, which can only be realized by filtration or ultracentrifugation. This will result in a loss of both drug-rich nanodroplets and carrier micelle/vesicle with a size larger than pore diameter due to retention. The ability of a carrier (PL and PVP-PL) to incorporate and stabilize drug-rich droplets can be masked in recrystallization test accordingly. This deviation is unlikely to be solved by adjusting experimental conditions as the working mechanism for each experiment cannot be changed. More types of experiment design would be needed to address this challenge. This study suggested that special considerations should be given to solutions containing micelle/vesicle structures larger than 200 nm when analyzing the LLPS and recrystallization results of supersaturated drug solutions. Overall, chapter 2 and 3 provided detailed views of LLPS and recrystallization behaviors of IDM and APX in the presence of different ASD carriers. The supersaturation properties for carriers including SA, PL, G48 and ATO, were revealed to fill the blank areas of these materials.

For chapter 4, the design of fluorescence spectroscopy and fluorescence microscopy was inspired by several pilot studies using these techniques to assess the physical state and drug-carrier miscibility with commonly used polymers. When using these methods to assess more types of drug-carrier systems, it was found that the interpretations of fluorescence spectroscopy signals should be different in order for spectroscopy and microscopy results to align. In this context, fluorescence imaging results were considered to be more effective and accurate in terms of confirming phase separation. Based on the results obtained in this chapter, assessment disciplines obtained from previous studies were supplemented with better accuracy. The methodology was validated to be able to assess drug-excipient miscibility for more types of ASD carriers, and the results can be used to facilitate the analysis of drug release behaviors of ASD formulations.

For chapter 5, it was found that the expression of both solid-state and in-solution properties of carriers during ASD dissolution was highly dependent on the dissolution of carrier materials. Without a fast and complete dissolution of carrier materials, the correlations between the above properties could not be established. On that note, “medium soluble” and “medium insoluble” were considered to be effective terms to describe the disintegration and dissolution characteristics of ASD carriers, as the direction of simplified categorization of carriers could be insufficient when they are used in different media. Materials that are well categorized as “hydrophilic” or “amphiphilic” could show poor dispersibility and dissolution in specific dissolution media. For example, while being commonly used as dissolution enhancing carrier, SOL showed a slow dissolution and poor drug release of IDM in pure water at 37 °C due to gelation. Although PL could load amorphous IDM and APX effectively and provided solubilization effect by its amphiphilicity, the buildup of drug supersaturation of PL-based ASD could be slow since a long time was required for PL to finely disperse in water due to intermolecular complexation. By analyzing the correlations between LLPS, recrystallization, drug amorphization and dissolution behaviors of different ASD formulations, this study stated the critical role of carrier dissolution, as it was seen as the prerequisite for the expression of solid-state and in-solution properties of carrier materials. As a limitation, the investigations into drug-carrier ratio, SI index, and supersaturation induction rate were not included in this study. These parameters could act as variables to influence the kinetic solubility profiles of ASD formulations and examine the discussed mechanisms in a more comprehensive way.

Overall, this study provided detailed characterizations of solid-state and in-solution properties for several polymer and lipid ASD carriers. For several carriers and APX, the LLPS, recrystallization,

and non-sink dissolution behaviors were revealed for the first time. The obtained results and implications could serve as fundamental information to benefit the development of ASD formulations. The employed characterization methods and assessment disciplines were optimized and expected to serve the investigation of more types of drugs and ASD carriers.

6.3 Future directions

Based on the fact that an ASD carrier could have different effects on the LLPS of different drugs, it is suggested that the methodology is used for more types of carrier materials and drugs to validate the proposed mechanisms underlying the non-universal effects. For the proposed mechanism of the synergistic effect of PVP-PL (i.e. the ability of PL to incorporate nanodroplets is enhanced by PVP), different PVP-PL ratios could be used to test the correlation between LLPS and recrystallization results. Temperature could also be an interesting factor to investigate, as SOL and PL exhibit different micelle/vesicle size with varying temperatures. The effect of micelle size on the stabilization of drug-rich nanodroplets could be better characterized with more experiments. As discussed, filtration of aliquot dissolution samples was another factor responsible for the deviation between LLPS and recrystallization results. To validate this speculation, a series of experiments could be designed using different grades of PL and membrane filters with different pore sizes (i.e. 0.22 μm, 0.45 μm and 0.80 μm) for the processing of dissolution samples. There are reasons to expect different concentrations of a same sample set determined by different filters if incorporated nanodroplets can pass through to different degrees. These efforts could benefit the development of ASD products using amphiphilic materials as carriers.

The effect of drug-carrier ratio and dose on the dissolution and supersaturation properties of IDM and APX could be of interest since these factors have been suggested to influence drug supersaturation. As implied by this study, the change in absolute amount of ASD carrier, which is associated with the change in drug-carrier ratio and dose, should be a consideration when analyzing the dissolution behaviors of ASDs. The rate and extent of dissolution of carrier material could be a significant determinant for the ASD dissolution. Especially for APX, the detailed investigations into these factors will greatly benefit the formulation process.

Fluorescence techniques are expected to serve the miscibility assessment for more drugs and carriers given the provided parameter optimization method and assessment disciplines. The identified amorphous-amorphous phase separation could facilitate the analysis of DSC and PXRD results and

used to explain the drug release behaviors of ASDs. The comprehensive research methodology of this study is expected to be used for the investigation of properties of more types of drug-carrier system and benefit the development of ASD formulations.

References

1. Sastry, S.V.; Nyshadham, J.R.; Fix, J.A. Recent Technological Advances in Oral Drug Delivery – a Review. *Pharmaceutical Science & Technology Today* **2000**, *3*, 138–145, doi:10.1016/S1461-5347(00)00247-9.
2. Homayun, B.; Lin, X.; Choi, H.-J. Challenges and Recent Progress in Oral Drug Delivery Systems for Biopharmaceuticals. *Pharmaceutics* **2019**, *11*, 129, doi:10.3390/pharmaceutics11030129.
3. Takano, R.; Sugano, K.; Higashida, A.; Hayashi, Y.; Machida, M.; Aso, Y.; Yamashita, S. Oral Absorption of Poorly Water-Soluble Drugs: Computer Simulation of Fraction Absorbed in Humans from a Miniscale Dissolution Test. *Pharm Res* **2006**, *23*, 1144–1156, doi:10.1007/s11095-006-0162-4.
4. Newby, D.; Freitas, A.A.; Ghafourian, T. Decision Trees to Characterise the Roles of Permeability and Solubility on the Prediction of Oral Absorption. *European Journal of Medicinal Chemistry* **2015**, *90*, 751–765, doi:10.1016/j.ejmech.2014.12.006.
5. Augustijns, P.; Wuyts, B.; Hens, B.; Annaert, P.; Butler, J.; Brouwers, J. A Review of Drug Solubility in Human Intestinal Fluids: Implications for the Prediction of Oral Absorption. *European Journal of Pharmaceutical Sciences* **2014**, *57*, 322–332, doi:10.1016/j.ejps.2013.08.027.
6. Balimane, P.V.; Chong, S.; Morrison, R.A. Current Methodologies Used for Evaluation of Intestinal Permeability and Absorption. *Journal of Pharmacological and Toxicological Methods* **2000**, *44*, 301–312, doi:10.1016/S1056-8719(00)00113-1.
7. Lennernäs, H. Intestinal Permeability and Its Relevance for Absorption and Elimination. *Xenobiotica* **2007**, *37*, 1015–1051, doi:10.1080/00498250701704819.
8. Dahan, A.; Miller, J.M.; Amidon, G.L. Prediction of Solubility and Permeability Class Membership: Provisional BCS Classification of the World's Top Oral Drugs. *AAPS J* **2009**, *11*, 740–746, doi:10.1208/s12248-009-9144-x.
9. Dokoumetzidis, A.; Macheras, P. A Century of Dissolution Research: From Noyes and Whitney to the Biopharmaceutics Classification System. *International Journal of Pharmaceutics* **2006**, *321*, 1–11, doi:10.1016/j.ijpharm.2006.07.011.
10. Stegemann, S.; Leveiller, F.; Franchi, D.; de Jong, H.; Lindén, H. When Poor Solubility Becomes an Issue: From Early Stage to Proof of Concept. *European Journal of Pharmaceutical Sciences* **2007**, *31*, 249–261, doi:10.1016/j.ejps.2007.05.110.
11. Lipinski, C.A.; Lombardo, F.; Dominy, B.W.; Feeney, P.J. Experimental and Computational Approaches to Estimate Solubility and Permeability in Drug Discovery and Development Settings1PII of Original Article: S0169-409X(96)00423-1. The Article Was Originally Published in Advanced Drug Delivery Reviews 23 (1997) 3–25.1. *Advanced Drug Delivery Reviews* **2001**, *46*, 3–26, doi:10.1016/S0169-409X(00)00129-0.
12. Lipinski, C.A. Drug-like Properties and the Causes of Poor Solubility and Poor Permeability. *Journal of Pharmacological and Toxicological Methods* **2000**, *44*, 235–249, doi:10.1016/S1056-8719(00)00107-6.
13. Loftsson, T.; Brewster, M.E. Pharmaceutical Applications of Cyclodextrins: Basic Science and Product Development. *Journal of Pharmacy and Pharmacology* **2010**, *62*, 1607–1621, doi:10.1111/j.2042-7158.2010.01030.x.

14. Paus, R.; Ji, Y.; Vahle, L.; Sadowski, G. Predicting the Solubility Advantage of Amorphous Pharmaceuticals: A Novel Thermodynamic Approach. *Mol. Pharmaceutics* **2015**, *12*, 2823–2833, doi:10.1021/mp500824d.
15. Taylor, L.S.; Zhang, G.G.Z. Physical Chemistry of Supersaturated Solutions and Implications for Oral Absorption. *Advanced Drug Delivery Reviews* **2016**, *101*, 122–142, doi:10.1016/j.addr.2016.03.006.
16. Sandler, S.I. *Chemical, Biochemical, and Engineering Thermodynamics*; John Wiley & Sons, 2017; ISBN 978-0-470-50479-6.
17. Jermain, S.V.; Brough, C.; Williams, R.O. Amorphous Solid Dispersions and Nanocrystal Technologies for Poorly Water-Soluble Drug Delivery – An Update. *International Journal of Pharmaceutics* **2018**, *535*, 379–392, doi:10.1016/j.ijpharm.2017.10.051.
18. Noyes, A.A.; Whitney, W.R. THE RATE OF SOLUTION OF SOLID SUBSTANCES IN THEIR OWN SOLUTIONS. *J. Am. Chem. Soc.* **1897**, *19*, 930–934, doi:10.1021/ja02086a003.
19. Kobayashi, M.; Sada, N.; Sugawara, M.; Iseki, K.; Miyazaki, K. Development of a New System for Prediction of Drug Absorption That Takes into Account Drug Dissolution and PH Change in the Gastro-Intestinal Tract. *International Journal of Pharmaceutics* **2001**, *221*, 87–94, doi:10.1016/S0378-5173(01)00663-9.
20. Jornada, D.H.; Dos Santos Fernandes, G.F.; Chiba, D.E.; De Melo, T.R.F.; Dos Santos, J.L.; Chung, M.C. The Prodrug Approach: A Successful Tool for Improving Drug Solubility. *Molecules* **2016**, *21*, 42, doi:10.3390/molecules21010042.
21. Callender, S.P.; Mathews, J.A.; Kobernyk, K.; Wettig, S.D. Microemulsion Utility in Pharmaceuticals: Implications for Multi-Drug Delivery. *Int J Pharm* **2017**, *526*, 425–442, doi:10.1016/j.ijpharm.2017.05.005.
22. Good, D.J.; Rodríguez-Hornedo, N. Solubility Advantage of Pharmaceutical Cocrystals. *Crystal Growth & Design* **2009**, *9*, 2252–2264, doi:10.1021/cg801039j.
23. Torchilin, V.P. Structure and Design of Polymeric Surfactant-Based Drug Delivery Systems. *Journal of Controlled Release* **2001**, *73*, 137–172, doi:10.1016/S0168-3659(01)00299-1.
24. Davis, M.E.; Brewster, M.E. Cyclodextrin-Based Pharmaceutics: Past, Present and Future. *Nat Rev Drug Discov* **2004**, *3*, 1023–1035, doi:10.1038/nrd1576.
25. Zhang, Y.; Zhi, Z.; Jiang, T.; Zhang, J.; Wang, Z.; Wang, S. Spherical Mesoporous Silica Nanoparticles for Loading and Release of the Poorly Water-Soluble Drug Telmisartan. *Journal of Controlled Release* **2010**, *145*, 257–263, doi:10.1016/j.jconrel.2010.04.029.
26. Loh, Z.H.; Samanta, A.K.; Sia Heng, P.W. Overview of Milling Techniques for Improving the Solubility of Poorly Water-Soluble Drugs. *Asian Journal of Pharmaceutical Sciences* **2015**, *10*, 255–274, doi:10.1016/j.ajps.2014.12.006.
27. Crowley, K.J.; Zografi, G. Cryogenic Grinding of Indomethacin Polymorphs and Solvates: Assessment of Amorphous Phase Formation and Amorphous Phase Physical Stability. *Journal of Pharmaceutical Sciences* **2002**, *91*, 492–507, doi:10.1002/jps.10028.
28. Tagami, T.; Imao, Y.; Ito, S.; Nakada, A.; Ozeki, T. Simple and Effective Preparation of Nano-Pulverized Curcumin by Femtosecond Laser Ablation and the Cytotoxic Effect on C6 Rat Glioma Cells in Vitro. *International Journal of Pharmaceutics* **2014**, *468*, 91–96, doi:10.1016/j.ijpharm.2014.04.013.
29. Chan, H.-K.; Kwok, P.C.L. Production Methods for Nanodrug Particles Using the Bottom-up Approach. *Advanced Drug Delivery Reviews* **2011**, *63*, 406–416, doi:10.1016/j.addr.2011.03.011.

30. de Waard, H.; Hinrichs, W.L.J.; Frijlink, H.W. A Novel Bottom–up Process to Produce Drug Nanocrystals: Controlled Crystallization during Freeze-Drying. *Journal of Controlled Release* **2008**, *128*, 179–183, doi:10.1016/j.jconrel.2008.03.002.
31. Vasconcelos, T.; Marques, S.; das Neves, J.; Sarmento, B. Amorphous Solid Dispersions: Rational Selection of a Manufacturing Process. *Advanced Drug Delivery Reviews* **2016**, *100*, 85–101, doi:10.1016/j.addr.2016.01.012.
32. Huang, S.; Mao, C.; Williams, R.O.; Yang, C.-Y. Solubility Advantage (and Disadvantage) of Pharmaceutical Amorphous Solid Dispersions. *Journal of Pharmaceutical Sciences* **2016**, *105*, 3549–3561, doi:10.1016/j.xphs.2016.08.017.
33. Kulikovsky, V.; Vorlíček, V.; Boháč, P.; Stranyánek, M.; Čtvrtlík, R.; Kurdyumov, A.; Jastrabik, L. Hardness and Elastic Modulus of Amorphous and Nanocrystalline SiC and Si Films. *Surface and Coatings Technology* **2008**, *202*, 1738–1745, doi:10.1016/j.surfcoat.2007.07.029.
34. Zhou, W.-X.; Cheng, Y.; Chen, K.-Q.; Xie, G.; Wang, T.; Zhang, G. Thermal Conductivity of Amorphous Materials. *Advanced Functional Materials* **2020**, *30*, 1903829, doi:10.1002/adfm.201903829.
35. Privitera, S.; Rimini, E.; Zonca, R. Amorphous-to-Crystal Transition of Nitrogen- and Oxygen-Doped Ge2Sb2Te5 Films Studied by in Situ Resistance Measurements. *Appl. Phys. Lett.* **2004**, *85*, 3044–3046, doi:10.1063/1.1805200.
36. Parks, G.S.; Thomas, S.B.; Light, D.W. Studies on Glass XII. Some New Heat Capacity Data for Organic Glasses. The Entropy and Free Energy of Dl-Lactic Acid. *J. Chem. Phys.* **1936**, *4*, 64–69, doi:10.1063/1.1749749.
37. Brick, M.C.; Palmer, H.J.; Whitesides, T.H. Formation of Colloidal Dispersions of Organic Materials in Aqueous Media by Solvent Shifting. *Langmuir* **2003**, *19*, 6367–6380, doi:10.1021/la034173o.
38. Murdande, S.B.; Pikal, M.J.; Shanker, R.M.; Bogner, R.H. Solubility Advantage of Amorphous Pharmaceuticals: II. Application of Quantitative Thermodynamic Relationships for Prediction of Solubility Enhancement in Structurally Diverse Insoluble Pharmaceuticals. *Pharm Res* **2010**, *27*, 2704–2714, doi:10.1007/s11095-010-0269-5.
39. Hancock, B.C.; Parks, M. What Is the True Solubility Advantage for Amorphous Pharmaceuticals? *Pharm Res* **2000**, *17*, 397–404, doi:10.1023/A:1007516718048.
40. Murdande, S.B.; Pikal, M.J.; Shanker, R.M.; Bogner, R.H. Solubility Advantage of Amorphous Pharmaceuticals: I. A Thermodynamic Analysis. *J Pharm Sci* **2010**, *99*, 1254–1264, doi:10.1002/jps.21903.
41. Barry, B.W.; Harrison, S.M.; Dugard, P.H. Vapour and Liquid Diffusion of Model Penetrants through Human Skin; Correlation with Thermodynamic Activity. *Journal of Pharmacy and Pharmacology* **1985**, *37*, 226–236, doi:10.1111/j.2042-7158.1985.tb05050.x.
42. Indulkar, A.S.; Gao, Y.; Raina, S.A.; Zhang, G.G.Z.; Taylor, L.S. Exploiting the Phenomenon of Liquid–Liquid Phase Separation for Enhanced and Sustained Membrane Transport of a Poorly Water-Soluble Drug. *Mol. Pharmaceutics* **2016**, *13*, 2059–2069, doi:10.1021/acs.molpharmaceut.6b00202.
43. Sun, D.D.; Wen, H.; Taylor, L.S. Non-Sink Dissolution Conditions for Predicting Product Quality and In Vivo Performance of Supersaturating Drug Delivery Systems. *Journal of Pharmaceutical Sciences* **2016**, *105*, 2477–2488, doi:10.1016/j.xphs.2016.03.024.
44. Bevernage, J.; Brouwers, J.; Brewster, M.E.; Augustijns, P. Evaluation of Gastrointestinal Drug Supersaturation and Precipitation: Strategies and Issues. *International Journal of Pharmaceutics* **2013**, *453*, 25–35, doi:10.1016/j.ijpharm.2012.11.026.

45. Sun, D.D.; Lee, P.I. Evolution of Supersaturation of Amorphous Pharmaceuticals: The Effect of Rate of Supersaturation Generation. *Mol. Pharmaceutics* **2013**, *10*, 4330–4346, doi:10.1021/mp400439q.
46. De Yoreo, J.J.; Vekilov, P.G. Principles of Crystal Nucleation and Growth. *Reviews in Mineralogy and Geochemistry* **2003**, *54*, 57–93, doi:10.2113/0540057.
47. Ozaki, S.; Kushida, I.; Yamashita, T.; Hasebe, T.; Shirai, O.; Kano, K. Inhibition of Crystal Nucleation and Growth by Water-Soluble Polymers and Its Impact on the Supersaturation Profiles of Amorphous Drugs. *Journal of Pharmaceutical Sciences* **2013**, *102*, 2273–2281, doi:10.1002/jps.23588.
48. Erdemir, D.; Lee, A.Y.; Myerson, A.S. Nucleation of Crystals from Solution: Classical and Two-Step Models. *Acc. Chem. Res.* **2009**, *42*, 621–629, doi:10.1021/ar800217x.
49. Leubner, I.H. Particle Nucleation and Growth Models. *Current Opinion in Colloid & Interface Science* **2000**, *5*, 151–159, doi:10.1016/S1359-0294(00)00048-0.
50. Laidler, K.J. The Development of the Arrhenius Equation. *J. Chem. Educ.* **1984**, *61*, 494, doi:10.1021/ed061p494.
51. B. Chavan, R.; Thipparaboina, R.; Kumar, D.; R. Shastri, N. Evaluation of the Inhibitory Potential of HPMC, PVP and HPC Polymers on Nucleation and Crystal Growth. *RSC Advances* **2016**, *6*, 77569–77576, doi:10.1039/C6RA19746A.
52. Terebetski, J.L.; Michniak-Kohn, B. Combining Ibuprofen Sodium with Cellulosic Polymers: A Deep Dive into Mechanisms of Prolonged Supersaturation. *International Journal of Pharmaceutics* **2014**, *475*, 536–546, doi:10.1016/j.ijpharm.2014.09.015.
53. Christian, S.D.; Scamehorn, J.F. *Solubilization in Surfactant Aggregates*; CRC Press, 2020; ISBN 978-1-00-014823-7.
54. Lawrence, M.J. Surfactant Systems: Their Use in Drug Delivery. *Chem. Soc. Rev.* **1994**, *23*, 417, doi:10.1039/cs9942300417.
55. Chen, J.; Ormes, J.D.; Higgins, J.D.; Taylor, L.S. Impact of Surfactants on the Crystallization of Aqueous Suspensions of Celecoxib Amorphous Solid Dispersion Spray Dried Particles. *Mol. Pharmaceutics* **2015**, *12*, 533–541, doi:10.1021/mp5006245.
56. Rodríguez-Hornedo, N.; Murphy, D. Surfactant-facilitated Crystallization of Dihydrate Carbamazepine during Dissolution of Anhydrous Polymorph. *Journal of Pharmaceutical Sciences* **2004**, *93*, 449–460, doi:10.1002/jps.10496.
57. Bodnár, K.; Hudson, S.P.; Rasmuson, Å.C. Promotion of Mefenamic Acid Nucleation by a Surfactant Additive, Docusate Sodium. *Crystal Growth & Design* **2019**, *19*, 591–603, doi:10.1021/acs.cgd.8b00995.
58. Ilevbare, G.A.; Taylor, L.S. Liquid–Liquid Phase Separation in Highly Supersaturated Aqueous Solutions of Poorly Water-Soluble Drugs: Implications for Solubility Enhancing Formulations. *Crystal Growth & Design* **2013**, *13*, 1497–1509, doi:10.1021/cg301679h.
59. Deneau, E.; Steele, G. An In-Line Study of Oiling Out and Crystallization. *Org. Process Res. Dev.* **2005**, *9*, 943–950, doi:10.1021/op050107c.
60. Bisrat, M.; Nyström, C. Physicochemical Aspects of Drug Release. VIII. The Relation between Particle Size and Surface Specific Dissolution Rate in Agitated Suspensions. *International Journal of Pharmaceutics* **1988**, *47*, 223–231, doi:10.1016/0378-5173(88)90235-9.
61. Imaizumi, H.; Nambu, N.; Nagai, T. Stability and Several Physical Properties of Amorphous and Crystalline Form of Indomethacin. *Chem Pharm Bull (Tokyo)* **1980**, *28*, 2565–2569, doi:10.1248/cpb.28.2565.

62. Lindfors, L.; Forssén, S.; Skantze, P.; Skantze, U.; Zackrisson, A.; Olsson, U. Amorphous Drug Nanosuspensions. 2. Experimental Determination of Bulk Monomer Concentrations. *Langmuir* **2006**, *22*, 911–916, doi:10.1021/la052367t.
63. Xie, T.; Gao, W.; Taylor, L.S. Impact of Eudragit EPO and Hydroxypropyl Methylcellulose on Drug Release Rate, Supersaturation, Precipitation Outcome and Redissolution Rate of Indomethacin Amorphous Solid Dispersions. *International Journal of Pharmaceutics* **2017**, *531*, 313–323, doi:10.1016/j.ijpharm.2017.08.099.
64. Almeida e Sousa, L.; Reutzel-Edens, S.M.; Stephenson, G.A.; Taylor, L.S. Assessment of the Amorphous "Solubility" of a Group of Diverse Drugs Using New Experimental and Theoretical Approaches. *Mol. Pharmaceutics* **2015**, *12*, 484–495, doi:10.1021/mp500571m.
65. Mosquera-Giraldo, L.I.; Taylor, L.S. Glass–Liquid Phase Separation in Highly Supersaturated Aqueous Solutions of Telaprevir. *Mol. Pharmaceutics* **2015**, *12*, 496–503, doi:10.1021/mp500573z.
66. Buckley, S.T.; Frank, K.J.; Fricker, G.; Brandl, M. Biopharmaceutical Classification of Poorly Soluble Drugs with Respect to "Enabling Formulations." *European Journal of Pharmaceutical Sciences* **2013**, *50*, 8–16, doi:10.1016/j.ejps.2013.04.002.
67. Tho, I.; Liepold, B.; Rosenberg, J.; Maegerlein, M.; Brandl, M.; Fricker, G. Formation of Nano/Micro-Dispersions with Improved Dissolution Properties upon Dispersion of Ritonavir Melt Extrudate in Aqueous Media. *European Journal of Pharmaceutical Sciences* **2010**, *40*, 25–32, doi:10.1016/j.ejps.2010.02.003.
68. Kanzer, J.; Hupfeld, S.; Vasskog, T.; Tho, I.; Hölig, P.; Mägerlein, M.; Fricker, G.; Brandl, M. In Situ Formation of Nanoparticles upon Dispersion of Melt Extrudate Formulations in Aqueous Medium Assessed by Asymmetrical Flow Field-Flow Fractionation. *Journal of Pharmaceutical and Biomedical Analysis* **2010**, *53*, 359–365, doi:10.1016/j.jpba.2010.04.012.
69. Mellaerts, R.; Aerts, A.; Caremans, T.P.; Vermant, J.; Van den Mooter, G.; Martens, J.A.; Augustijns, P. Growth of Itraconazole Nanofibers in Supersaturated Simulated Intestinal Fluid. *Mol. Pharmaceutics* **2010**, *7*, 905–913, doi:10.1021/mp900300j.
70. LaPlante, S.R.; Aubry, N.; Bolger, G.; Bonneau, P.; Carson, R.; Coulombe, R.; Sturino, C.; Beaulieu, P.L. Monitoring Drug Self-Aggregation and Potential for Promiscuity in Off-Target In Vitro Pharmacology Screens by a Practical NMR Strategy. *J. Med. Chem.* **2013**, *56*, 7073–7083, doi:10.1021/jm4008714.
71. Raina, S.A.; Van Eerdenbrugh, B.; Alonzo, D.E.; Mo, H.; Zhang, G.G.Z.; Gao, Y.; Taylor, L.S. Trends in the Precipitation and Crystallization Behavior of Supersaturated Aqueous Solutions of Poorly Water-Soluble Drugs Assessed Using Synchrotron Radiation. *Journal of Pharmaceutical Sciences* **2015**, *104*, 1981–1992, doi:10.1002/jps.24423.
72. Aisha, A.F.A.; Ismail, Z.; Abu-Salah, K.M.; Majid, A.M.S.A. Solid Dispersions of α-Mangostin Improve Its Aqueous Solubility through Self-Assembly of Nanomicelles. *Journal of Pharmaceutical Sciences* **2012**, *101*, 815–825, doi:10.1002/jps.22806.
73. Ilevbare, G.A.; Liu, H.; Pereira, J.; Edgar, K.J.; Taylor, L.S. Influence of Additives on the Properties of Nanodroplets Formed in Highly Supersaturated Aqueous Solutions of Ritonavir. *Mol. Pharmaceutics* **2013**, *10*, 3392–3403, doi:10.1021/mp400228x.
74. Vo, C.L.-N.; Park, C.; Lee, B.-J. Current Trends and Future Perspectives of Solid Dispersions Containing Poorly Water-Soluble Drugs. *European Journal of Pharmaceutics and Biopharmaceutics* **2013**, *85*, 799–813, doi:10.1016/j.ejpb.2013.09.007.
75. Baghel, S.; Cathcart, H.; O'Reilly, N.J. Polymeric Amorphous Solid Dispersions: A Review of Amorphization, Crystallization, Stabilization, Solid-State Characterization, and Aqueous

Solubilization of Biopharmaceutical Classification System Class II Drugs. *Journal of Pharmaceutical Sciences* **2016**, *105*, 2527–2544, doi:10.1016/j.xphs.2015.10.008.
76. Schittny, A.; Huwyler, J.; Puchkov, M. Mechanisms of Increased Bioavailability through Amorphous Solid Dispersions: A Review. *Drug Delivery* **2020**, *27*, 110–127, doi:10.1080/10717544.2019.1704940.
77. Sekiguchi, K.; Obi, N. Studies on Absorption of Eutectic Mixture. I. A Comparison of the Behavior of Eutectic Mixture of Sulfathiazole and That of Ordinary Sulfathiazole in Man. *Chemical & Pharmaceutical Bulletin* **1961**, *9*, 866–872, doi:10.1248/cpb.9.866.
78. Jachowicz, R. Dissolution Rates of Partially Water-Soluble Drugs from Solid Dispersion Systems. I. Prednisolone. *International Journal of Pharmaceutics* **1987**, *35*, 1–5, doi:10.1016/0378-5173(87)90067-6.
79. Craig, D.Q.M. The Mechanisms of Drug Release from Solid Dispersions in Water-Soluble Polymers. *International Journal of Pharmaceutics* **2002**, *231*, 131–144, doi:10.1016/S0378-5173(01)00891-2.
80. van Drooge, D.J.; Hinrichs, W.L.J.; Visser, M.R.; Frijlink, H.W. Characterization of the Molecular Distribution of Drugs in Glassy Solid Dispersions at the Nano-Meter Scale, Using Differential Scanning Calorimetry and Gravimetric Water Vapour Sorption Techniques. *International Journal of Pharmaceutics* **2006**, *310*, 220–229, doi:10.1016/j.ijpharm.2005.12.007.
81. Desai, J.; Alexander, K.; Riga, A. Characterization of Polymeric Dispersions of Dimenhydrinate in Ethyl Cellulose for Controlled Release. *International Journal of Pharmaceutics* **2006**, *308*, 115–123, doi:10.1016/j.ijpharm.2005.10.034.
82. Design of Sustained-Release Nitrendipine Microspheres Having Solid Dispersion Structure by Quasi-Emulsion Solvent Diffusion Method. *Journal of Controlled Release* **2003**, *91*, 375–384, doi:10.1016/S0168-3659(03)00275-X.
83. Passerini, N.; Albertini, B.; González-Rodríguez, M.L.; Cavallari, C.; Rodriguez, L. Preparation and Characterisation of Ibuprofen–Poloxamer 188 Granules Obtained by Melt Granulation. *European Journal of Pharmaceutical Sciences* **2002**, *15*, 71–78, doi:10.1016/S0928-0987(01)00210-X.
84. Damian, F.; Blaton, N.; Naesens, L.; Balzarini, J.; Kinget, R.; Augustijns, P.; Van den Mooter, G. Physicochemical Characterization of Solid Dispersions of the Antiviral Agent UC-781 with Polyethylene Glycol 6000 and Gelucire 44/14. *European Journal of Pharmaceutical Sciences* **2000**, *10*, 311–322, doi:10.1016/S0928-0987(00)00084-1.
85. Kalivoda, A.; Fischbach, M.; Kleinebudde, P. Application of Mixtures of Polymeric Carriers for Dissolution Enhancement of Oxeglitazar Using Hot-Melt Extrusion. *International Journal of Pharmaceutics* **2012**, *439*, 145–156, doi:10.1016/j.ijpharm.2012.10.013.
86. Huang, Y.; Dai, W.-G. Fundamental Aspects of Solid Dispersion Technology for Poorly Soluble Drugs. *Acta Pharmaceutica Sinica B* **2014**, *4*, 18–25, doi:10.1016/j.apsb.2013.11.001.
87. Qian, F.; Huang, J.; Hussain, M.A. Drug–Polymer Solubility and Miscibility: Stability Consideration and Practical Challenges in Amorphous Solid Dispersion Development. *Journal of Pharmaceutical Sciences* **2010**, *99*, 2941–2947, doi:10.1002/jps.22074.
88. Tian, B.; Tang, X.; Taylor, L.S. Investigating the Correlation between Miscibility and Physical Stability of Amorphous Solid Dispersions Using Fluorescence-Based Techniques. *Mol. Pharmaceutics* **2016**, *13*, 3988–4000, doi:10.1021/acs.molpharmaceut.6b00803.
89. Doherty, C.; York, P. Evidence for Solid- and Liquid-State Interactions in a Furosemide-Polyvinylpyrrolidone Solid Dispersion. *Journal of Pharmaceutical Sciences* **1987**, *76*, 731–737, doi:10.1002/jps.2600760912.

90. Que, C.; Qi, Q.; Zemlyanov, D.Y.; Mo, H.; Deac, A.; Zeller, M.; Indulkar, A.S.; Gao, Y.; Zhang, G.G.Z.; Taylor, L.S. Evidence for Halogen Bonding in Amorphous Solid Dispersions. *Crystal Growth & Design* **2020**, *20*, 3224–3235, doi:10.1021/acs.cgd.0c00073.
91. Song, Y.; Yang, X.; Chen, X.; Nie, H.; Byrn, S.; Lubach, J.W. Investigation of Drug–Excipient Interactions in Lapatinib Amorphous Solid Dispersions Using Solid-State NMR Spectroscopy. *Mol. Pharmaceutics* **2015**, *12*, 857–866, doi:10.1021/mp500692a.
92. Nie, H.; Su, Y.; Zhang, M.; Song, Y.; Leone, A.; Taylor, L.S.; Marsac, P.J.; Li, T.; Byrn, S.R. Solid-State Spectroscopic Investigation of Molecular Interactions between Clofazimine and Hypromellose Phthalate in Amorphous Solid Dispersions. *Mol. Pharmaceutics* **2016**, *13*, 3964–3975, doi:10.1021/acs.molpharmaceut.6b00740.
93. Yoshihashi, Y.; Iijima, H.; Yonemochi, E.; Terada, K. Estimationof Physical Stability of Amorphous Solid Dispersion Using Differential Scanningcalorimetry. *J Therm Anal Calorim* **2006**, *85*, 689–692, doi:10.1007/s10973-006-7653-8.
94. Tian, Y.; Booth, J.; Meehan, E.; Jones, D.S.; Li, S.; Andrews, G.P. Construction of Drug–Polymer Thermodynamic Phase Diagrams Using Flory–Huggins Interaction Theory: Identifying the Relevance of Temperature and Drug Weight Fraction to Phase Separation within Solid Dispersions. *Mol. Pharmaceutics* **2013**, *10*, 236–248, doi:10.1021/mp300386v.
95. Sun, D.D.; Lee, P.I. Probing the Mechanisms of Drug Release from Amorphous Solid Dispersions in Medium-Soluble and Medium-Insoluble Carriers. *Journal of Controlled Release* **2015**, *211*, 85–93, doi:10.1016/j.jconrel.2015.06.004.
96. Knopp, M.M.; Olesen, N.E.; Holm, P.; Langguth, P.; Holm, R.; Rades, T. Influence of Polymer Molecular Weight on Drug–Polymer Solubility: A Comparison between Experimentally Determined Solubility in PVP and Prediction Derived from Solubility in Monomer. *Journal of Pharmaceutical Sciences* **2015**, *104*, 2905–2912, doi:10.1002/jps.24410.
97. Franco, P.; De Marco, I. The Use of Poly(N-Vinyl Pyrrolidone) in the Delivery of Drugs: A Review. *Polymers (Basel)* **2020**, *12*, 1114, doi:10.3390/polym12051114.
98. Tekade, A.R.; Yadav, J.N. A Review on Solid Dispersion and Carriers Used Therein for Solubility Enhancement of Poorly Water Soluble Drugs. *Adv Pharm Bull* **2020**, *10*, 359–369, doi:10.34172/apb.2020.044.
99. Bavishi, D.D.; Borkhataria, C.H. Spring and Parachute: How Cocrystals Enhance Solubility. *Progress in Crystal Growth and Characterization of Materials* **2016**, *62*, 1–8, doi:10.1016/j.pcrysgrow.2016.07.001.
100. Liu, C.; Chen, Z.; Chen, Y.; Lu, J.; Li, Y.; Wang, S.; Wu, G.; Qian, F. Improving Oral Bioavailability of Sorafenib by Optimizing the "Spring" and "Parachute" Based on Molecular Interaction Mechanisms. *Mol. Pharmaceutics* **2016**, *13*, 599–608, doi:10.1021/acs.molpharmaceut.5b00837.
101. Li, Y.-W.; Zhang, H.-M.; Cui, B.-J.; Hao, C.-Y.; Zhu, H.-Y.; Guan, J.; Wang, D.; Jin, Y.; Feng, B.; Cai, J.-H.; et al. "Felodipine-Indomethacin" Co-Amorphous Supersaturating Drug Delivery Systems: "Spring-Parachute" Process, Stability, in Vivo Bioavailability, and Underlying Molecular Mechanisms. *European Journal of Pharmaceutics and Biopharmaceutics* **2021**, *166*, 111–125, doi:10.1016/j.ejpb.2021.05.030.
102. Bevernage, J.; Forier, T.; Brouwers, J.; Tack, J.; Annaert, P.; Augustijns, P. Excipient-Mediated Supersaturation Stabilization in Human Intestinal Fluids. *Mol. Pharmaceutics* **2011**, *8*, 564–570, doi:10.1021/mp100377m.
103. Gao, P.; Akrami, A.; Alvarez, F.; Hu, J.; Li, L.; Ma, C.; Surapaneni, S. Characterization and Optimization of AMG 517 Supersaturatable Self-Emulsifying Drug Delivery System (S-

SEDDS) for Improved Oral Absorption. *Journal of Pharmaceutical Sciences* **2009**, *98*, 516–528, doi:10.1002/jps.21451.
104. Miller, D.A.; DiNunzio, J.C.; Yang, W.; McGinity, J.W.; Williams, R.O. Enhanced In Vivo Absorption of Itraconazole via Stabilization of Supersaturation Following Acidic-to-Neutral PH Transition. *Drug Development and Industrial Pharmacy* **2008**, *34*, 890–902, doi:10.1080/03639040801929273.
105. Balani, P.N.; Wong, S.Y.; Ng, W.K.; Widjaja, E.; Tan, R.B.H.; Chan, S.Y. Influence of Polymer Content on Stabilizing Milled Amorphous Salbutamol Sulphate. *International Journal of Pharmaceutics* **2010**, *391*, 125–136, doi:10.1016/j.ijpharm.2010.02.029.
106. Xie, S.; Poornachary, S.K.; Chow, P.S.; Tan, R.B.H. Direct Precipitation of Micron-Size Salbutamol Sulfate: New Insights into the Action of Surfactants and Polymeric Additives. *Crystal Growth & Design* **2010**, *10*, 3363–3371, doi:10.1021/cg901270x.
107. Yani, Y.; Chow, P.S.; Tan, R.B.H. Molecular Simulation Study of the Effect of Various Additives on Salbutamol Sulfate Crystal Habit. *Mol. Pharmaceutics* **2011**, *8*, 1910–1918, doi:10.1021/mp200277u.
108. Feng, D.; Peng, T.; Huang, Z.; Singh, V.; Shi, Y.; Wen, T.; Lu, M.; Quan, G.; Pan, X.; Wu, C. Polymer–Surfactant System Based Amorphous Solid Dispersion: Precipitation Inhibition and Bioavailability Enhancement of Itraconazole. *Pharmaceutics* **2018**, *10*, 53, doi:10.3390/pharmaceutics10020053.
109. Kramarenko, E.Yu.; Winkler, R.G.; Khalatur, P.G.; Khokhlov, A.R.; Reineker, P. Molecular Dynamics Simulation Study of Adsorption of Polymer Chains with Variable Degree of Rigidity. I. Static Properties. *J. Chem. Phys.* **1996**, *104*, 4806–4813, doi:10.1063/1.471175.
110. Hauss, D.J. Oral Lipid-Based Formulations. *Advanced Drug Delivery Reviews* **2007**, *59*, 667–676, doi:10.1016/j.addr.2007.05.006.
111. Rosiaux, Y.; Jannin, V.; Hughes, S.; Marchaud, D. Solid Lipid Excipients as Matrix Agents for Sustained Drug Delivery. In *Excipient Applications in Formulation Design and Drug Delivery*; Narang, A.S., Boddu, S.H.S., Eds.; Springer International Publishing: Cham, 2015; pp. 237–271 ISBN 978-3-319-20206-8.
112. Rydhag, L.; Wilton, I. The Function of Phospholipids of Soybean Lecithin in Emulsions. *J Am Oil Chem Soc* **1981**, *58*, 830–837, doi:10.1007/BF02665591.
113. Aburahma, M.H.; Badr-Eldin, S.M. Compritol 888 ATO: A Multifunctional Lipid Excipient in Drug Delivery Systems and Nanopharmaceuticals. *Expert Opinion on Drug Delivery* **2014**, *11*, 1865–1883, doi:10.1517/17425247.2014.935335.
114. Kumar, S.; Kaur Randhawa, J. Solid Lipid Nanoparticles of Stearic Acid for the Drug Delivery of Paliperidone. *RSC Advances* **2015**, *5*, 68743–68750, doi:10.1039/C5RA10642G.
115. Li, Y.; Wong, H.L.; Shuhendler, A.J.; Rauth, A.M.; Wu, X.Y. Molecular Interactions, Internal Structure and Drug Release Kinetics of Rationally Developed Polymer–Lipid Hybrid Nanoparticles. *Journal of Controlled Release* **2008**, *128*, 60–70, doi:10.1016/j.jconrel.2008.02.014.
116. Kuche, K.; Bhargavi, N.; Dora, C.P.; Jain, S. Drug-Phospholipid Complex—a Go Through Strategy for Enhanced Oral Bioavailability. *AAPS PharmSciTech* **2019**, *20*, 43, doi:10.1208/s12249-018-1252-4.
117. Peng, Q.; Gong, T.; Zuo, J.; Liu, J.; Zhao, D.; Zhang, Z. Enhanced the Oral Bioavailability of Salvianolic Acid B by Phospholipid Complex Loaded Nanoparticles. *Die Pharmazie - An International Journal of Pharmaceutical Sciences* **2008**, *63*, 661–666, doi:10.1691/ph.2008.8053.

118. Bombardelli, E.; Curri, S.; Loggia, R.D.; Negro, P.; Gariboldi, P.; Tubaro, A. Complexes between Phospholipids and Vegetal Derivates of Biological Interest. **1989**.
119. Zhang, S.; Niu, H.; Zhang, Y.; Liu, J.; Shi, Y.; Zhang, X.; Cai, Y. Biocompatible Phosphatidylcholine Bilayer Coated on Magnetic Nanoparticles and Their Application in the Extraction of Several Polycyclic Aromatic Hydrocarbons from Environmental Water and Milk Samples. *Journal of Chromatography A* **2012**, *1238*, 38–45, doi:10.1016/j.chroma.2012.03.056.
120. Hamai, C.; Yang, T.; Kataoka, S.; Cremer, P.S.; Musser, S.M. Effect of Average Phospholipid Curvature on Supported Bilayer Formation on Glass by Vesicle Fusion. *Biophysical Journal* **2006**, *90*, 1241–1248, doi:10.1529/biophysj.105.069435.
121. Kaffash, E.; Badiee, A.; Akhgari, A.; Akhavan Rezayat, N.; Abbaspour, M.; Saremnejad, F. Development and Characterization of a Multiparticulate Drug Delivery System Containing Indomethacin-Phospholipid Complex to Improve Dissolution Rate. *Journal of Drug Delivery Science and Technology* **2019**, *53*, 101177, doi:10.1016/j.jddst.2019.101177.
122. Amirinejad, M.; Davoodi, J.; Abbaspour, M.R.; Akhgari, A.; Hadizadeh, F.; Badiee, A. Preparation, Characterization and Improved Release Profile of Ibuprofen-Phospholipid Association. *Journal of Drug Delivery Science and Technology* **2020**, *60*, 101951, doi:10.1016/j.jddst.2020.101951.
123. Guo, B.; Liu, H.; Li, Y.; Zhao, J.; Yang, D.; Wang, X.; Zhang, T. Application of Phospholipid Complex Technique to Improve the Dissolution and Pharmacokinetic of Probucol by Solvent-Evaporation and Co-Grinding Methods. *International Journal of Pharmaceutics* **2014**, *474*, 50–56, doi:10.1016/j.ijpharm.2014.08.006.
124. Fong, S.Y.K.; Ibisogly, A.; Bauer-Brandl, A. Solubility Enhancement of BCS Class II Drug by Solid Phospholipid Dispersions: Spray Drying versus Freeze-Drying. *International Journal of Pharmaceutics* **2015**, *496*, 382–391, doi:10.1016/j.ijpharm.2015.10.029.
125. Engelhard, D.; Eldor, A.; Polacheck, I.; Hardan, I.; Ben-yehuda, D.; Amselem, S.; Salkin, I.F.; Lopez-berestein, G.; Sacks, T.; Rachmilewitz, E.A.; et al. Disseminated Visceral Fusariosis Treated with Amphotericin B-Phospholipid Complex. *Leukemia & Lymphoma* **1993**, *9*, 385–392, doi:10.3109/10428199309148539.
126. Maiti, K.; Mukherjee, K.; Gantait, A.; Saha, B.P.; Mukherjee, P.K. Curcumin–Phospholipid Complex: Preparation, Therapeutic Evaluation and Pharmacokinetic Study in Rats. *International Journal of Pharmaceutics* **2007**, *330*, 155–163, doi:10.1016/j.ijpharm.2006.09.025.
127. Song, Y.; Song, Y.; Zhuang, J.; Guo, J.; Xiao, Y.; Ping, Q. Preparation and Properties of a Silybin-Phospholipid Complex. *Die Pharmazie - An International Journal of Pharmaceutical Sciences* **2008**, *63*, 35–42, doi:10.1691/ph.2008.7132.
128. Singh, D.; S.M. Rawat, M.; Semalty, A.; Semalty, M. Rutin-Phospholipid Complex: An Innovative Technique in Novel Drug Delivery System- NDDS. *Current Drug Delivery* **2012**, *9*, 305–314, doi:10.2174/156720112800389070.
129. Zhou, Y.; Dong, W.; Ye, J.; Hao, H.; Zhou, J.; Wang, R.; Liu, Y. A Novel Matrix Dispersion Based on Phospholipid Complex for Improving Oral Bioavailability of Baicalein: Preparation, in Vitro and in Vivo Evaluations. *Drug Delivery* **2017**, *24*, 720–728, doi:10.1080/10717544.2017.1311968.
130. Pathan, R.A.; Bhandari, U. Preparation & Characterization of Embelin–Phospholipid Complex as Effective Drug Delivery Tool. *J Incl Phenom Macrocycl Chem* **2011**, *69*, 139–147, doi:10.1007/s10847-010-9824-2.

131. Huang, J.; Chen, P.X.; Wettig, S. Fluorescence-Based Techniques to Assess the Miscibility and Physical Stability of a Drug–Lipid Complex. *Can. J. Chem.* **2019**, *97*, 496–503, doi:10.1139/cjc-2018-0404.
132. Vora, A.K.; Londhe, V.Y.; Pandita, N.S. Preparation and Characterization of Standardized Pomegranate Extract-Phospholipid Complex as an Effective Drug Delivery Tool. *J Adv Pharm Technol Res* **2015**, *6*, 75–80, doi:10.4103/2231-4040.154542.
133. Hüsch, J.; Dutagaci, B.; Glaubitz, C.; Geppert, T.; Schneider, G.; Harms, M.; Müller-Goymann, C.C.; Fink, L.; Schmidt, M.U.; Setzer, C.; et al. Structural Properties of So-Called NSAID–Phospholipid-Complexes. *European Journal of Pharmaceutical Sciences* **2011**, *44*, 103–116, doi:10.1016/j.ejps.2011.06.010.
134. Sikarwar, M.S.; Sharma, S.; Jain, A.K.; Parial, S.D. Preparation, Characterization and Evaluation of Marsupsin–Phospholipid Complex. *AAPS PharmSciTech* **2008**, *9*, 129–137, doi:10.1208/s12249-007-9020-x.
135. Huang, J.; Chen, P.X.; Rogers, M.A.; Wettig, S.D. Investigating the Phospholipid Effect on the Bioaccessibility of Rosmarinic Acid-Phospholipid Complex through a Dynamic Gastrointestinal in Vitro Model. *Pharmaceutics* **2019**, *11*, 156, doi:10.3390/pharmaceutics11040156.
136. Gao, H.; Wei, Y.; Xi, L.; Sun, Y.; Zhang, T. Evaluation of Intestinal Absorption and Bioavailability of a Bergenin–Phospholipid Complex Solid Dispersion in Rats. *AAPS PharmSciTech* **2018**, *19*, 1720–1729, doi:10.1208/s12249-018-0984-5.
137. Zhang, Z.; Chen, Y.; Deng, J.; Jia, X.; Zhou, J.; Lv, H. Solid Dispersion of Berberine–Phospholipid Complex/TPGS 1000/SiO2: Preparation, Characterization and in Vivo Studies. *International Journal of Pharmaceutics* **2014**, *465*, 306–316, doi:10.1016/j.ijpharm.2014.01.023.
138. Wang, J.; Wang, L.; Zhang, L.; He, D.; Ju, J.; Li, W. Studies on the Curcumin Phospholipid Complex Solidified with Soluplus®. *Journal of Pharmacy and Pharmacology* **2018**, *70*, 242–249, doi:10.1111/jphp.12857.
139. Peng, R.; Huang, J.; He, L.; Zhao, L.; Wang, C.; Wei, W.; Xia, T.; Mao, Y.; Wen, Y.; Wang, L.; et al. Polymer/Lipid Interplay in Altering in Vitro Supersaturation and Plasma Concentration of a Model Poorly Soluble Drug. *European Journal of Pharmaceutical Sciences* **2020**, *146*, 105262, doi:10.1016/j.ejps.2020.105262.
140. Kaur, A.; Parmar, P.K.; Bansal, A.K. Evaluation of Different Techniques for Size Determination of Drug Nanocrystals: A Case Study of Celecoxib Nanocrystalline Solid Dispersion. *Pharmaceutics* **2019**, *11*, 516, doi:10.3390/pharmaceutics11100516.
141. Hassouna, F.; Abo El Dahab, M.; Fulem, M.; De Lima Haiek, A.; Laachachi, A.; Kopecký, D.; Šoóš, M. Multi-Scale Analysis of Amorphous Solid Dispersions Prepared by Freeze Drying of Ibuprofen Loaded Acrylic Polymer Nanoparticles. *Journal of Drug Delivery Science and Technology* **2019**, *53*, 101182, doi:10.1016/j.jddst.2019.101182.
142. Lee, S.; Nam, K.; Kim, M.S.; Jun, S.W.; Park, J.-S.; Woo, J.S.; Hwang, S.-J. Preparation and Characterization of Solid Dispersions of Itraconazole by Using Aerosol Solvent Extraction System for Improvement in Drug Solubility and Bioavailability. *Arch Pharm Res* **2005**, *28*, 866–874, doi:10.1007/BF02977355.
143. Zhang, X.; Sun, N.; Wu, B.; Lu, Y.; Guan, T.; Wu, W. Physical Characterization of Lansoprazole/PVP Solid Dispersion Prepared by Fluid-Bed Coating Technique. *Powder Technology* **2008**, *182*, 480–485, doi:10.1016/j.powtec.2007.07.011.

144. Lang, B.; McGinity, J.W.; Williams, R.O. Hot-Melt Extrusion – Basic Principles and Pharmaceutical Applications. *Drug Development and Industrial Pharmacy* **2014**, *40*, 1133–1155, doi:10.3109/03639045.2013.838577.
145. Nalamachu, S.; Wortmann, R. Role of Indomethacin in Acute Pain and Inflammation Management: A Review of the Literature. *Postgraduate Medicine* **2014**, *126*, 92–97, doi:10.3810/pgm.2014.07.2787.
146. Takeuchi, H.; Nagira, S.; Yamamoto, H.; Kawashima, Y. Solid Dispersion Particles of Amorphous Indomethacin with Fine Porous Silica Particles by Using Spray-Drying Method. *International Journal of Pharmaceutics* **2005**, *293*, 155–164, doi:10.1016/j.ijpharm.2004.12.019.
147. Fini, A.; Cavallari, C.; Ospitali, F. Raman and Thermal Analysis of Indomethacin/PVP Solid Dispersion Enteric Microparticles. *European Journal of Pharmaceutics and Biopharmaceutics* **2008**, *70*, 409–420, doi:10.1016/j.ejpb.2008.03.016.
148. Greco, K.; Bogner, R. Crystallization of Amorphous Indomethacin during Dissolution: Effect of Processing and Annealing. *Mol. Pharmaceutics* **2010**, *7*, 1406–1418, doi:10.1021/mp1000197.
149. Byon, W.; Garonzik, S.; Boyd, R.A.; Frost, C.E. Apixaban: A Clinical Pharmacokinetic and Pharmacodynamic Review. *Clin Pharmacokinet* **2019**, *58*, 1265–1279, doi:10.1007/s40262-019-00775-z.
150. ELIQUIS (Apixaban) Product Monograph, Https://Www.Pfizer.ca/Sites/Default/Files/201910/ELIQUIS_PM_229267_07Oct2019_Marketed_E.Pdf.
151. Patel, J.; Frost, C.; Jia, J.; Vemavarapu, C. Apixaban Formulations 2016.
152. Chen, Y.; Li, L.; Yao, J.; Ma, Y.-Y.; Chen, J.-M.; Lu, T.-B. Improving the Solubility and Bioavailability of Apixaban via Apixaban–Oxalic Acid Cocrystal. *Crystal Growth & Design* **2016**, *16*, 2923–2930, doi:10.1021/acs.cgd.6b00266.
153. Crystalline Form of Apixaban 2014.
154. Zhang, L.; Kong, D.; Wang, H.; Jiao, L.; Zhao, X.; Song, J.; Yang, D.; Yang, H.; Yang, S.; Du, G.; et al. Cocrystal of Apixaban–Quercetin: Improving Solubility and Bioavailability of Drug Combination of Two Poorly Soluble Drugs. *Molecules* **2021**, *26*, 2677, doi:10.3390/molecules26092677.
155. Malley, M.; Pommier, C. Crystalline Solvates of Apixaban 2007.
156. Badawy, S.I.F.; Lum, S. Apixaban Solution Formulations 2016.
157. Asati, A.V.; Salunkhe, K.S.; Chavan, M.J.; Chintamani, R.B.; Singh, R.P. Solubility Enhancement of BCS Classified II/IV Drug – Solid Dispersion of Apixaban by Solvent Evaporation. *International Journal of Pharmaceutical Investigation* **2020**, *10*, 430–436, doi:10.5530/ijpi.2020.4.76.
158. Nause, R.G. Dosage Forms of Apixaban 2019.
159. Yani, Y.; Kanaujia, P.; Chow, P.S.; Tan, R.B.H. Effect of API-Polymer Miscibility and Interaction on the Stabilization of Amorphous Solid Dispersion: A Molecular Simulation Study. *Ind. Eng. Chem. Res.* **2017**, *56*, 12698–12707, doi:10.1021/acs.iecr.7b03187.
160. Shamma, R.N.; Basha, M. Soluplus®: A Novel Polymeric Solubilizer for Optimization of Carvedilol Solid Dispersions: Formulation Design and Effect of Method of Preparation. *Powder Technology* **2013**, *237*, 406–414, doi:10.1016/j.powtec.2012.12.038.
161. Zhong, Y.; Jing, G.; Tian, B.; Huang, H.; Zhang, Y.; Gou, J.; Tang, X.; He, H.; Wang, Y. Supersaturation Induced by Itraconazole/Soluplus® Micelles Provided High GI Absorption in

Vivo. *Asian Journal of Pharmaceutical Sciences* **2016**, *11*, 255–264, doi:10.1016/j.ajps.2015.07.001.
162. Daâssi, D.; Rodríguez-Couto, S.; Nasri, M.; Mechichi, T. Biodegradation of Textile Dyes by Immobilized Laccase from Coriolopsis Gallica into Ca-Alginate Beads. *International Biodeterioration & Biodegradation* **2014**, *90*, 71–78, doi:10.1016/j.ibiod.2014.02.006.
163. Hashim, I.B.; Khalil, A.H.; Habib, H. Quality and Acceptability of a Set-Type Yogurt Made from Camel Milk. *Journal of Dairy Science* **2009**, *92*, 857–862, doi:10.3168/jds.2008-1408.
164. Sood, A.; Arora, V.; Shah, J.; Kotnala, R.K.; Jain, T.K. Multifunctional Gold Coated Iron Oxide Core-Shell Nanoparticles Stabilized Using Thiolated Sodium Alginate for Biomedical Applications. *Materials Science and Engineering: C* **2017**, *80*, 274–281, doi:10.1016/j.msec.2017.05.079.
165. Varaprasad, K.; Raghavendra, G.M.; Jayaramudu, T.; Seo, J. Nano Zinc Oxide–Sodium Alginate Antibacterial Cellulose Fibres. *Carbohydrate Polymers* **2016**, *135*, 349–355, doi:10.1016/j.carbpol.2015.08.078.
166. Sow, L.C.; Toh, N.Z.Y.; Wong, C.W.; Yang, H. Combination of Sodium Alginate with Tilapia Fish Gelatin for Improved Texture Properties and Nanostructure Modification. *Food Hydrocolloids* **2019**, *94*, 459–467, doi:10.1016/j.foodhyd.2019.03.041.
167. Desai, R.M.; Koshy, S.T.; Hilderbrand, S.A.; Mooney, D.J.; Joshi, N.S. Versatile Click Alginate Hydrogels Crosslinked via Tetrazine–Norbornene Chemistry. *Biomaterials* **2015**, *50*, 30–37, doi:10.1016/j.biomaterials.2015.01.048.
168. Quinlan, E.; López-Noriega, A.; Thompson, E.; Kelly, H.M.; Cryan, S.A.; O'Brien, F.J. Development of Collagen-Hydroxyapatite Scaffolds Incorporating PLGA and Alginate Microparticles for the Controlled Delivery of RhBMP-2 for Bone Tissue Engineering. *J Control Release* **2015**, *198*, 71–79, doi:10.1016/j.jconrel.2014.11.021.
169. Pradhan, R.; Tran, T.H.; Choi, J.Y.; Choi, I.S.; Choi, H.-G.; Yong, C.S.; Kim, J.O. Development of a Rebamipide Solid Dispersion System with Improved Dissolution and Oral Bioavailability. *Arch Pharm Res* **2015**, *38*, 522–533, doi:10.1007/s12272-014-0399-0.
170. Borba, P.A.A.; Pinotti, M.; de Campos, C.E.M.; Pezzini, B.R.; Stulzer, H.K. Sodium Alginate as a Potential Carrier in Solid Dispersion Formulations to Enhance Dissolution Rate and Apparent Water Solubility of BCS II Drugs. *Carbohydr Polym* **2016**, *137*, 350–359, doi:10.1016/j.carbpol.2015.10.070.
171. Guan, J.; Liu, Q.; Zhang, X.; Zhang, Y.; Chokshi, R.; Wu, H.; Mao, S. Alginate as a Potential Diphase Solid Dispersion Carrier with Enhanced Drug Dissolution and Improved Storage Stability. *Eur J Pharm Sci* **2018**, *114*, 346–355, doi:10.1016/j.ejps.2017.12.028.
172. França, M.T.; O'Reilly Beringhs, A.; Nicolay Pereira, R.; Martins Marcos, T.; Bazzo, G.C.; Stulzer, H.K. The Role of Sodium Alginate on the Supersaturation State of the Poorly Soluble Drug Chlorthalidone. *Carbohydrate Polymers* **2019**, *209*, 207–214, doi:10.1016/j.carbpol.2019.01.007.
173. Guan, J.; Liu, Q.; Liu, J.; Cui, Z.; Zhang, X.; Mao, S. Elucidation of Alginate-Drug Miscibility on Its Crystal Growth Inhibition Effect in Supersaturated Drug Delivery System. *Carbohydrate Polymers* **2020**, *230*, 115601, doi:10.1016/j.carbpol.2019.115601.
174. Wasilewska, K.; Winnicka, K. Ethylcellulose–A Pharmaceutical Excipient with Multidirectional Application in Drug Dosage Forms Development. *Materials* **2019**, *12*, 3386, doi:10.3390/ma12203386.
175. Small, D.M. Surface and Bulk Interactions of Lipids and Water with a Classification of Biologically Active Lipids Based on These Interactions. *Fed Proc* **1970**, *29*, 1320–1326.

176. Cerpnjak, K.; Zvonar, A.; Gašperlin, M.; Vrečer, F. Lipid-Based Systems as a Promising Approach for Enhancing the Bioavailability of Poorly Water-Soluble Drugs. *Acta Pharm* **2013**, *63*, 427–445, doi:10.2478/acph-2013-0040.
177. van Hoogevest, P.; Wendel, A. The Use of Natural and Synthetic Phospholipids as Pharmaceutical Excipients. *Eur J Lipid Sci Technol* **2014**, *116*, 1088–1107, doi:10.1002/ejlt.201400219.
178. Shinde, U.K.; Suryawanshi, D.G.; Amin, P.D. Development of Gelucire® 48/16 and TPGS Mixed Micelles and Its Pellet Formulation by Extrusion Spheronization Technique for Dissolution Rate Enhancement of Curcumin. *AAPS PharmSciTech* **2021**, *22*, 182, doi:10.1208/s12249-021-02032-8.
179. Jannin, V.; Chevrier, S.; Michenaud, M.; Dumont, C.; Belotti, S.; Chavant, Y.; Demarne, F. Development of Self Emulsifying Lipid Formulations of BCS Class II Drugs with Low to Medium Lipophilicity. *International Journal of Pharmaceutics* **2015**, *495*, 385–392, doi:10.1016/j.ijpharm.2015.09.009.
180. Aldosari, B.N.; Almurshedi, A.S.; Alfagih, I.M.; AlQuadeib, B.T.; Altamimi, M.A.; Imam, S.S.; Hussain, A.; Alqahtani, F.; Alzait, E.; Alshehri, S. Formulation of Gelucire®-Based Solid Dispersions of Atorvastatin Calcium: In Vitro Dissolution and In Vivo Bioavailability Study. *AAPS PharmSciTech* **2021**, *22*, 161, doi:10.1208/s12249-021-02019-5.
181. Sarabu, S.; Kallakunta, V.R.; Butreddy, A.; Janga, K.Y.; Ajjarapu, S.; Bandari, S.; Zhang, F.; Murthy, S.N.; Repka, M.A. A One-Step Twin-Screw Melt Granulation with Gelucire 48/16 and Surface Adsorbent to Improve the Solubility of Poorly Soluble Drugs: Effect of Formulation Variables on Dissolution and Stability. *AAPS PharmSciTech* **2021**, *22*, 79, doi:10.1208/s12249-021-01945-8.
182. Thomson, J.A.; Schurtenberger, P.; Thurston, G.M.; Benedek, G.B. Binary Liquid Phase Separation and Critical Phenomena in a Protein/Water Solution. *Proceedings of the National Academy of Sciences* **1987**, *84*, 7079–7083, doi:10.1073/pnas.84.20.7079.
183. Raina, S.A.; Alonzo, D.E.; Zhang, G.G.Z.; Gao, Y.; Taylor, L.S. Using Environment-Sensitive Fluorescent Probes to Characterize Liquid-Liquid Phase Separation in Supersaturated Solutions of Poorly Water Soluble Compounds. *Pharm Res* **2015**, *32*, 3660–3673, doi:10.1007/s11095-015-1725-z.
184. Akbar, J.; Tavakoli, N.; Gerrard Marangoni, D.; Wettig, S.D. Mixed Aggregate Formation in Gemini Surfactant/1,2-Dialkyl-Sn-Glycero-3-Phosphoethanolamine Systems. *Journal of Colloid and Interface Science* **2012**, *377*, 237–243, doi:10.1016/j.jcis.2012.03.048.
185. Kalyanasundaram, K.; Thomas, J.K. Environmental Effects on Vibronic Band Intensities in Pyrene Monomer Fluorescence and Their Application in Studies of Micellar Systems. *J. Am. Chem. Soc.* **1977**, *99*, 2039–2044, doi:10.1021/ja00449a004.
186. Aso, Y.; Yoshioka, S. Molecular Mobility of Nifedipine−PVP and Phenobarbital−PVP Solid Dispersions as Measured by 13C-NMR Spin-Lattice Relaxation Time. *Journal of Pharmaceutical Sciences* **2006**, *95*, 318–325, doi:10.1002/jps.20545.
187. Wang, B.; Wang, D.; Zhao, S.; Huang, X.; Zhang, J.; Lv, Y.; Liu, X.; Lv, G.; Ma, X. Evaluate the Ability of PVP to Inhibit Crystallization of Amorphous Solid Dispersions by Density Functional Theory and Experimental Verify. *European Journal of Pharmaceutical Sciences* **2017**, *96*, 45–52, doi:10.1016/j.ejps.2016.08.046.
188. Kothari, K.; Ragoonanan, V.; Suryanarayanan, R. The Role of Drug–Polymer Hydrogen Bonding Interactions on the Molecular Mobility and Physical Stability of Nifedipine Solid Dispersions. *Mol. Pharmaceutics* **2015**, *12*, 162–170, doi:10.1021/mp5005146.

189. Jin, J.; Ooi, C.H.; Dao, D.V.; Nguyen, N.-T. Coalescence Processes of Droplets and Liquid Marbles. *Micromachines (Basel)* **2017**, *8*, E336, doi:10.3390/mi8110336.
190. Bannow, J.; Yorulmaz, Y.; Löbmann, K.; Müllertz, A.; Rades, T. Improving the Drug Load and in Vitro Performance of Supersaturated Self-Nanoemulsifying Drug Delivery Systems (Super-SNEDDS) Using Polymeric Precipitation Inhibitors. *International Journal of Pharmaceutics* **2020**, *575*, 118960, doi:10.1016/j.ijpharm.2019.118960.
191. Usui, F.; Maeda, K.; Kusai, A.; Nishimura, K.; Keiji Yamamoto Inhibitory Effects of Water-Soluble Polymers on Precipitation of RS-8359. *International Journal of Pharmaceutics* **1997**, *154*, 59–66, doi:10.1016/S0378-5173(97)00129-4.
192. Rahimi, P.; Ward, C.A. Contact Angle Hysteresis on Smooth and Homogenous Surfaces in Gravitational Fields. *Microgravity sci. Technol.* **2005**, *16*, 231–235, doi:10.1007/BF02945982.
193. Xu, B.; Nguyen, N.-T.; Neng Wong, T. Droplet Coalescence in Microfluidic Systems. *Micro and Nanosystems* **2011**, *3*, 131–136.
194. Liu, P.; Zhou, J.; Chang, J.; Liu, X.; Xue, H.; Wang, R.; Li, Z.; Li, C.; Wang, J.; Liu, C. Soluplus-Mediated Diosgenin Amorphous Solid Dispersion with High Solubility and High Stability: Development, Characterization and Oral Bioavailability. *Drug Des Devel Ther* **2020**, *14*, 2959–2975, doi:10.2147/DDDT.S253405.
195. Zhang, K.; Yu, H.; Luo, Q.; Yang, S.; Lin, X.; Zhang, Y.; Tian, B.; Tang, X. Increased Dissolution and Oral Absorption of Itraconazole/Soluplus Extrudate Compared with Itraconazole Nanosuspension. *European Journal of Pharmaceutics and Biopharmaceutics* **2013**, *85*, 1285–1292, doi:10.1016/j.ejpb.2013.03.002.
196. Po, H.N.; Senozan, N.M. The Henderson-Hasselbalch Equation: Its History and Limitations. *J. Chem. Educ.* **2001**, *78*, 1499, doi:10.1021/ed078p1499.
197. Indulkar, A.S.; Box, K.J.; Taylor, R.; Ruiz, R.; Taylor, L.S. PH-Dependent Liquid–Liquid Phase Separation of Highly Supersaturated Solutions of Weakly Basic Drugs. *Mol. Pharmaceutics* **2015**, *12*, 2365–2377, doi:10.1021/acs.molpharmaceut.5b00056.
198. De Mel, J.U.; Gupta, S.; Willner, L.; Allgaier, J.; Stingaciu, L.R.; Bleuel, M.; Schneider, G.J. Manipulating Phospholipid Vesicles at the Nanoscale: A Transformation from Unilamellar to Multilamellar by an n-Alkyl-Poly(Ethylene Oxide). *Langmuir* **2021**, *37*, 2362–2375, doi:10.1021/acs.langmuir.0c03302.
199. Liu, J.; Nicholson, C.E.; Cooper, S.J. Direct Measurement of Critical Nucleus Size in Confined Volumes. *Langmuir* **2007**, *23*, 7286–7292, doi:10.1021/la063650a.
200. Vyazovkin, S.; Dranca, I. Physical Stability and Relaxation of Amorphous Indomethacin. *J. Phys. Chem. B* **2005**, *109*, 18637–18644, doi:10.1021/jp052985i.
201. Shi, Q.; Chen, H.; Wang, Y.; Wang, R.; Xu, J.; Zhang, C. Amorphous Solid Dispersions: Role of the Polymer and Its Importance in Physical Stability and In Vitro Performance. *Pharmaceutics* **2022**, *14*, 1747, doi:10.3390/pharmaceutics14081747.
202. Li, N.; Taylor, L.S. Tailoring Supersaturation from Amorphous Solid Dispersions. *Journal of Controlled Release* **2018**, *279*, 114–125, doi:10.1016/j.jconrel.2018.04.014.
203. Li, Y.; Qian, F.; Li, Z. Reduction of Second-Order Scattering Interference by Variable-Angle Synchronous Luminescence Spectroscopy. *Chem J Internet* **2000**, *2*, 30.
204. Belovolova, L.V.; Glushkov, M.V.; Vinogradov, E.A.; Babintsev, V.A.; Golovanov, V.I. Ultraviolet Fluorescence of Water and Highly Diluted Aqueous Media. *Phys. Wave Phen.* **2009**, *17*, 21–31, doi:10.3103/S1541308X0901004X.
205. Investigating the Correlation between Miscibility and Physical Stability of Amorphous Solid Dispersions Using Fluorescence-Based Techniques | Molecular Pharmaceutics Available online:

https://pubs.acs.org/doi/abs/10.1021/acs.molpharmaceut.6b00803?casa_token=_2yARziy2R4AAAAA:pAunJWuDO2epFNi7vKJQtfjFiAAdH6zbrIdW4IZHbVAm2tvcHAjgnPufqmt8rLB2lBbZsqDPB31F4z3V (accessed on 16 April 2022).
206. Deng, H.; Ray, P.C.; Ghann, W.E.; Uddin, J.; Samokhvalov, A.; Yu, H. Distance-Dependent Fluorescence Quenching on a Silver Nanoparticle Surface. *Chem. Lett.* **2019**, *48*, 1504–1506, doi:10.1246/cl.190684.
207. Lebold, T.P.; Yeow, E.K.L.; Steer, R.P. Fluorescence Quenching of the S1 and S2 States of Zinc Meso-Tetrakis(4-Sulfonatophenyl)Porphyrin by Halide Ions. *Photochem. Photobiol. Sci.* **2004**, *3*, 160–166, doi:10.1039/B310980A.
208. Qi, J.; Hu, X.; Dong, X.; Lu, Y.; Lu, H.; Zhao, W.; Wu, W. Towards More Accurate Bioimaging of Drug Nanocarriers: Turning Aggregation-Caused Quenching into a Useful Tool. *Advanced Drug Delivery Reviews* **2019**, *143*, 206–225, doi:10.1016/j.addr.2019.05.009.
209. Husain, M.A.; Ishqi, H.M.; Sarwar, T.; Rehman, S.U.; Tabish, M. Interaction of Indomethacin with Calf Thymus DNA: A Multi-Spectroscopic, Thermodynamic and Molecular Modelling Approach. *Med. Chem. Commun.* **2017**, *8*, 1283–1296, doi:10.1039/C7MD00094D.
210. Rumondor, A.C.F.; Ivanisevic, I.; Bates, S.; Alonzo, D.E.; Taylor, L.S. Evaluation of Drug-Polymer Miscibility in Amorphous Solid Dispersion Systems. *Pharm Res* **2009**, *26*, 2523–2534, doi:10.1007/s11095-009-9970-7.
211. Walden, D.M.; Bundey, Y.; Jagarapu, A.; Antontsev, V.; Chakravarty, K.; Varshney, J. Molecular Simulation and Statistical Learning Methods toward Predicting Drug–Polymer Amorphous Solid Dispersion Miscibility, Stability, and Formulation Design. *Molecules* **2021**, *26*, 182, doi:10.3390/molecules26010182.
212. Frenette, M.; Cosa, G.; Friščić, T. Characterisation of Organic Solid Forms and Real-Time in Situ Monitoring of Their Transformations Using Solid-State Fluorescence. *CrystEngComm* **2013**, *15*, 5100–5106, doi:10.1039/C3CE40604K.
213. Dash, S.; Murthy, P.N.; Nath, L.; Chowdhury, P. Kinetic Modeling on Drug Release from Controlled Drug Delivery Systems. *Acta Pol Pharm* **2010**, *67*, 217–223.
214. Higuchi, T. Mechanism of Sustained-Action Medication. Theoretical Analysis of Rate of Release of Solid Drugs Dispersed in Solid Matrices. *Journal of Pharmaceutical Sciences* **1963**, *52*, 1145–1149, doi:10.1002/jps.2600521210.
215. Hixson, A.W.; Crowell, J.H. Dependence of Reaction Velocity upon Surface and Agitation. *INDUSTRIAL AND ENGINEERING CHEMISTRY* **1931**, 9.
216. Korsmeyer, R.W.; Peppas, N.A. Solute and Penetrant Diffusion in Swellable Polymers. III. Drug Release from Glassy Poly(HEMA-Co-NVP) Copolymers. *Journal of Controlled Release* **1984**, *1*, 89–98, doi:10.1016/0168-3659(84)90001-4.
217. McIlvaine, T.C. A BUFFER SOLUTION FOR COLORIMETRIC COMPARISON. *Journal of Biological Chemistry* **1921**, *49*, 183–186, doi:10.1016/S0021-9258(18)86000-8.
218. Patel, J.; Frost, C.; Jia, J.; Vemavarapu, C. Apixaban Formulations 2017.
219. Bhattacharyya, S.; Ahammed, S.M.; Saha, B.P.; Mukherjee, P.K. The Gallic Acid–Phospholipid Complex Improved the Antioxidant Potential of Gallic Acid by Enhancing Its Bioavailability. *AAPS PharmSciTech* **2013**, *14*, 1025–1033, doi:10.1208/s12249-013-9991-8.
220. Alshahrani, S.M.; Lu, W.; Park, J.-B.; Morott, J.T.; Alsulays, B.B.; Majumdar, S.; Langley, N.; Kolter, K.; Gryczke, A.; Repka, M.A. Stability-Enhanced Hot-Melt Extruded Amorphous Solid Dispersions via Combinations of Soluplus® and HPMCAS-HF. *AAPS PharmSciTech* **2015**, *16*, 824–834, doi:10.1208/s12249-014-0269-6.

221. Browne, E.; Worku, Z.A.; Healy, A.M. Physicochemical Properties of Poly-Vinyl Polymers and Their Influence on Ketoprofen Amorphous Solid Dispersion Performance: A Polymer Selection Case Study. *Pharmaceutics* **2020**, *12*, 433, doi:10.3390/pharmaceutics12050433.
222. Soares, J.P.; Santos, J.E.; Chierice, G.O.; Cavalheiro, E.T.G. Thermal Behavior of Alginic Acid and Its Sodium Salt. *Eclet. Quím.* **2004**, *29*, 57–64, doi:10.1590/S0100-46702004000200009.
223. Xiong, M.; Tang, H.; Wang, Y.; Pan, M. Ethylcellulose-Coated Polyolefin Separators for Lithium-Ion Batteries with Improved Safety Performance. *Carbohydrate Polymers* **2014**, *101*, 1140–1146, doi:10.1016/j.carbpol.2013.10.073.
224. Hasankhan, S.; Tabibiazar, M.; Hosseini, S.M.; Ehsani, A.; Ghorbani, M. Fabrication of Curcumin-Zein-Ethyl Cellulose Composite Nanoparticles Using Antisolvent Co-Precipitation Method. *International Journal of Biological Macromolecules* **2020**, *163*, 1538–1545, doi:10.1016/j.ijbiomac.2020.08.045.
225. Haq, M.; Chun, B.-S. Characterization of Phospholipids Extracted from Atlantic Salmon By-Product Using Supercritical CO2 with Ethanol as Co-Solvent. *Journal of Cleaner Production* **2018**, *178*, 186–195, doi:10.1016/j.jclepro.2018.01.024.
226. Altamimi, M.A.; Neau, S.H. Investigation of the in Vitro Performance Difference of Drug-Soluplus® and Drug-PEG 6000 Dispersions When Prepared Using Spray Drying or Lyophilization. *Saudi Pharmaceutical Journal* **2017**, *25*, 419–439, doi:10.1016/j.jsps.2016.09.013.
227. Asare-Addo, K.; Alshafiee, M.; Walton, K.; Ward, A.; Totea, A.-M.; Taheri, S.; Mawla, N.; Adebisi, A.O.; Elawad, S.; Diza, C.; et al. Effect of Preparation Method on the Surface Properties and UV Imaging of Indomethacin Solid Dispersions. *Eur J Pharm Biopharm* **2019**, *137*, 148–163, doi:10.1016/j.ejpb.2019.03.002.
228. Salah, I.; Shamat, M.A.; Cook, M.T. Soluplus Solutions as Thermothickening Materials for Topical Drug Delivery. *Journal of Applied Polymer Science* **2019**, *136*, 46915, doi:10.1002/app.46915.
229. Chakravarti, R.K.; Kaur, S.; Samal, S.K.; Kashyap, M.C.; Sangamwar, A.T. Combination of Phospholipid Complex and Matrix Dispersion. *AAPS PharmSciTech* **2021**, *22*, 189, doi:10.1208/s12249-021-02067-x.
230. Boggs, J.M. Lipid Intermolecular Hydrogen Bonding: Influence on Structural Organization and Membrane Function. *Biochimica et Biophysica Acta (BBA) - Reviews on Biomembranes* **1987**, *906*, 353–404, doi:10.1016/0304-4157(87)90017-7.

Appendix

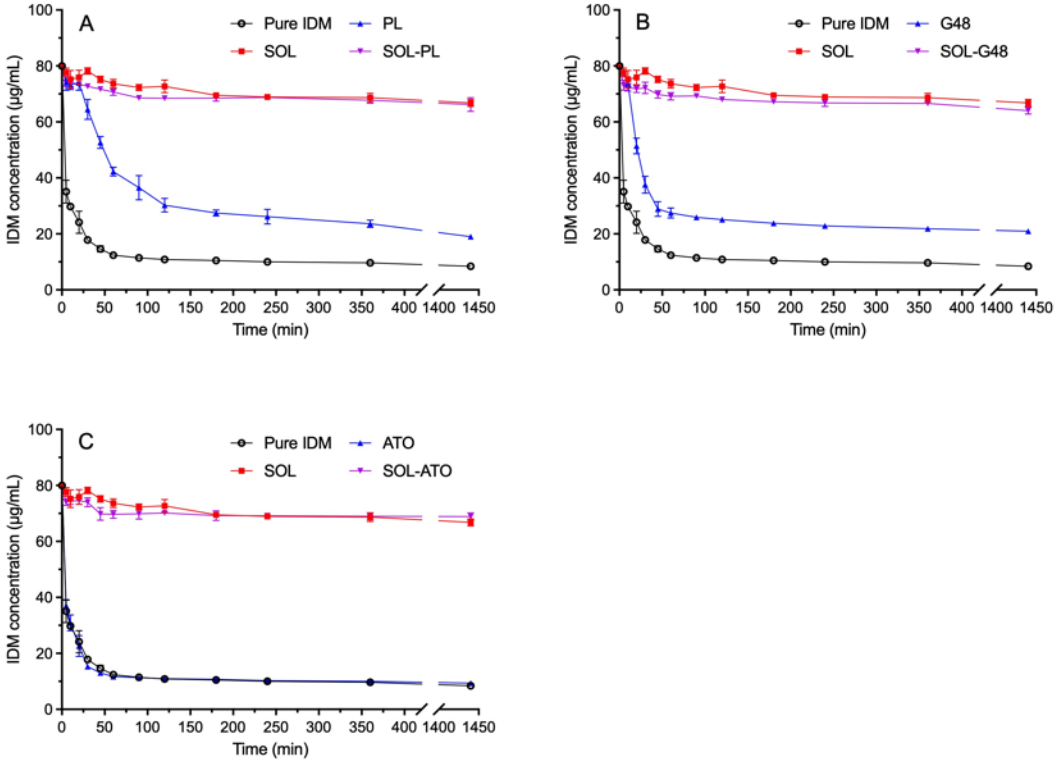

Figure A-1. Recrystallization of IDM in the presence of pre-dissolved (A) SOL-PL, (B) SOL-G48 and (C) SOL-ATO.

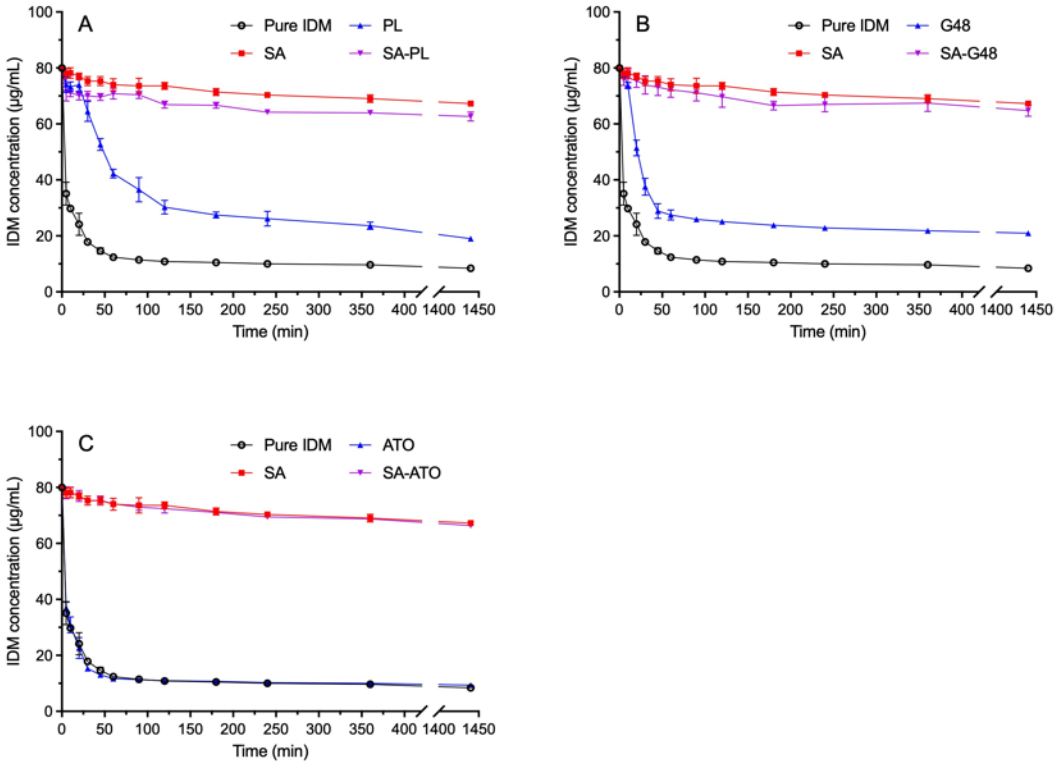

Figure A-2. Recrystallization of IDM in the presence of pre-dissolved (A) SA-PL, (B) SA-G48 and (C) SA-ATO.

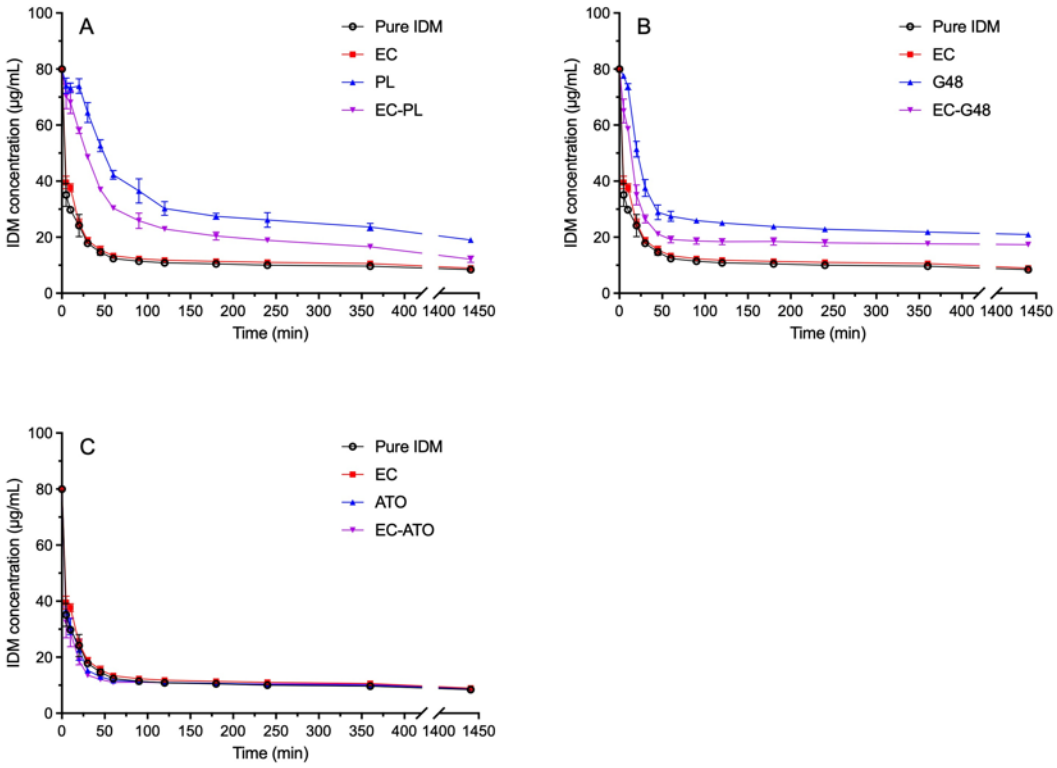

Figure A-3. Recrystallization of IDM in the presence of pre-dissolved (A) EC-PL, (B) EC-G48 and (C) EC-ATO.

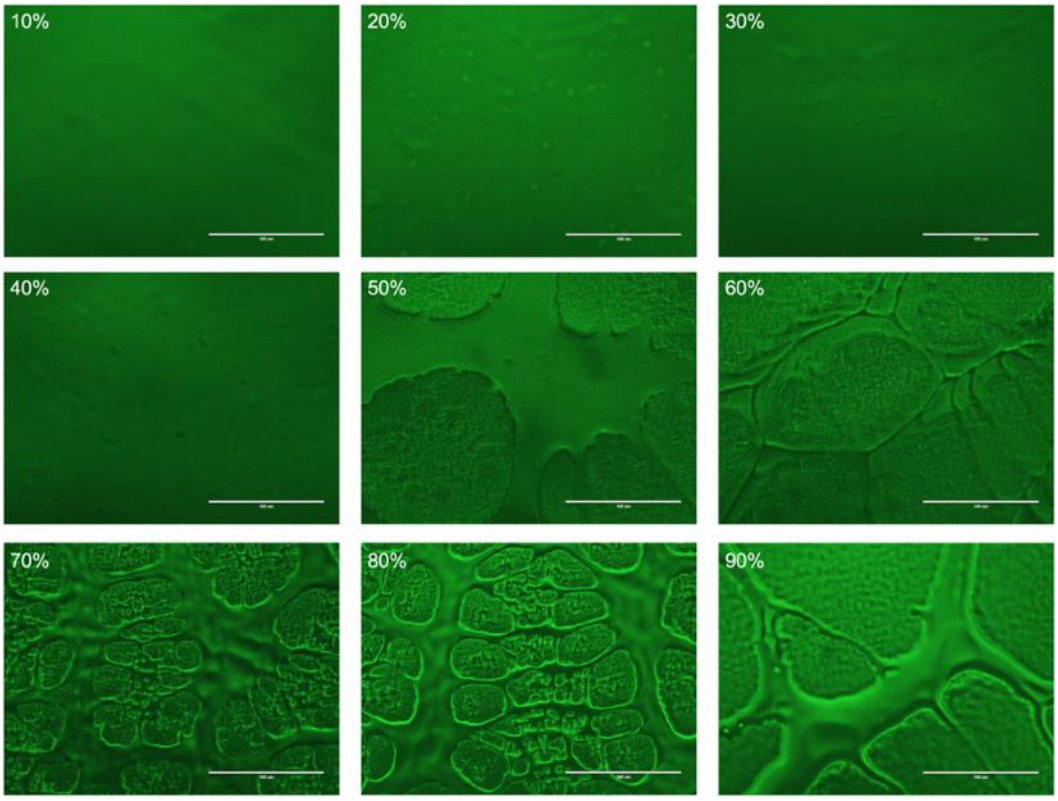

Figure B-1. Fluorescence images of IDM-PVP ASDs after storage for 1-week at 40 °C. Percentage refers to drug loading degree (w/w). Scale bar is 100 μm.

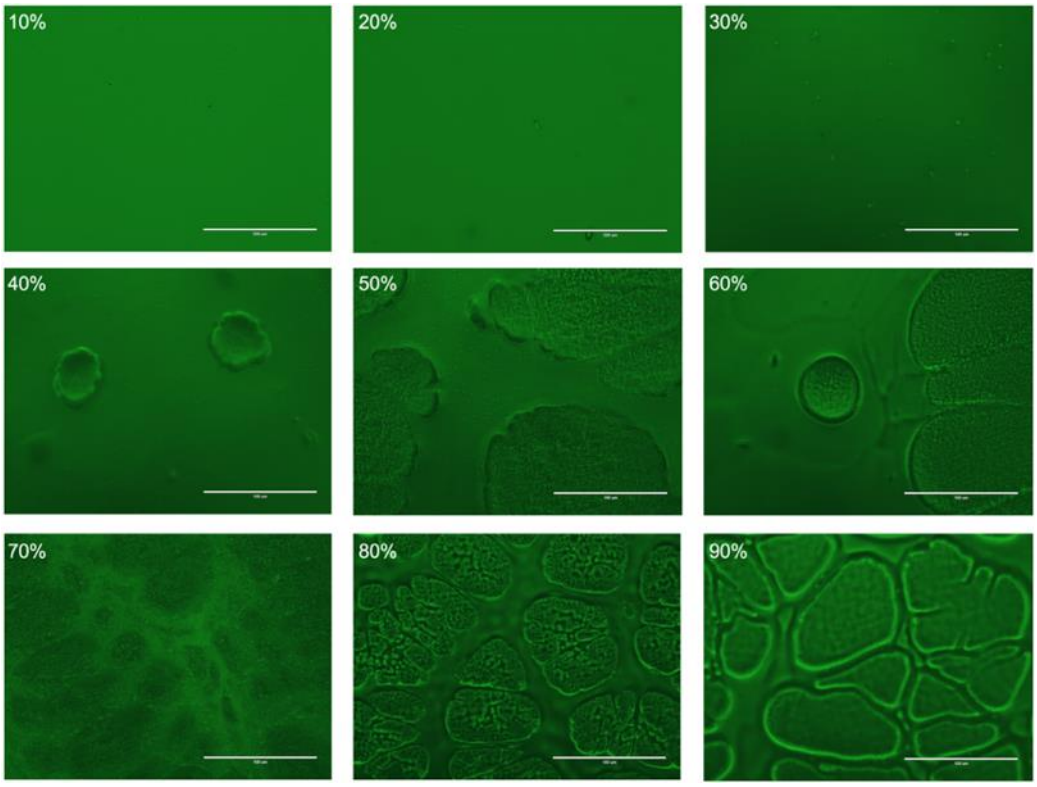

Figure B-2. Fluorescence images of IDM-PVP ASDs storage for 2-week at 40 °C. Percentage refers to drug loading degree (w/w). Scale bar is 100 μm.

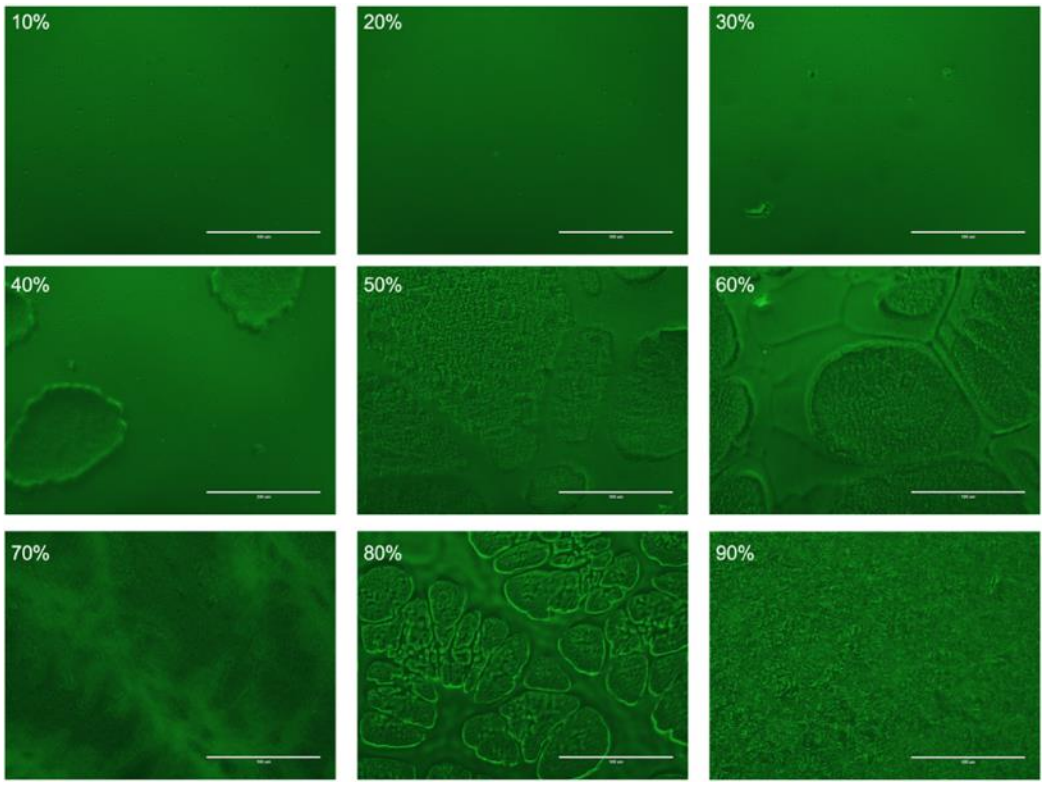

Figure B-3. Fluorescence images of IDM-PVP ASDs storage for 1-week at 40 °C. Percentage refers to drug loading degree (w/w). Scale bar is 100 μm.

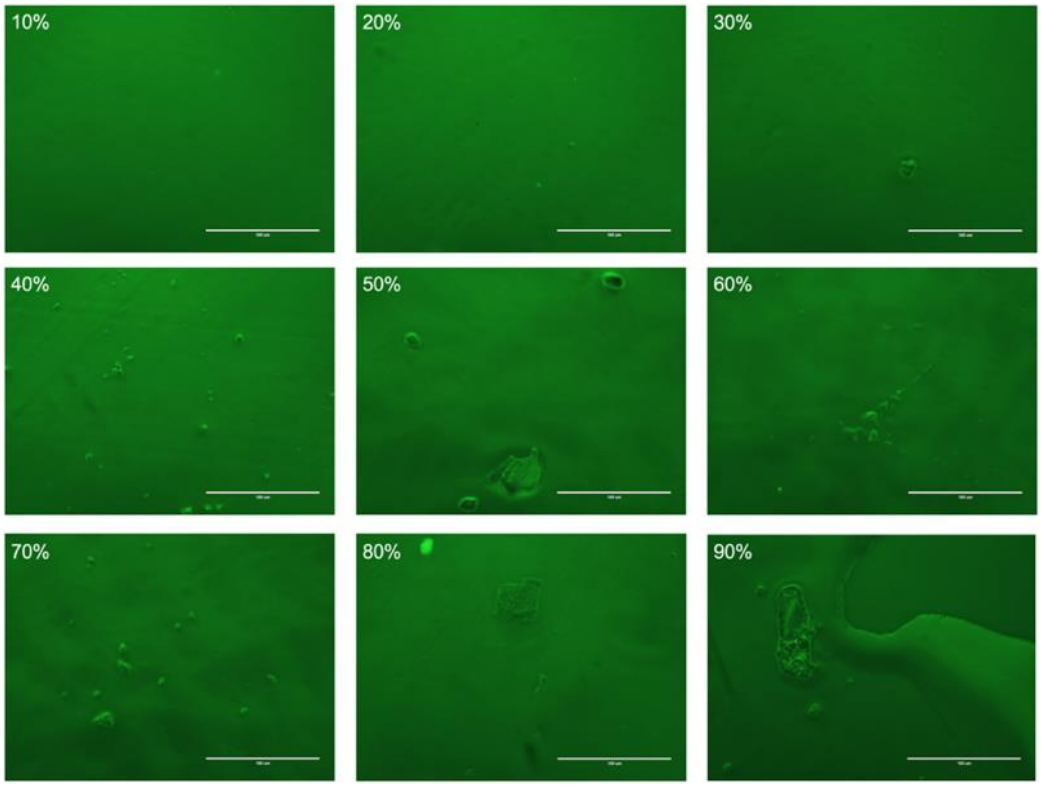

Figure B-4. Fluorescence images of IDM-SOL ASDs storage for 1-week at 40 °C. Percentage refers to drug loading degree (w/w). Scale bar is 100 μm.

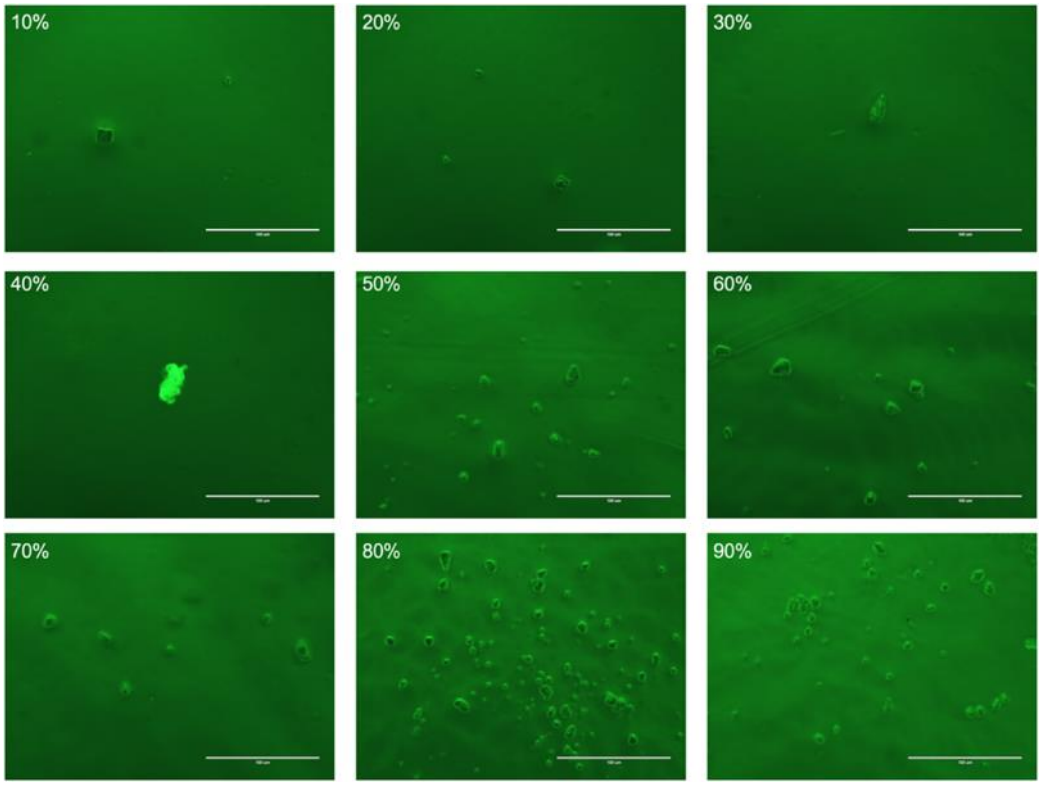

Figure B-5. Fluorescence images of IDM-SOL ASDs storage for 2-week at 40 °C. Percentage refers to drug loading degree (w/w). Scale bar is 100 μm.

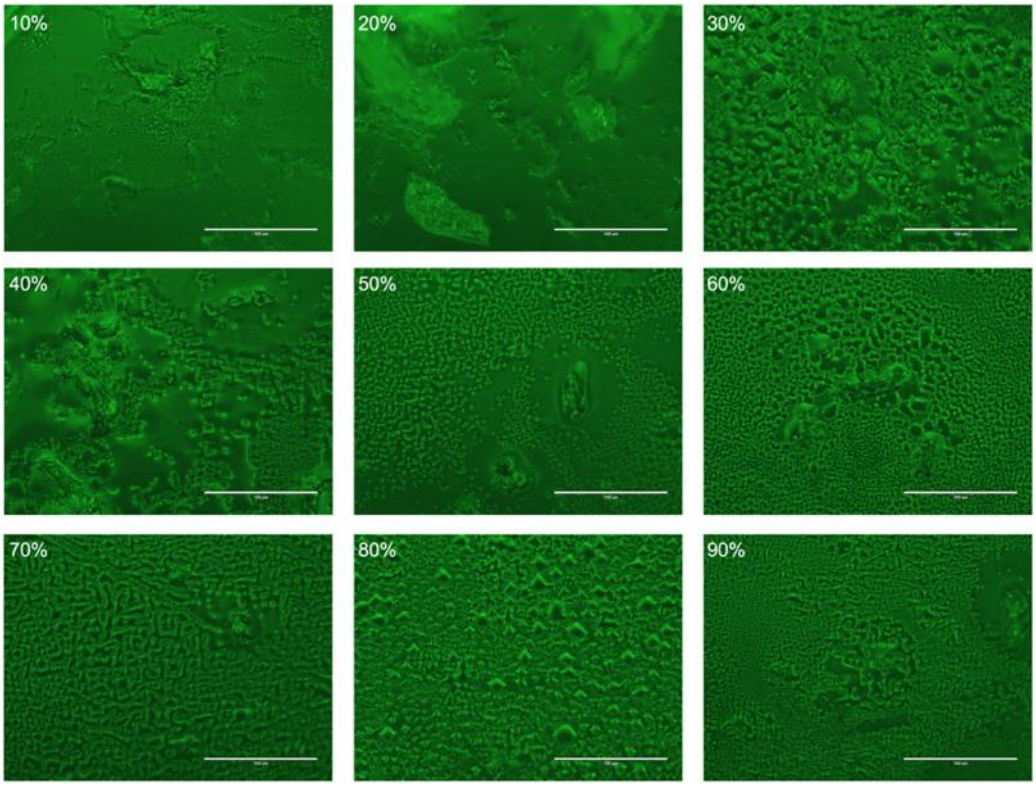

Figure B-6. Fluorescence images of IDM-SA ASDs storage for 1-week at 40 °C. Percentage refers to drug loading degree (w/w). Scale bar is 100 μm.

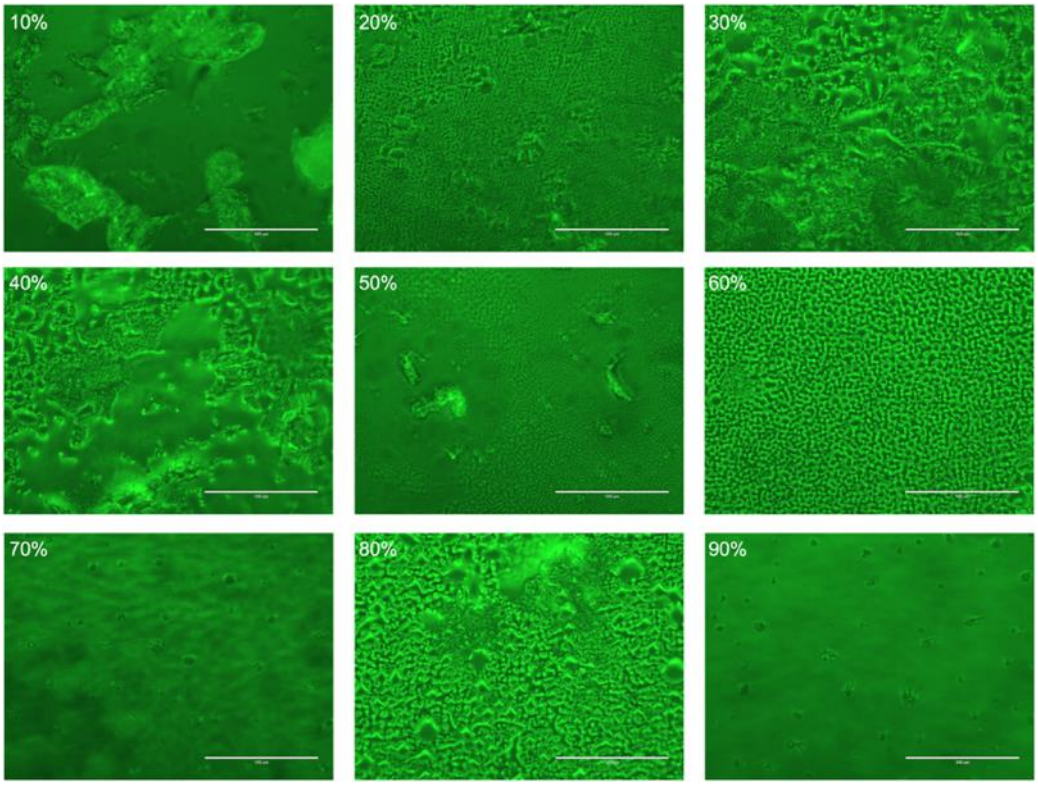

Figure B-7. Fluorescence images of IDM-SA ASDs storage for 2-week at 40 °C. Percentage refers to drug loading degree (w/w). Scale bar is 100 μm.

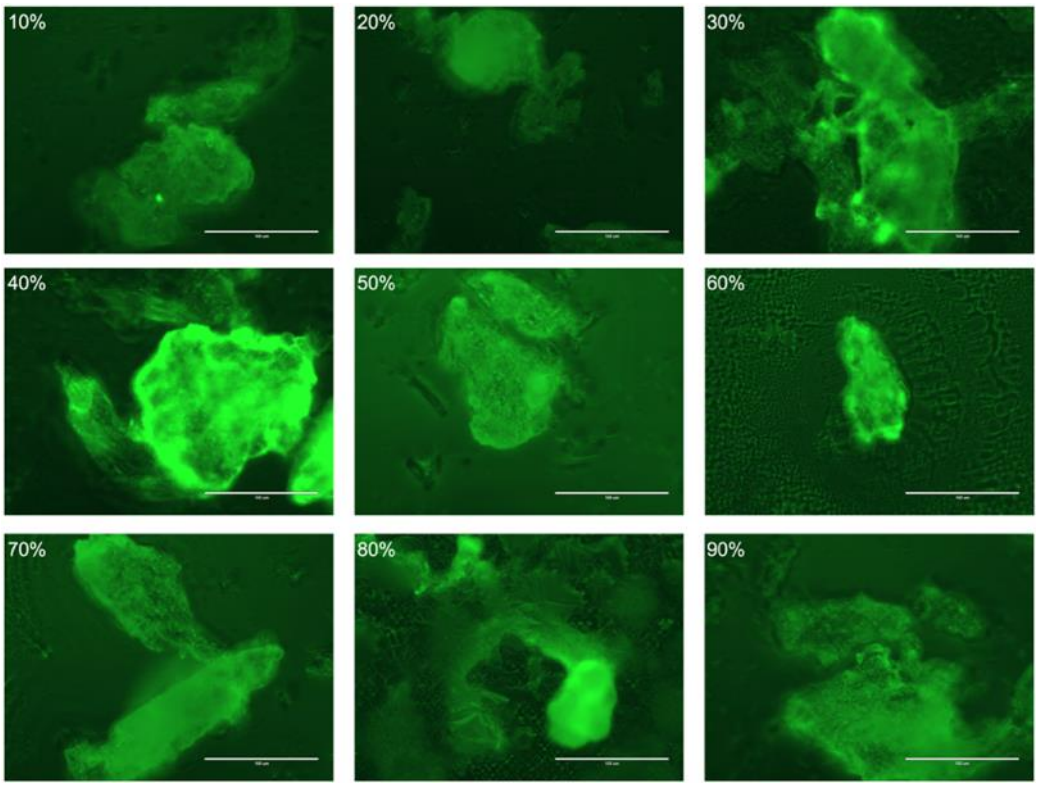

Figure B-8. Fluorescence images of IDM-SA ASDs storage for 3-week at 40 °C. Percentage refers to drug loading degree (w/w). Scale bar is 100 μm.

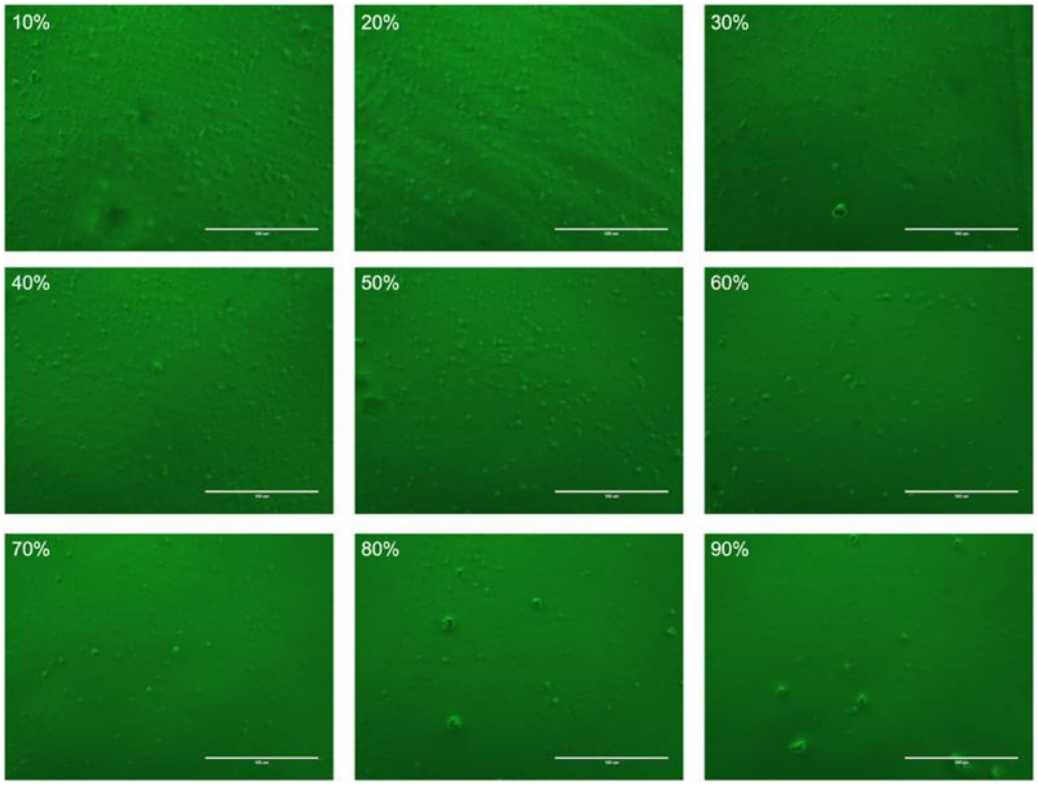

Figure B-9. Fluorescence images of IDM-EC ASDs storage for 1-week at 40 °C. Percentage refers to drug loading degree (w/w). Scale bar is 100 μm.

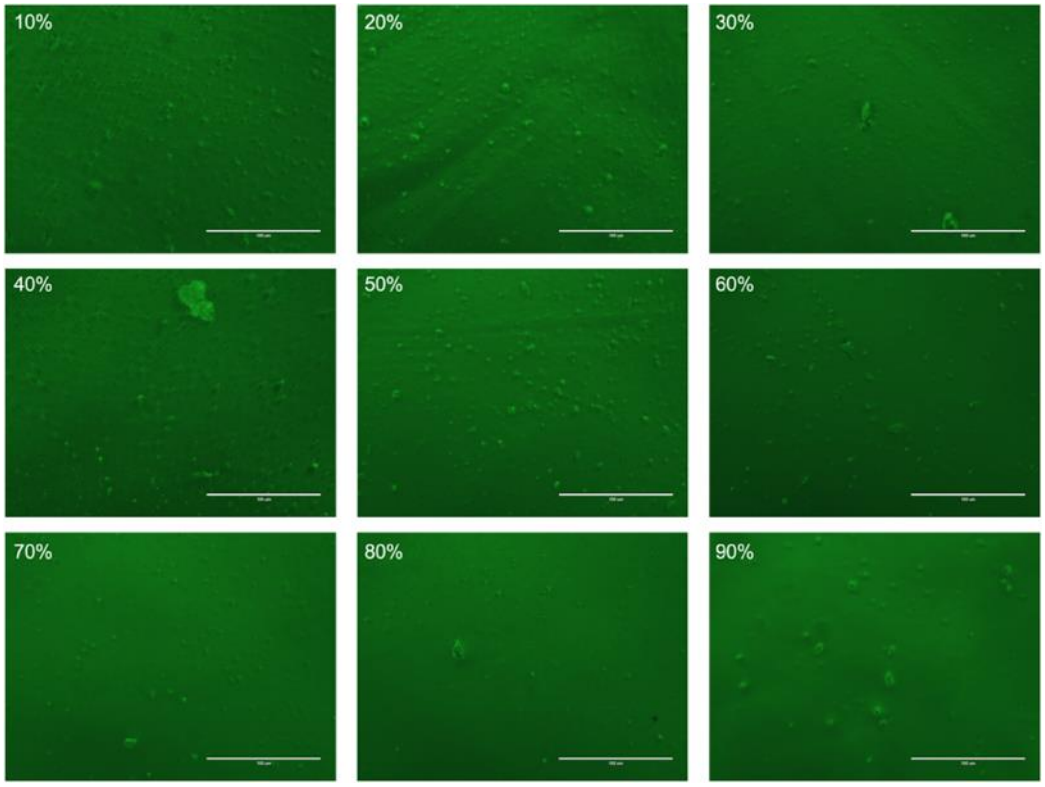

Figure B-10. Fluorescence images of IDM-EC ASDs storage for 2-week at 40 °C. Percentage refers to drug loading degree (w/w). Scale bar is 100 μm.

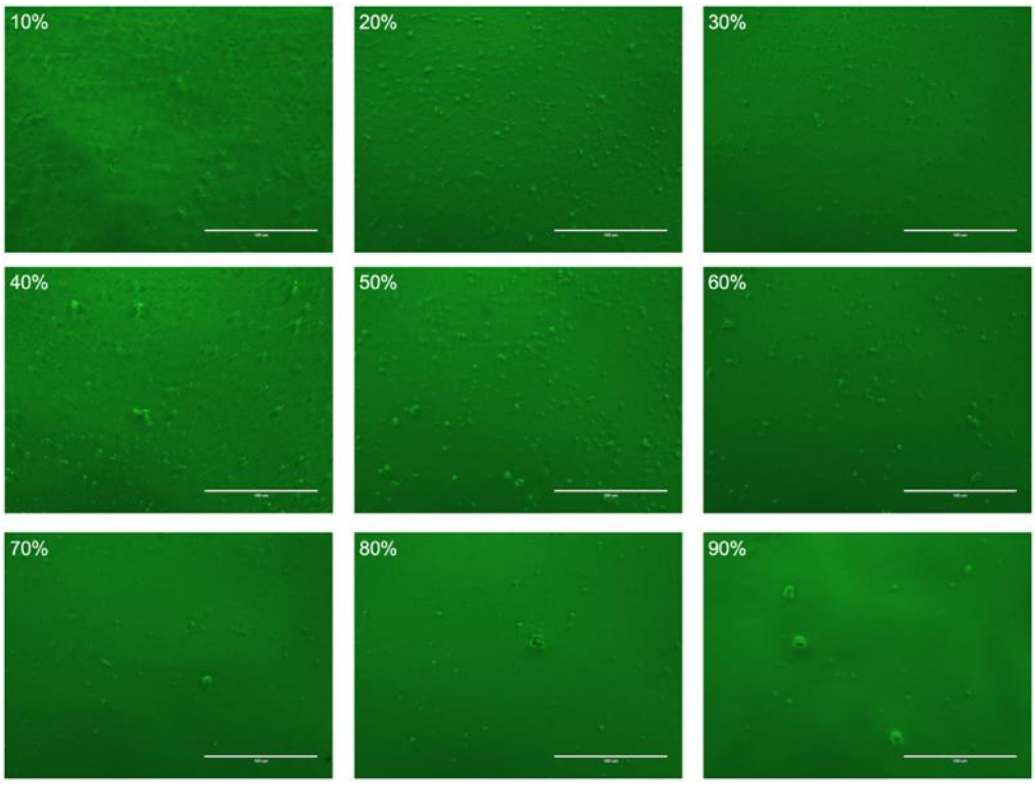

Figure B-11. Fluorescence images of IDM-EC ASDs storage for 3-week at 40 °C. Percentage refers to drug loading degree (w/w). Scale bar is 100 μm.

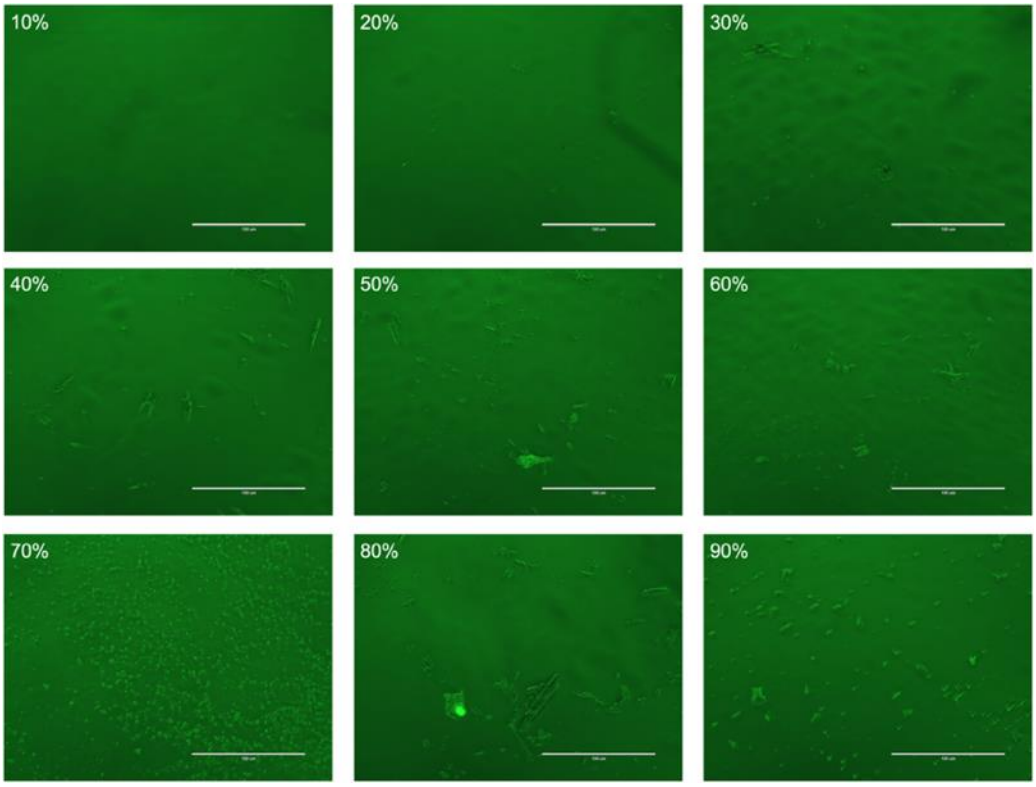

Figure B-12. Fluorescence images of IDM-PL ASDs storage for 2-week at 40 °C. Percentage refers to drug loading degree (w/w). Scale bar is 100 μm.

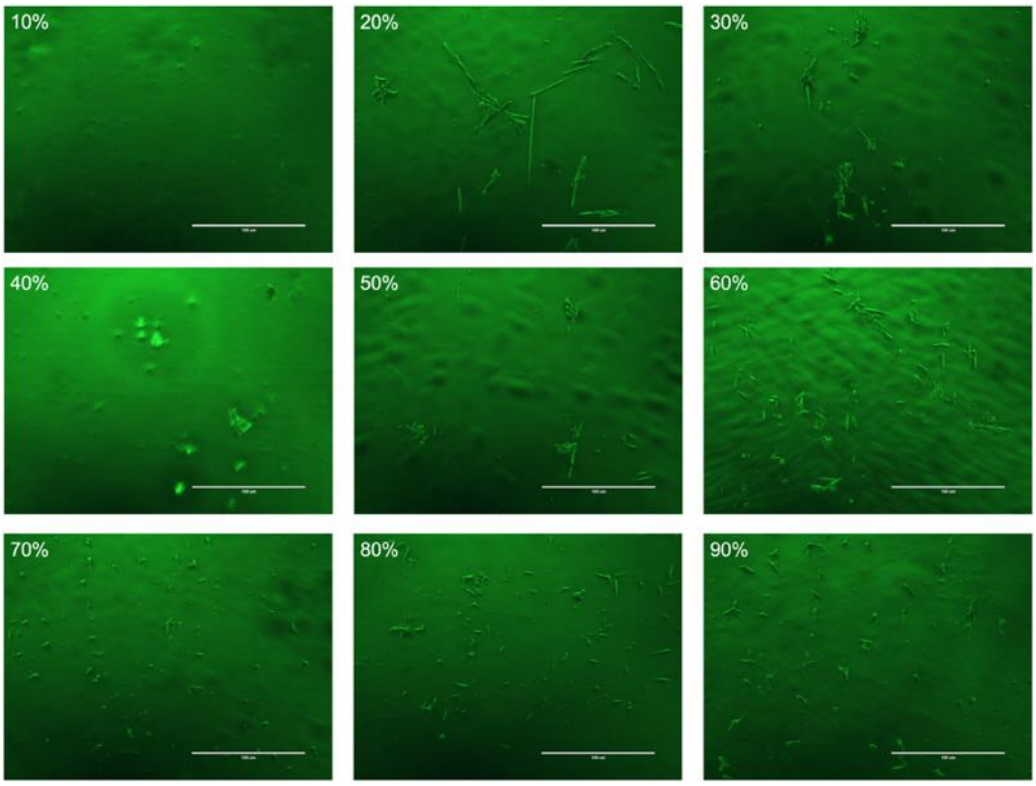

Figure B-13. Fluorescence images of IDM-PL ASDs storage for 3-week at 40 °C. Percentage refers to drug loading degree (w/w). Scale bar is 100 μm.

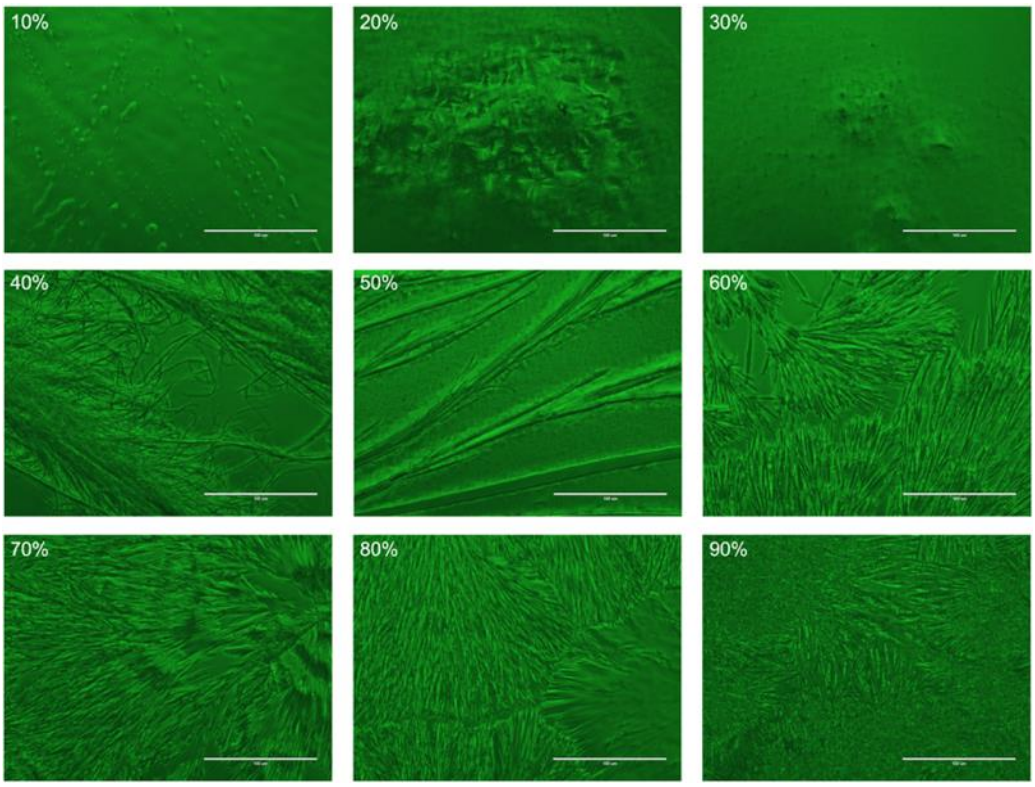

Figure B-14. Fluorescence images of IDM-G48 ASDs storage for 2-week at 40 °C. Percentage refers to drug loading degree (w/w). Scale bar is 100 μm.

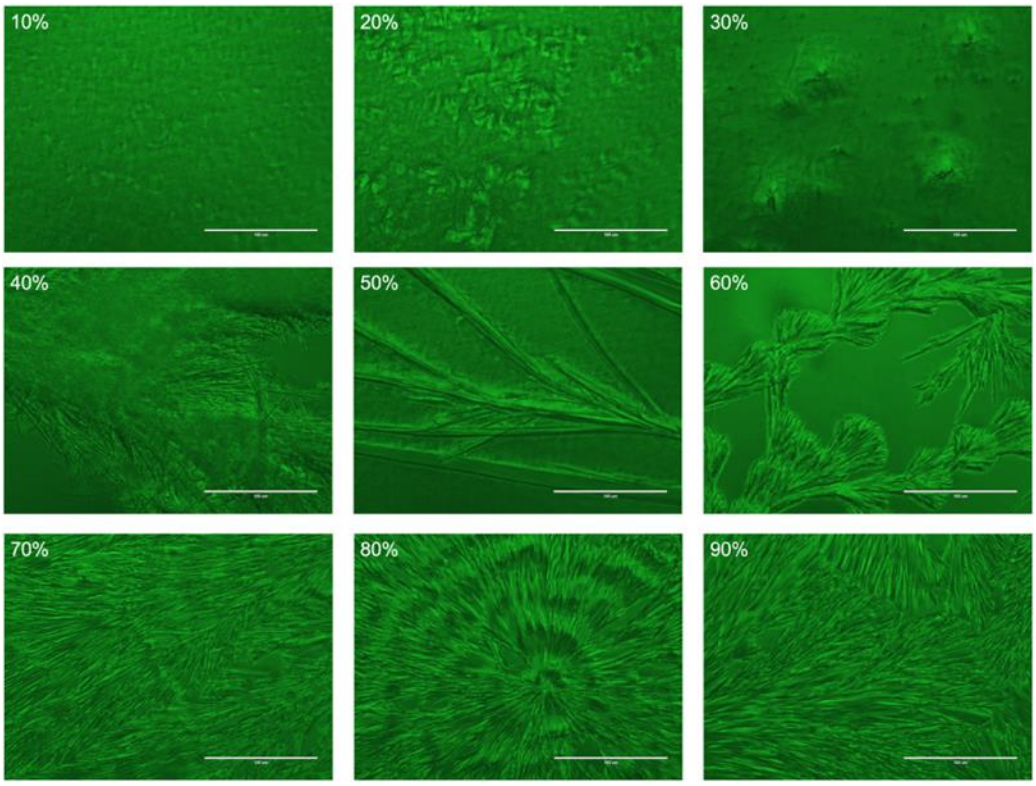

Figure B-15. Fluorescence images of IDM-G48 ASDs storage for 3-week at 40 °C. Percentage refers to drug loading degree (w/w). Scale bar is 100 μm.

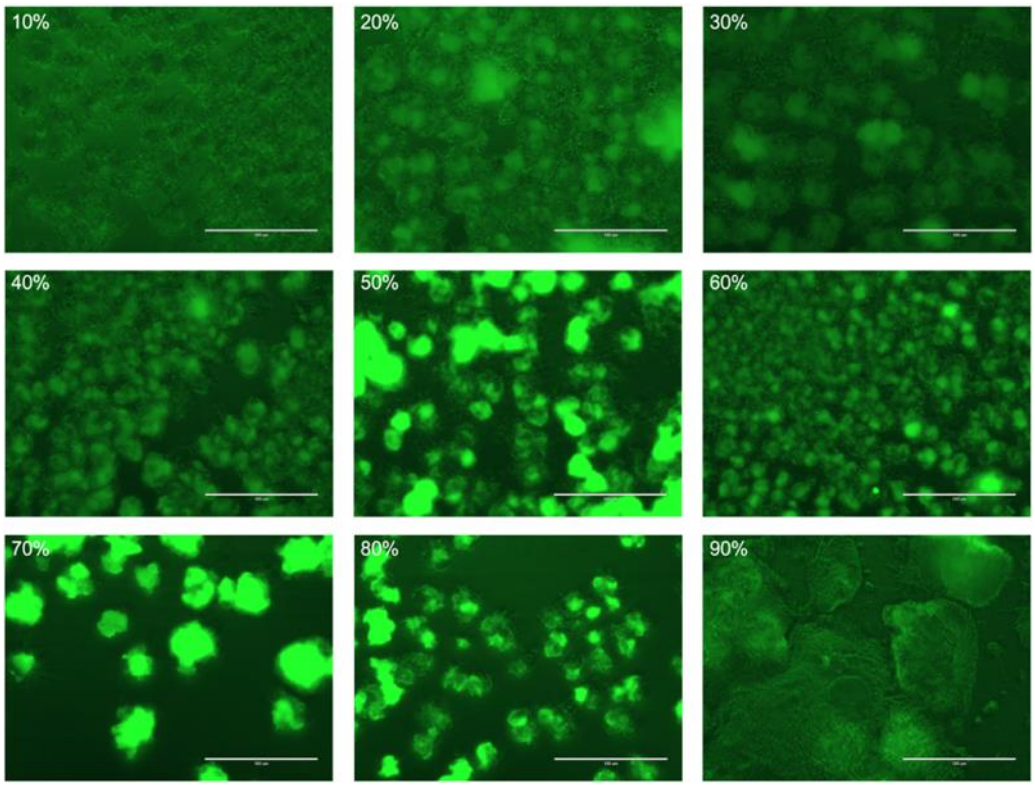

Figure B-16. Fluorescence images of IDM-ATO ASDs storage for 2-week at 40 °C. Percentage refers to drug loading degree (w/w). Scale bar is 100 μm.

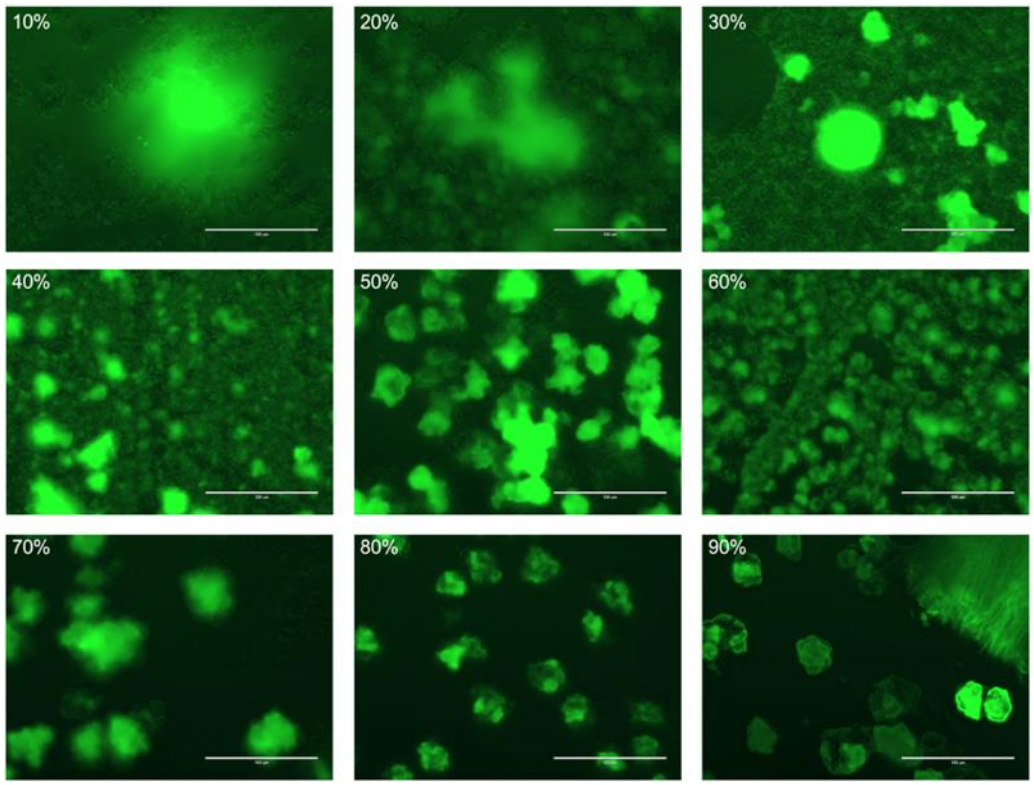

Figure B-17. Fluorescence images of IDM-ATO ASDs storage for 3-week at 40 °C. Percentage refers to drug loading degree (w/w). Scale bar is 100 μm.

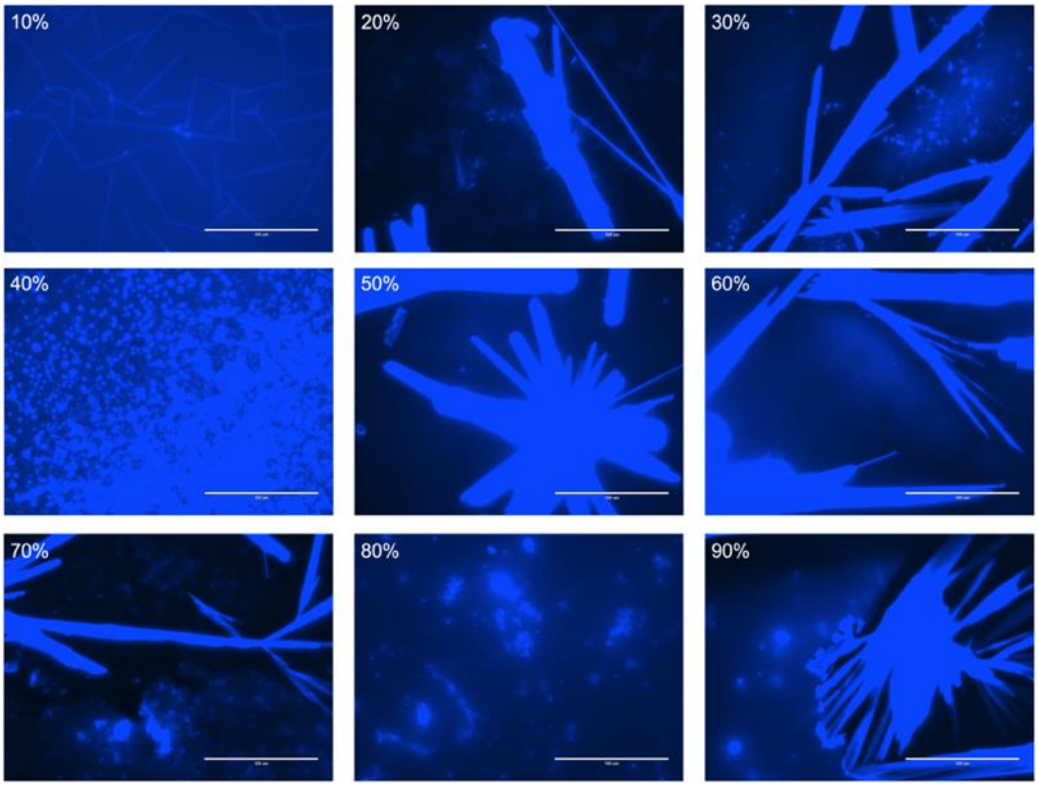

Figure B-18. Fluorescence images of APX-PVP ASDs storage for 1-week at 40 °C. Percentage refers to drug loading degree (w/w). Scale bar is 100 μm.

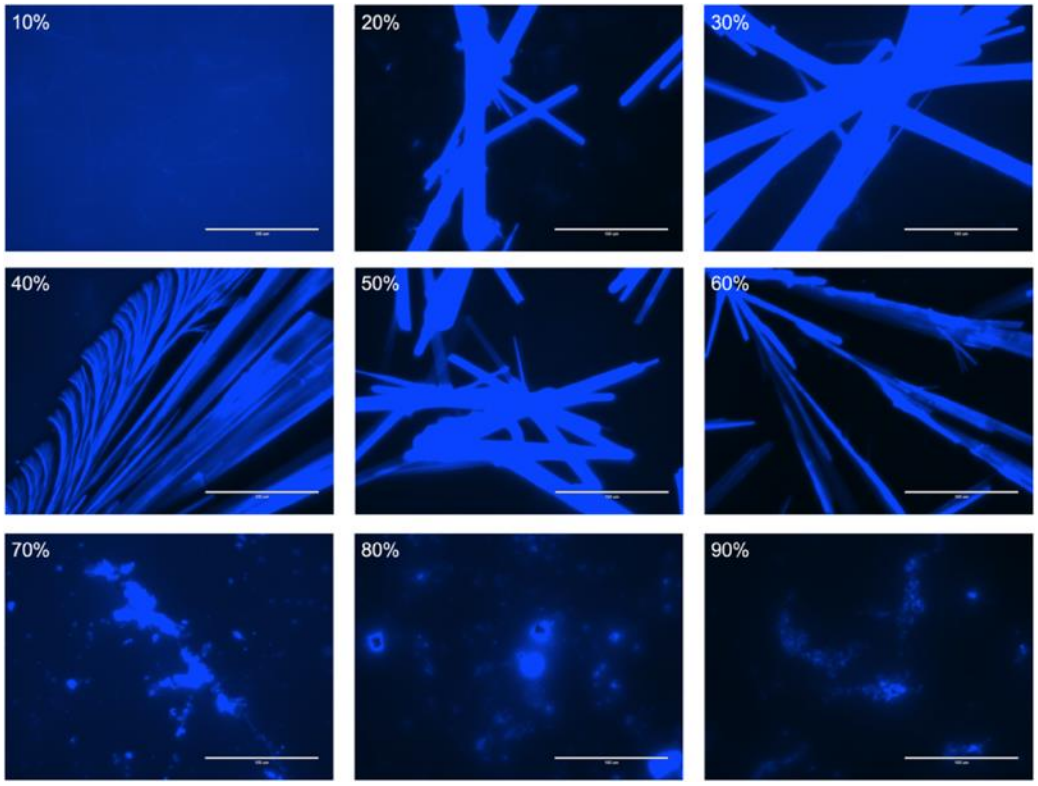

Figure B-19. Fluorescence images of APX-PVP ASDs storage for 3-week at 40 °C. Percentage refers to drug loading degree (w/w). Scale bar is 100 μm.

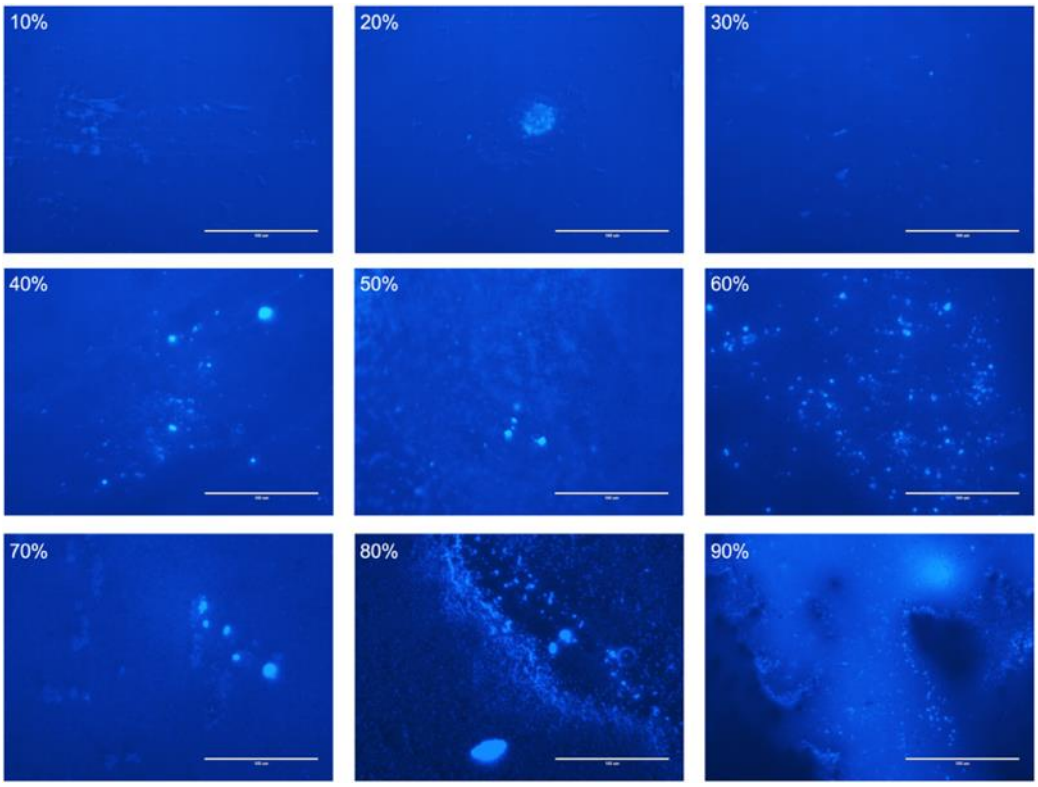

Figure B-20. Fluorescence images of APX-SOL ASDs storage for 1-week at 40 °C. Percentage refers to drug loading degree (w/w). Scale bar is 100 μm.

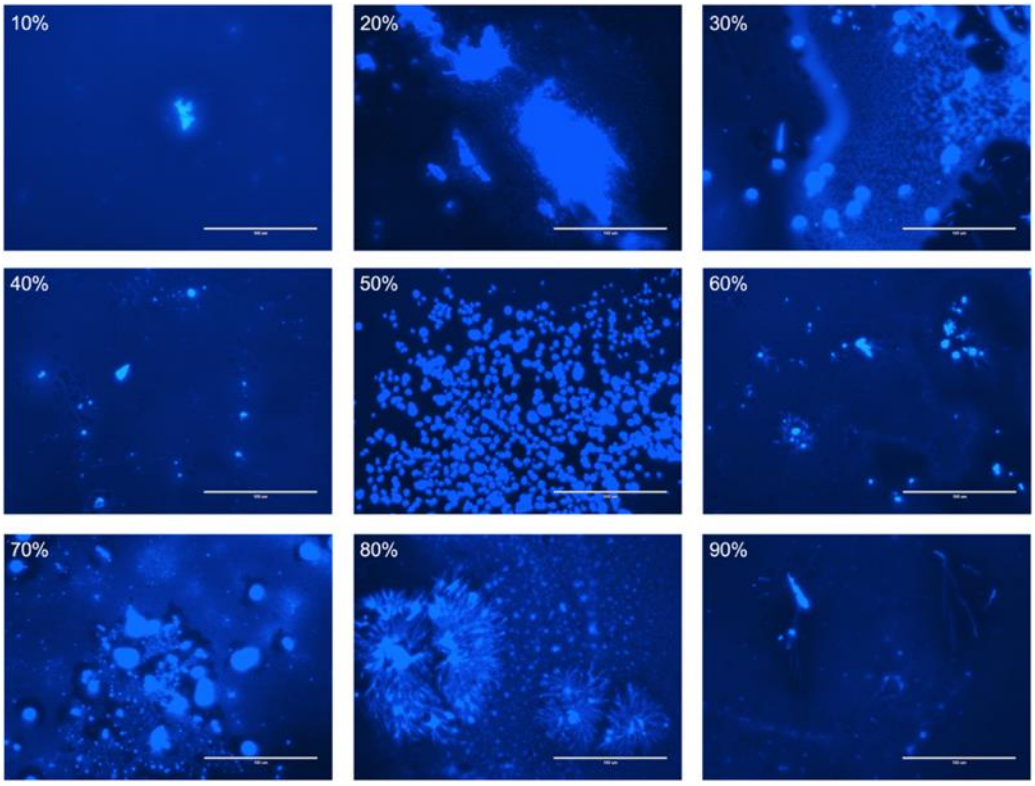

Figure B-21. Fluorescence images of APX-SOL ASDs storage for 2-week at 40 °C. Percentage refers to drug loading degree (w/w). Scale bar is 100 μm.

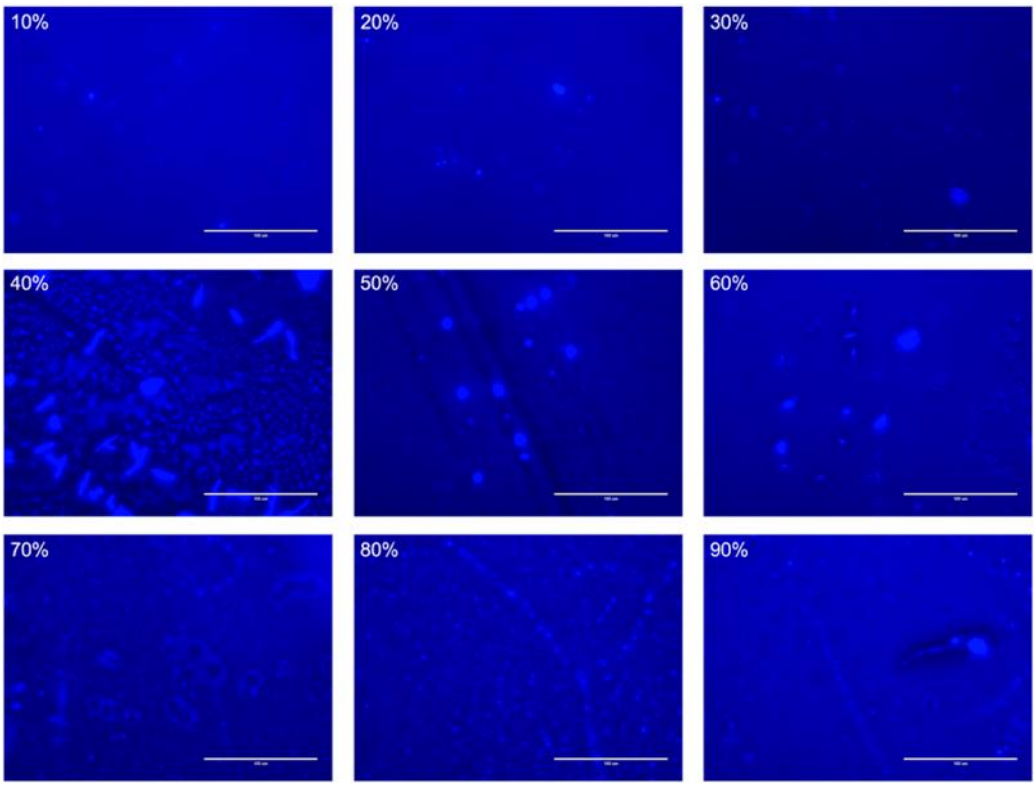

Figure B-22. Fluorescence images of APX-SOL ASDs storage for 3-week at 40 °C. Percentage refers to drug loading degree (w/w). Scale bar is 100 μm.

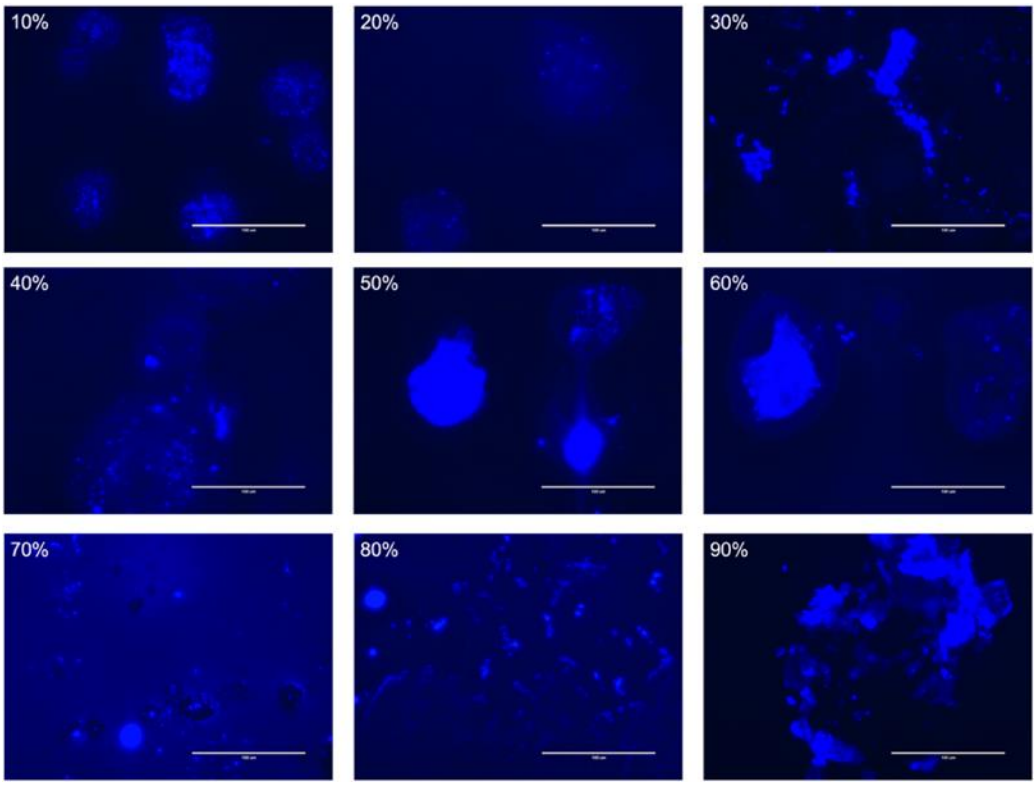

Figure B-23. Fluorescence images of APX-SA ASDs storage for 1-week at 40 °C. Percentage refers to drug loading degree (w/w). Scale bar is 100 μm.

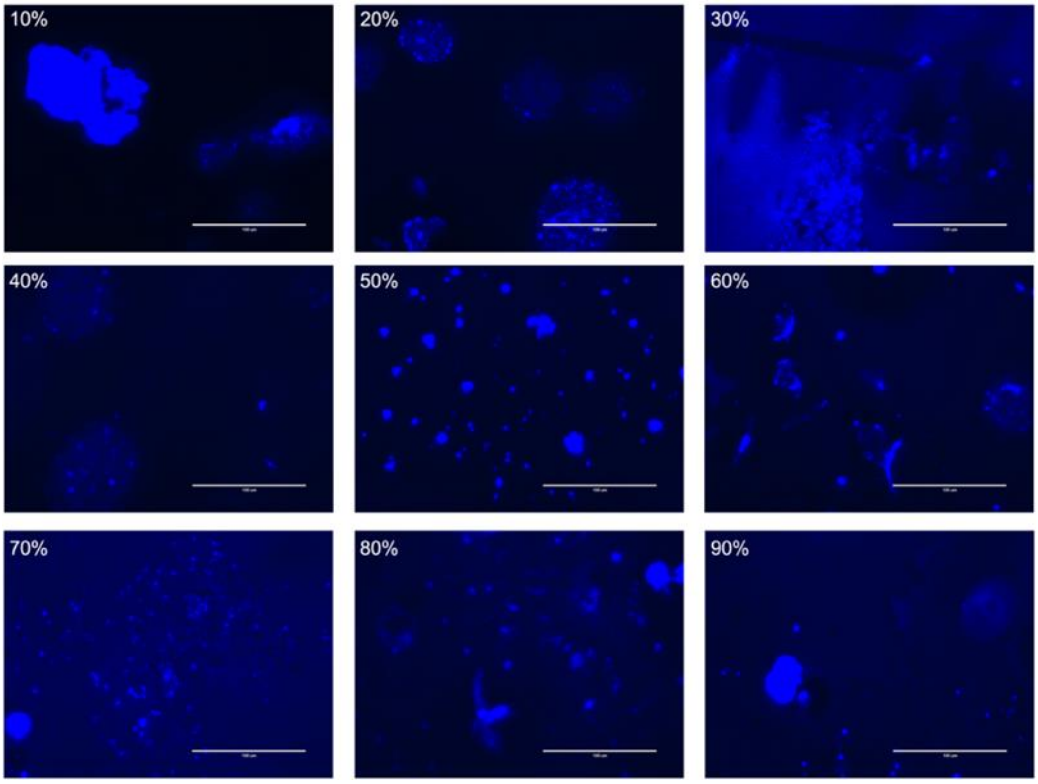

Figure B-24. Fluorescence images of APX-SA ASDs storage for 2-week at 40 °C. Percentage refers to drug loading degree (w/w). Scale bar is 100 μm.

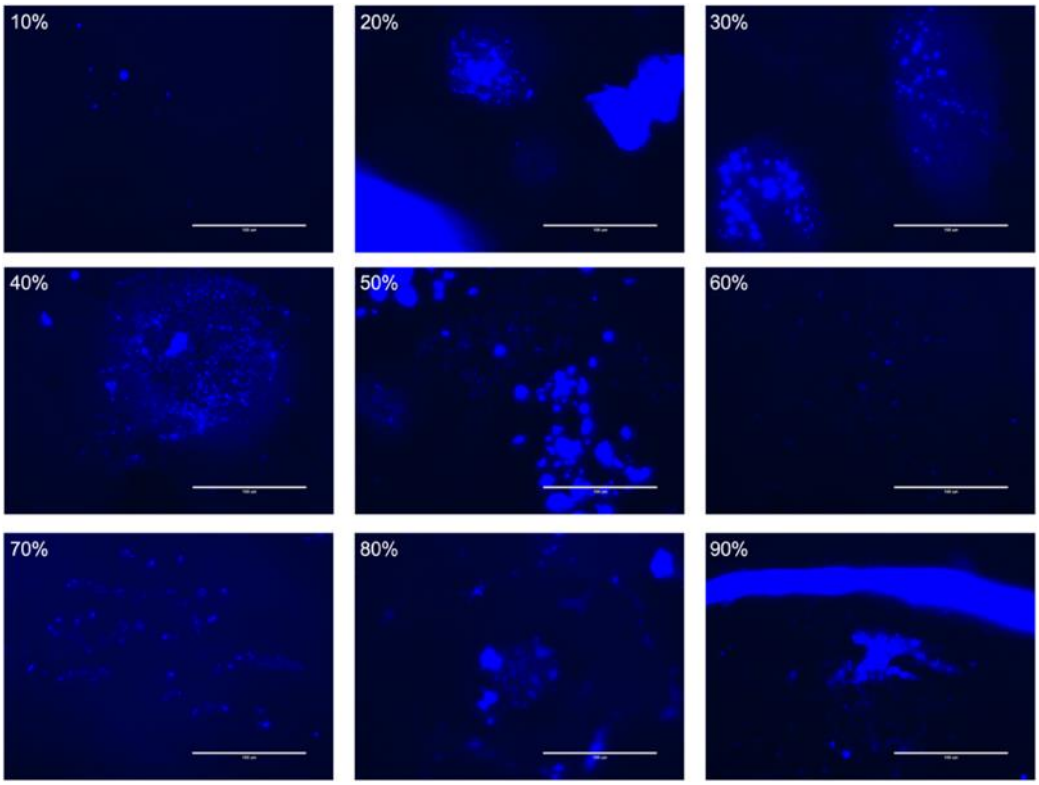

Figure B-25. Fluorescence images of APX-SA ASDs storage for 3-week at 40 °C. Percentage refers to drug loading degree (w/w). Scale bar is 100 μm.

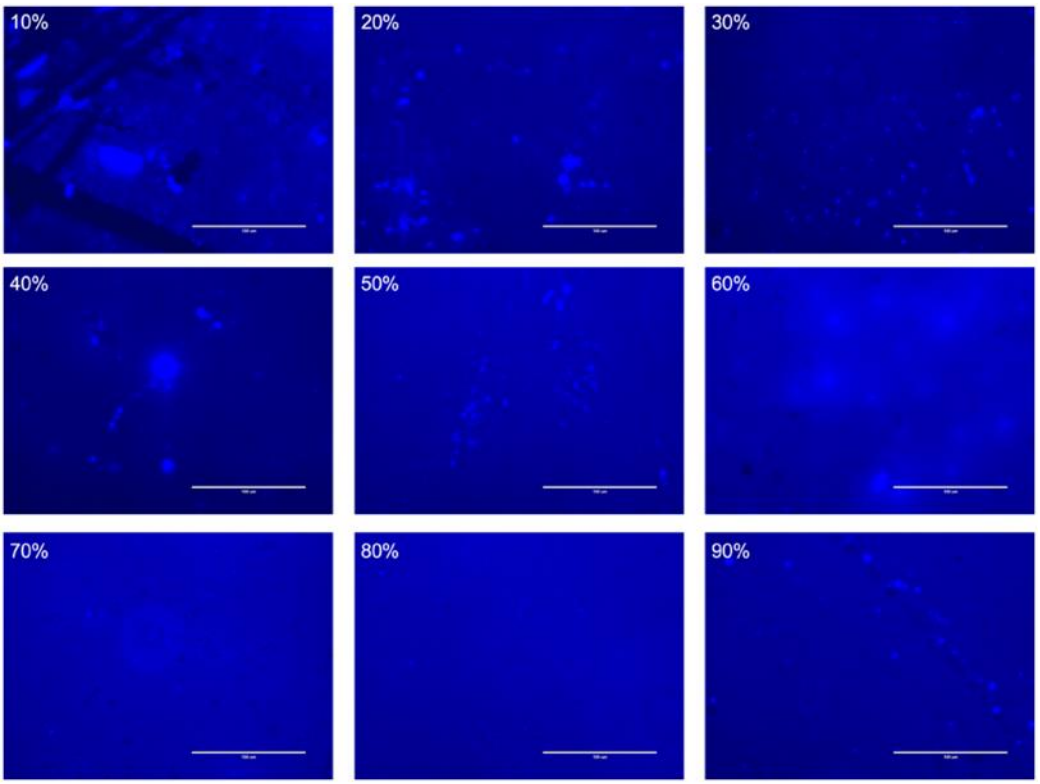

Figure B-26. Fluorescence images of APX-EC ASDs storage for 1-week at 40 °C. Percentage refers to drug loading degree (w/w). Scale bar is 100 μm.

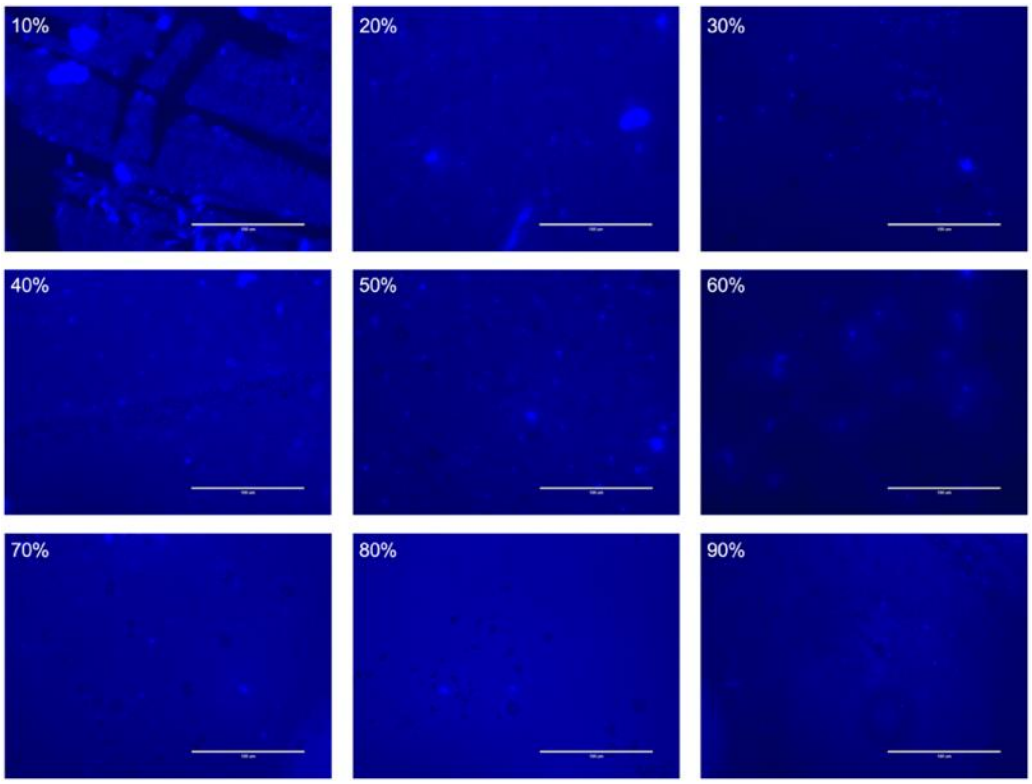

Figure B-27. Fluorescence images of APX-EC ASDs storage for 2-week at 40 °C. Percentage refers to drug loading degree (w/w). Scale bar is 100 μm.

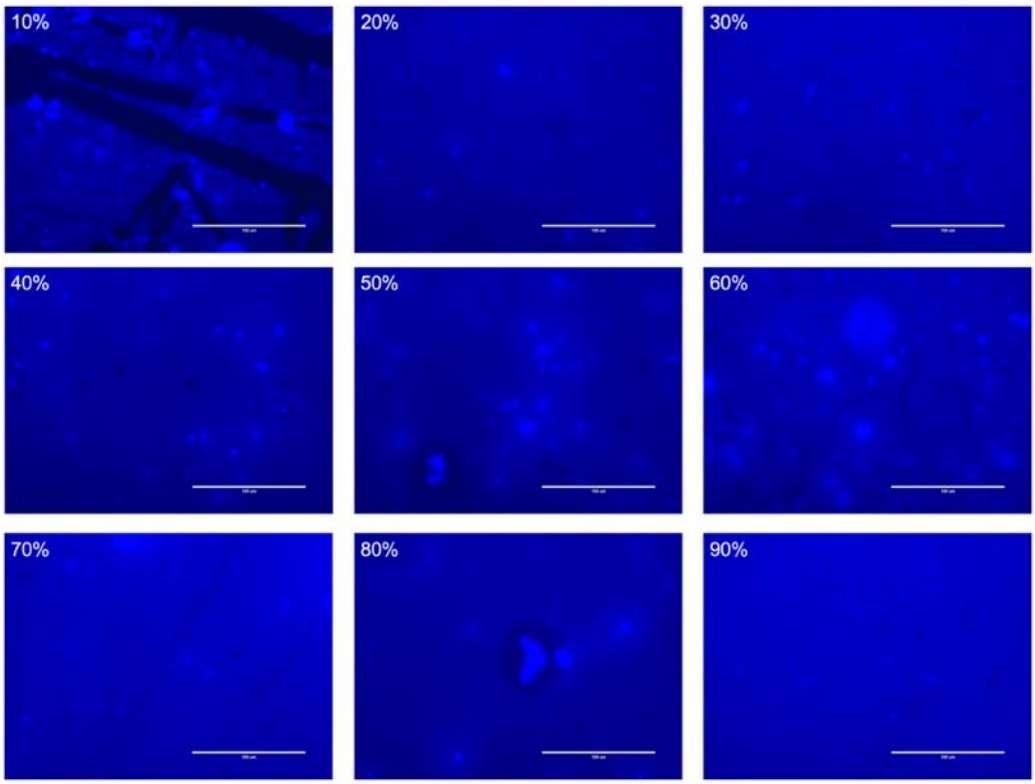

Figure B-28. Fluorescence images of APX-EC ASDs storage for 3-week at 40 °C. Percentage refers to drug loading degree (w/w). Scale bar is 100 μm.

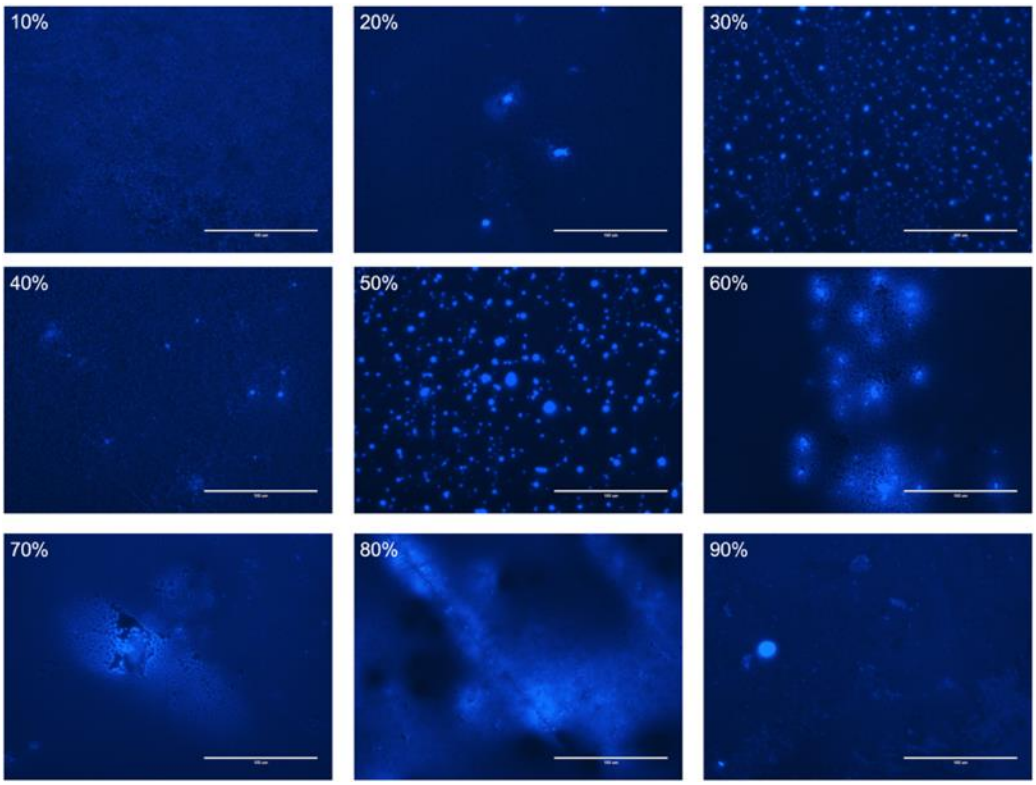

Figure B-29. Fluorescence images of APX-PL ASDs storage for 1-week at 40 °C. Percentage refers to drug loading degree (w/w). Scale bar is 100 μm.

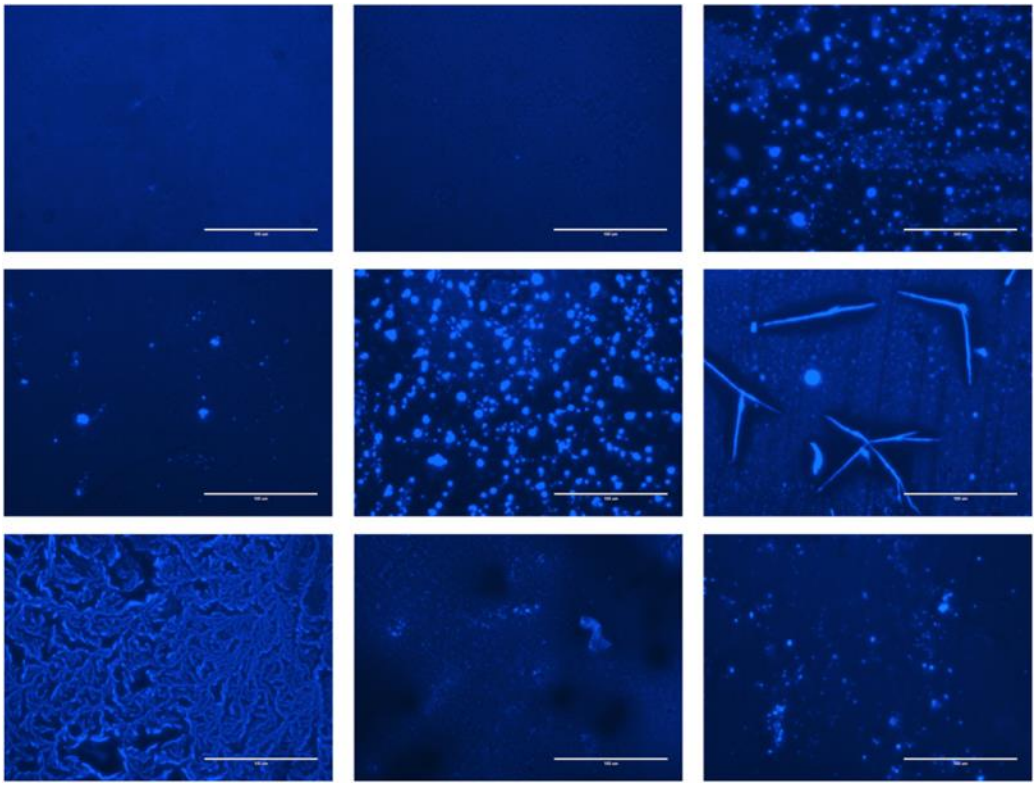

Figure B-30. Fluorescence images of APX-PL ASDs storage for 2-week at 40 °C. Percentage refers to drug loading degree (w/w). Scale bar is 100 μm.

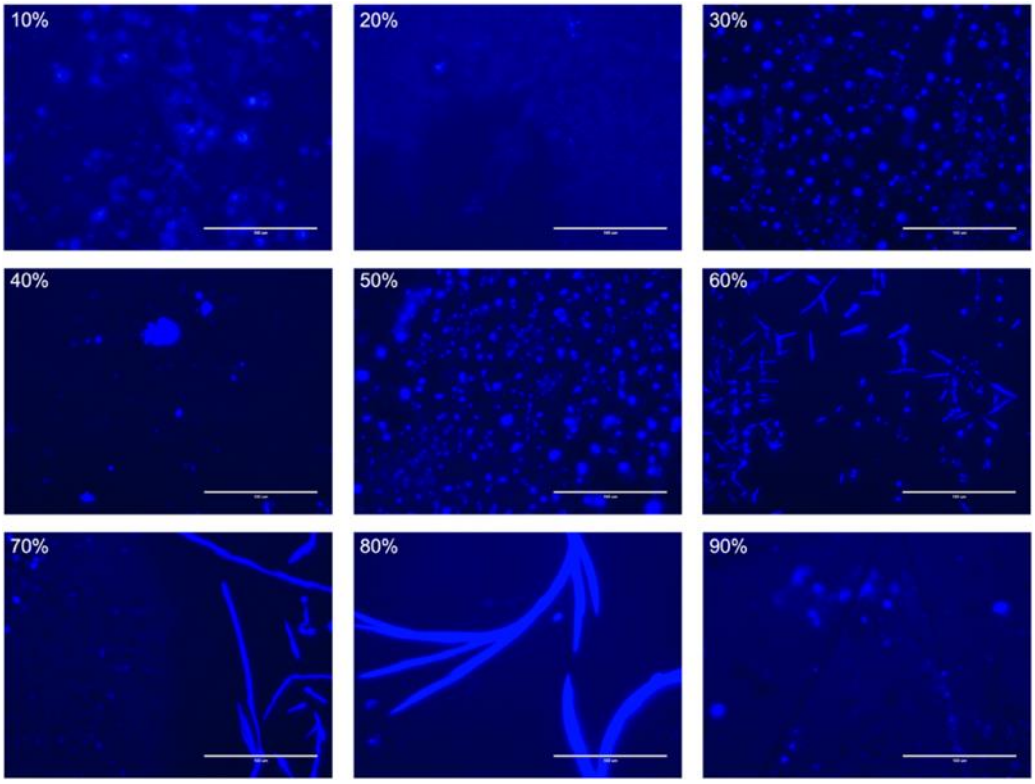

Figure B-31. Fluorescence images of APX-PL ASDs storage for 3-week at 40 °C. Percentage refers to drug loading degree (w/w). Scale bar is 100 μm.

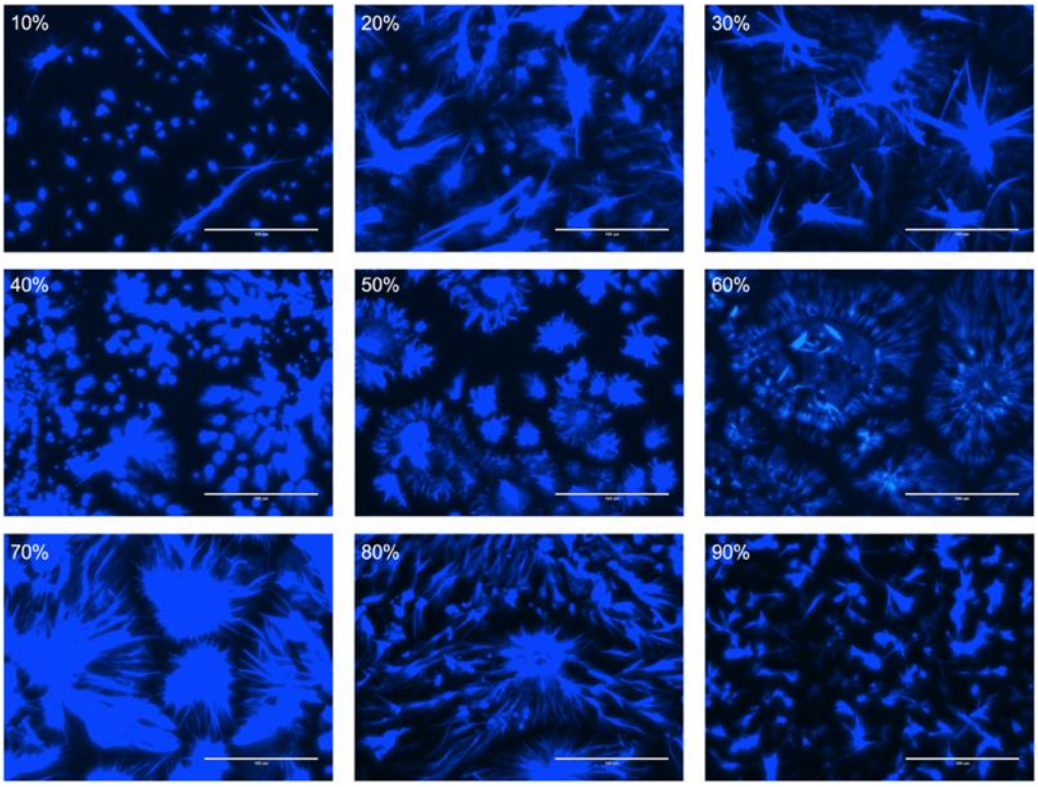

Figure B-32. Fluorescence images of APX-G48 ASDs storage for 2-week at 40 °C. Percentage refers to drug loading degree (w/w). Scale bar is 100 μm.

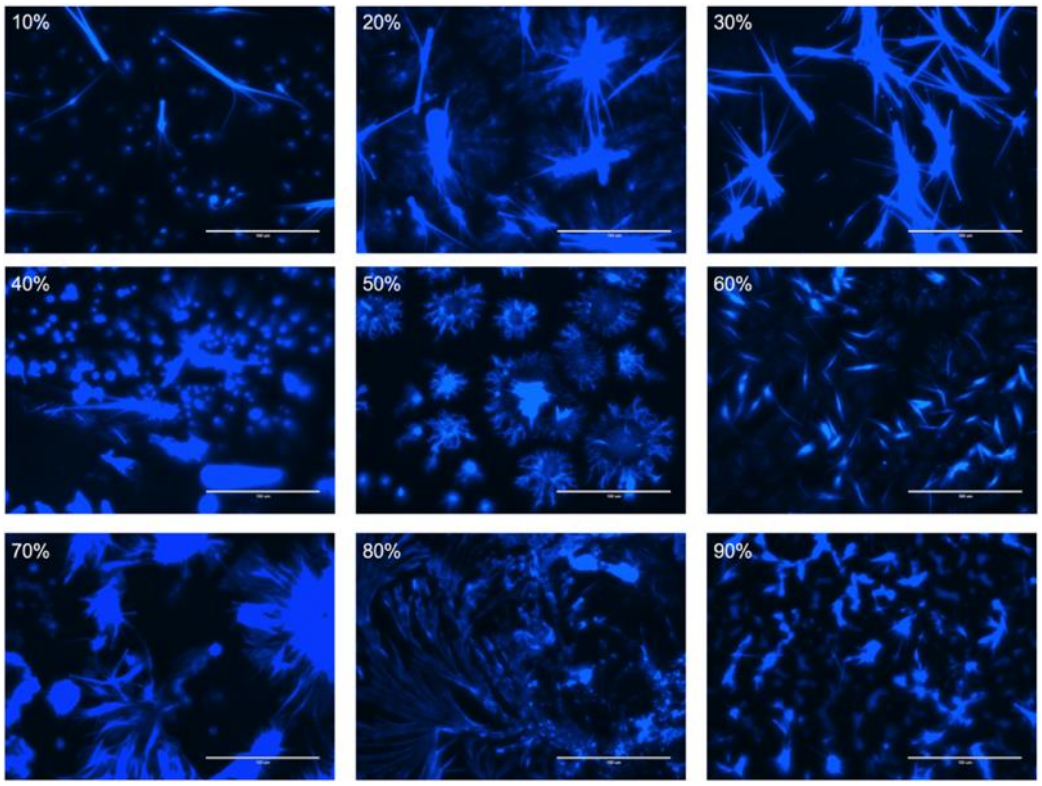

Figure B-33. Fluorescence images of APX-G48 ASDs storage for 3-week at 40 °C. Percentage refers to drug loading degree (w/w). Scale bar is 100 μm.

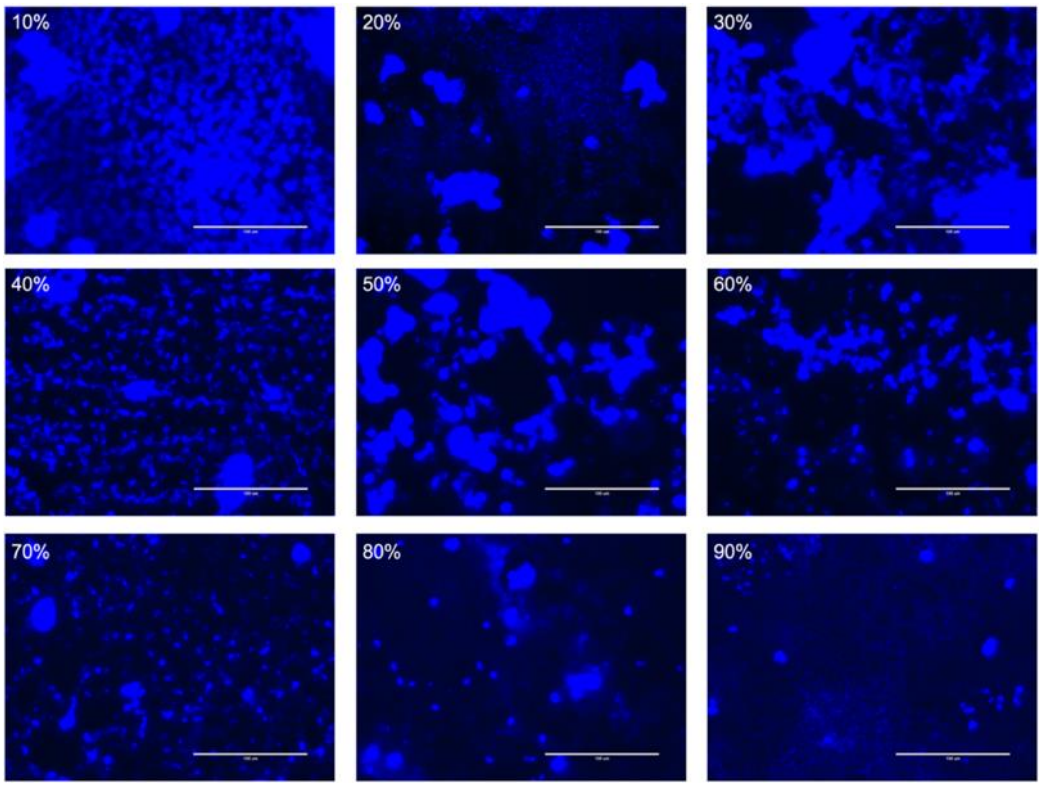

Figure B-34. Fluorescence images of APX-ATO ASDs storage for 1-week at 40 °C. Percentage refers to drug loading degree (w/w). Scale bar is 100 μm.

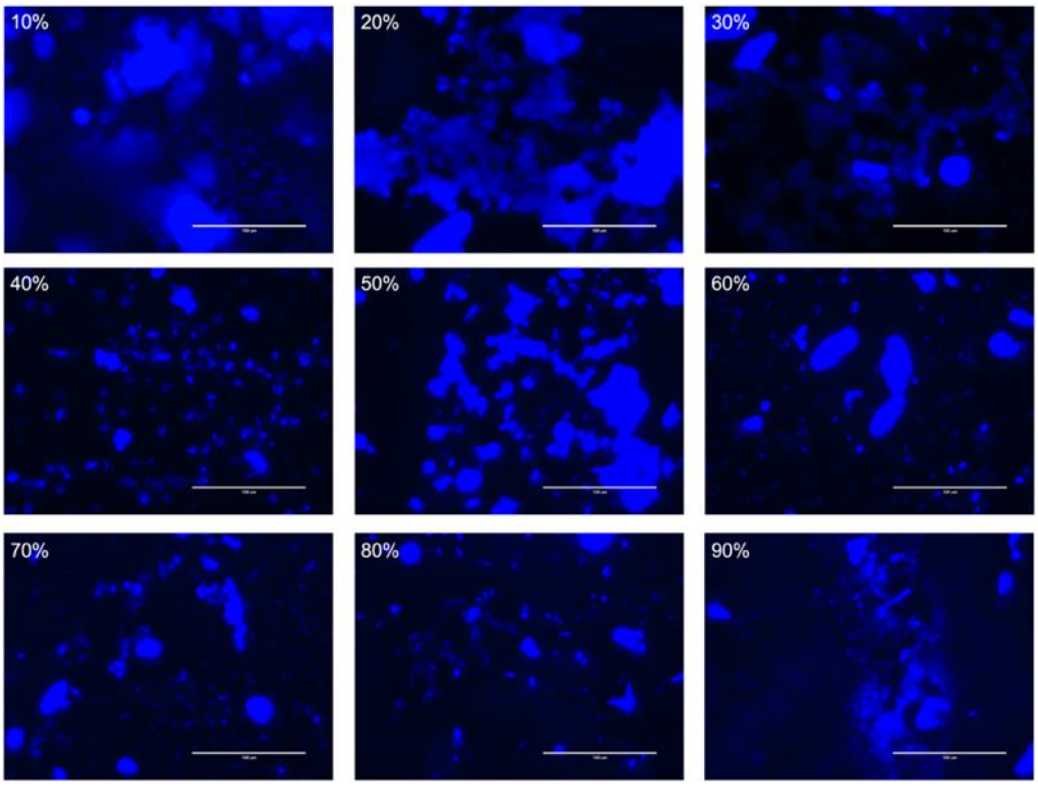

Figure B-35. Fluorescence images of APX-ATO ASDs storage for 2-week at 40 °C. Percentage refers to drug loading degree (w/w). Scale bar is 100 μm.

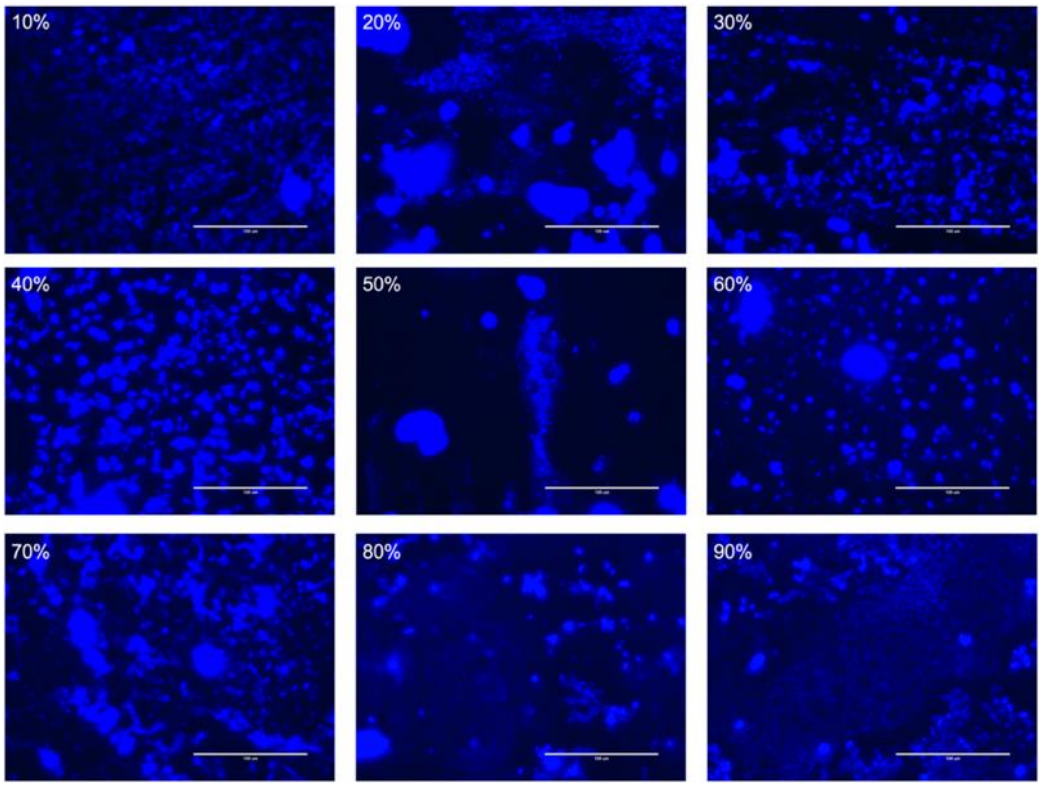

Figure B-36. Fluorescence images of APX-ATO ASDs storage for 3-week at 40 °C. Percentage refers to drug loading degree (w/w). Scale bar is 100 μm.

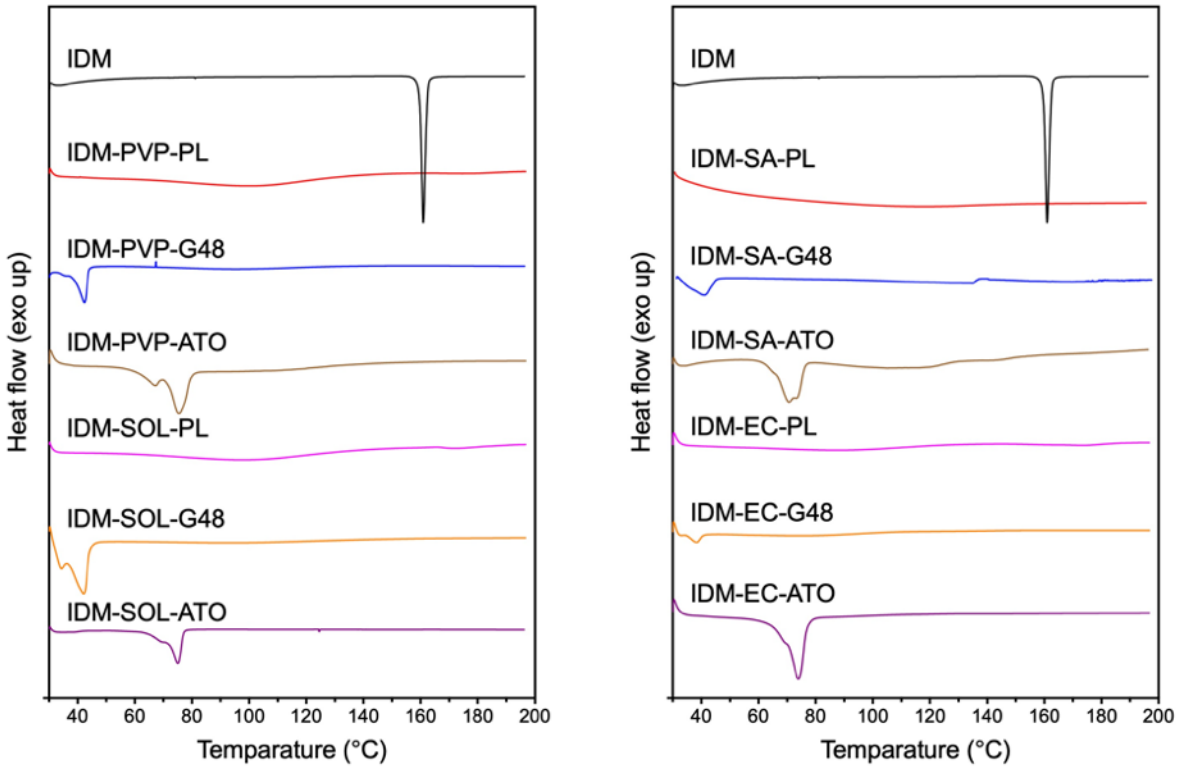

Figure C-1. DSC thermograms of solvent-based IDM ASDs prepared with polymer-lipid combination carriers.

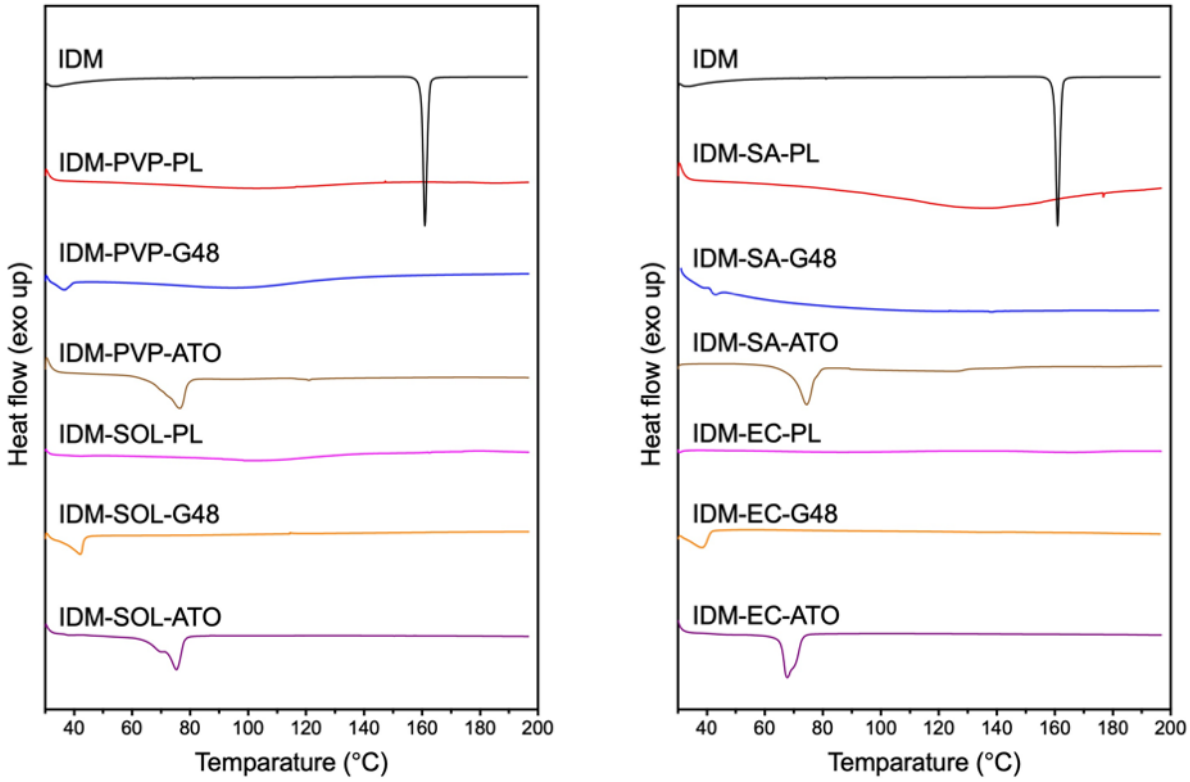

Figure C-2. DSC thermograms of freeze-dried IDM ASDs prepared with polymer-lipid combination carriers.

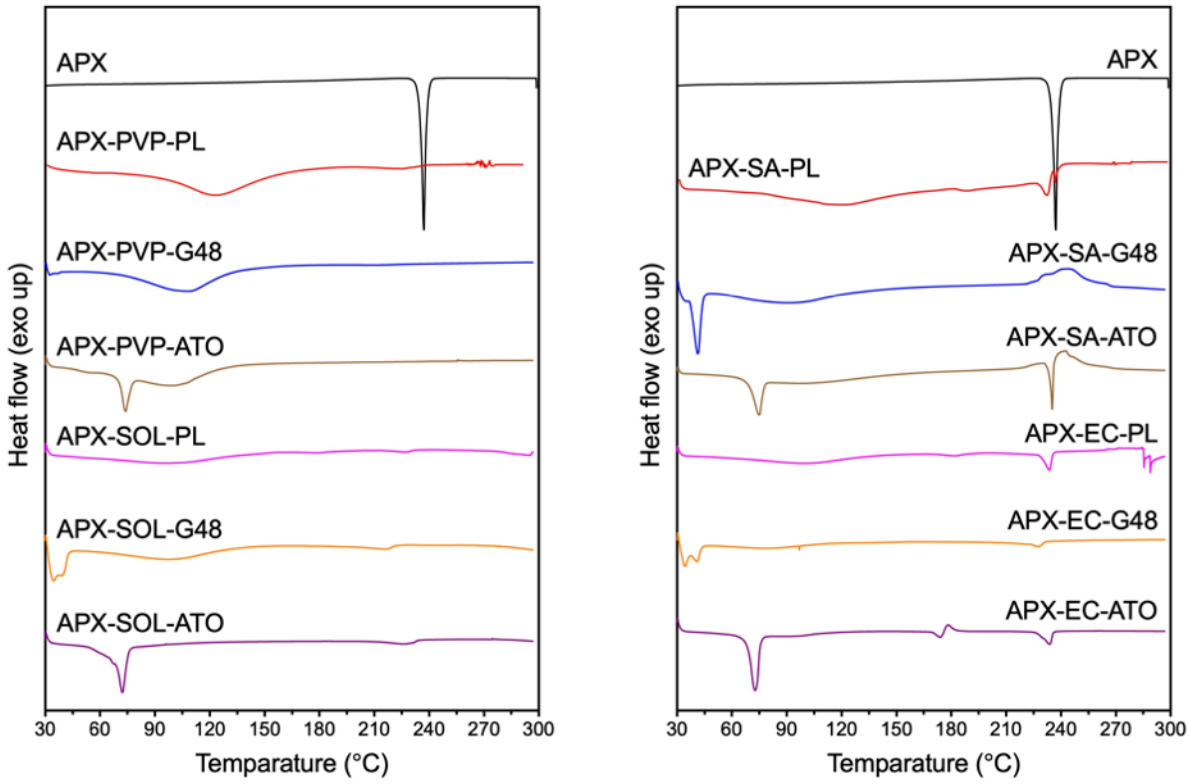

Figure C-3. DSC thermograms of solvent-based APX ASDs prepared with polymer-lipid combination carriers.

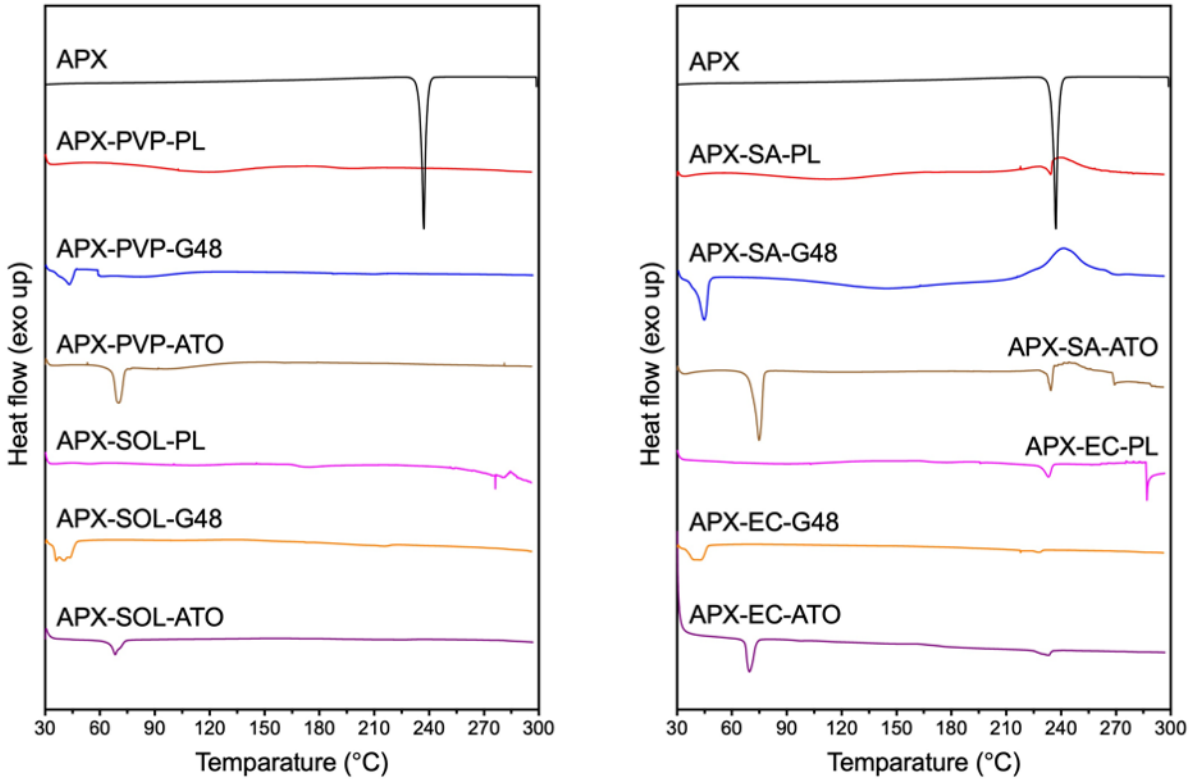

Figure C-4. DSC thermograms of freeze-dried APX ASDs prepared with polymer-lipid combination carriers.

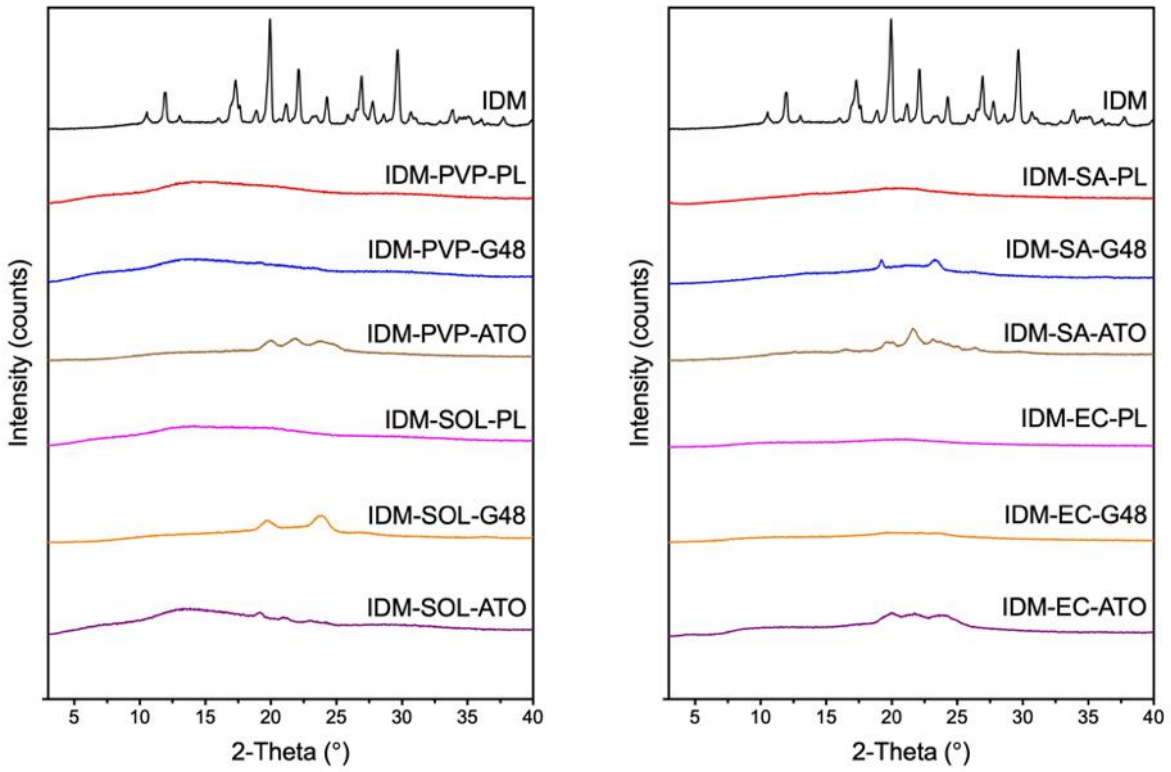

Figure C-5. PXRD diffractograms of solvent-based IDM ASDs prepared with polymer-lipid combination carriers.

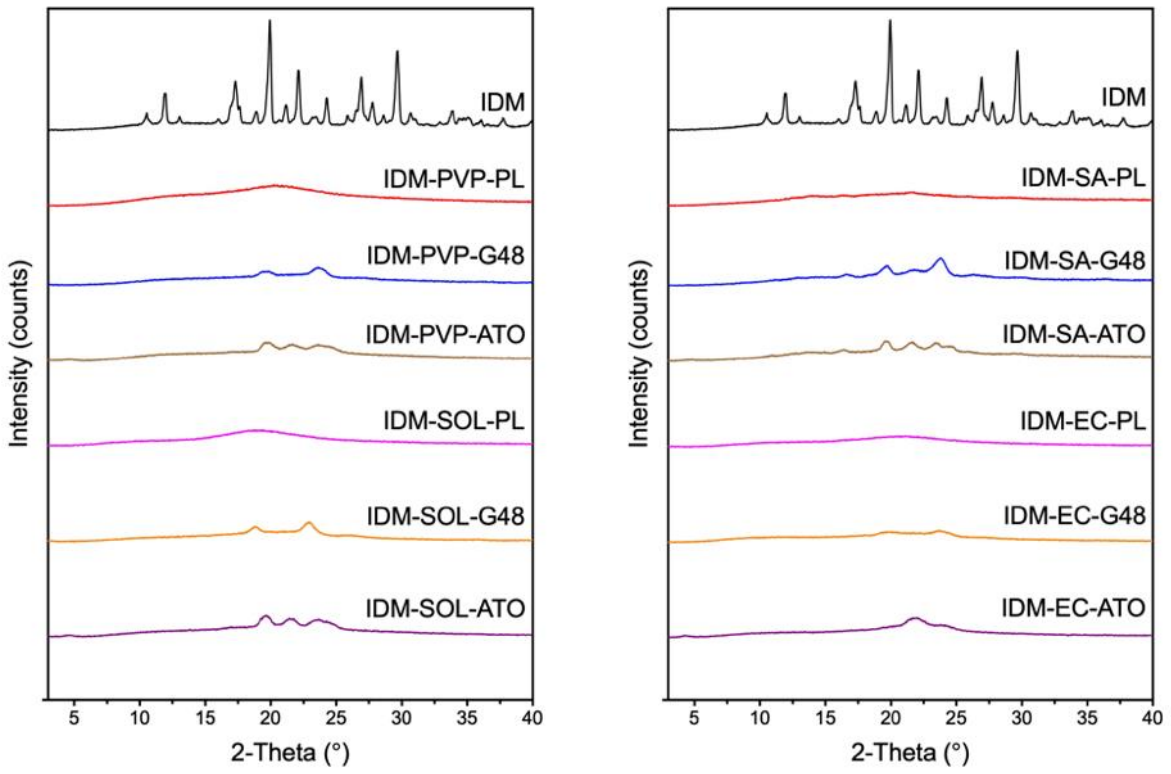

Figure C-6. PXRD diffractograms of freeze-dried IDM ASDs prepared with polymer-lipid combination carriers.

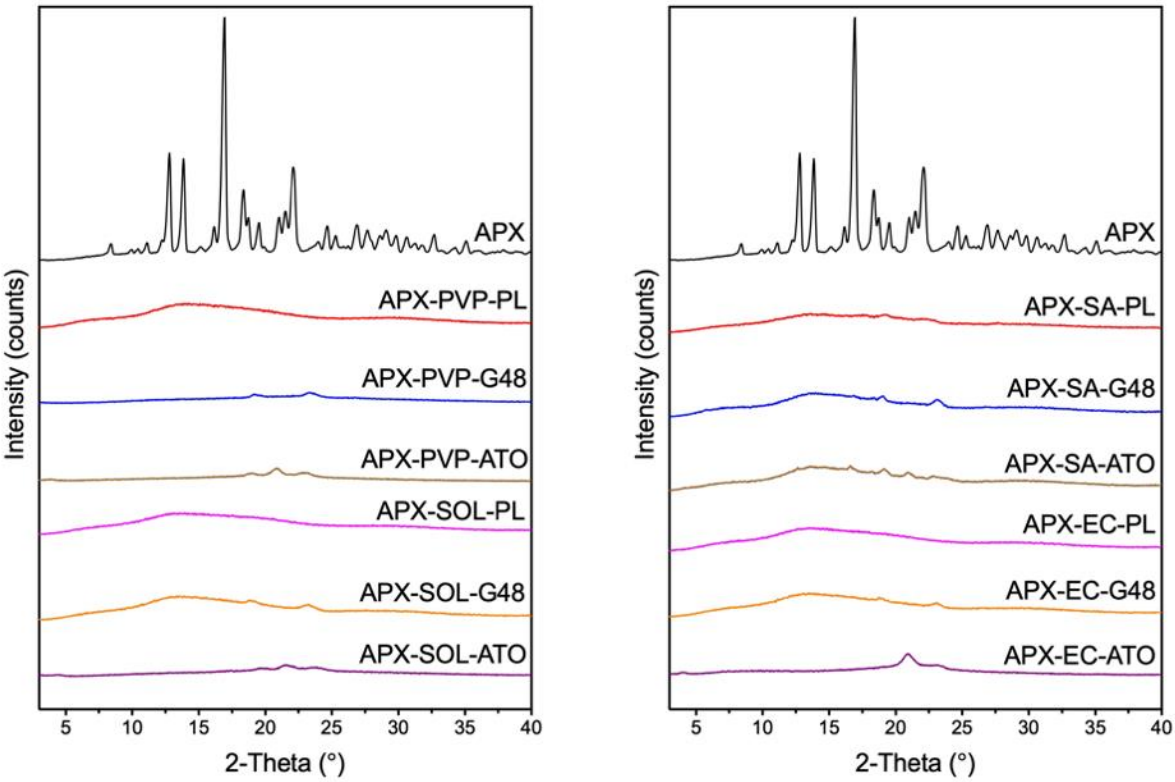

Figure C-7. PXRD diffractograms of solvent-based APX ASDs prepared with polymer-lipid combination carriers.

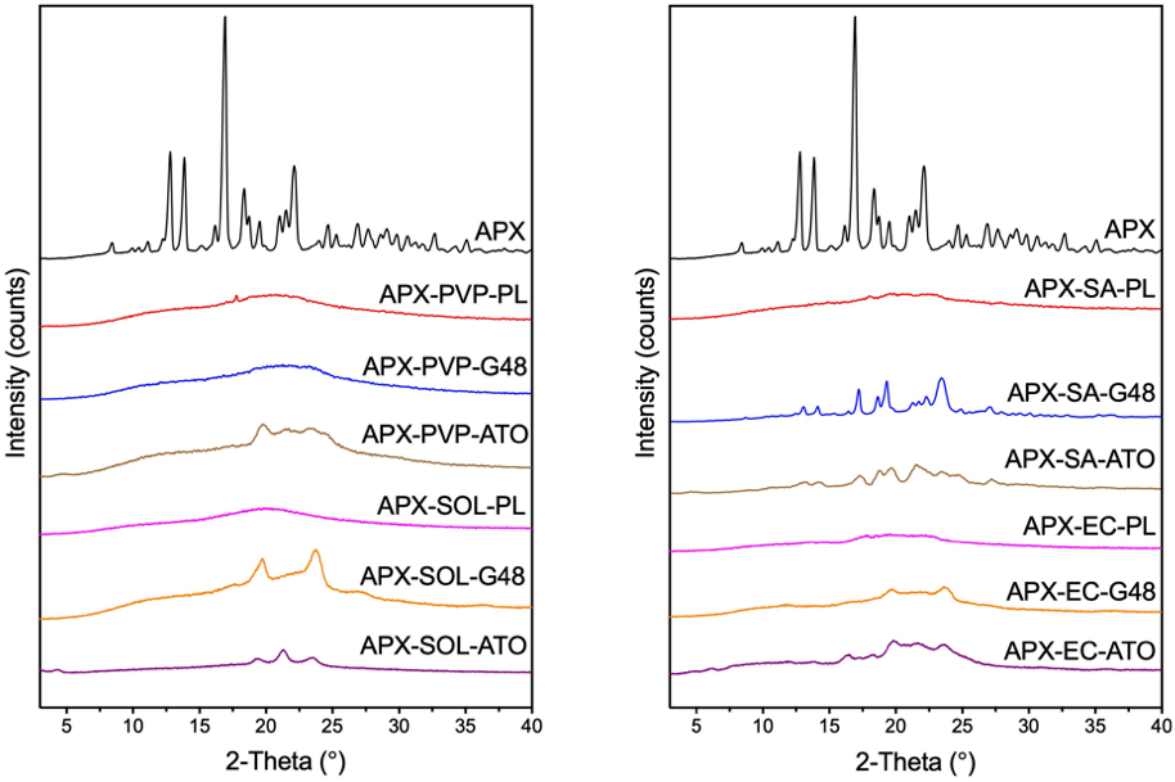

Figure C-8. PXRD diffractograms of freeze-dried APX ASDs prepared with polymer-lipid combination carriers.

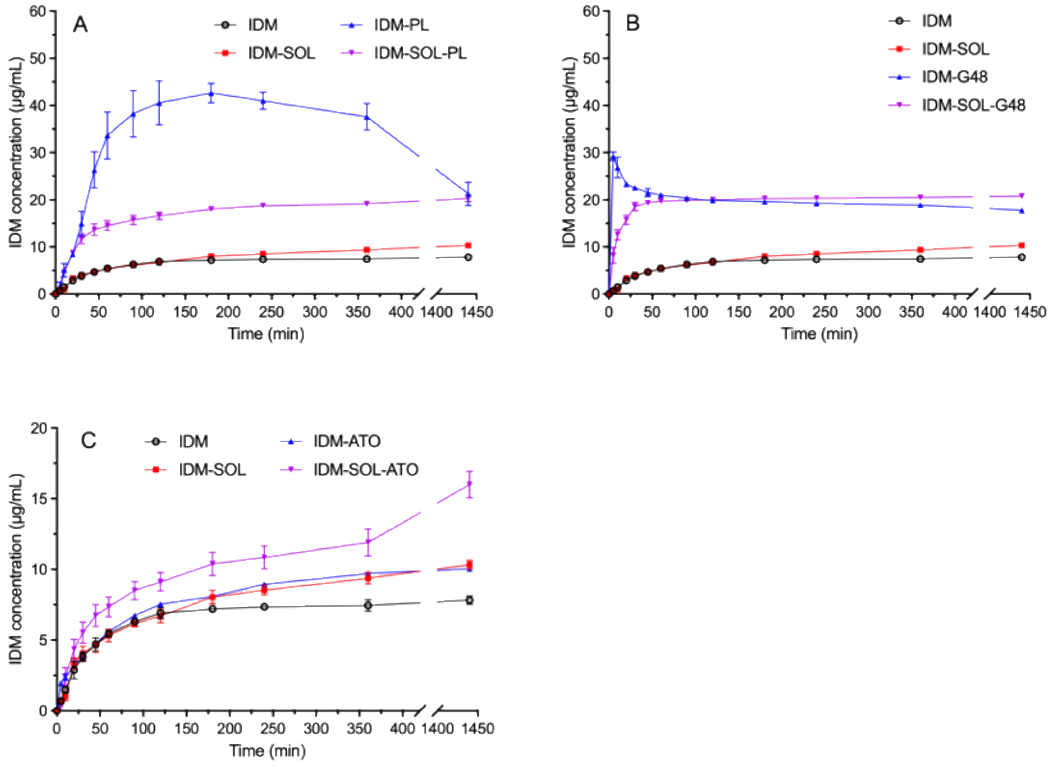

Figure C-9. Dissolution of solvent-based IDM ASDs prepared with (A) SOL-PL, (B) SOL-G48 and (C) SOL-ATO carriers in water.

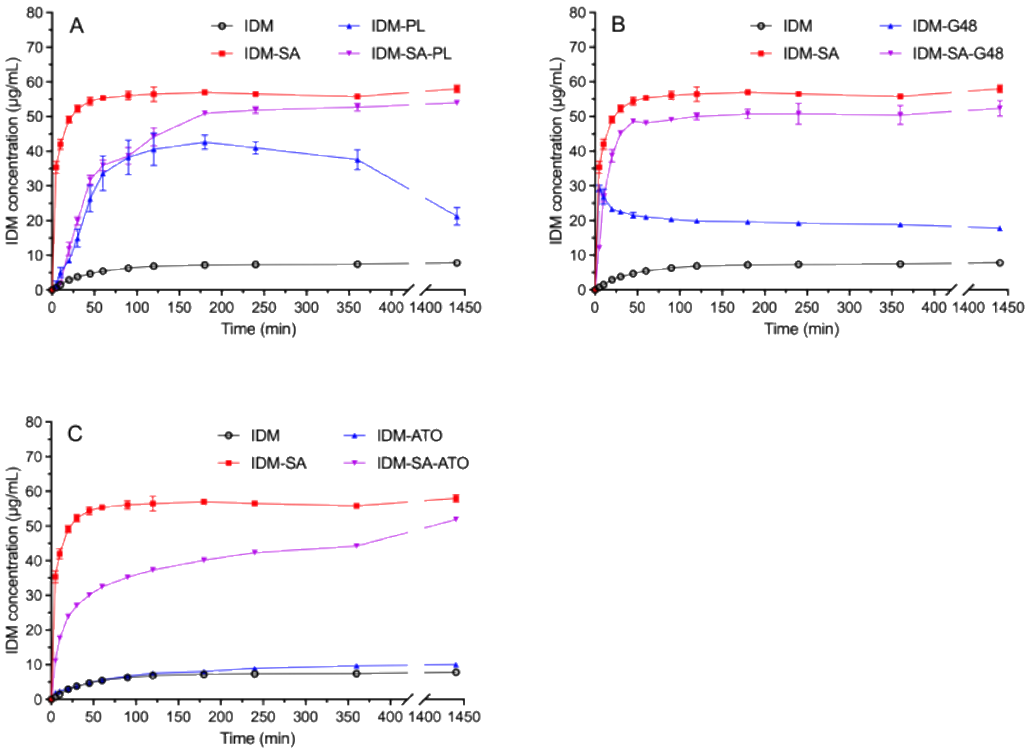

Figure C-10. Dissolution of solvent-based IDM ASDs prepared with (A) SA-PL, (B) SA-G48 and (C) SA-ATO carriers in water.

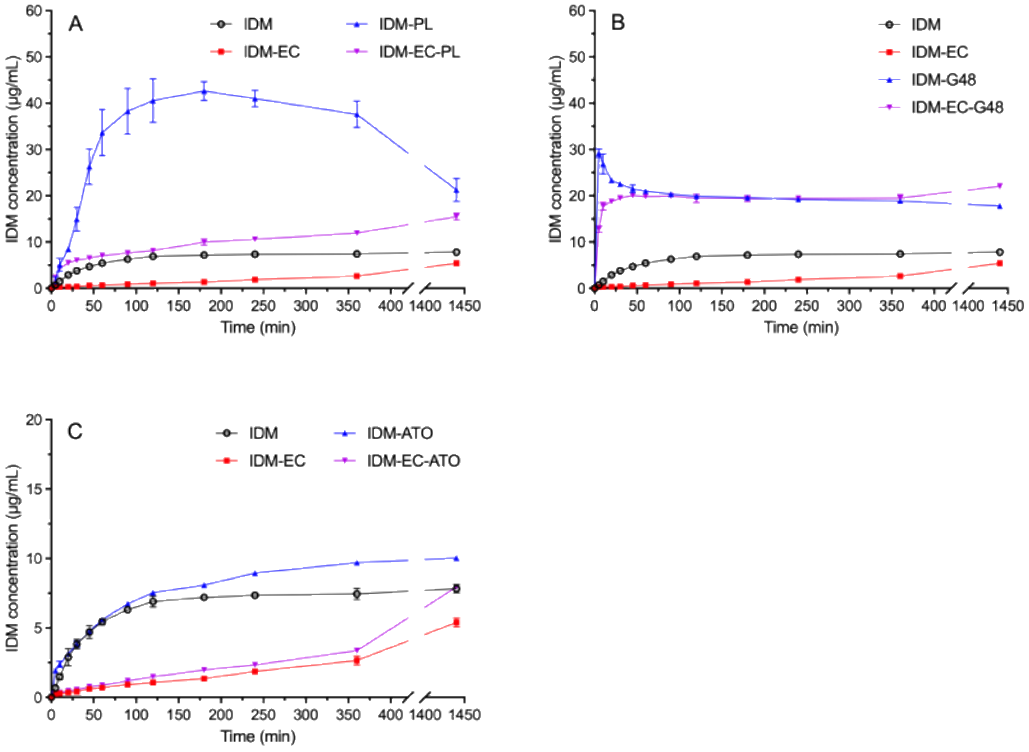

Figure C-11. Dissolution of solvent-based IDM ASDs prepared with (A) EC-PL, (B) EC-G48 and (C) EC-ATO carriers in water.

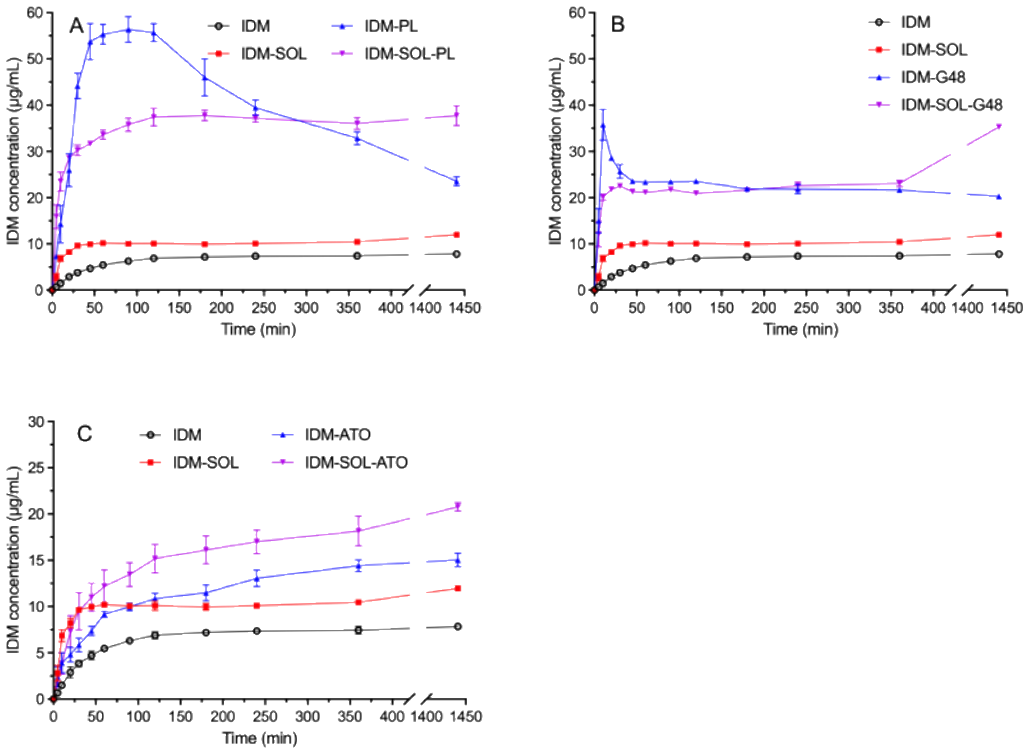

Figure C-12. Dissolution of freeze-dried IDM ASDs prepared with (A) SOL-PL, (B) SOL-G48 and (C) SOL-ATO carriers in water.

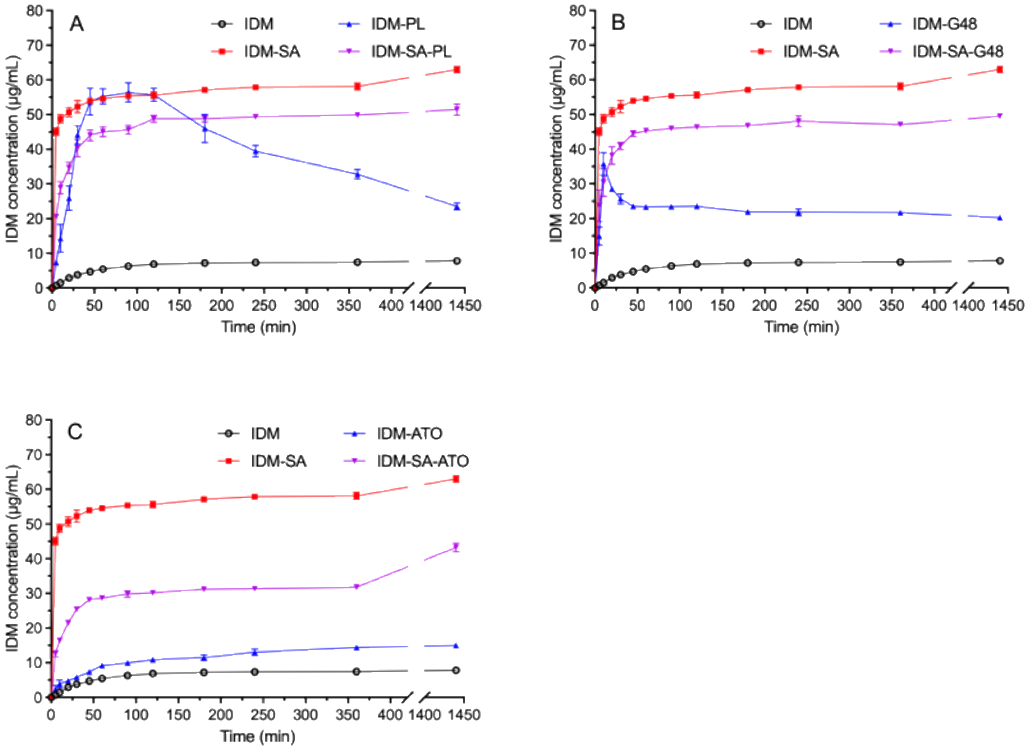

Figure C-13. Dissolution of freeze-dried IDM ASDs prepared with (A) SA-PL, (B) SA-G48 and (C) SA-ATO carriers in water.

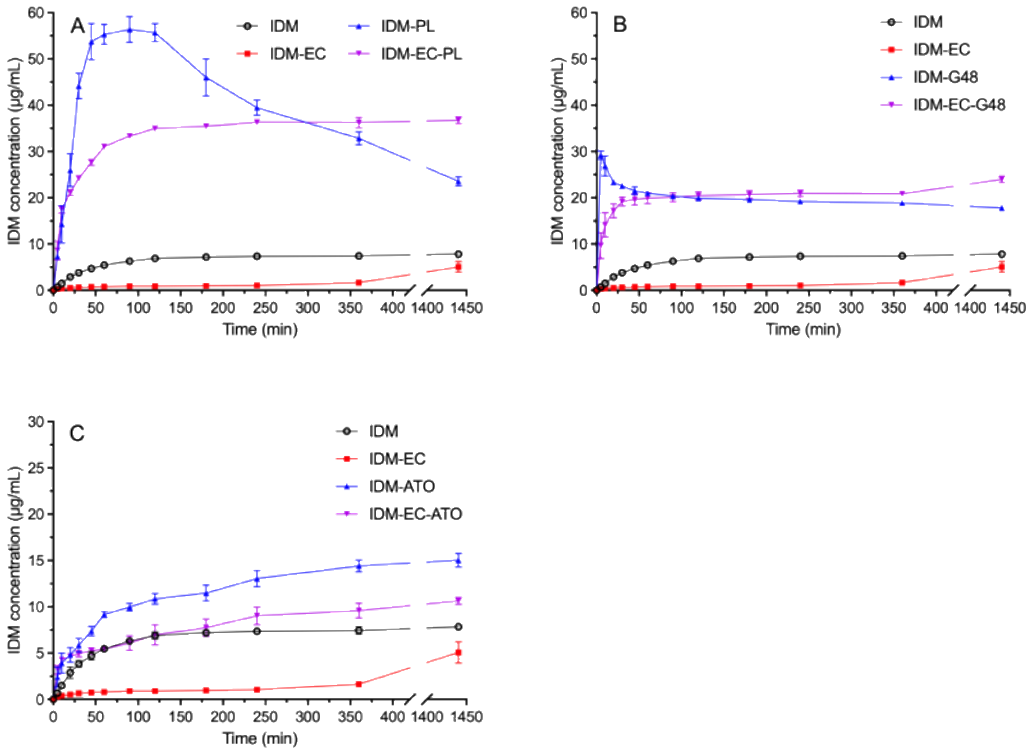

Figure C-14. Dissolution of freeze-dried IDM ASDs prepared with (A) EC-PL, (B) EC-G48 and (C) EC-ATO carriers in water.

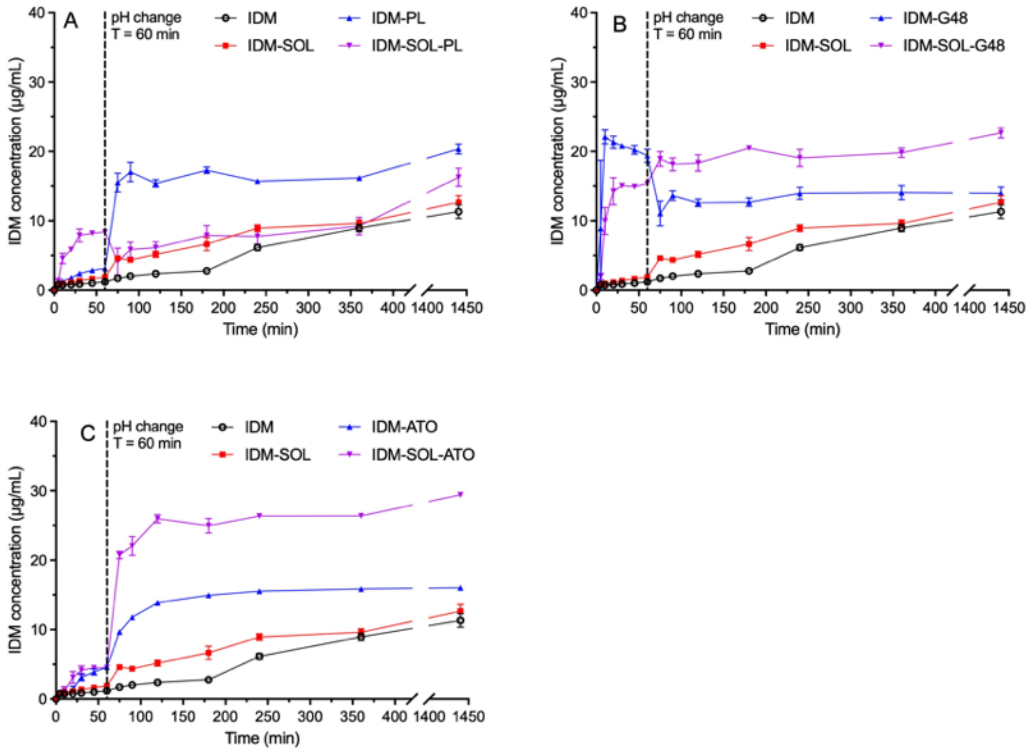

Figure C-15. Two-stage dissolution of freeze-dried IDM ASDs prepared with (A) SOL-PL, (B) SOL-G48 and (C) SOL-ATO.

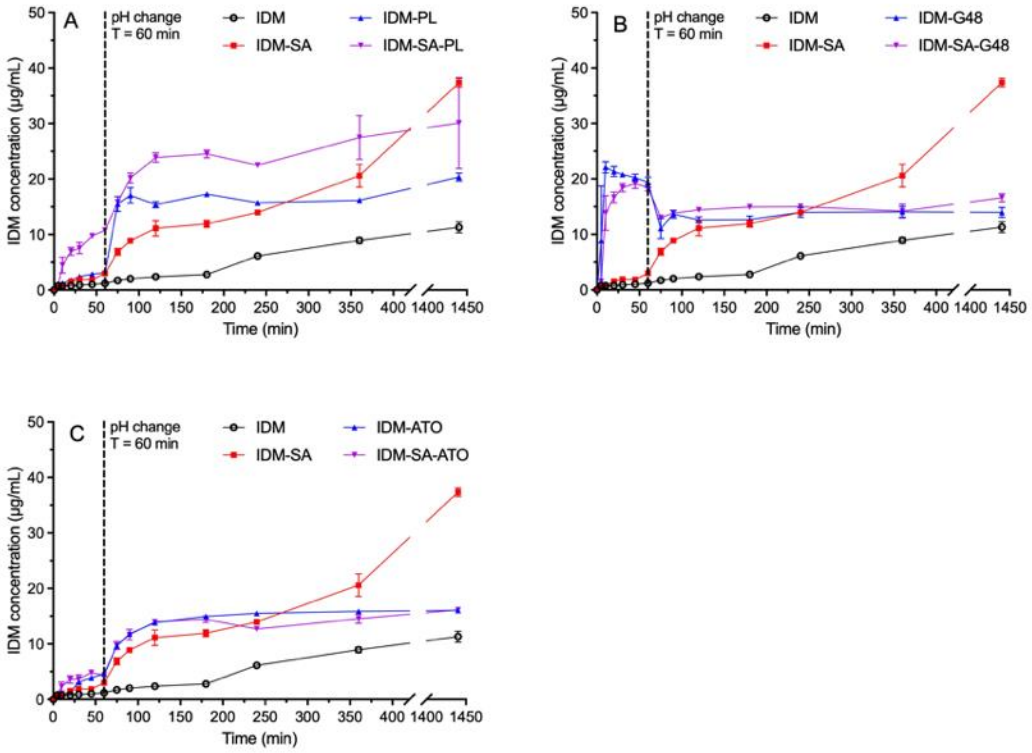

Figure C-16. Two-stage dissolution of freeze-dried IDM ASDs prepared with (A) SA-PL, (B) SA-G48 and (C) SA-ATO.

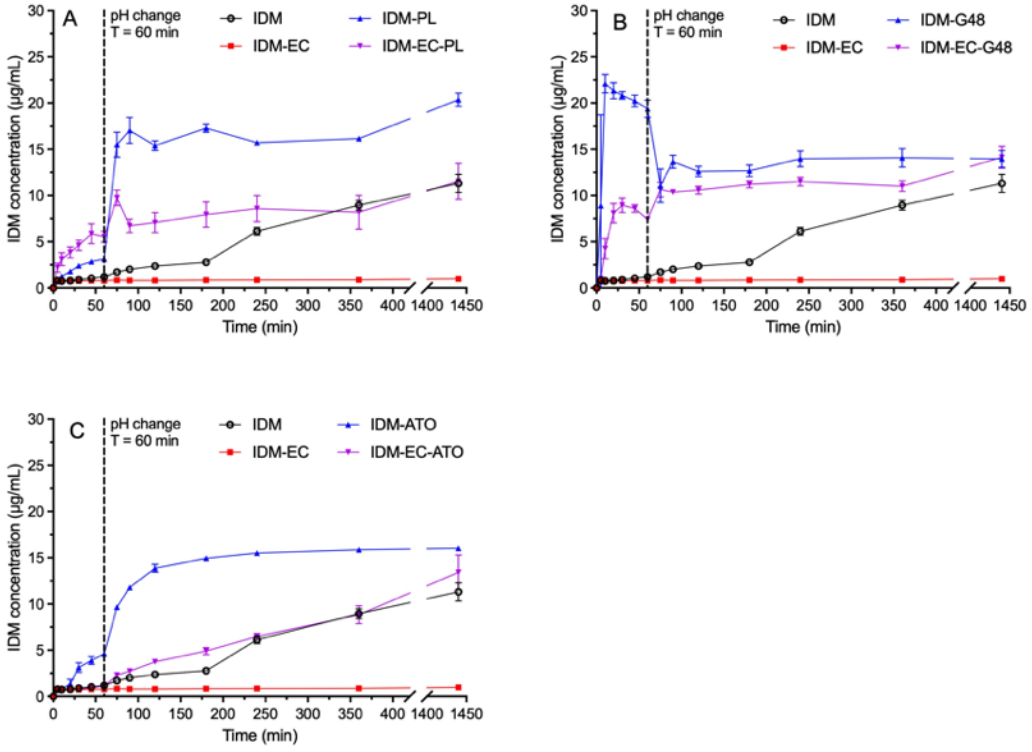

Figure C-17. Two-stage dissolution of freeze-dried IDM ASDs prepared with (A) EC-PL, (B) EC-G48 and (C) EC-ATO.

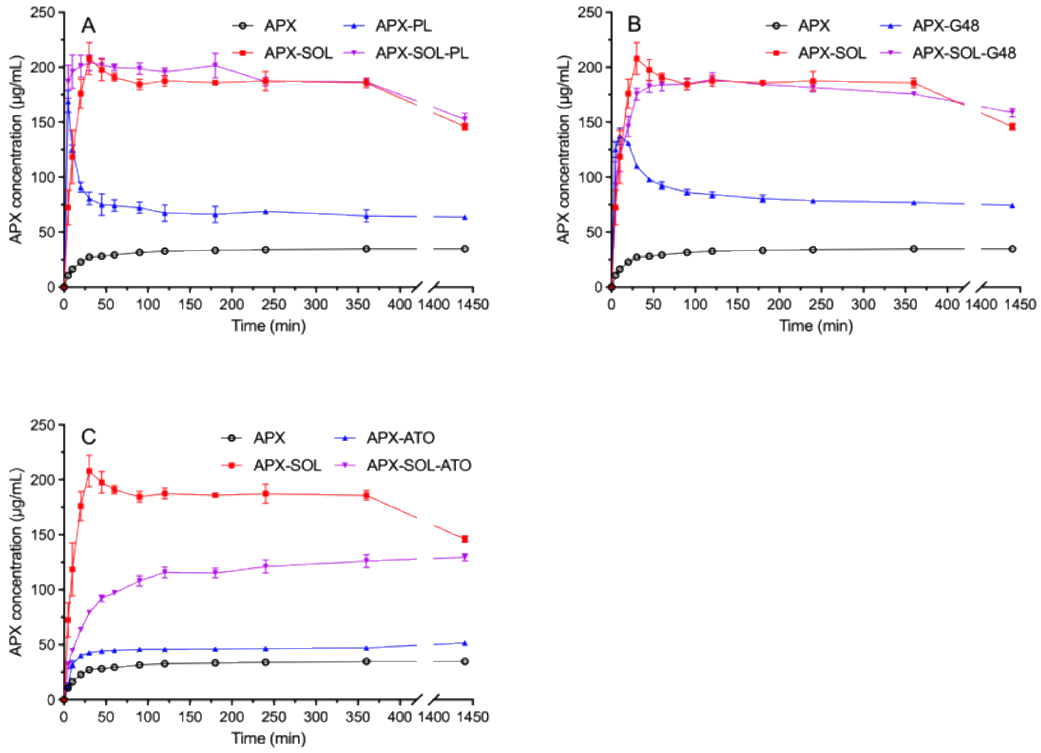

Figure C-18. Dissolution of solvent-based APX ASDs prepared with (A) SOL-PL, (B) SOL-G48 and (C) SOL-ATO carriers in water.

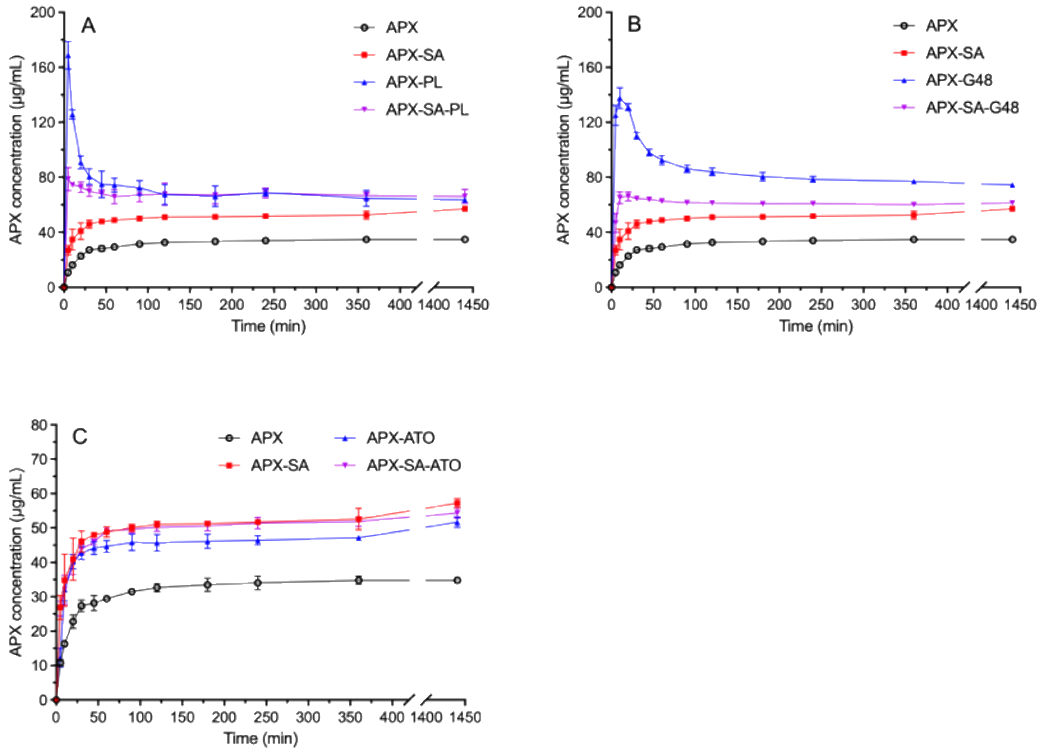

Figure C-19. Dissolution of solvent-based APX ASDs prepared with (A) SA-PL, (B) SA-G48 and (C) SA-ATO carriers in water.

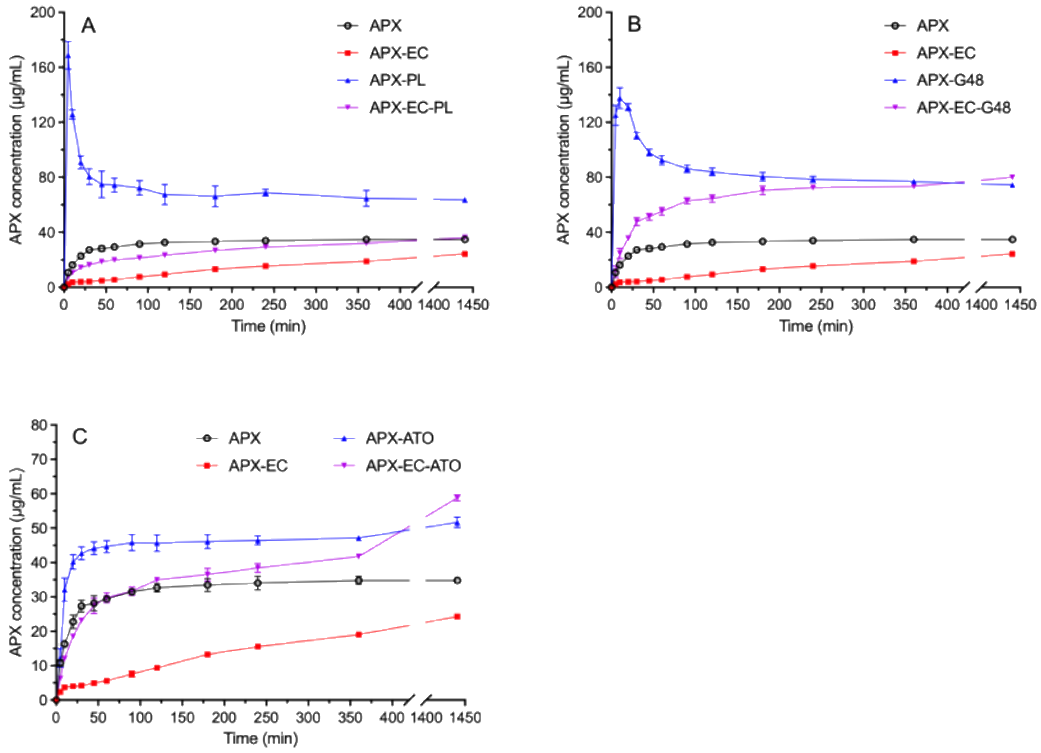

Figure C-20. Dissolution of solvent-based APX ASDs prepared with (A) EC-PL, (B) EC-G48 and (C) EC-ATO carriers in water.

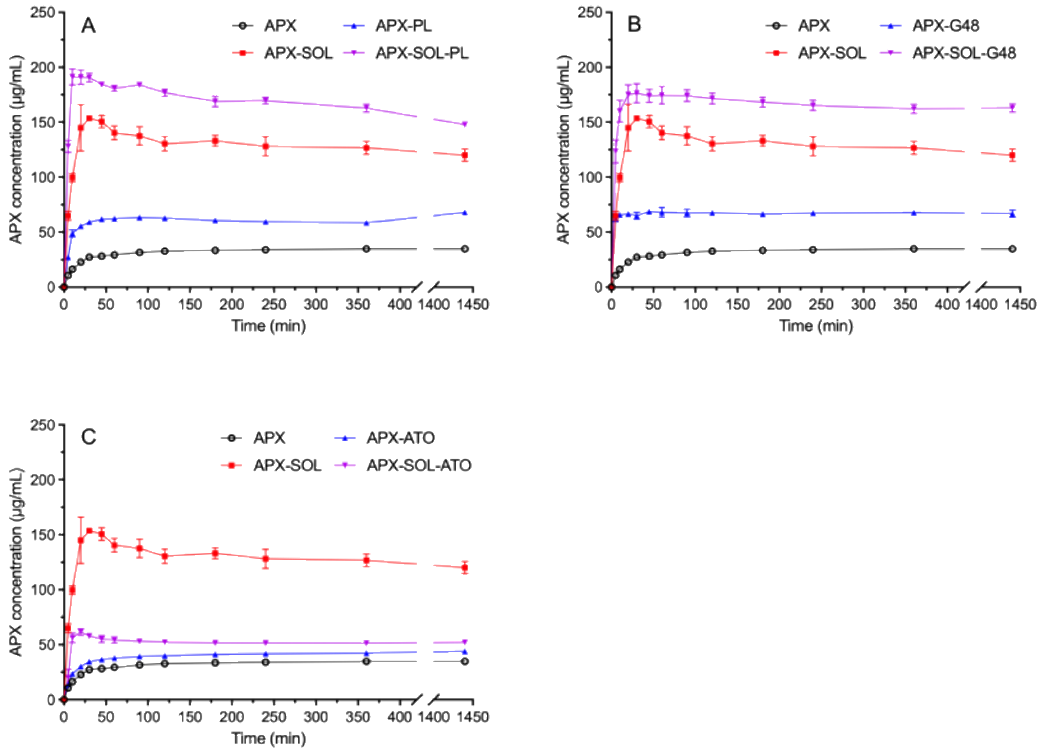

Figure C-21. Dissolution of freeze-dried APX ASDs prepared with (A) SOL-PL, (B) SOL-G48 and (C) SOL-ATO carriers in water.

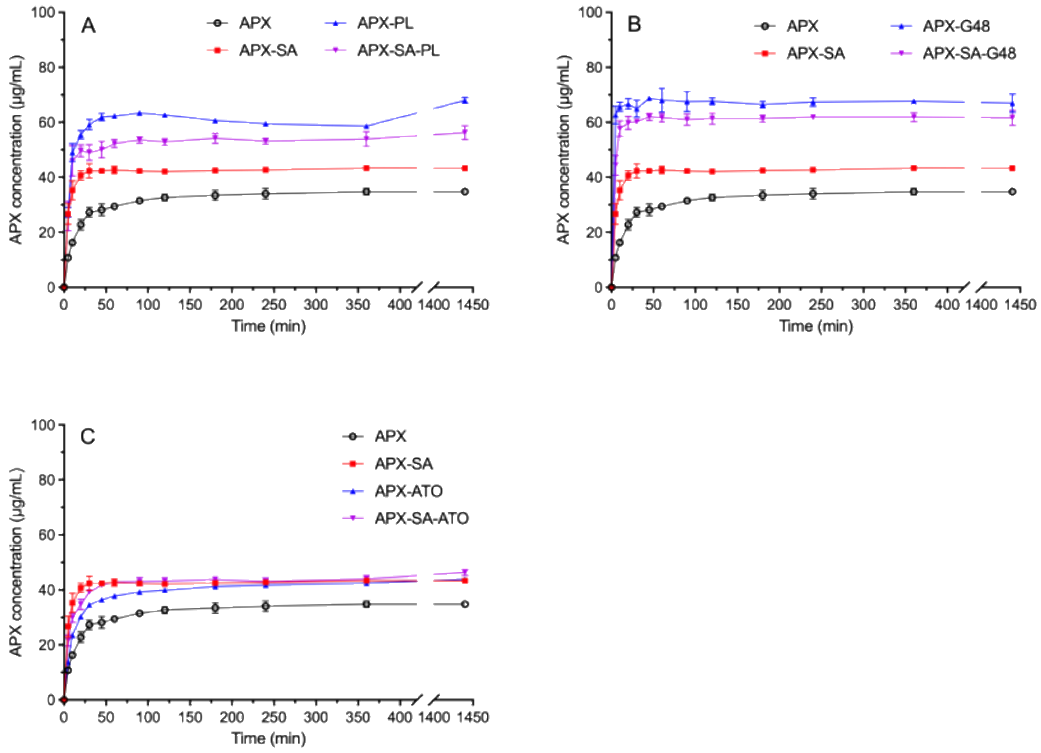

Figure C-22. Dissolution of freeze-dried APX ASDs prepared with (A) SA-PL, (B) SA-G48 and (C) SA-ATO carriers in water.

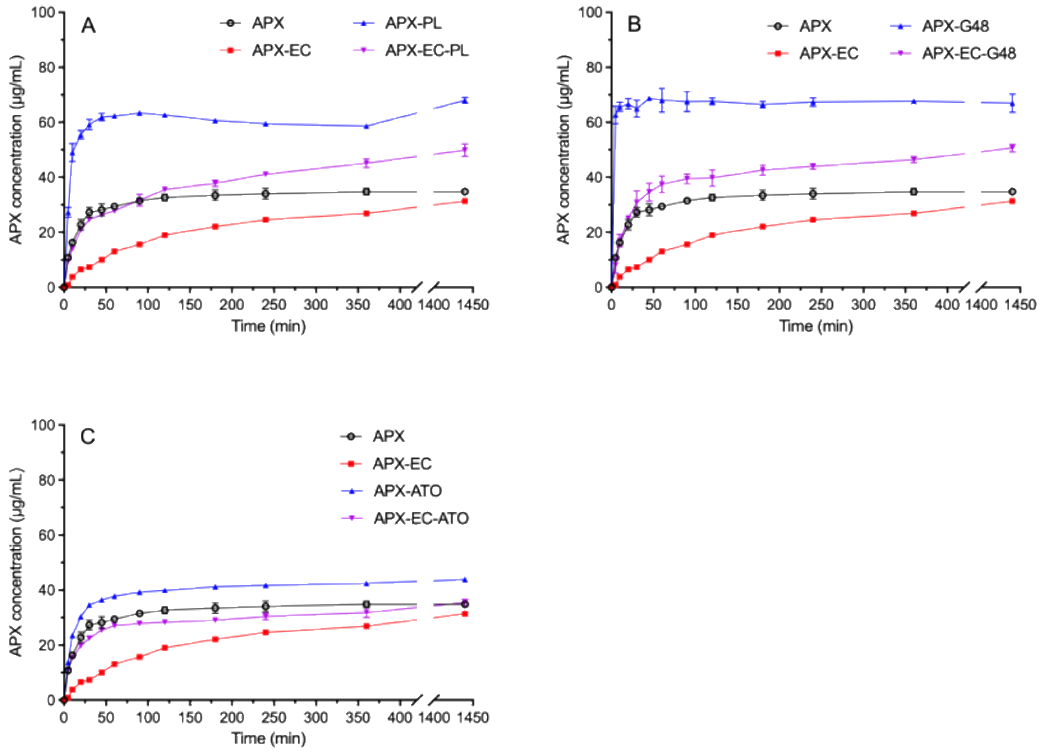

Figure C-23. Dissolution of freeze-dried APX ASDs prepared with (A) EC-PL, (B) EC-G48 and (C) EC-ATO carriers in water.

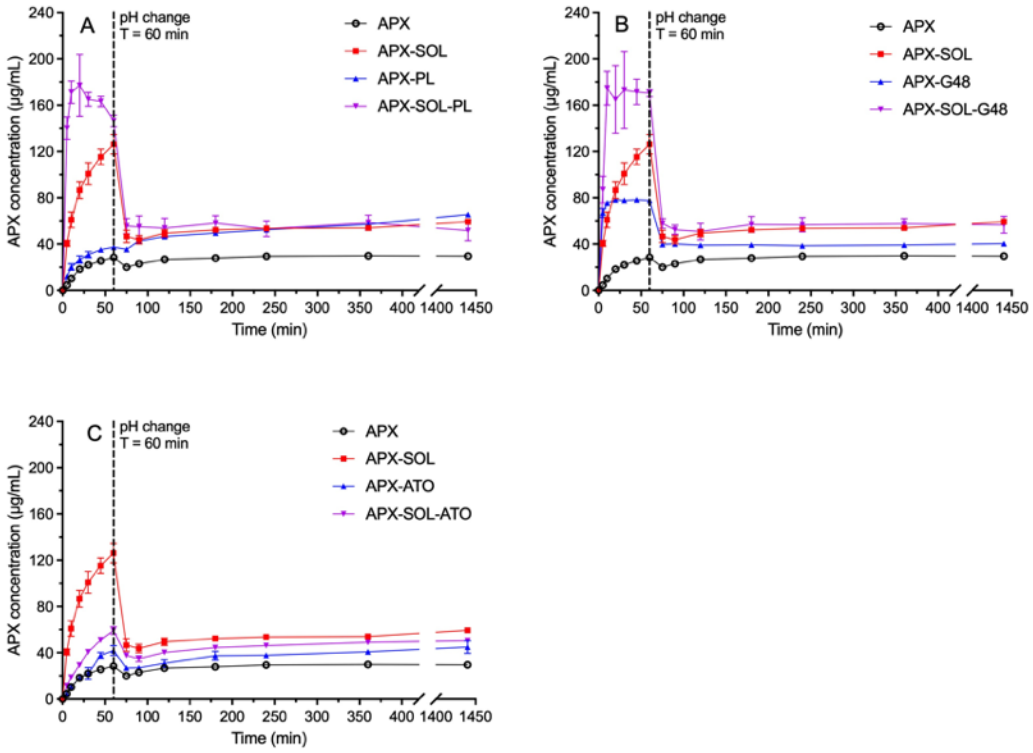

Figure C-24. Two-stage dissolution of freeze-dried APX ASDs prepared with (A) SOL-PL, (B) SOL-G48 and (C) SOL-ATO.

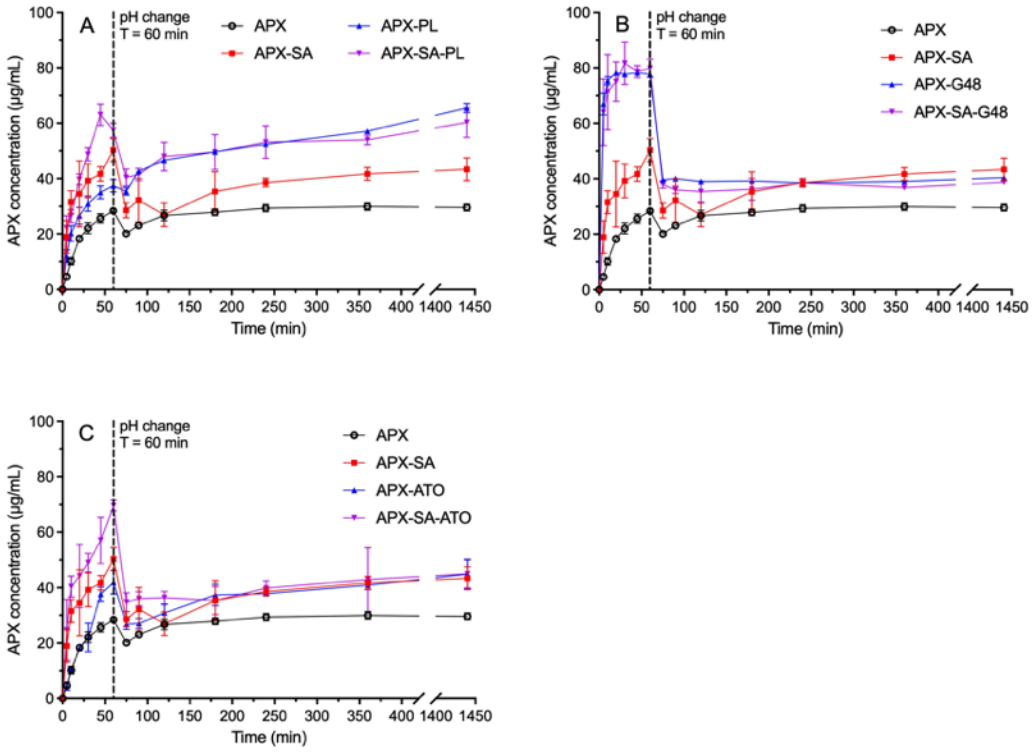

Figure C-25. Two-stage dissolution of freeze-dried APX ASDs prepared with (A) SA-PL, (B) SA-G48 and (C) SA-ATO.

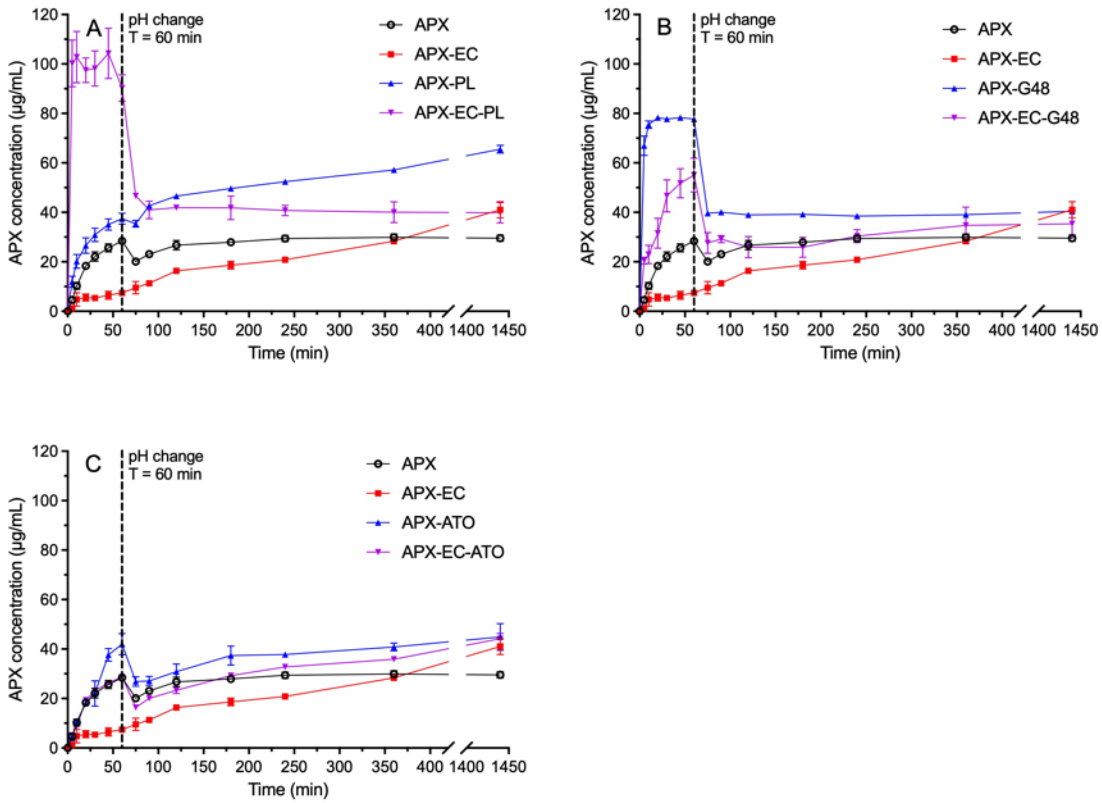

Figure C-26. Two-stage dissolution of freeze-dried APX ASDs prepared with (A) EC-PL, (B) EC-G48 and (C) EC-ATO.